LARGE DISPLACEMENT DEFORMATION OF PLATES

SUBJECT TO PROJECTILE IMPACT

A thesis submitted for the degree of Doctor of Philosophy

in the Department of Civil Engineering

at The City University

by

N. M. HALLETT

JUNE, 1987

ABSTRACT

The principle aim of the research reported in this thesis is to develop simple analytical techniques which can be confidently used to predict the amount and type of permanent damage to plates subject to projectile impact. In addition, it is intended to assess the validity of the scale similarity laws which are applicable to impact generated structural response involving large plastic deformations.

Existing literature involving analytical, experimental and numerical treatment of impact phenomena is reviewed. The need for the work conducted herein arises because, in general, simple design formulae for structural damage estimation do not exist. Furthermore, when structural testing is deemed necessary, it is uncertain whether scale models will faithfully represent prototype behaviour in situations involving structural impact.

The analytical procedures proposed are based on a rigid plastic material idealisation and, in addition, rely on many other assumptions. The implications of the assumptions inherent in the techniques are critically examined and discussed in detail. Simple relationships are proposed for both quasi-static and dynamic target response. Furthermore, square target panels are analysed as 'equivalent circular plates' to enable axisymmetric treatment of the problem.

An experimental programme involving fifty-nine tests on isotropic mild steel plates is reported. An experimental rig was designed and

built both for the purposes of this research and to provide a general impact test facility for future use. Two test series were conducted: the first provided data to validate analytical methods and the second was specifically designed to validate scale similarity laws. The special instrumentation problems associated with tests involving impact are discussed.

The experimental results are compared with the various analytical techniques proposed. In addition, a small number of case studies are presented to demonstrte the capabilities and versatility of the proposed methods.

It is concluded that approximate rigid plastic methods can provide good estimates of target damage from projectile impact loading. The particular analytical approach necessary for a given problem is dependent on the initial problem parameters. A wide range of problems can be solved, however, with careful use of the proposed methods.

The use of small scale models to predict prototype behaviour is valid for the work reported in this thesis. It is concluded, however, that impact events involving tearing, fracture or buckling in response are less likely to scale successfully and further work is suggested.

The validity of the proposed analytical methods is limited to the range of parameters studied epxerimentally. There is no reason to suppose, however, that use of the techniques outside this range will be unsuccessful and further experimental work is suggested to support this conjecture. The main limitation of the proposed methods is the lack of

a criterion defining failure. For example, in one test the target was perforated completely and this was not predicted by the theoretical techniques used.

Although there exist limitations with simple analytical design methods, the various techniques developed herein have predicted good results for a wide range of problem parameters.

CONTENTS

LIST OF TABLES

LIST OF FIGURES

NOTATION

A,B	half lengths of rectangular plate sides
A_L,A_p	area integration limits of plates
A_o,B_o	constants in equation (3.46)
A^1,B^1,C^1,D^1	cubic polynomial coefficients equation (5.11)
C,D	parameters defining rectangular plate geometry
$[BR]$	$= \frac{ab}{AB} + \frac{1}{3}\left(\frac{b}{B} + \frac{a}{A} + 1\right)$ - see equation (3.27)
C_o	constant in equation (5.7)
D	$= \frac{Eh^2}{12(1-\nu)^2}$ - plate elasticity constant
D_E	external work rate
D_f	plate dissipation function
$D_i D_b$	internal, boundary dissipation functions
D_o	material constant equation (2.9)
E	Young's modulus
G	missile mass
K	elastic stiffness
$K_1,K_2,K_3,K_4,$	constants in equations (3.38) and (3.41)
Kg	strain gauge factor
K_p	Kinetic energy of plate
K_s	Kinetic energy of striker
$K.E$	Kinetic energy
$K(t)$	Kinetic energy of system at time t
L	length of beam or side length of square plate
M_{ij}	internal bending stress resultants
M_o	$= \frac{\sigma_y h^2}{4}$ - plastic bending moment per unit width of plate
N_{ij}	internal in-plane stress resultants

N_o	$= \sigma_y h$ - fully plastic axial force per unit width of plate
P	total applied load
P_L	limit load of beam or plate
Q_i	internal shear stress resultants
$Q_1, Q_2 .. Q_n$	generalised stress resultants, equation (2.1)
R	radius of circular plate
SR	$= \frac{4h}{3R^2 (1-\nu^2)}$, strain rate correction constant
T	fundamental natural period of plate
V_o	missile velocity
V_A	measured value of missile velocity
V_{TH}	theoretical value of missile velocity
V_i	actual velocity, equation (3.23)
a_c	acceleration of plate
a_L	radius of plate loaded area
a,b	linear dimensions of plate loaded area
a_o, b_o	empirical shape functions, equation (5.8)
d	power of dissipation, equation (2.1)
d_1	constant in section 3.5
e	axial extension
e_1, e_2, e_3, e_4, e_5	constants, equations (3.40) and (3.42)
f	fundamental natural plate frequency
g	gravitational acceleration constant
h	thickness of plate
m	number of straight line plastic hinges
lm	length of m^{th} plastic hinge line

p_i	load per unit area of plate
p_o	material constant, equation (2.9)
$\dot{q}_1, \dot{q}_2 .. \dot{q}_n$	generalized strain rate, equation (2.1)
t	time
t_f	duration of impact response
u_i	in-plane displacement components of plate
w	plate out of plane deflection
w_o	maximum permanent plate deflection
w_e	maximum elastic plate deflection
$\bar{w}_o$	normalised maximum permanent deflection
$\dot{w}_i, \dot{w}*^o, \dot{w}*$	values of plate velocity, section 3.4
w_f	permanent deflection at time $t = t_f$
x, y	co-ordinate axes in plate mid-plane
z	co-ordinate axis normal to plate mid-plane
Δ	positive function expressing difference in assumed and actual velocities, equation (3.23)
Φ_1, Φ_2	constants, equation (3.45)
Ψ_1, Ψ_2, Ψ_3	constants, equation (3.45)
Γ	$= \frac{\Theta \beta^2}{6} (3-2\xi_o) (1- \xi_o + 1/ (2-\xi_o))$
Ω	aspect ratio of plate
Θ	$= \frac{\mu V_o^2 \beta^2}{M_o h}$, constant in equation (2.7)
α	$= \frac{a}{C} + \frac{b}{D}$, rectangular plate geometrical constant
β	$= \frac{C}{D} + \frac{D}{C}$, rectangular plate geometrical constant
β_o	scale factor (less than unity)
γ	rectangular plate limits of moving boundary
δ	variational function equation (3.33)
ϵ	strain
ϵy	yield strain

ϵr	radial strain
ϵ	circumferential strain
ϵre	recorded value from strain gauge
$\dot{\epsilon}$	strain rate
$\dot{\epsilon} e$	equivalent strain rate for 3D strain field
ζ	rectangular plate limit of moving boundary
η	$= \frac{4\mu ab}{G}$, equation (3.26)
θ	angular displacement
$\dot{\theta}$	rotation rate at a plastic hinge
$\dot{\kappa}$	rate of plate curvature
ϕ	angle defining rectangular plate geometry
χ	$= \frac{4\mu AB}{G}$, plate/striker mass ratio
ψ	normalised deflection shape functions
ω	circular natural frequency of plate
$\bar{\omega}$	circular plate geometric constant defining shape change
λ	$= \frac{GV_o^2}{8M_o h}$ Kinetic energy constant
μ	mass per unit area of plate
ν	Poisson's ratio
ξo	$= \Omega \tan \phi$, constant equation (2.7)
$\pi i \cdots \pi n$	Buckingham-pi method similarity constants
ρ	material density
σ	stress
σ_y	yield stress
σ_{yd}	dynamic yield stress
τ	strain rate constant

ACKNOWLEDGEMENTS

I am indebted to the Science and Engineering Research Council for providing the funding necessary to carry out this research.

I would also like to express thanks to the following people:

Dr. L.F. Boswell who supervised the work.

[redacted] and the technician staff in the Department of Civil Engineering; all made valuable contributions during the experimental programme.

[redacted] who assisted in the preparation of text and tables.

Finally, I would like to express deep gratitude to [redacted], who typed the bulk of the text and gave me constant encouragement and support at all times.

CHAPTER 1

GENERAL INTRODUCTION

1.1 Introduction

Permanent damage or destruction can occur to a structure when it is subjected to intense short term loading which may be referred to as an impact. It is likely that the time history of the impact is complex and the associated structural response can be investigated by a number of methods. Analytical methods range from crude empirical equations to full numerical solutions of the governing equations of motion. In many cases, however, lack of confidence in analytical approaches will demand recourse to experimental testing of the prototype, or of scale models.

Two recent papers [1,2] report the results from full scale tests carried out to assess the integrity of structural components subject to projectile impact loading. The tests were conducted to provide data to design stiffened and unstiffened structural plating in the wellhead module area of offshore drilling platforms. The function of the plating was to absorb the kinetic energy possessed by an object which had been accidentally dropped from an overhead crane thus ensuring the safety of equipment and personnel in areas beneath. In both reports it was concluded that the normal impact of a standard 3 tonne drill collar 9m long and 0.24m in diameter would represent the worse case for this hypothetical impact. During the experiments, therefore, drill collars were dropped on to specimens from heights up to 42m.

In the above studies, theoretical correlations to the problem are attempted, but final design recommendations are exclusively based on the test results. In reference [1], however, a formula from a paper by DeOliveira [3] is used to predict the result of one test with apparent success. It is the author's opinion that this result is somewhat coincidental. The formula in question, used in reference [1] for stiffened plate design, was derived for unstiffened plating and is shown in Chapter 5 to seriously underestimate plate damage for the projectile impact tests reported herein.

Presumably it was thought necessary in references [1,2] to test at full scale to avoid potential scale effects associated with small scale model testing. It is well known that certain structures subjected to impact loading can be successfully modelled at small scale, while others cannot [4]. There is little doubt that more experimental evidence is necessary to reinforce the literature on impact scale similarity. Significant time and cost savings can usually be achieved if the results from small scale models can be successfully extrapolated to predict prototype behaviour.

It is evident from references [1,2] that existing analytical techniques for target damage estimation are inadequate. Impact Engineering is in its infancy and generally the Engineer does not have the benefit of design manuals and codes of practice. The response of a given target is dependent on many parameters such as impact velocity, target and missile hardness, missile mass etc., and alteration of these may cause the target to respond elastically, plastically or fail completely.

Early analytical work involved the determination of empirical equations to predict critical velocities for target perforation [5,6]. The use of these equations, however, is generally limited to a small range of parameters. Many analytical developments have occurred since and are discussed in Chapter 2 but there clearly exists a certain lack of knowledge concerning the range of applicability of such methods.

The work presented in this thesis represents the initial part of a research programme to propose and validate simple analytical techniques for predicting damage to structures subject to projectile impact loading. The research also aims to provide further information regarding the controversial subject of scale model testing of dynamically loaded structures.

Reports regarding the integrity of offshore platform components provided the initiative to commence this research programme. The problem of designing structures subject to impact loading, however, occurs in many industries. For example, the Naval Architect may be concerned with slamming damage to ships [7], collision between ships [8], or the structural effects of aircraft landing on aircraft carriers [9]. The Nuclear Engineer is concerned with the integrity of a reactor building under many impact loading conditions including explosion, crashing aircraft or fragment impact due to turbine failure [10]. The Aeronautical Engineer may be concerned with the potential hazard of birds causing impact loading of compressor blades [11].

1.2 Thesis Objectives

The original objective of this research was to re-examine the tests reported in reference [1,2], both theoretically and experimentally at small scale. It is apparent that analytical design methods are inadequate for such events and that results from small scale impact tests should be treated with caution [4]. The laws of dynamic similarity (see section 2.6) mean that small scale simulation of the events reported in references [1,2] is not possible under laboratory conditions, due to the missile velocity remaining invariant. Furthermore, it is apparent that investigations of a problem often results in conclusions which are specific to a particular structural configuration.

In view of the above comments, no attempt has been made to consider a particular design impact condition or model any prototype. It is intended that the research be undertaken as a fundamental investigation of the problem. If the results of fundamental tests can be properly understood and explained, then it should be possible to predict the behaviour of a prototype structure.

The work presented in this thesis has four objectives and these are

a) To review the literature concerning structures subject to impact loading of sufficient intensity to cause plastic deformation.

   Perforation and penetration of structural components, however, is not a consideration in this thesis.

b) To propose and critically examine approximate analytical techniques which enable estimates of damage to structures subject to projectile impact.

Although sophisticated numerical treatment of impact phenomena is now possible, time and cost restrictions mean simple approximate methods remain an invaluable, inexpensive design aid.

c) To assess the validity of scale model testing for projectile impact structural response.

It is obvious that, in many cases, recourse to testing is necessary either to validate proposed design methods or because no design methods are immediately available. If applicable, testing at small scale is usually more economical than full scale tests [12], and

d) To compare analytical proposals with the results of an experimental test programme.

1.3 Outline of the Thesis

In Chapter 1 the introduction and objectives are followed by a brief introduction to general impact phenomena. The introduction to impact outlines the mechanics involved, some of the complexities encountered, the extreme range of behaviour possible and the simplifying assumptions which are necessary for the theoretical treatment of impact events.

In Chapter 2, a literature review is presented and particular attention is given to the analytical treatment of impact events. Experimental studies, which are still surprisingly scarce, are also reviewed. A comprehensive review of the numerical treatment of impact phenomena is not attempted, but papers directly relevant to the current work are mentioned. Finally, mention is made of studies which have particular relevance to scale similarity of structures and strain rate sensitivity of structural response.

The most common simplifying assumption enabling analytical treatment of impact events involving gross plastic deformations, is that of assuming rigid plastic material behaviour. The consequences of this assumption are discussed in Chapter 3 where rigid plastic methods are used to derive equations for the design of isotropic plates subject to projectile impact load. Analyses include both quasi-static and dynamic treatment of plate response. The formulae derived are found to disagree with previously published design formulae.

Chapter 4 describes the design and construction of a general purpose impact testing facility. The 'drop hammer' apparatus was required to produce test results for the current investigation and, in addition, be as versatile as possible for maximum future usage. The instrumentation associated with the apparatus plus the two series of tests carried out and the testing procedure adopted are also described.

In Chapter 5, the results from the two test series are presented and compared with analytical predictions. Discussions on accuracy and effects such as material strain rate sensitivity and scale similarity

are presented together with an approximate method to determine maximum permanent target displacement. This approximate method is based on the final deformed profiles of the specimens. Case studies using the formulae derived in Chapter 3 are also presented and discussed.

Finally, Chapter 6 lists the conclusions of the research work presented and suggests recommendations for further work.

1.4 Introduction to Impact Phenomena

Modern construction techniques and material developments has encouraged the study of the dynamic behaviour of structures. The economic necessity of lowering structural factors of safety has produced lighter, more flexible structures, which in turn has resulted in an increasing industrial need to accurately determine the response of such structures to periodic, transient or impulsive excitation.

Furthermore, the availability of powerful computational hardware has allowed, at least in principal, numerical analysis of such events.

The type of dynamic loading of interest in this thesis is the short term excitation associated with the more specialised subject of Impact Mechanics. For this type of loading it is often necessary to estimate the maximum dynamic energy which a structure could absorb without failure, or to predict the damage which a structure would sustain if it were involved in a collision with another body, or subjected to explosive loading.

In certain circumstances, blast loading and projectile impact loading will produce similar structural response and consequently theoretical methods have been developed in parallel for both types of response. To-date, however, it would appear that many workers have concentrated on analyses which rely on the initial specification of a force-time function and are, therefore, most suited to blast loading conditions.

Much work in the field of projectile impact has military application. This is generally in the category of 'high velocity' impact where load intensity causes a highly localised response governed by the constitution of the material in the vicinity of load application rather than the geometry and the boundary conditions of the structure as a whole. In many situations involving impact at high velocity the boundary conditions of the problem will be irrelevant and a description of the problem in terms of elastic, plastic and shock wave propagation becomes appropriate.

In contrast to the above, and of particular interest in this work, is 'low velocity' impact. In this regime structural behaviour is controlled by a relatively small number of low frequency modes and local indentations or perforations are strongly coupled to the overall deformation of the structure.

A quantitative measure of when 'low' velocity becomes 'high' velocity is difficult to define, but often low velocity impact is defined as being associated with velocities of less than about 100 m/s [4].

The loading and response times in the different velocity regimes differ by orders of magnitude. High velocities are associated with 'early time' response, are governed by stress wave propogation and have durations typically of the order of microseconds. A common practical problem of interest here is the spalling of a concrete slab on the opposite face to that subject to impact. This spalling is caused by a compressive pulse transmitted through the thickness of the slab which is subsequently reflected as a tensile wave.

Low velocities are associated with 'late time' response and have durations typically of the order of milliseconds. In this case it is generally assumed that an impact imparts instantaneous momentum to the mid-surface of a structural component.

The theoretical treatment of impact phenomena is extremly complex whichever velocity regime is of interest. When one body impacts another, both instantaneously experience excitation of elastic modes. If the contact force created is of sufficient magnitude, the material will reach yield at certain times and locations within the structure and plastic deformation will occur in regions with time dependant boundary locations. Furthermore these boundaries will be separated by regions where the yield criteria has not been satisfied and elastic action continues.

Evaluation of the problem requires the solution of partial differential equations with moving boundaries and, furthermore, these equations will become non-linear if finite deflections are to be considered. When the energy required to continue plastic deformation

expires, the third phase of motion, consisting of elastic vibration in the deformed state, concludes the structural response.

In view of the complex behaviour of impact phenomena analytical solutions are out of the question unless gross simplifying assumptions are made. The definition of material properties is a further difficulty. The properties of a structural material which are commonly determined from uni-axial 'static' tests may be quite inappropriate when that material is subject to high rates of strain.

It is clear that the theoretical and experimental study of structures subject to impact loading is still in its infancy despite a considerable research effort over the past three decades. This chapter has briefly examined the complexities involved in the theoretical study of impact events.

Although many theoretical techniques have been proposed, very few have been applied in practical analyses. The authors of references [1] and [2] were unable to successfully correlate theoretical methods of damage estimation with their experimental results.

The single test in reference [1] which did appear to correlate with an equation proposed in reference [3] was not sufficient to prove the validity of this approach. The proposed equation for the tests reported in reference [3] is found to seriously underestimate permanent target damage.

A main objective of this work is to initiate a research programme to propose and identify the limitations of simple analytical techniques for permanent damage estimation of plates subject to low velocity projectile impact. In addition, the experiments which provide data to validate the analytical methods are designed to enable an investigation of the scale similarity of impact loaded structures.

CHAPTER 2

LITERATURE REVIEW

2.1 Introduction

The literature associated with developments in Impact Mechanics has followed two distinct directions. There is the development of sophisticated computer programs for purely numerical treatment of impact phenomena, which invariably incorporate spatial discretization of the structural system and time integration of the equations of motion. Alternatively, there is the development of simplified analytical methods, which typically allow solutions to problems without recourse to extensive numerical methods or computer programs. These simplified methods may produce time histories of plastic deformation, or simply predict only the final deformation state. Between these two extremes are hybrid methods which may treat only a few degrees of structural freedom by numerical methods using lumped mass idealisation of the structure, for example.

With each approach there exists advantages and limitations but, without question, their separate development is both necessary and complementary. The solution to problems in Impact Mechanics requires the application of the basic laws of mechanics, as well as a description of the behaviour of the material being considered. Analytical methods must, therefore, incorporate gross simplifications in order that the solution be tractable.

If these simplified methods can be validated, however, and their limits of application defined, they represent an extremely useful method of design. In many cases the results obtained will be good enough for engineering design purposes. Bodner [13] has stated that, for damage assessment on large structures, an accuracy of 10% for the deformation parameters would be considered extremely good, an accuracy of 25% - 50% would probably be sufficient for most purposes and often only an order of magnitude estimate is desired. If a more refined analysis is required, however, the preliminary analytical design may be used as initial data for a full numerical solution.

Typically finite element or finite difference techniques are employed to solve impact problems numerically. Comprehensive time histories of displacements, stresses, strains, etc., within the structure, can be obtained. Although the numerical solution will invariably be more accurate than the analytical solution, it will also be markedly more expensive both in terms of initial development costs and subsequent execution of the computer program. Furthermore, it must be remembered that the solution obtained is still approximate and will rely on many assumptions. In particular, the characteristics of the dynamic load in impact problems are often difficult to define. The approximations inherent in the material constitutive equations, however, are of greater significance. This is due to the paucity of information on material properties at high rates of strain.

The quasi-static stress-strain curve is often treated as the inherent property of a given material, but is a valid description only at the strain rate at which the uni-axial test was conducted. In many

materials, strain rate can significantly alter material properties as discussed in section 2.7. The most general form of material constitutive equation should include the description of the material behaviour under the total range of strain rates that may be encountered. The problem is so complex that, in general, such equations do not exist. It is hardly surprising that the Institute of Physics have devoted several international conferences exclusively to the subject of material properties at high rates of strain [14]. It is accepted that, at present, numerical analysis capabilities far exceed the knowledge of dynamic material properties of the structure being analysed [15,16].

The remainder of this Chapter reviews the literature relevant to the current investigation. Most emphasis is placed on analytical methods and experimental investigations, although a brief, but by no means comprehensive survey is given of numerical investigations. Finally, the subjects of scale similarity and material strain rate sensitivity, in impact loaded structures, are discussed in further detail.

2.2 Analytical Developments

The development of theoretical methods to predict damage estimation of structural components necessarily involve the use of fundamental theorems of plasticity. The development of theoretical plasticity has continued steadily for over a century and no attempt is made here to provide a concise review. However, a brief summary of the relevant 'milestones' in plasticity development follows.

The two popular theories of elastic failure are attributed to Tresca [17] and Von Mises [18]. The former states that material will begin to flow when the shear stress reaches a critical value, and the latter states that failure will occur when the shear strain energy in the material reaches the value at yield in simple tension. Theorems regarding the subsequent flow of material, once yield had occurred at some point in a structure, were published by Prandtl [19] and Reuss [20].

The above developments were to result in two fundamental concepts of theoretical plasticity. The concept of a yield criterion being expressed as a function of the stress tensor and related to the yield stress of the material in uniaxial tension, and the concept of a yield locus defining the conditions of flow possible after initial 'failure'.

In 1950 Hill [21] published his mathematical theory of plasticity. From this work the two fundamental theorems of limit analysis were derived by Hill [22], for the case of the rigid perfectly plastic body and by Drucker et al [23], for the case of the elastic-perfectly plastic body.

Use of the theorems of limit analysis and plasticity theory in general rely on simplifications introduced by assuming idealised material behaviour. Figure 2.1 shows the kinematic model and corresponding stress-strain curve of two common material idealisations: (a) the rigid-perfectly plastic solid and (b) the elastic-perfectly plastic solid.

The above mentioned material idealisations may be used in the design of beams and frames in which the transition from purely elastic behaviour to contained plastic deformation and then to unrestricted plastic flow can be considered at specific 'hinge' locations. For more complex structures, however, the study of structural behaviour throughout deformation becomes difficult and the emphasis then turns to the direct determination of the limit state. In this condition the plastic deformation in the plastic zones is no longer contained by the adjacent non-plastic zones and the structure begins to flow under constant load. The intensity of loading for this limit state is called the limit load. The above definition of limit load can be fairly meaningless in some structures, however, as strengthening of the structure will occur under increasing load due to favourable geometry changes. This aspect will be discussed in section 3.2.1.

The two fundamental theorems of limit analysis for perfectly plastic continua are based on three concepts:

a) The yield criterion and related flow rule.
b) A statically admissible stress field, and
c) A kinematically admissible flow mechanism.

The 'lower bound' theorem must satisfy both (a) and (b) and the 'upper bound' theorem must satisfy (a) and (c). If the two theorems produce the same collapse load, then the solution is 'exact'.

The theorems of limit analysis are absolutely identical for both material idealisations shown in figure 2.1 as they are based exclusively

on concepts of statically admissable stress fields and kinematically admissible plastic strain rate fields with no reference to the elastic or rigid nature of the material which is not at yield.

Of particular interest in this work is the upper bound theorem where the flow mechanism satisfies the kinematic boundary conditions of the body and through conservation of energy, the power of the applied loads is equal to the power dissipated in plastic flow, which is essentially positive. In its simplest form, the theorem considers only infinitesimal deflection and all time effects such as influence of strain rate sensitivity, creep or work hardening, are ignored. The strain rates are small, but of sufficient magnitude to be considered large compared to the elastic strains at yield. Yield line theory [25] is a common application of this theorem which, to-date, has found most application in the analysis of reinforced concrete slabs.

Great simplification is achieved when these concepts can be applied without the need to consider three-dimensional stress and displacement fields. Fortunately, the stress resultant description, familiar in linear elastic theory of beams, plates and shells and based on the Bernouilli hypothesis of plane sections remaining plane, is equally valid in the elastic and plastic regimes [24].

The limit analysis of structures, using assumed collapse velocity fields, can therefore proceed using 'generalised strain rates', $\dot{q}_n$, as descriptions of these mechanisms. A familiar example is the rates of curvature ($\dot{\kappa}$) and axial extension ($\dot{\varepsilon}$) in the mid-plane of a simple beam. Generalised stresses Q_1---Q_n, are the stress type variables

associated with the generalized strain rates such that the 'power of dissipation',

$$d = Q_1\dot{q}_1 + Q_2\dot{q}_2 + \text{------} + Q_n\dot{q}_n \qquad \text{.....(2.1)}$$

The yield condition adopted will be a function of the generalized stresses which appear in equation 2.1. Generalized stresses which do not appear in equation 2.1 are those associated with vanishing generalized strain rates. For example, the transverse shear strains in simple beam theory do not contribute to energy dissipation by virtue of the Bernouilli hypothesis. The choice of the yield criterion adopted is generally made for convenience rather than on physical grounds, as the differences, which are important from the fundamental view of material behaviour, are of minor importance for the determination of load carrying capacity or 'post-limit' behaviour.

The neglect of material elasticity in a rigid plastic treatment of a dynamic problem can be justified if the energy ratio is larger than about three [26]. The energy ratio is defined as the external dynamic energy divided by the maximum amount of strain energy which can be absorbed by the structure in a wholly elastic manner.

In addition, the duration of the load should be short compared to the fundamental period of elastic vibration of the structure. If the problem is quasi-static, the latter consideration may be unimportant providing the energy ratio is large (see also section 3.2.1).

The rigid-perfectly plastic idealisation was used by Lee and Symonds [27], to investigate the somewhat unrealistic problem of a completely free beam struck at midspan by an impulive load. The analysis includes three phases of motion based on rigid body dynamics of segments of beam joined at plastic hinges where the entire deformation was assumed to take place. It was observed that plastic deformation of the beam continued long after the force ceased to act. Conray [28] subsequently re-worked the same problem with a triangular load function.

Although an impulsive load is defined in various ways by different authors, essentially the same concept has been described. Strictly, impulsive loading implies a delta function loading, which instantaneously imparts some velocity profile to a structure i.e. a condition of initial velocity with zero initial deflection.

A somewhat looser definition is a force or pressure pulse applied in a time short enough for the structural response to be only a function of the integral of the pulse, rather than details of its time history [29]. This is in contrast to initial conditions specified as a known force time function, which is applicable in certain cases of explosive loading. It is also in contrast to the impact of two bodies, where momentum and energy conservation considerations may need to be applied to determine initial conditions.

Symonds [30] studied the more realistic case of a simply supported beam under central impulse loading and in 1955 Parkes [31] published his classic paper on a cantilever struck at its tip by a mass. The latter paper clearly showed, both experimentally and theoretically, the

importance of the mass ratio between the missile and the structure. For 'light' strikers (a rifle bullet) the structure behaved in true dynamic fashion with evidence of what was considered at the time to be a plastic hinge travelling from tip to root. This concept is now thought to occur as a consequence of initial elastic effects [32]. For 'heavy' strikers (a free fall mass significantly heavier than the mass of the cantilever), the structure behaved quasi-statically with a rigid body rotation about the root dissipating the striker kinetic energy. The paper also attempted to make an allowance for material strain rate sensitivity by modifying the fully plastic bending moment of the section. This 'dynamic plastic moment' was calculated by considering approximate rotation rates at the plastic hinge.

Parkes later extended his investigations [33] to study a fully fixed beam struck at any point along its length by a falling mass, and again, strain rate approximations were included in the analysis.

In many structures the kinematic boundary conditions mean that out of plane deflections greatly enhance the structure load carrying capacity. The response of a fully fixed beam, for example, would change with increasing deflection, from initial flexure to predominant axial extension i.e. from bending to membrane behaviour.

It became clear that finite deflections, or geometry changes, had to be included in the analysis in many practical cases because of the somewhat contradictory requirements demanded by elementary rigid-plastic theory. Martin and Symonds [34] stated,

"The range of validity of the theory is bounded at one end by the requirement that the deflections should not be so large that geometry changes are significant and at the other end by the requirement that the energy of the disturbance should be large compared with the energy that could be stored elastically".

For many structural configurations this range does not exist at all.

Mentel [35] re-examined the cantilever tip-mass problem first reported by Parkes [31] and included geometry changes and material strain hardening effects. Bodner and Symonds [36] studied the same problem both experimentally and theoretically with the loading now due to a uniform impulse. In reference [36] geometry changes, strain hardening and material strain rate sensitivity were all considered approximately.

Symonds and Mentel [37] again highlighted the importance of geometry changes when studying encastre and pin-ended beams subject to blast loading.

A new approach which avoided tedious solution of coupled equations of motion was proposed by Martin in 1964 [38]. The 'bound theorems' proposed by Martin enabled simple calculations for a lower bound on response time and an upper bound on permanent deflection for impulsively loaded continua, but were restricted to structures undergoing infinitesimal deflection.

A further development of these theorems, by Martin and Symonds [34]

introduced the 'mode approximation' technique which involved the choice of an initial mode shape for transverse velocity which remainded invariant during deformation. The mode approximation technique has been steadily developed ever since, largely by Symonds and his co-workers, and is now a very powerful method of analysis [39].

Another possible method of approach was reported by Newmark [40] and involved a lumped mass, limited degree of freedom idealisation. For example, a single degree of freedom approximation will involve the calculation of an equivalent mass, stiffness and loading function. These constants are evaluated by assuming the deflected shape of the actual structure. A common assumption is the structural shape taken up by static application of the dynamic load. In general, however, the stresses and forces in the idealised system are not directly equivalent to the same quantities in the actual structure.

The earliest work concerning blast loading of plates appears to be due to Wang in 1955 [41]. The study considered a simply supported plate undergoing bending deformation only. Florence studied circular plates under uniform [42] and localised [43] blast loading, assuming total energy dissipation through plate curvature. Florence concluded from an experimental correlation [44] that the bending only theory was inadequate and geometry changes must be included. Examining essentially the same problem, Wierzbicki included a strain hardening parameter [45], Perrone included material strain rate sensitivity [46] and Jones included membrane effects [47,48]. The latter showed improved correlation with the experiments of Florence [44].

Jones [49] theoretically studied an annular plate subject to a linearly varying impulse load and included geometry changes, strain hardening and strain rate sensitivity approximations. It was concluded that, in most problems of interest, strain hardening is of minor importance, material strain rate sensitivity is somewhat more important and inclusion of geometry changes is critical. The lack of importance of material strain hardening implies that the actual material behaviour approaches the rigid perfectly plastic idealisation, but with a raised yield stress.

The aforementioned conclusion by Jones [49] was reinforced in studies by Jones [50] and Symonds and Jones [51] where a beam is the structure under consideration.

Wierzbicki and Kelly [52] studied circular plates subjected to projectile impact load and noted the "virtual non-existence" of literature regarding the motion of plates subject to impact from a moving mass. Earlier work by Goldsmith et al [53] had considered elastic effects and plate penetration by projectiles. Wierzbicki and Kelly [52] used a static collapse velocity profile originally proposed by Onat and Haythornthwaite [54] which itself was a continuation of earlier work by Hopkins and Prager [55]. Wierzbicki and Kelly [52] included an approximate correction for material strain rate sensitivity. They concluded that, for the range of energies studied, the inertia of the plate was unimportant and the analysis effectively considered a massless plate.

It is of importance to consider static analysis of structures which

experience large plastic deformations due to the quasi-static nature of many low velocity impact events. Onat and Haythornthwaite [54] studied simply supported and clamped circular plates under various loading conditions to obtain 'post-limit' equations for load-deflection behaviour. Their analysis was carried out by initially assuming a velocity field which can describe the position of the mid-surface of the plate throughout deformation. The rate of energy dissipation due to this velocity profile was calculated and equated to the external load applied using virtual work principles. The rate of energy dissipation is found directly from the yield criterion and the strain rate diagrams resulting from the velocity profile assumptions, hence direct use is not made of the equilibrium equations.

The load-deflection relationships for a simply supported circular plate of radius R and with a centrally applied load P, is given as [54],

$$\frac{P}{P_L} = 1 + \frac{4}{3}\left(\frac{w_o}{h}\right)^2 \qquad \text{for} \quad \frac{w_o}{h} \leqslant \frac{1}{2} \qquad \text{.....(2.2a)}$$

$$\frac{P}{P_L} = \frac{2w_o}{h} + \frac{h}{6w_o} \qquad \text{for} \quad \frac{w_o}{h} \geqslant \frac{1}{2} \qquad \text{.....(2.2b)}$$

where w_o = central deflection

h = plate thickness

$$P_L = \frac{2\pi M_o}{1 - 2a_L / 3R}$$

$$M_o = \frac{\sigma_y h^2}{4}$$

a_L = radius of loaded area

Equations 3.45 in section 3.5 give the corresponding relationships for a fully clamped circular plate under the same loading condition.

The theory developed in [54] agreed well with experimental results for fully clamped plates, although extremely slender plates were found to behave according to plastic membrane theory, (also reported in [54]). Simply supported plates were in good agreement with experimental results if a correction was made for elastic effects, but it was noted that no theoretical justification could be made for simple addition of an elastic deflection in a rigid-plastic analysis.

Calladine [56] proposed an alternative approach to the same problem by treating the axisymmetric plate as a three dimensional solid and commented that adaptation to alternative plate configurations and loading conditions would be feasible.

The equations given by Calladine for a simply supported centrally loaded circular plate are

$$\frac{P}{P_L} = 1 + \frac{1}{3}\left(\frac{w_o}{h}\right)^2 \qquad \text{for } \frac{w_o}{h} \leqslant 1 \qquad \text{.....(2.3a)}$$

$$\frac{P}{P_L} = \frac{w_o}{h} + \frac{h}{3w_o} \qquad \text{for } \frac{w_o}{h} \geqslant 1 \qquad \text{.....(2.3b)}$$

in which the symbols are the same as those in equation 2.2.

Hooke and Rawlings carried out experimental studies [57,58] on uniformly loaded rectangular plates. Hooke [59] proposed a graphical method of analysis for uniformly loaded rectangular plates experiencing large plastic deformations. Jones and Walters [60] considered this problem theoretically following earlier work by Sawczuk [61,62] and Jones [63].

The method proposed in [60] relies on a suitable choice of velocity profile and in this case was formulated and observed experimentally by Wood [25]. Although resulting deflections are large compared to the plate thickness, they are still considered sufficiently small to enable replacement of tan θ with θ radians (see figure 3.4). The equations derived in [60] showed excellent agreement with the experiments of Hooke and Rawlings [57,58] and also Greenspon [64], but showed the graphical method due to Hooke [59] to be inadequate for the analysis of square plates.

In reference [60] formulae are given for load-deflection relationships of the plate shown in figure 3.4, under uniform loading, with clamped and simply supported edge conditions.

For the clamped edge condition:

$$\frac{P}{P_L} = 1 + \frac{1}{3}\left(\frac{w_o}{h}\right)^2 \left[\frac{\xi_o + (3 - 2\xi_o)^2}{3 - 2\xi_o}\right] \qquad \text{for } \frac{w_o}{h} \leqslant 1 \qquad \text{.....(2.4a)}$$

$$\frac{P}{P_L} = \frac{2w_o}{h}\left[1 + \frac{\xi_o (2 - \xi_o)}{(3 - \xi_o)}\left(\frac{h^2}{3w_o^2} - 1\right)\right] \qquad \text{for } \frac{w_o}{h} \geqslant 1 \qquad \text{.....(2.4b)}$$

where $$P_L = \frac{12M_o}{A^2 \tan^2 \phi}$$

and for the simply supported edge condition:

$$\frac{P}{P_L} = 1 + \frac{4}{3}\left(\frac{w_o}{h}\right)^2 \left[\frac{\xi_o + (3-2\xi_o)^2}{(3-\xi_o)}\right] \qquad \text{for } \frac{w_o}{h} \leqslant \tfrac{1}{2} \qquad \text{.....(2.5a)}$$

$$\frac{P}{P_L} = \frac{4w_o}{h}\left[1 + \frac{\xi_o (\xi_o - 2)}{(3-\xi_o)}\left(1 - \frac{h^2}{12w_o^2}\right)\right] \qquad \text{for } \frac{w_o}{h} \geqslant \tfrac{1}{2} \qquad \text{.....(2.5b)}$$

where $$P_L = \frac{6\,M_o}{A^2(3-2\xi_o)}$$

and $$\tan \phi = (3 + \Omega^2)^{1/2} - \Omega$$
$$\xi_o = \Omega \tan \phi$$
$$\Omega = A/B$$

The method presented in [60] was extended by Kling [9] to incorporate concentrated loading and the following equations for the plate shown in figure 3.2 with clamped edge condition, are given as

$$P = 8M_o \left[\alpha + \beta + \left(\alpha + \frac{1}{3}\beta\right)\left(\frac{w_o}{h}\right)^2\right] \qquad \text{for } \frac{w_o}{h} \leqslant 1 \qquad \text{.....(2.6a)}$$

$$P = 4M_o \left[\alpha + 10\beta - 9\beta \left(\frac{w_o}{h}\right) + 3\left(\frac{w_o}{h}\right)^2 \left(\alpha - \frac{11}{9}\beta\right) - 2Ln\left(\frac{h}{w_o}\right)\right]$$

$$\text{for } \frac{w_o}{h} \geqslant 1 \qquad \text{.....(2.6b)}$$

where $\alpha = \frac{a}{C} + \frac{b}{D}$

$\beta = \frac{C}{D} + \frac{D}{C}$

and $C = B-b$, $D = A-a$

Equations 2.6 disagree with equations 3.12 derived in section 3.3. Both sets of equations are compared with experimental data in Chapter 5, where equations 2.6 are shown to seriously underestimate plate deflection.

In a classic paper in 1971, Jones [63] studied rectangular plates subject to uniform blast loading and included geometry changes in the analysis. The collapse velocity profile used was reported by Wood [25]. The initial condition of the method is an assumption concerning the load-time history, which must be of short duration compared to the fundamental natural period of the structure under consideration. Estimates of structural response time and permanent displacement are ultimately obtained through solution of non-linear differential equations.

Jones [63] derived the following expression for the permanent deformation of the plate shown in figure 3.4 subject to uniform blast loading,

$$\frac{w_o}{h} = \frac{(3 - \xi_o)\left[(1 + \Gamma)^{1/2} - 1\right]}{2\left[1 + (\xi_o - 1)(\xi_o - 2)\right]} \qquad \text{.....(2.7)}$$

where $$\Gamma = \frac{\Theta \beta^2}{6} (3 - 2\xi_o)\,(1 - \xi_o + 1/(2 - \xi_o))$$

$$\Theta = \frac{\mu V_o B^2}{M_o h}$$

Taya and Mura [65] used the "Extended Hamilton's Principle" to solve the same problem. The use of this principle results in the more manageable task of solving non-linear algeabraic equations, instead of non-linear differential equations. In both [63] and [65] good agreement was obtained with tests conducted by Jones et al [66,67]. In the analyses in references [63] and [65] the Tresca yield condition was used, including interaction between the membrane and bending generalized stress resultants. This criterion is discussed by Symonds and Jones [51] and shown in figure 3.5. The generalized stress resultant due to transverse shear is generally ignored (see, for example Drucker [68]) although certain analyses have critically reviewed this assumption [69-72].

A critical examination of the fully fixed support condition, assumed in theoretical work, and non-existent in practice, was made by Jones [73] for rigid-plastic analysis of beams and plates. It was concluded that very small in-plane displacements at supports can significantly effect resulting behaviour and, therefore, the validity of such idealised analyses in treating practical situations is questionable. Jones also extended his studies to anisotropic structures, specifically, fibre-reinforced beams [74].

Forrestal et al [75-77] developed a simple, and accurate method of incorporating the effect of material elasticity in the dynamic plastic response of beams. The 'half sine' impulse loading used was chosen specifically to excite the fundamental natural period of the beam during the elastic phase and hence, simplify the analysis. Approximations for material strain rate sensitivity were also made and excellent agreement was observed with their tests.

DeOliveira [3] proposed a design method for rectangular plates subject to projectile impact. His analysis followed earlier work by Haythornthwaite [78] and Kling [9]. The method is essentially an energy method in which the time history of structural response is completely ignored. The kinetic energy imparted to the system is equated to the energy dissipated by the structure in deforming from its initial to its final shape.

For the plate shown in figure 3.2, DeOliveira gives the following equation for estimation of permanent damage resulting from the impact of a mass G, travelling at velocity V_o and striking at the central area of dimensions 2a x 2b:

$$\left(\alpha + \frac{11}{9}\beta\right)\left(\frac{w_o}{h}\right)^3 - \frac{9}{2}\beta\left(\frac{w_o}{h}\right)^2 + \left(\alpha + 10\beta\right)\frac{w_o}{h} - 2\beta Ln\left(\frac{w_o}{h}\right)$$

$$+\frac{2}{3}\alpha - \frac{9}{2}\beta = \frac{\lambda}{\chi\left[\frac{ab}{AB} + \frac{1}{3}\left(\frac{b}{B} + \frac{a}{A} + 1\right)\right] + 2} \qquad \text{.....(2.8)}$$

where $\lambda = \frac{GV_o^2}{8M_o h}$

$\chi = \frac{4\mu AB}{G}$

μ = mass/unit area of plate.

Equation 2.8 was used by Samuelides and Frieze [78,80] in connection with ship collision damage assessment, but is shown in Chapter 5 to predict unsafe results.

The mode approximation technique [38] can now study more complex problems, but as more accuracy and sophistication is sought, the simplicity of the method is reduced. For example, Symonds and Chon [81] studied the response of a circular clamped strain-rate sensitive plate subject to blast loading. A series of successive velocity fields were used in the analysis and each was individually determined as an eigen problem solved by using the finite element method with iterations. Symonds has recently extended this to include elastic effects [82] under the name "SEP" or simple elastic-plastic methods. The method allows calculation of maximum as well as final displacements.

The significant advantage of the technique is its ability to treat structures subject to pulses which are long compared to the fundamental natural period of the structure. This is achieved by explicitly considering three stages of motion, an elastic phase followed by a plastic phase and finally the elastic vibration phase of the deformed structure on cessation of plastic flow.

Yankelevsky [83] has included elastic effects into the method

originally proposed by Jones [63]. Using a central difference method of solution, time histories of stress resultants at plastic hinges can be determined.

It is evident that, as these simple analytical methods become more complex [e.g. 81,82], some of their advantages over full numerical solutions are lost. It is questionable whether the increase in accuracy obtained is sufficient to warrant the extra computation involved.

2.3 Review Articles

Despite the practical importance and widespread applications of Impact Engineering, very few text books devoted to the subject have been published. Early examples include Goldsmith [84], Critescu [85] and Johnson [86], while more recently Zukas et al [16] devote most of their book to high velocity impact. The proceedings of two recent International Conferences [87,88] provide valuable information on all aspects of collision.

In an early review article Symonds [89] discussed analytical methods for solution of dynamic plasticity problems with particular reference to beams. In reference [13] Bodner discussed the merits of rigid plastic theory and material strain rate effects for impulsively loaded structures and Keil [90] reported specifically on the Naval applications of impulsive loading studies.

Following an initial review in 1975 [91], Jones has regularly published up-to-date information on the plastic response of structures

subject to dynamic loading [92-94]. Baker has also published a series of three review articles [29,95,96].

Solutions based on modal techniques are reviewed by Griffin and Martin [97]. In a recent paper, Bodner [98] compares the merits of analytical, numerical and experimental studies for impact behaviour. In [98], Bodner reports that a major treatise on the subject of analytical methods is in preparation by Symonds and Martin at Brown University.

Neilson [99] reviews published empirical equations for calculation of critical velocities for perforation of plates by projectiles. Although perforation and penetration are not examined explicitly in this work, it is relevant to mention review articles by Backman and Goldsmith [100], Sheih [101], Wilkins [102] and Bodner [103], for completeness.

2.4 Experimental Investigations

Early experimental work concerned the determination of empirical equations to calculate critical velocities of target perforation [99]. The critical velocity is defined as the minimum velocity necessary to perforate a given structural component. These equations must be used with extreme caution as they are only valid within a limited range of parameters and extrapolation of results outside the range of applicability can lead to serious errors.

Very little experimental work has been reported concerning structures which are loaded well into the plastic range [67]. Under

conditions of 'static' loading, Cambell and Charlton [104] tested fully clamped beams and Onat and Haythornthwaite [54] tested clamped and simply supported circular plates. Hooke and Rawlings [57] tested rectangular plates under uniform pressure loading with different aspect ratios and thicknesses. In reference [57] great care was taken to prevent slippage at the supports.

Goldsmith et al [53] and Calder and Goldsmith [105] tested clamped circular plates under projectile impact. In reference [105] high speed photography recorded the event and non-contacting eddy current displacement transducers provided a dynamic time history of the event. Florence [44] blast loaded circular plates in an attempt to validate his theoretical predictions [42]. Parkes [31] and Bodner and Symonds [36] have experimentally studied the response of cantilever beams to impact loading.

The deflection of plates under projectile impact was experimentally determined using streak camera and Moire fringe techniques by Duffey and Key [106] and Beynet and Plunket [107]. Beynet and Plunket observed from strain gauge output that plastic energy dissipation was almost entirely due to radial in-plane membrane behaviour and involved negligible bending or shear.

Rawlings [108] utilised dynamic buckling for energy absorption purposes as did Davis and Pih [109] in their examination of the integrity of nuclear fuel transportation casks. Zaid and Travis [110] tested multi-layered targets to determine optimum energy absorption configurations.

Jones et al [66] used sheet explosive to impart a uniform impulse to clamped rectangular plates. The impulse was measured experimentally using a ballistic pendulum device. In a subsequent investigation, Jones et al [67] examined wide beams and rectangular plates clamped at two ends only.

Witmer et al [111,112] report tests on plates and spherical shells to validate their numerical predictions. Barr, Neilson and others at UKAEA [8,10,113,114] have been involved for some time in test series aimed at validating computer codes for impact situations applicable to the Nuclear Industry. Neilson [113] reports projectile impact tests at low velocity on circular, triangular end square clamped plates. The instrumentation included a specially developed displacement transducer [115] capable of the high frequency response required by such tests. Another aim of the UKAEA investigations has been to validate scale model testing for reinforced and prestressed concrete slabs [103].

Brown and Perry [116,117] have reported tests on reinforced and prestressed concrete slabs and shells. Displacement-time histories at various locations on specimens were obtained by integrating acceleration-time signals from piezoelectric acceleration transducers.

Miyamoto et al [118] fired projectiles at fully clamped steel plates up to 30mm thick. Dynamic measurements included strain across the plate and load at the supports. Two accompanying papers [119,120] discuss analytical and numerical treatment of the problem.

Ellis et al [2] and Wenger et al [1] report full scale tests on offshore platform structural configurations. The projectile in both cases was a standard three tonne drill collar which was dropped from heights up to 42m. Theoretical correlations were attempted but were unsuccessful.

Since it is desirable to have criteria for determining how the various properties of the target and missile influence material damage, Corren et al [121] carried out an experimental study to identify favourable parameters in both missiles and targets. The parametric study included variation of missile mass, nose shape, hardness and target support condition. Multi-layered targets were also tested and design recommendations as well as approximate formulae for energy absorbtion calculations, are given.

Booth et al [122], Jones et al [123] and Duffey et al [124] all report tests aimed at validating scale similarity laws for impact loaded structures. These investigations are discussed further in section 2.6.

Finally, Ghosh et al [125] and Nurrick and Martin [126] report recent novel experimental techniques for load application and dynamic displacement measurement respectively in impact investigations.

2.5 Numerical Work

The literature on non-linear dynamic analysis using numerical methods is vast and no attempt is made here to present a concise review. It is apparent, however, that most numerical schemes use finite

element spatial discretization of the structure and integrate through time using difference equations. Generally for global structural dynamics problems, 'implicit' integration of the equations of motion is appropriate while for localised wave propogation problems, 'explicit' integration, which is only conditionally stable, is required.

Many 'late-time' impact problems where global response is most significant can be analysed using general purpose finite element computer programmes which contain time-marching integration routines and are capable of modelling material and geometric non-linearities [4]. For example, a low velocity projectile impacting a plate, has been modelled by Neilson [113] by assuming contact between missile and plate throughout response. The initial conditions were a velocity applied to the explicitly modelled missile and time integration was carried out using implicit routines. Yamamoto et al [120] conducted a similar analysis, but gap elements were used to model contact between missile and plate.

A more specialised program will be required when localised effects or 'early-time' response is of importance. These computer codes generally use explicit time integration, where very small time steps are used in the integration (e.g. one to three orders of magnitude smaller than those needed for implicit methods). In addition, they avoid matrix assembly and inversion, which is very expensive for large structures and they provide fine tracking of physical phenomena by virtue of the minute time steps. Within each time step the internal stress state caused by impact is calculated and the extent of incremental material damage can be determined by applying failure criteria to the multi-axial stress

state within the body. Specialised facilities such as automatic mesh re-zoning may also be provided.

An exception to the use of finite element idealisation is reported by Samuelides and Frieze [79] who use a real time version of the dynamic relaxation technique (RTDR) to investigate critical velocities for ship collision.

The book by Zukas et al [16] and the conference proceedings [87] and [88] give considerable information and references on numerical modelling of impact phenomena.

2.6 Scale Modelling of Impact Phenomena

The use of small scale models is often preferable when testing is required either for practical or economic reasons, or both. It has been estimated that the comparable cost of scale model testing is proportional to the scale factor cubed [12].

Reports of scale model testing appear in the literaure with somewhat contradictory conclusions. It would appear that some structures obey the laws of dynamic similarity while others do not [4].

In a recent paper, Jones [127] remarks that few experimental investigations have examined the validity, or otherwise, of the scale modelling of structures, because until recently most structures were designed to remain elastic.

A paper by Duffey [124] used the 'Buckingham π ' theorem [128] to generate nineteen dimensionless parameters which govern the behaviour of fuel capsules subject to blast fragment and earth impact loading. Duffey concluded that scale similarity laws were valid for the range of velocities tested.

Jones [127] has commented, however, that Duffey's conclusion is open to some doubt, due to the lack of accurate data concerning the experimental arrangement.

Development of scaling laws using the Buckingham π method [118] is well known. A complete set of dimensionless pi-terms is formed from the isolated parameters and equality of pi-terms for model and prototype yield the similitude requirements or scaling laws to be satisfied.

A summary of the results of a dimensional analysis for the impact parameters relevant to this work is shown in table 2.1. It is apparent that there are two exceptions to model-prototype scale similarity in this case:

a) Strain rate.
b) Gravitational acceleration.

Booth et al [122] carried out thirteen drop tests on thin plated steel structures. Their results indicated that for mild steel specimens, post impact deformations might be as much as 2.5 times greater in a full scale prototype than would be expected from a quarter scale model test. Their general conclusion from observations of the

three different configurations of structure tested stated that scale similarity for small scale impact testing would be open to some question if either the yield stress was strain rate sensitive, or the structure had a collapse strength which falls off sharply with increasing deflection, or tearing or fracture was involved in failure. These comments were accompanied by the observation that much more experimental evidence is required before concise conclusions can be drawn.

Booth et all mentioned the difficulties in obtaining perfect model structures. Of particular significance is the problem associated with matching material properties of steel plates of different thickness. In view of the aforementioned, Jones [127] reproduced results from [122] incorporating corrections for different material properties, but found only marginal improvement in results.

In an appendix to reference [122], Calladine [129] proposed an experimental technique, incorporating modified scaling laws, to overcome the difficulty of the strain rate scale discrepancy. In his scheme, and contrary to conventional theory, Calladine proposes that the velocity and drop height of free fall objects should be proportionalo to the scale factor and the scale factor squared respectively. To the authors knowledge, no experiments have yet tested this hypothesis.

Jones et al [123] report tests involving tearing of mild steel plates and show the deformations of a prototype are 2.283 times larger than those predicted from a quarter scale model, according to the principles of elementary geometrical scaling. Scaling laws which consider the elementary principles of elastic fracture mechanics are

discussed at length in [127] and it is stated that, in certain circumstances, a model could behave in a ductile fashion while a geometrically similar protype could fracture, Hagiwara et al [130].

In an earlier paper, Jones [8] discusses the particular problems associated with the successful modelling of structural aspects of ship collisions.

Barr [12] reports on tests, during a six year period, carried out by UKAEA, to determine the validity of scale modelling for prestressed and reinforced concrete structures subject to projectile impact.

Recently Duffey et al [124] have concluded that scale similarity laws apply, to within 10%, for punch loaded clamped steel plates. Booth et al [4] attempt to categorize structural behaviour into five basic groups and comment on the applicability of scale modelling to each individual group.

2.7 Material Strain Rate Sensitivity

It is well known that material strain rate effects are exaggerated in small scale models of a prototype [e.g. 4]. This is because strain is invariant under the laws of dynamic similarity but events happen $1/\beta$ times faster in models, where β is a scale factor less than unity.

The literature surveys by Jones [91-94] discuss in detail the importance of strain rate effects on the dynamic plastic response of structures.

Many constitutive equations for materials subject to high rates of strain have been proposed [85, 131]. The Cowper-Symonds relationship [131], however, which was derived from uni-axial tests, is used almost exclusibvely in theoretical and numerical studies of the dynamic plastic behaviour of structures made from strain rate sensitive materials [6]. Mainstone [132] has summarised test datsa for various materials under high strain rate conditions.

The Cowper-Symonds equation is given as:

$$\frac{\sigma_{yd}}{\sigma_y} = \left[1 + \left(\frac{\dot{\epsilon}}{D_o}\right)^{1/p_o}\right] \qquad .....(2.9)$$

where σ_y and σ_{yd} are the yield stress and 'dynamic yield stress' respectively, $\dot{\epsilon}$ is the current rate of strain and p_o and D_o are material constants which are generally taken as 5 and 40.4 respectively for mild steel following tests reported in [133].

Symonds and Jones [51] proposed a dynamic correction factor from equation 2.9 for both the plastic bending moment and plastic axial force to allow for the strain rate effect in the response of a fully clamped beam. The average strain rate and curvature rate were both determined when the transition to plastic behaviour occurred. Similar approximate strain rate corrections are ported in [31] and [65] and are shown to agree well with experiments.

The method of a stress resultant correction, which is assumed valid throughout response, would therefore appear to be a reasonable method to account for rate effects, Perrone [46]. This is due, in part, to the

form of equation 2.9, which, for example, means that a 50% error in an estimate of average strain rate, over a range of strain rates from 0.1/sec to 10/sec would only result in an error of less than 5% for the modified yield stress if the material under consideration is mild steel.

Hobbs [134] proposed a strain rate correction method particularly suited to structures where a single-degree-of-freedom idealisation can be used. The estimated strain rate, which is subsequently used in equation 2.9, is calculated by dividing the maximum elastic strain of the equivalent system by the estimated time required to reach it.

Use of equation 2.9 in a numerical scheme is reported by Samuelides and Frieze [79]. The dynamic yield stress is updated during each time step by replacing $\dot{\varepsilon}$ in equation 2.9, with $\dot{\varepsilon}_e$, an equivalent strain rate corresponding to the equivalent stress for defining material yield criteria.

It should be noted [4] that material strain rate sensitivity is still a fairly controversial subject. There are many different constitutive equations which have been proposed and no clear evidence suggests that any one is more accurate or versatile than all others. In reference [89] mention is made of a proposal that rate sensitivity is not a material property at all, but an effect which results from the inertia of the material as it is loaded at high rates of strain.

As the quality of analytical or numerical predictions in quasi-static or dynamic analyses will be directly related to the accuracy of the material constitutive equations employed, it is a

subject of considerable importance, and for this reason, it has been the subject of three international conferences over the past fifteen years, [e.g. 14].

2.8 Concluding Remarks

This chapter has reviewed the literature concerning structures subject to impulsive loading which is of sufficient intensity to cause plastic deformation in response. Analytical and numerical solution techniques have been reviewed together with relevant experimental investigations. The subjects of material strain rate sensitivity and dynamic similarity have been discussed in some detail.

The review of analytical techniques has shown that, in general, simple limit analyses are inadequate for permanent damage estimation. Invariably finite deflections or geometry changes must be considered and in many cases an approximation for the effect of material strain rate sensitivity must be included. Generally the effect of strain hardening is negligible and a single correction for material strain rate sensitivity is sufficient. The resulting analysis effectively uses a rigid plastic material idealisation with a raised yield stress.

Previous investigations have shown that simple analytical methods are capable of accurately predicting the permanent damage of structures subject to impact. Many of these methods rely on the choice of a single mode shape to represent deformation throughout response. In many cases it is doubtful whether an increase in accuracy resulting from rigorous consideration of several stages of motion is worth the extra analysis

effort. Furthermore, much time, effort and money is often wasted employing expensive numerical methods when simple calculations are adequate.

It is apparent that many analytical methods are available in the literature, but there is little information regarding their use in practical situations. This is due to uncertainties concerning their range of validity and their limitations. Analytical methods which are proposed without experimental correlation may subsequently be found to have serious limitations in their application. It is the intention of this work to recommend analysis methods for isotropic plates subject to impact at low velocity and to establish the limitations of these methods.

TABLE 2.1 SCALE SIMILARITY

PROBLEM GOVERNING VARIABLES		
Variable	Definition	Unit
L	Length	L
w_o	Displacement	L
ϵ	Strain	-
σ	Stress	$ML^{-1}T^{-2}$
t	Time	T
V	Velocity	LT^{-1}
a_c	Acceleration	LT^{-2}
$\dot{\epsilon}$	Strain Rate	T^{-1}
E	Stress Constant	$ML^{-1}T^{-2}$
τ	Rate Constant	T
ρ	Density	ML^{-3}
G	Mass	M
g	Gravitational Acceleration	LT^{-2}
P	Force	MLT^{-2}

14 Variables - 3 Dimensions = 11 Dimensionless Groups

$$\frac{w_o}{L} = f\left(\frac{\rho v^2}{\sigma}, \epsilon, \frac{Vt}{L}, \frac{GV^2}{\sigma L^3}, \dot{\epsilon}t, \frac{V\tau}{L}, \frac{a_c L}{V^2}, \frac{E}{\sigma}, \frac{gL}{V^2}, \frac{P}{\sigma L^2}\right)$$

(...contd.)

TABLE 2.1 (contd.)

RESULTING SCALE SIMILARITY LAWS: (β_o = SCALE FACTOR LESS THAN UNITY)		
Variable	Prototype	Model
L	1	β_o
w_o	1	β_o
ϵ	1	1
σ	1	1
t	1	β_o
V	1	1
a_c	1	$1/\beta_o$
$\dot{\epsilon}$	1	$1/\beta_o$
E	1	1
τ	1	β_o
ρ	1	1
G	1	β_o^3
g	1	$1/\beta_o$
P	1	β_o^2

FIGURE 2.1 IDEALISED MATERIAL MODELS

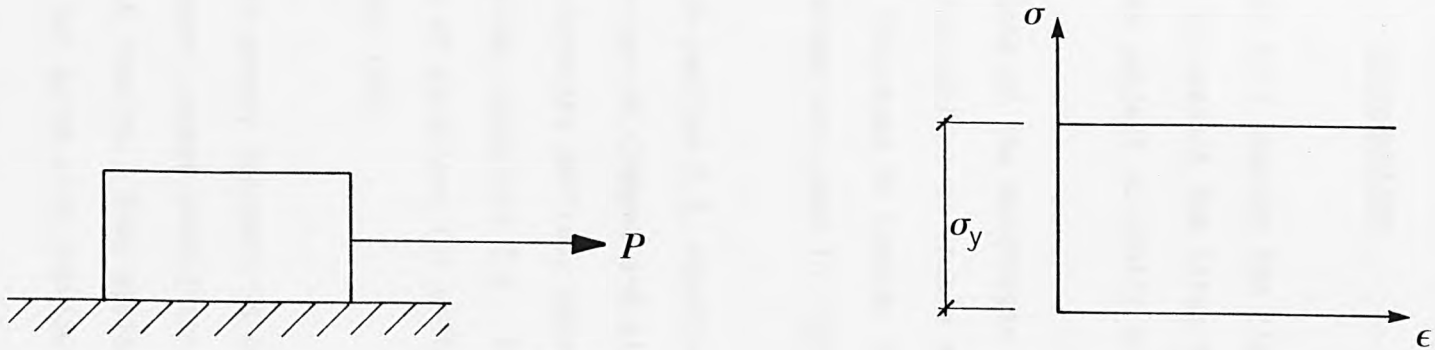

a) RIGID PERFECTLY PLASTIC IDEALISATION

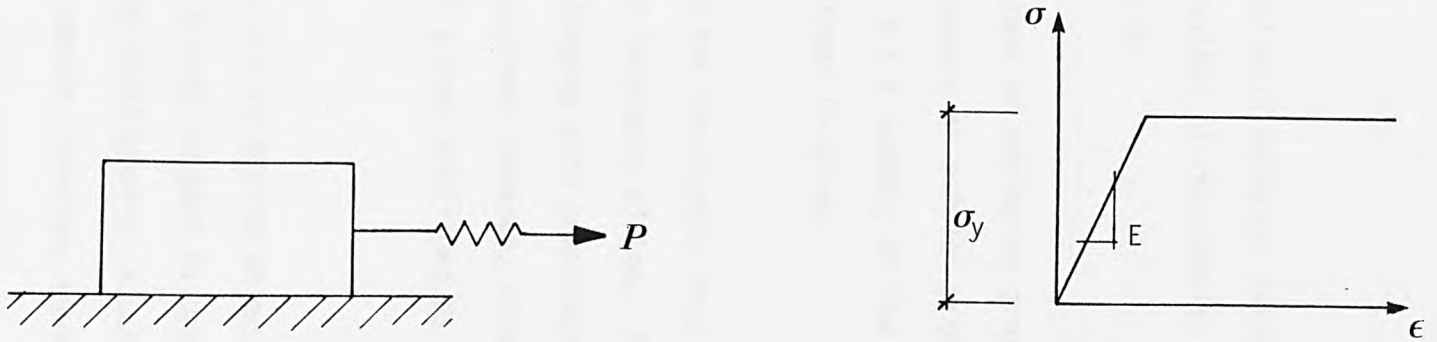

b) ELASTIC PERFECTLY PLASTIC IDEALISATION

CHAPTER 3

THEORETICAL DEVELOPMENT

3.1 Introduction

In this chapter the rigid perfectly plastic material idealisation is used to predict the large deflection behaviour of rectangular isotropic plates subject to static and impact loading.

Some of the advantages and disadvantages of employing gross simplifications to enable analytical treatment of complex problems have been discussed in Chapter 2. In section 3.2 a summary of the main approximations used in rigid plastic analyses is given.

In section 3.3, equations are derived for the static load deflection behaviour of clamped and simply supported isotropic plates. The relationships derived, equations 3.12, disagree with previously published formulae, equations 2.6. Agreement is obtained, however, with reduced forms of equations for uniform loading of plates published by Jones and Walters [60].

An energy approach is used in section 3.4 to derive an equation for permanent damage prediction of isotropic plates subject to projectile impact loading. Once again, the resulting relationship, equation 3.27, does not agree with previously published design formulae, equation 2.8.

In section 3.5, a rigid plastic approach which includes inertia effects is formulated. The technique involves consideration of two stages of motion and results in the solution of non-linear differential equations. In order to simplify the approach, a method using Hamilton's principle is also presented. The relationships derived, equations 3.40 and 3.42, enable estimates of final permanent deflection and duration of response.

Finally, in section 3.6, square plates are idealised as 'equivalent circular plates' and an axisymmetric formulation is therefore utilised to derive equations for plate damage estimation. The method uses static load-deflection relationships originally proposed by Onat and Haythornthwaite [54].

3.2 Rigid Plastic Idealisation

Figure 2.1 shows two rigid plastic material behaviour idealisations. Analytical methods are greatly simplified if the rigid-perfectly plastic idealisation can be assumed. The resulting analysis omits the initial elastic phase of motion, material hardening effects and the final phase of motion when elastic recovery will occur after plastic deformation has ceased.

Although the techniques to be employed are analogous to some applications of limit analysis, the relationships developed do not necessarily give an upper bound to the problem solution because, in general, the assumed shape of the system velocity field will not be correct. This velocity field is often assumed to be constant

throughout response. A more realistic approach can be made by considering several stages in the analysis. At each stage velocity fields are consistent with conditions existing at the end of the previous phase of motion. The solutions found are, therefore, upper bounds to an assumed set of initial conditions and not necessarily upper bounds to the actual solution.

3.2.1 Material Elasticity

Although analyses are simpler when elastic effects are ignored, the implications of this simplifying assumption have to be assessed. The theorems of limit analysis are identical for both material idealisations shown in figure 2.1. For a given structure, the determination of the limit load involves the choice of a suitable velocity profile consistent with the applied loading and boundary conditions of the problem. On initiation of motion, at infinitesimal deflection, the work associated with internal and external energies are equated and solved for P_L, the limit load.

It is intuitively obvious that, quantitatively, the above definition of limit load is only meaningful when initial elastic behaviour invokes insignificant displacement. Plates with high slenderness ratios (the slenderness ratio of a plate is defined as the ratio of the longest side to the mean thickness), may experience significant elastic deflection before the yield stress is reached at any point on the plate. It has been estimated that the fundamental limit load definition is only valid for plates with slenderness ratios between 10 and 40, approximately [24]. For

plates with slenderness ratios less than about 10 even a thick plate formulation with inclusion of shear effects may not be adequate and analyses will require the consideration of a three dimensional stress state.

Furthermore the fundamental definition of limit load refers to the load at which increasing plastic strain occurs at constant load. In plates, membrane action will cause an increase in load carrying capacity with increasing deflection during 'post limit' behaviour. Theoretically, the limit load now refers to a kink in the load deflection curve, originating on or very near to a positive intercept of the load axis at P_L.

The effect of material elasticity is, therefore, dependent on the slenderness ratio of the plate. For plates where the fundamental definition of limit load applies, rigid plastic analyses may be used with confidence. Most practical plates, however, are more flexible and elastic deflections will invariably prove significant. The effect of material elasticity becomes less with increasing permanent deflection during post limit behaviour, as the elastic strain vector becomes a smaller proportion of the total strain vector. The load-deflection graph will, therefore, approach the load-permanent deflection graph [58].

It is apparent, therefore, that rigid plastic analyses should provide increasingly accurate predictions as permanent deflection increases even if material elasticity has adversely affected results at smaller displacement values [54,60]. In reference [54] Symonds and Jones added a correction for elastic effects to the load deflection graph, but it is stated that no

theoretical justification will support this arbitrary correction.

In a rigid plastic dynamic analysis the neglect of material elasticity appears reasonable, provided the energy ratio is larger than about 3 [13,26,36], where the energy ratio is defined as the external dynamic energy available divided by the elastic strain energy capacity of the structure under consideration. A hypothetical estimate of the elastic strain energy, when the entire structure just reaches the yield stress is made [26] to obtain a conservative estimate of the strain energy capacity of the system, (See Appendix 3).

Symonds [89] has stated, however, that material elasticity may be important in a dynamic analysis when the external load duration is long compared to the fundamental period of elastic vibration of the structure.

3.2.2 Material Strain Hardening

Studies which include strain hardening approximations have been mentioned in section 2.2. The most significant studies by Jones and Symonds [51] and Jones [50] conclude that strain hardening effects are relatively unimportant compared to the effects of change in geometry and strain rate sensitivity for most engineering materials. A material which exhibits unusually high hardening capabilities, however, may require a hardening correction in the analysis.

3.2.3 Material Strain Rate Sensitivity

If the constitutive equations of a material are dependent on the rate of straining, then a rigid perfectly plastic approximation might require further refinement. Strain rate sensitivity tends to be associated with materials exhibiting a sharp yield point (e.g. mild steel). Materials which yield gradually have shown little or no rate effects [13].

The Cowper-Symonds formula (equation 2.9) has proved very popular for analytical and numerical analyses which attempt to include strain rate effects. In references [36], [51] and [75] the authors demonstrated the use of a single raised yield stress, calculated from equation 2.9, and in each case found good agreement with experimental results on beams. The use of a single raised yield stress is valid provided an estimation of the value of average strain rate can be made and provided the greater part of deformation occurs at a uniform rate of strain. In practical situations the latter is highly unlikely and the former is likely to be determined empirically, at least to some extent.

For complex redundant structures, the strain rate will vary in time and space throughout the structure. A redistribution of energy absorption will take place where high strain rate effects occur, according to the structural kinematic boundary conditions or kinematically available mechanisms. This would tend to decrease the influence of strain rate on the final deformation and hence restrict the applicability of a single correction factor on the results of basic theory.

In principal, a numerical method can employ equation 2.9 to update the yield stress value at each spatial location during each time increment, in accordance with the current strain rate values. Under these conditions the programme should reasonably account for material strain rate effects. It must be remembered, however, that the coefficients used in equation 2.9 are derived from uniaxial material tests.

Bodner [13] has listed general conclusions concerning strain rate effects on material behaviour (see also figure 3.1) and these are,

i) The yield stress and flow stresses increase nonlinearly with strain rate for all strain levels.

ii) Strain rate sensitivity diminishes with increasing strain.

iii) Strain hardening after yield diminishes with increasing strain rate, and

iv) Strain rate dependance of flow stresses increase with increasing temperature.

3.2.4 Finite Deflections

It is apparent from the literature survey in Chapter 2 that the influence of geometry changes must be accounted for in all practical rigid plastic analyses where transverse deflections are larger than, say, the

thickness of the structure. This is particularly important for axially restrained beams and plates under transverse loading where out of plane deflections as small as 0.2 times the structure thickness can induce membrane effects.

Most analyses assume deflections can be large compared to the thickness of the specimen, but are sufficiently small to replace tan θ, the angular change across a plastic hinge, with θ radians. Further refinement of methods must be made when significant differences occur in these quantities

It is apparent from the literature that, when discussing the implications of approximate analyses, uncertainty is involved. The conclusions drawn invariably state that inclusion or omission of a certain effect may be of importance. The nature and variety of impact studies is such that many problems are essentially individual.

Strong justification for approximate analyses remain, however, due to the paucity of information on dynamic material properties and the assumptions which are often included in defining a given problem, particularly the characteristics of the dynamic loading. It is unrealistic to employ methods having precision much greater than the input to the analysis.

3.3 Rectangular Plate Under Static Loading

Jones and Walters [60] developed a rigid perfectly plastic analysis,

which retained the influence of finite deflections, for a uniformly loaded, fully clamped rectangular plate. Their predictions produced "reasonable engineering estimates" of the permanent deflections of plates tested by Hooke and Rawlings [57]. The analysis in [60] was an extension of earlier work by Sawzcuk [61].

In this section this analysis is extended to allow a condition of central concentrated loading. The plate under investigation is shown in figure 3.2. The resulting load-deflection relationships disagree with equations 2.6 which were developed by Kling [9].

The method relies on a choice of a velocity field, which is assumed to remain constant throughout response, and the summation of work rates due to internal and external energy dissipation.

The governing relationship developed (equation 3.5) is analogous to the upper bound theorem of limit analysis in producing an energy balance between external work rate and internal energy dissipation rate for an assumed velocity field which is consistent with kinematic boundary conditions for the problem. The solution, however, represents an upper bound to an assumed set of initial conditions and, as such, is not necessarily an upper bound to the actual structural behaviour.

Figure 3.3 shows the external forces, P_L, internal stress resultants, M_{ij}, N_{ij}, Q_i, and displacements, u_i,w, acting on an element in the mid-plane of a plate.

The external work rate for a plate with no displacement at the boundary, and with no external moment or force acting at the boundary is,

$$D_E = \int_{A_L} [p_i \dot{u}_i + p_3 \dot{w}] \, dA_L \qquad .....(3.1)$$

Where A_L refers to the loaded area of the plate and can be taken as the undeformed mid-plane loaded area for moderate deflections.

The symbols $\dot{u}_i$, $i = 1,2$ and $\dot{w}$ are respectively, the in-plane and transverse velocity components of a point in the mid-plane of the plate and p_i, $i = 1,2$ and p_3 are respectively, the in-plane and transverse components of load per unit area.

Referring to figure 3.3, the equilibrium equations are:

$$N_{ij},i + P_j = 0 \qquad .....(3.2a)$$

$$(Q_i + N_{ij} w,i),i + p_3 = 0 \qquad .....(3.2b)$$

$$Q_i = - M_{ji},j \qquad .....(3.2c)$$

where commas represent spatial differentiation.

Substituting from equations 3.2 into equation 3.1 gives the external work rate in terms of internal stress resultants:

$$D_E = -\int_{A_p} [N_{ij},_i u_j + (Q_i + N_{ij} w,_j),_i \dot{w}]\, dA_p \qquad .....(3.3)$$

The following expression is obtained [63] after applying Green's theorem to the terms in equation 3.3 together with the conditions of kinematic continuity. It has been assumed that the influence of u_i is negligible when $p_i = 0$.

$$\int p_3 \dot{w}\, dA_L = \sum_{o}^{m} \int_{L_m} (N_{ij} w - M_{ji})\, \dot{w},_i n_j dL_m + \int_{A_p} (M_{ji} - N_{ij} w)\, \dot{w},_j dA_p \qquad .....(3.4)$$

Where m is the number of hinge lines of length L_m and A_p is the undeformed mid-plane area of the plate. The first term on the right-hand side of equation 3.4 represents internal energy dissipated at any plastic hinges and the remaining term is the energy dissipated in continuous deformation fields.

In order to simplify the analysis, Jones [63] assumed the yield line collapse velocity profile shown in figure 3.4 which has been used by Wood [25] for infinitesimal collapse analyses. This mechanism was subsequently confirmed experimentally for uniform loading conditions [66].

The corresponding collapse profile used in this analysis and observed experimentally by Kling [9], is shown in figure 3.2. The test results

reported in Chapter 5, however, would appear to question the validity of this profile for concentrated loading. Despite this doubt, however, predictions obtained using the following analysis have been encouraging.

The mechanism in figure 3.2 assumes a series of rigid body segments separated by m straight line hinges of length L_m where all the deformation takes place. As a result the last term in equation 3.4, which represents energy dissipated in continuous deformation fields, will vanish. Equation 3.4 now becomes

$$\int_{A_L} p_3 \, \dot{w} \, dA_L = \sum_{o}^{m} \int_{L_m} (Nw - M) \, \dot{\theta}_m \, dL_m \qquad .....(3.5)$$

Where $\dot{\theta}_m$ is the rotation rate across a straight line hinge.

The quantity:

$$D_f = (Nw - M) \, \dot{\theta}_m \qquad ....(3.5a)$$

is a 'dissipation function' and represents the internal energy dissipation rate per unit length of a hinge.

The effect of finite deflection is evident in the membrane contribution to internal energy dissipation expressed by the production of the stress resultant N and the axial strain rate $w\dot{\theta}_m$.

The explicit form of D_f, for a given problem, will depend on both the boundary conditions and the material yield criteria. The structure dissipation functions will collectively give the energy dissipation for the system as a whole rather than at individual hinges i.e. the interaction existing between boundary and internal dissipation functions mean physical energy dissipation at a particular hinge cannot be evaluated.

The yield criterion used in this study is the maximum shear stress or Tresca criterion, with interaction between bending and membrane stress resultants at a hinge, (see Appendix A)

$$\frac{M}{M_o} = 1 - \left(\frac{N}{N_o}\right)^2 \qquad \text{.....(3.6)}$$

Where M_o = fully plastic bending moment $= \frac{\sigma_y h^2}{4}$

N_o = fully plastic axial force $= \sigma_y h$

The yield condition given by equation 3.6 is shown in figure 3.5 along with inscribing and circumscribing square yield curves.

The plate shown in figure 3.2 has external dimensions 2A x 2B and has a central loaded area 2a x 2b subjected to uniform pressure p per unit area. The following transverse displacements exist in regions I, II and III:

$$\text{I}: \quad w = w_o \frac{[(B-b)-x^1]}{B-b} = \frac{w_o\,(c-x^1)}{C} \qquad \ldots.(3.7a)$$

$$\text{II}: \quad w = w_o \frac{[(A-a)-y^1]}{A-a} = w_o \frac{(D-y^1)}{D} \qquad \ldots.(3.7b)$$

$$\text{III}: \quad w = w_o \qquad \ldots.(3.7c)$$

where $C = B - b$

$D = A - a$

It can be shown that the following dissipation functions are applicable for interior hinges of a clamped plate (See Appendix B):

$$D_i = M_o \left(1 + 3\frac{w^2}{h^2}\right)\dot{\theta}_m \qquad \text{where } \frac{w}{h} \leqslant 1 \qquad \ldots.(3.8a)$$

$$D_i = 4 M_o \frac{w}{h} \cdot \dot{\theta}_m \qquad \text{where } \frac{w}{h} \geqslant 1 \qquad \ldots.(3.8b)$$

and those for a boundary hinge:

$$D_b = M_o \left(1 - \frac{w^2}{h^2}\right) \dot{\theta}_m \qquad \ldots.(3.8c)$$

which becomes zero where the applicable value of w/h exceeds unity as $N = N_o$.

It is apparent that when w/h>1 there will be two regions of deformation with different dissipation functions separated by a moving boundary located at w/h = 1.

Referring to figure 3.2, the explicit form of the dissipation functions, equations 3.8, become:

$$D_b = M_o \left(1 - \frac{w^2}{h^2}\right) \frac{\dot{w}_o}{C} \qquad \text{for } O \leqslant y^1 \leqslant D \qquad x^1 = \pm C \qquad \ldots.(3.9a)$$

where w = displacement of the inclined hinge at y^1

$$D_b = M_o \left(1 - \frac{w^2}{h^2}\right) \frac{\dot{w}_o}{D} \qquad \text{for } O \leqslant x^1 \leqslant C \qquad y^1 = \pm D \qquad \ldots.(3.9b)$$

where w = displacement of the inclined hinge at x^1

$$D_b = M_o \left(1 - \frac{w_o^2}{h^2}\right) \frac{\dot{w}_o}{D} \qquad \text{for } -b \leqslant x \leqslant b \qquad y = \pm a \qquad \ldots.(3.9c)$$

$$D_b = M_o \left(1 - \frac{w_o^2}{h^2}\right) \frac{\dot{w}_o}{C} \qquad \text{for } -a \leqslant y \leqslant a \qquad x = \pm b \qquad \ldots.(3.9d)$$

when $\frac{w}{h} < 1$, and

$$D_b = M_o\left(1 - \frac{w^2}{h^2}\right)\frac{\dot{w}_o}{C} \qquad \text{for } \gamma \leqslant y^1 \leqslant D$$

$$x^1 = \pm C \qquad \ldots.(3.9e)$$

where w = displacement of the inclined hinge at y^1

$$D_b = M_o\left(1 - \frac{w^2}{h^2}\right)\frac{\dot{w}_o}{D} \qquad \text{for } \zeta \leqslant x^1 \leqslant C$$

$$y^1 = \pm D \qquad \ldots.(3.9f)$$

where w = displacement of the inclined hinge at x^1

when $\frac{w}{h} > 1$

When $\frac{w}{h} > 1$ the boundary hinges located at:

$$0 \leqslant x^1 \leqslant \zeta, \quad -b \leqslant x \leqslant b, \quad y = \pm A$$

$$0 \leqslant y^1 \leqslant \gamma, \quad -a \leqslant y \leqslant a, \quad x = \pm B$$

have no further contribution to energy dissipation as $N = N_o$ when $\frac{w}{h} > 1$.

The dissipation functions for the internal hinges become

$$D_i = M_o\left(1 + \frac{3w_o^2}{h^2}\right)\frac{\dot{w}_o}{D} \qquad \text{for } -b \leqslant x \leqslant b$$

$$y = \pm a \qquad \ldots.(3.10a)$$

$$D_i = M_o\left(1 + \frac{3w_o^2}{h^2}\right)\frac{\dot{w}_o}{C} \quad \text{for} \quad -a \leqslant y \leqslant a$$

$$x = \pm b \qquad \ldots.(3.10b)$$

$$D_i = M_o\left(1 + \frac{3w^2}{h^2}\right)\frac{\dot{w}_o}{D\sin\phi} \qquad \ldots.(3.10c)$$

for inclined hinges

when $\frac{w}{h} < 1$ and

$$D_i = 4M_o \frac{w_o}{h} \cdot \frac{w_o}{D} \quad \text{for} \quad -b \leqslant x \leqslant b$$

$$y = \pm a \qquad \ldots.(3.10d)$$

$$D_i = 4M_o \frac{w_o}{h} \cdot \frac{w_o}{C} \quad \text{for} \quad -a \leqslant y \leqslant a$$

$$x = \pm b \qquad \ldots.(3.10e)$$

$$D_i = 4M_o \frac{w}{h} \cdot \frac{w_o}{D\sin\phi} \qquad \ldots.(3.10f)$$

for inclined hinges with

$$\frac{w}{h} > 1$$

$$D_i = M_o\left(1 - \frac{w^2}{h^2}\right)\frac{w_o}{D} \qquad \ldots.(3.10g)$$

for inclined hinges with

$$\frac{w}{h} < 1$$

when $\frac{w}{h} > 1$

The right-hand side of the governing relationship, equation 3.5, is evaluated by substituting the appropriate dissipation functions, equations 3.9 and 3.10 with the geometric relationships, equations 3.7, and then integrating along all hinges.

The left-hand side of equation 3.5 is the external work rate and is given by:

$$P\dot{w}_o \qquad \ldots.(3.11)$$

where P = p2a2b

Equating the right and left-hand sides of equation 3.5 yields the final load-deflection relationships:

$$P = 8M_o\left[\alpha+\beta+\left(\alpha+\frac{1}{3}\beta\right)\frac{w_o^2}{h^2}\right] \quad \text{when} \quad \frac{w_o}{h} \leqslant 1 \qquad \ldots.(3.12a)$$

$$P = 4M_o\left[\alpha\left(\frac{4w_o}{h}\right)+\beta\left(\frac{2w_o}{h}\right)+\beta\left(\frac{2h}{3w_o}\right)\right] \text{when} \quad \frac{w_o}{h} \geqslant 1 \qquad \ldots.(3.12b)$$

where

$$\alpha = \frac{a}{C}+\frac{b}{D}$$

$$\beta = \frac{C}{D}+\frac{D}{C}$$

If a = b = 0 and A = B, the problem reduces to a square plate under 'point load' and equations 3.12 become:

$$\frac{P}{P_L} = 1 + \frac{w_o^2}{3h^2} \qquad \text{for } \frac{w_o}{h} \leqslant 1 \qquad \ldots.(3.13a)$$

$$\frac{P}{P_L} = \left(\frac{w_o}{h} + \frac{h}{3w_o}\right) \qquad \text{for } \frac{w_o}{h} \geqslant 1 \qquad \ldots.(3.13b)$$

where

$$P_L = 16M_o$$

Equations 3.13 correspond exactly to the reduced form of equations 2.4 for a square clamped plate under uniform pressure loading.

The value $P_L = 16M_o$ is the infinitesimal collapse load calculated assuming a yield line collapse pattern similar to figure 3.2 with a = b = 0. Using infinitesimal yield line theory, a number of authors [e.g. 9] have shown this result to be incorrect for the case of a square plate under point loading, and it is used here for comparative purposes only.

In fact, the whole concept of 'collapse load' for steel plates is fairly meaningless as discussed in section 3.2.1. A reinforced concrete slab may well become unserviceable, perhaps due to cracking, by forming a yield line collapse pattern at infinitesimal deflection [25]. A steel plate, however, will invariably strengthen with increasing deflection and, in some cases, will deflect elastically to several times its thickness. Collapse in steel plates will therefore usually be defined as a maximum permissible deflection or a maximum permissible rate of increase of

deflection. The parameter P_L used in the plate expressions should therefore not be taken as a quantative definition of collapse.

Equations 3.12 also reduce to those derived by Haythornthwaite [78] for a fully clamped beam loaded at mid-span:

i.e. $\beta \to 0, \alpha \to \frac{1}{A} = \frac{1}{L}$ where L = length of beam,

equations 3.12 become:

$$\frac{P}{P_L} = 1 + \frac{w_o^2}{h^2} \quad \text{for } \frac{w_o}{h} \leqslant 1 \qquad \ldots.(3.14a)$$

$$\frac{P}{P_L} = \frac{2w_o}{h} \quad \text{for } \frac{w_o}{h} \geqslant 1 \quad P_L = \frac{8M_o}{L} \qquad \ldots.(3.14b)$$

where $P_L = \frac{8M_o}{L}$ from basic plastic beam theory.

A more simple approximate analysis can be carried out by using the square yield interaction curves shown in figure 3.5. For this condition the dissipation function can be shown to be:

$$D = M_o \left(1 + \frac{4w}{h}\right) \dot{\theta}_m \qquad \ldots.(3.15)$$

and in this case applies throughout the range of deflection.

The left-hand side of equation 3.5 is again given by equation 3.11, while the right-hand side is evaluated by using the dissipation function, equation 3.15, and geometrical relationships, equations 3.7, and integrating along all hinges.

Equating the right and left-hand sides of equation 3.5 yields the final result:

$$P = 8M_o \left[\alpha/2 + \beta + (\alpha+\beta) \frac{w_o}{h} \right] \qquad \ldots.(3.16)$$

Once more, the reduced form of equation 3.16 will agree with the reduced form of equations derived by Jones and Walters [60] for a uniformly loaded plate.

Equation 3.16 gives a solution based on a square yield curve which circumscribes the parabolic interaction curve in figure 3.5. If the results of equation 3.16 are multiplied by 0.618, however, they then represent a solution which corresponds to a square yield curve which inscribes the maximum shear stress yield curve.

Similar large deflection equations may be derived for plates under various load and boundary conditions. For example, if the plate shown in figure 3.2 has a simply supported edge condition, the dissipation functions can be shown to be

$$D_i = M_o \left(1 + 4\frac{w^2}{h^2} \right) \dot{\theta}_m \qquad \text{for } \frac{w_o}{h} \leqslant \frac{1}{2} \qquad \ldots.(3.17a)$$

$$D_i = 4M_o \frac{w}{h} \cdot \dot{\theta}_m \qquad \text{for } \frac{w_o}{h} \geqslant \frac{1}{2} \qquad \ldots.(3.17b)$$

The analysis proceeds as before, based on the governing relationship, equation 3.5, with the final result given by

$$P = 4M_o\left[\alpha + \beta + \left(4\alpha + {}^4/_3\beta\right)\frac{w_o^2}{h^2}\right] \qquad \text{for } \frac{w_o}{h} \leqslant \frac{1}{2} \qquad \ldots.(3.18a)$$

$$P = 4M_o\left[\alpha\left(\frac{4w_o}{h}\right) + \beta\left(\frac{w_o}{h}\right) + \beta\left(\frac{h}{6w_o}\right)\right] \qquad \text{for } \frac{w_o}{h} \geqslant \frac{1}{2} \qquad \ldots.(3.18b)$$

Equations 3.18 can be shown to agree with reduced forms of equations 2.2, derived by Onat and Haythornthwaite [54] for a simply supported circular plate, and reduced forms of equations 2.5, derived by Jones and Walters [60] for a simply supported rectangular plate loaded uniformly.

3.4 Rectangular Plate Under Central Impact Load

DeOliveira [3] developed an approximate method for the design of beams and plates subject to low velocity projectile impact. The method used is essentially an energy approach which equates the initial kinetic energy of the plate and impacting body at time t =0, to the area under the static load-deflection curve. The method, therefore, relies on the structure response being quasi-static. The static load-deflection equations used by DeOliveira were those derived by Kling (equations 2.6), which disagree with equations 3.12 derived in section 3.3.

The analysis assumes the same collapse profile shown in figure 3.2, where impact from a mass G, travelling at some velocity V_o, occurs over the central area 2a x 2b. In the analysis the mass is assumed to remain in contact with the plate throughout response.

If at any time t>0 (where t = 0 at the instant of impact), the velocity at the plate centre is $\dot{w}_*$, it can be shown that the system kinetic energy, K(t) is given by:

$$K(t) = \frac{1}{2} G \dot{w}_*^2 \left[\frac{1}{2} \chi \left[\frac{ab}{AB} + \frac{1}{3} \left(\frac{b}{B} + \frac{a}{A} + 1 \right) \right] + 1 \right] \qquad ....(3.19)$$

where $\chi = \frac{4 \mu AB}{G}$ = plate/striker mass ratio

μ = mass/unit area of plate

Equation 3.19 is obtained through summation of the kinetic energy possessed by the plate,

$$K_p = \mu \dot{w}_*^2 \left(ab + \frac{bA}{3} + \frac{aB}{3} + \frac{AB}{3} \right) \qquad ....(3.20)$$

and that possessed by the impacting body,

$$K_s = \frac{1}{2} G \dot{w}_*^2 \qquad ....(3.21)$$

The initial velocity of the system, $\dot{w}^o_*$, is found by the 'minimum Δ method', which has been used in mode approximation techniques [e.g. 98].

The minimum Δ technique states that a positive function of the actual and assumed modal velocities should be a relative minimum.

The assumed general mode field of velocity is presented as

$$\dot{w}_i\ (x, y, t) = \dot{w}_*\ (t)\ .\ \psi\ (x, y) \qquad \ldots.(3.22)$$

where $\dot{w}_*(t)$ is the velocity at the main point of interest and $\psi(x,y)$ are normalised shape functions of space variables (x,y).

The positive function Δ is a measure of the difference of the velocity distributions and is expressed as

$$\Delta\ (t) = \frac{1}{2}\ \rho \int_{vol} \left(\dot{v}_i - \dot{w}_*\right) \left(\dot{v}_i - \dot{w}_*\right)\ \ dvol \qquad \ldots.(3.23)$$

where $\dot{v}_i$ is the actual velocity of the system.

Minimising $\Delta(t)$ at time $t = 0$, at which time the modal form is assumed operative, determines the initial value of the velocity amplitude for the assumed mode shape.

$$\dot{w}_*{}^o = \frac{\int_{vol} \rho\ .\ \psi i\ .\ \dot{v}_i{}^o\ \ dvol}{\int_{vol} \rho\ .\ \psi_i\ .\ \psi_i\ \ dvol} \qquad \ldots.(3.24)$$

For the plate shown in figure 3.2, the mode fields are given by normalised forms of equations 3.7:

$$\text{I} \qquad \psi_{\text{I}}\ (x, y) = 1 - \frac{x^1}{C} \qquad \ldots.(3.25a)$$

$$\text{II} \qquad \psi_{\text{II}}\ (x, y) = 1 - \frac{y^1}{D} \qquad \ldots.(3.25b)$$

$$\text{III} \qquad \psi_{III}\,(x, y) = 1 \qquad \ldots.(3.25c)$$

The plate is initially at rest and $\dot{v}_i^{o}\,(x, y) = O$ everywhere except in region III, where $\dot{v}_i^{o}\,(x, y) = V_o$.

Substituting the initial conditions and equations 3.25 into equation 3.24 and carrying out the integration gives the initial velocity of the system,

$$\dot{w}_*^{o} = \frac{V_o\,(1+\eta)}{\chi/_2\left(\frac{ab}{AB} + \frac{b}{3B} + \frac{a}{3A} + \frac{1}{3}\right) + 1} \qquad \ldots.(3.26)$$

where $\eta = \dfrac{4\mu ab}{G}$

It can be seen from equation 3.26 that, as the mass of the striker becomes significantly greater than the mass of the plate, the initial velocity of the system approaches the initial velocity of the striker just prior to impact i.e. the analysis effectively reduces to that of a massless plate which is a similar situation to that noted by Wierzbicki and Kelly [52].

i.e. as $G >> 4\mu AB$, $\dot{w}_*^{o} \longrightarrow V_o$

The value of velocity from equation 3.26 is substituted into equation 3.19 to give a value of kinetic energy at time t = 0.

The kinetic energy at time t = 0 is then equated to the area under the

static load-deflection curve, which is found from integration of equations 3.12.

The final relationship, for values of $\frac{w}{h} > 1$, is obtained after considerable manipulation and simplification,

$$\frac{2}{3}\alpha + \frac{11}{9}\beta + (2\alpha+\beta)\left(\frac{w_o}{h}\right)^2 + \frac{2}{3}\beta \,\mathrm{Ln}\left(\frac{w_o}{h}\right) = \frac{2\lambda(1+\eta)^2}{\chi[BR]+2} \quad \ldots.(3.27)$$

where

$$[BR] = \frac{ab}{AB} + \frac{1}{3}\left(\frac{b}{B} + \frac{a}{A} + 1\right)$$

$$\lambda = \frac{G V_o^2}{8 M_o h}$$

If a similar procedure is followed for the plate shown in figure 3.2, with simply supported edge condition, the final relationship can be shown to be

$$\frac{1}{6}\alpha + 0.4211\beta + (2\alpha+\beta)\left(\frac{w_o}{h}\right)^2 + \frac{1}{6}\beta \,\mathrm{Ln}\left(\frac{w_o}{h}\right) = \frac{2\lambda(1+\eta)^2}{\chi[BR]+2} \quad \ldots.(3.28)$$

Simplified solutions can again be obtained by using the square yield conditions shown in figure 3.5. In particular, for a clamped plate with a

yield condition circumscribing the parabolic yield condition, the solution is given by

$$(\alpha+2\beta)\left(\frac{w_o}{h}\right)+(\alpha+\beta)\left(\frac{w_o}{h}\right)^2=\frac{2\lambda(1+\eta)^2}{\chi[BR]+2} \qquad \ldots.(3.29)$$

and the corresponding result for the inscribing yield condition is found by multiplying the solution from equation 3.29 by 0.618.

3.5 Dynamic Formulation for Central Impact Load

If the inertia of the system is included in the method described in section 3.3, equation 3.1 becomes,

$$D_E=\int_{A_L} p_i\,.\,\dot{u}_i\,dA_L-\int_{A_p}\mu\ddot{u}_i\dot{u}_i\,dAp+\int_{A_L} p_3\,.\,\dot{w}\,dA_L-\int\mu\,\ddot{w}\,\dot{w}\,dA_p \qquad \ldots.(3.30)$$

where A_p is the midplane area of the plate and can be taken as the undeformed area for moderate deflections.

Similarly the equilibrium equations, equations 3.2, become,

$$N_{ij},i+P_j-\mu\ddot{u}_i=0 \qquad \ldots.(3.31a)$$

$$(Qi+N_{ij}w,j),i+p_3-\mu\ddot{w}=0 \qquad \ldots.(3.31b)$$

$$Q_i=-M_{ji},j \qquad \ldots.(3.31c)$$

If the analysis proceeds as in section 3.2, and similar use is made of Green's theorem and kinematic boundary conditions, the governing equation for the problem becomes,

$$\int_{A_L} p_3 \, \dot{w} \, dA_L - \int_{A_p} \mu \, \ddot{w} \, \dot{w} \, dA_p = \sum_{o}^{m} \int_{Lm} (Nw - M) \, \dot{\theta}_m \, dL_m \qquad \ldots.(3.32)$$

This corresponds to the governing equation developed by Jones (equation 10, ref.63), for plates and beams subject to uniform blast loading. In [63] a detailed analysis is given for a simply supported beam and a fully clamped rectangular plate, both loaded uniformly with an assumed initial pressure-time pulse which is short compared to the fundamental period of the respective systems.

The problem at hand is tackled by substituting the appropriate dissipation functions and geometrical relations for the assumed velocity field, along with the assumed load-time function, into equation 3.32 and integrating along all hinge lines. This results in a non-linear differential equation which has to be solved for w_o. The solution involves two stages of motion, one in which the load is acting, and subsequently when no load acts and initial conditions are given by the values of w and $\dot{w}$ existing at the end of the first phase of motion.

Even when solving the resulting non-linear differential equation approximately [63], considerable algebraic manipulation is involved both in obtaining and using the resulting expressions for final displacement and duration of response. Equation 2.8 shows only the simplified expression

for the blast loaded plate, obtained using the circumscribing square yield condition shown in figure 3.5.

In view of the discussion presented in section 3.2, it is unlikely that a dynamic rigid plastic analysis is suitable in this case because:

a) The load duration will probably not be short compared to the fundamental natural period of the system.

b) A load-time history for arbitrary projectile impact is difficult to define and is very often the information required from such an analysis.

Taya and Mura [65] however, solved the plate problem in [63] by method they termed the 'extended Hamilton's principle'. In this approach, initial conditions are given as an applied velocity field rather than an applied force-time function. Furthermore, resulting expressions require the more manageable task of solving non-linear algebraic equations instead of non-linear differential equations. In view of the above, the present problem is formulated using the extended Hamilton's principle to give an indication of whether rigid plastic dynamic analysis is applicable in this case.

Taya and Mura [65] show that the governing variational relationship to apply Hamilton's principle to a non-conservative system is

$$\delta \int_0^{t_f} \int_{A_p} \left(\frac{1}{2} \mu \dot{w}^2 + pw \right) dA_p dt = \int_0^{t_f} \int_{L_m} \left(N_w - M \right) \delta \dot{\theta}_m \, dL_m \, dt \qquad \ldots.(3.33)$$

which, for the problem being considered here, becomes,

$$\delta\left[\int_0^{t_f}\frac{1}{2}G\dot{w}_o^{\,2}\,dt+\int_0^{t_f}\int_{A_p}\frac{1}{2}\mu\dot{w}^{\,2}\,dA_p\,dt\right]=\int_0^{t_f}\int_{L_m}\left(N_w-M\right)\delta\,\dot{\theta}_m\,dL_m\,dt \qquad ....(3.34)$$

where t_f is the duration of response.

In the analysis, it is assumed that the mass, G, stays in contact with the plate throughout the response until time t_f.

The deflection at time t, is related to the initial velocity, and a constant d_1, as yet undetermined, by

$$w_o(t) = V_o t + d_1 t^2 \qquad ....(3.35)$$

$$\dot{w}_o(t) = V_o + 2d_1 t \qquad ....(3.36)$$

Equations 3.35 and 3.36 satisfy the initial conditions:

$w_o = 0$ when $t = 0$

$\dot{w}_o = V_o$ when $t = 0$

The velocity field shown in figure 3.2 is used, hence the second term on the left-hand side of equation 3.34 is given by equation 3.20.

Substituting for $\dot{w}_o$ from equation 3.36, carrying out the time integration and taking variation with respect to d_1, evaluates the left-hand side of equation 3.34:

$$\left[\frac{GV_o^3}{12d_1^2} + \frac{\mu V_o^3}{6d_1^2}\left(ab + \frac{bA}{3} + \frac{aB}{3} + \frac{AB}{3}\right)\right]\delta d_1 \qquad \ldots.(3.37)$$

If the square yield criterion is assumed, the appropriate dissipation function is given by equation 3.15. Using equation 3.15 and the appropriate geometrical relationships, the right-hand side of equation 3.34 is evaluated by integrating along all hinge lines and subsequently through time, before finally taking variation with respect to d_1 to give

$$\frac{M_o V_o^3}{d_1^3}\left(-\frac{K_1}{24} + \frac{3K_2 V_o^2}{320 d_1 h}\right)\delta d_1 \qquad \ldots.(3.38)$$

where

$$K_1 = \left(\frac{8D}{C} + \frac{8C}{D} + \frac{16b}{D} + \frac{16a}{C}\right)$$

$$K_2 = \left(\frac{8D}{C} + \frac{8C}{D} + \frac{32b}{D} + \frac{32a}{C}\right)$$

Equating the left and right-hand sides of equation 3.34, produces a quadratic in d_1 given by

$$e_1 d_1^2 + e_2 d_1 - e_3 = 0 \qquad \ldots.(3.39)$$

where $e_1 = \frac{1}{12}\left[G + 2\mu\left(ab + \frac{bA}{3} + \frac{aB}{3} + \frac{AB}{3}\right)\right]$

$$e_2 = \frac{M_o K_1}{24}$$

$$e_3 = \frac{3 M_o K_2 V_o^2}{320h}$$

Solution of this quadratic equation gives the following expressions for the final permanent deflection and duration of response,

$$w_{of} = \frac{e_1 V_o^2}{2\left[e_2 + \left(e_2^2 + 4e_1 e_3\right)^{1/2}\right]} \qquad \ldots.(3.40a)$$

$$t_f = \frac{e_1 V_o}{e_2 + \left(e_2^2 + 4 e_1 e_3\right)^{1/2}} \qquad \ldots.(3.40b)$$

If the parabolic yield curve shown in figure 3.5 is used, the left-hand side of equation 3.34 remains unchanged, while the right-hand side becomes,

$$\frac{M_o V_o}{d_1^2}\left[\frac{3K_3 V_o^4}{320hd_1^2} - \frac{K_4 h}{2}\left(1 + 2\mathrm{Ln}\frac{V_o}{2} - 2\mathrm{Ln}V_o\right)\right]\delta d_1 \qquad \ldots.(3.41)$$

where

$$K_3 = \left(8\frac{C}{D} + 8\frac{D}{C} + 16\frac{b}{D} + 16\frac{a}{C}\right)$$

$$K_4 = \left(\frac{8}{3}\frac{D}{C} + \frac{8}{3}\frac{C}{D}\right)$$

Equating the right and left-hand sides of equation 3.34, solving for and utilising equation 3.36 produces the following expressions for d_1 permanent displacement and duration of response

$$w_{of} = \frac{V_o^2}{4\left(\frac{e_4}{e_5 + e_6}\right)^{1/2}} \qquad \ldots.(3.42a)$$

$$t_f = \frac{V_o}{2\left(\frac{e_4}{e_5 + e_6}\right)^{1/2}} \qquad \ldots.(3.42b)$$

where

$$e_4 = \frac{3 M_o K_3 V_o^4}{320h}$$

$$e_5 = \frac{1}{2}\left[G + 2\mu\left(ab + \frac{bA}{3} + \frac{aB}{3} + \frac{AB}{3}\right)\right]$$

$$e_6 = \frac{K_2 h M_o}{2}\left(1 + 2\mathrm{Ln}\,\tfrac{1}{2}\right)$$

The corresponding analysis in reference [65] for uniformly blast loaded plates agreed well with the experimental [66] and theoretical [63] results of Jones. The method was also used with success to predict the behaviour of the cantilever, struck at its tip by a mass, Parkes [31]. An approximate technique was used to include material strain rate effects by using an estimated average strain rate and equation 2.9, to calculate a value of dynamic yield stress valid throughout the response. The effect of the increase in magnitude of the yield stress is to reduce the permanent displacement for a given impact velocity.

3.6 Axisymmetric Idealisation of Rectangular Plate Under Central Impact

Throughout the experimental program reported in Chapters 4 and 5 it was observed that the velocity profile shown in figure 3.2 did not occur. The experimentally measured collapse profiles, for all tests, were virtually axisymmetric. This is in contrast to experimental observations made by Kling [9] and Samuelides [79], who both noted under conditions of concentrated loading, collapse profiles similar to figure 3.2. It is also in contrast to the collapse profile of a rectangular plate under uniform blast loading, figure 3.4 [66].

The experiments reported in Chapters 4 and 5, however, do confirm, that for the range of parameters tested, the plate response is essentially quasi-static.

The following analysis treats the square plates tested as 'equivalent circular plates'. The quasi-static approach used in section 3.4 is adopted. The available kinetic energy is equated to the work done, by plastic deformation, in displacing the plate from its initial to its final position.

The method utilises the static load-deflection relationships for circular plates, originally proposed by Onat and Haythornthwaite [54]. The clamped circular plate is shown in figure 3.6. The main assumption used in the derivation in [54] is that the radial velocity during deformation is zero i.e. all points in the deforming structure move vertically. The maximum shear stress criterion is used to control yielding

and the subsequent deformation obeys the corresponding flow rate. The rate of energy dissipation per unit volume during plastic flow is $\sigma_y |\dot{\epsilon}|$ max, where σ_y is the yield stress in simple tension and $|\dot{\epsilon}|$ max is the greatest principal strain rate, which is determined from initial velocity field assumptions. Since no energy is recoverable from a rigid plastic structure, the total rate of energy dissipation must equal the rate at which the applied loads do work and hence the magnitude of the applied load follows by virtual work considerations.

The velocity field used in reference [54] was used by Hopkins and Prager [55] for infinitesimal analysis and is shown in the latter to be correct for zero deflection. The velocity field has two parts

(i) Central zone, $r = \bar{\omega}$, where the plate deforms to a conical shape:

$$w(r) = w_o \left[\frac{\text{Ln } \frac{R}{r}}{1 + \text{Ln } \frac{R}{\bar{\omega}}} \right] \qquad \text{for } \bar{\omega} \leqslant r \leqslant R \qquad \ldots.(3.43a)$$

(ii) and a zone where $r > \bar{\omega}$ in which deformation is logarithmic:

$$w(r) = w_o \left[\frac{1 + \text{Ln } \frac{R}{\bar{\omega}} - \frac{r}{\bar{\omega}}}{1 + \text{Ln } \frac{R}{\bar{\omega}}} \right] \qquad \text{for } 0 \leqslant r \leqslant \bar{\omega} \qquad \ldots.(3.43b)$$

where $\bar{\omega}$ is found from the transcendental equation

$$1 - \frac{2}{3} \frac{a_L}{\bar{\omega}} \left(1 + \text{Ln } \frac{R}{\bar{\omega}} \right) = 0 \qquad \text{for } \frac{a_L}{R} \leqslant e^{-\frac{1}{2}} \qquad \ldots.(3.44a)$$

or from

$$1 - \frac{a_L^2}{\bar{\omega}^2}\left(1 + 2\mathrm{Ln}\frac{R}{a}\right) + \frac{2}{3}\left(1 + \mathrm{Ln}\frac{R}{\bar{\omega}}\right) = 0 \qquad \text{for } \frac{a_L}{R} \geqslant e^{-1/2} \qquad \ldots.(3.44b)$$

Equations for static load-deflection, which allow for geometry changes, can then be derived by integration of the strain rate diagrams which are consistent with the velocity field assumptions, and inclusion of a plastic hinge at r = R.

The final relationship is given by

$$\frac{P}{P_L} = 1 + \Phi_1\left(\frac{w_o}{h}\right) + \Phi_2\left(\frac{w_o}{h}\right)^2 \qquad \text{for } \frac{w_o}{h} \leqslant \tfrac{1}{2} + \tfrac{1}{2}\,\mathrm{Ln}\,\frac{R}{\bar{\omega}} \qquad \ldots.(3.45a)$$

$$\frac{P}{P_L} = \psi_1 + \psi_2\left(\frac{w_o}{h}\right) + \psi_3\left(\frac{h}{w_o}\right) \qquad \text{for } \frac{w_o}{h} \geqslant \tfrac{1}{2} + \tfrac{1}{2}\,\mathrm{Ln}\,\frac{R}{\bar{\omega}} \qquad \ldots.(3.45b)$$

where

$$\Phi_1 = \frac{\left(1 + 2\mathrm{Ln}\frac{R}{\bar{\omega}}\right)}{\left(2 + \mathrm{Ln}\frac{R}{\bar{\omega}}\right)\left(1 + \mathrm{Ln}\frac{R}{\bar{\omega}}\right)} \qquad \Phi_2 = \frac{2\left(1 + 3\,\mathrm{Ln}\frac{R}{\bar{\omega}}\right)}{3\left(2 + \mathrm{Ln}\frac{R}{\bar{\omega}}\right)\left(1 + \mathrm{Ln}\frac{R}{\bar{\omega}}\right)^2}$$

$$\psi_1 = \frac{\left(3 + \mathrm{Ln}\frac{R}{\bar{\omega}}\right)}{2\left(2 + \mathrm{Ln}\frac{R}{\bar{\omega}}\right)} \qquad \psi_2 = \frac{2\left(1 + 2\mathrm{Ln}\frac{R}{\bar{\omega}}\right)}{\left(2 + \mathrm{Ln}\frac{R}{\bar{\omega}}\right)\left(1 + \mathrm{Ln}\frac{R}{\bar{\omega}}\right)} \qquad \psi_3 = \frac{\left(1 + \mathrm{Ln}\frac{R}{\bar{\omega}}\right)}{12\left(2 + \mathrm{Ln}\frac{R}{\bar{\omega}}\right)}$$

and

$$P_L = 2\pi M_o \cdot \frac{A_o}{B_o} \qquad \ldots.(3.46)$$

where

$$A_o = 2 + \text{Ln}\,\frac{R}{\bar{\omega}}$$

$$B_o = 1 + \text{Ln}\,\frac{R}{\bar{\omega}} - \frac{2a_L}{3\bar{\omega}} \qquad \text{for } \bar{\omega} \geqslant a_L$$

or $$B_o = \frac{1}{2} + 1_n\,\frac{R}{a_L} - \frac{\bar{\omega}^2}{6a_L^2} \qquad \text{for } \bar{\omega} \leqslant a_L$$

Again P_L has no real physical significance in these formulae. It naturally occurs in the derivation and is the value of 'collapse load' at infinitesimal deflection.

The analysis of a plate under central impact follows the same procedure as that in section 3.4. The initial kinetic energy of the system is found using the mode approximation technique and equated to the area under the static load-deflection curve evaluated by integration of equations 3.45.

In this case the integration cannot be carried out explicitly and no final expression analogous to equation 3.27 can be formulated.

All methods for static and impact loading proposed in this chapter, are programmed in the FORTRAN computer language into programmes RELDEF, which treats rectangular plate formulations, and CILDEF, which treats axisymmetric simulations of the problem. Numerical integration is achieved using Simpson's rule and Newton Raphson iteration solves the transcendental equations 3.44.

Also programmed into CILDEF is an alternative approach for axisymmetric simulation, based on a static load-deflection relationship found from plastic membrane theory [54]. The velocity profile for the plate in figure 3.5 is obtained by using the equilibrium equations and the maximum shear stress yield criterion and is given by

$$w(r) = w_o \left(1 - \frac{r^2}{a_L^2\left(1 + 2\mathrm{Ln}\, R/a_L\right)}\right) \qquad \text{for } r \leqslant a_L \qquad \ldots.(3.47a)$$

$$w(r) = -w_o \cdot \frac{\mathrm{Ln}\, \frac{r}{R}}{\frac{1}{2} + \mathrm{Ln}\, \frac{R}{a_L}} \qquad \text{for } r \geqslant a_L \qquad \ldots.(3.47b)$$

and the load-deflection relationship becomes

$$P = 2\pi N_o \cdot \frac{w_o}{\frac{1}{2} + \mathrm{Ln}\, \frac{R}{a_L}} \qquad \ldots.(3.48)$$

where $P = \pi . a_L^2 . p$

$N_o = \sigma_y h$

Several possibilities exist for axisymmetric idealisation of a square plate. The plate can be either idealised as an inscribed or circumscribing circle, or alternatively as an 'equivalent circular plate', found by equating the elastic stiffness of square and circular plates under central concentrated load conditions, [113].

In reference [113] Neilson showed experimentally that square plates and inscribed circular plates, under clamped edge conditions, had deflection-time histories which agreed to within 10%. Using the

'equivalent circular plate', based on elastic stiffness, the numerical calculations showed results agreeing to within 5% of experimental data.

The elastic stiffness relationships:

$$w = \frac{0.0056\, PL^2}{D}$$ for square plates under concentrated loading

and $$w = \frac{PR^2}{16\,\pi\, D}$$ for circular plates under concentrated loading

where $$D = \frac{Eh^3}{12\left(1 - \upsilon^2\right)}$$

may be equated to give the 'equivalent radius'

$$R = 0.53055\ L \qquad \ldots.(3.49)$$

Where L is the length of the square plate side.

3.7 Concluding Remarks

In this chapter, various rigid plastic techniques have been used to derive equations for permanent damage estimation in isotropic plates subject to static and impact loading. Equations are presented for fully clamped and simply supported rectangular plates undergoing gross deformation. In two cases, the equations derived are found to disagree with previously published design formulae.

The behaviour of plates under central impact loading has been studied assuming both dynamic and quasi-static response. Equations are

presented for both the final permanent deformation and the duration of response when inertia effects are included.

All the analytical methods presented in this chapter have been coded in FORTRAN and incorporated into two computer programmes, one to analyse rectangular plates and the other to analyse rectangular plates using an axisymmetric idealisation. In addition, all formulae derived in this chapter are critically compared with the experimental data from the tests reported in chapter 5.

FIGURE 3.1 MATERIAL STRAIN RATE SENSITIVITY

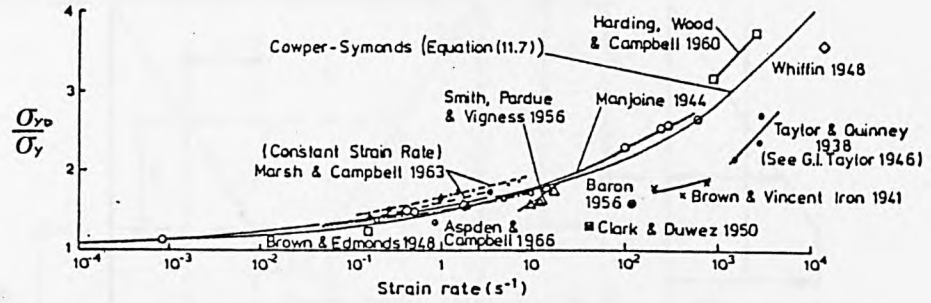

a) COMPARISON BETWEEN COWPER-SYMONDS EMPIRICAL RELATION (EQN. 2.9) FOR MILD STEEL ($D_{\bar{\sigma}}=40.45^{-1}$; $P_0=5$) AND EXPERIMENTAL UNIAXIAL DATA GATHERED BY SYMONDS [89]

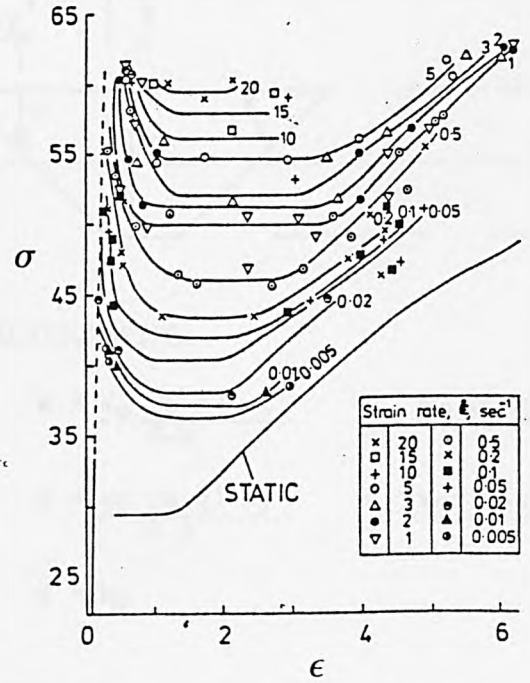

b) STRESS-STRAIN CURVES FOR MILD STEEL AT VARIOUS STRAIN RATES, FROM [8]. (1 UNIT OF ORDINATE = 10^3 1b in^{-2}).

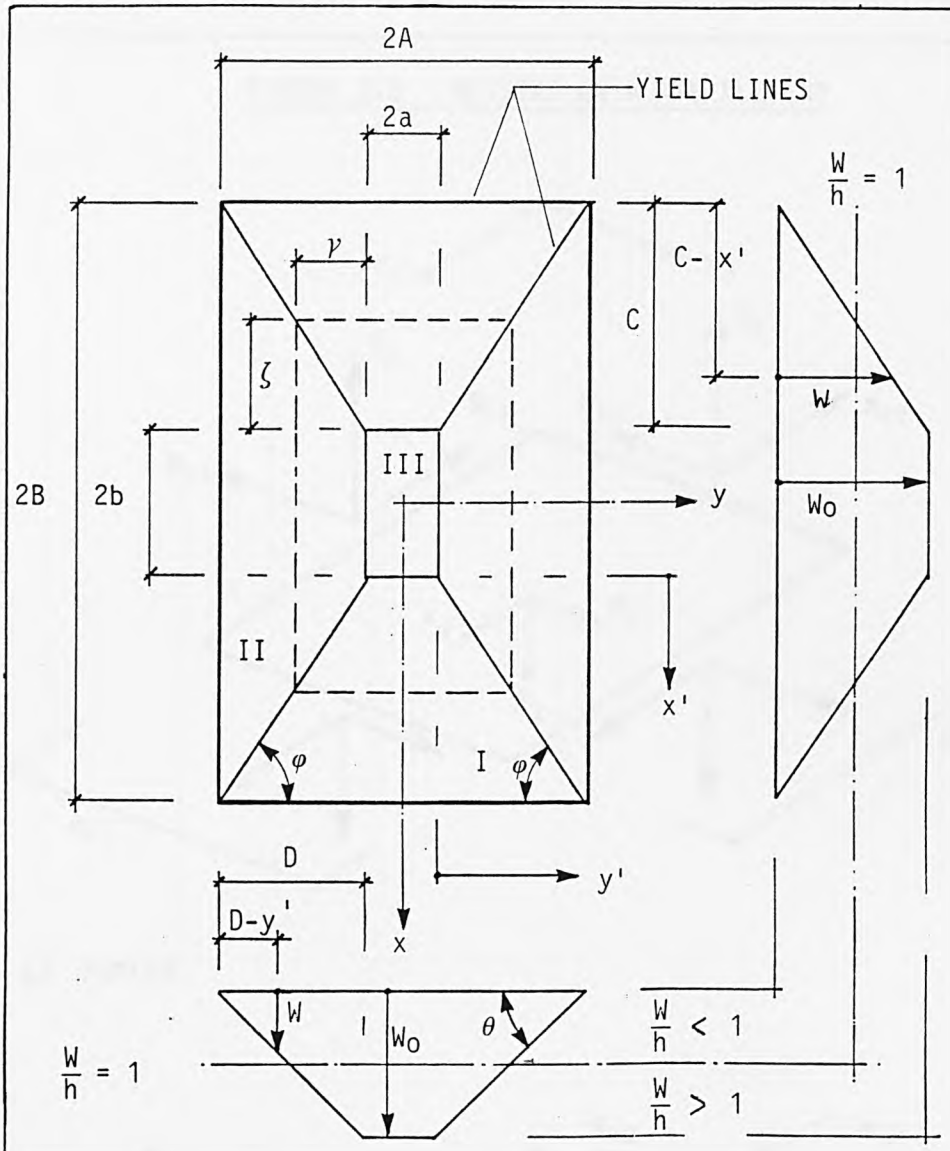

GEOMETRICAL RELATIONSHIPS:

REGION I : $W = \frac{W_o\,(B-b) - x'}{B-b} = \frac{W_o\,(C-x')}{C}$

REGION II : $W = \frac{W_o\,(A-a) - y'}{A-a} = \frac{W_o\,(D-y')}{D}$

REGION III: $W = W_o$

FIGURE 3.2, PLATE COLLAPSE MECHANISM

FIGURE 3.3 ACTIONS ON PLATE ELEMENT

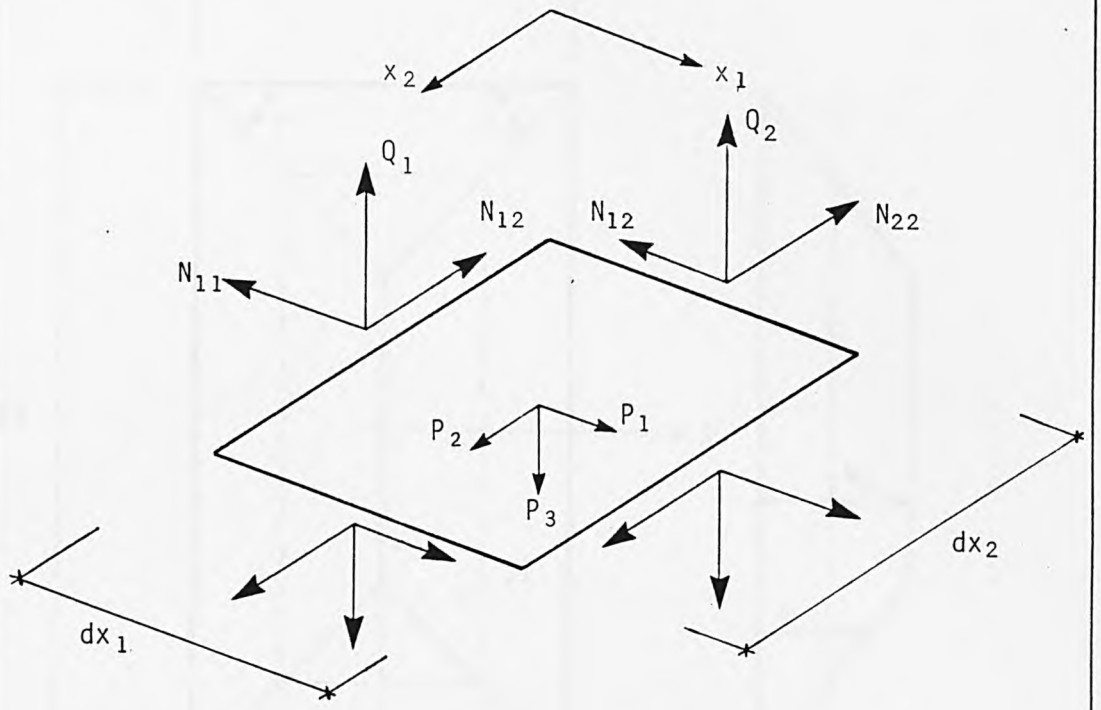

a) FORCES

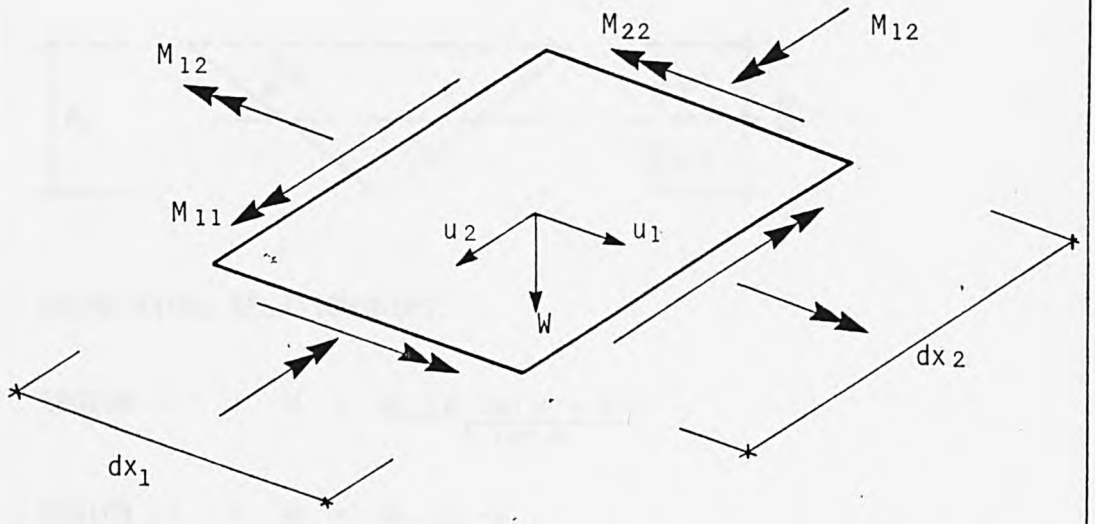

b) MOMENTS AND DEFLECTIONS

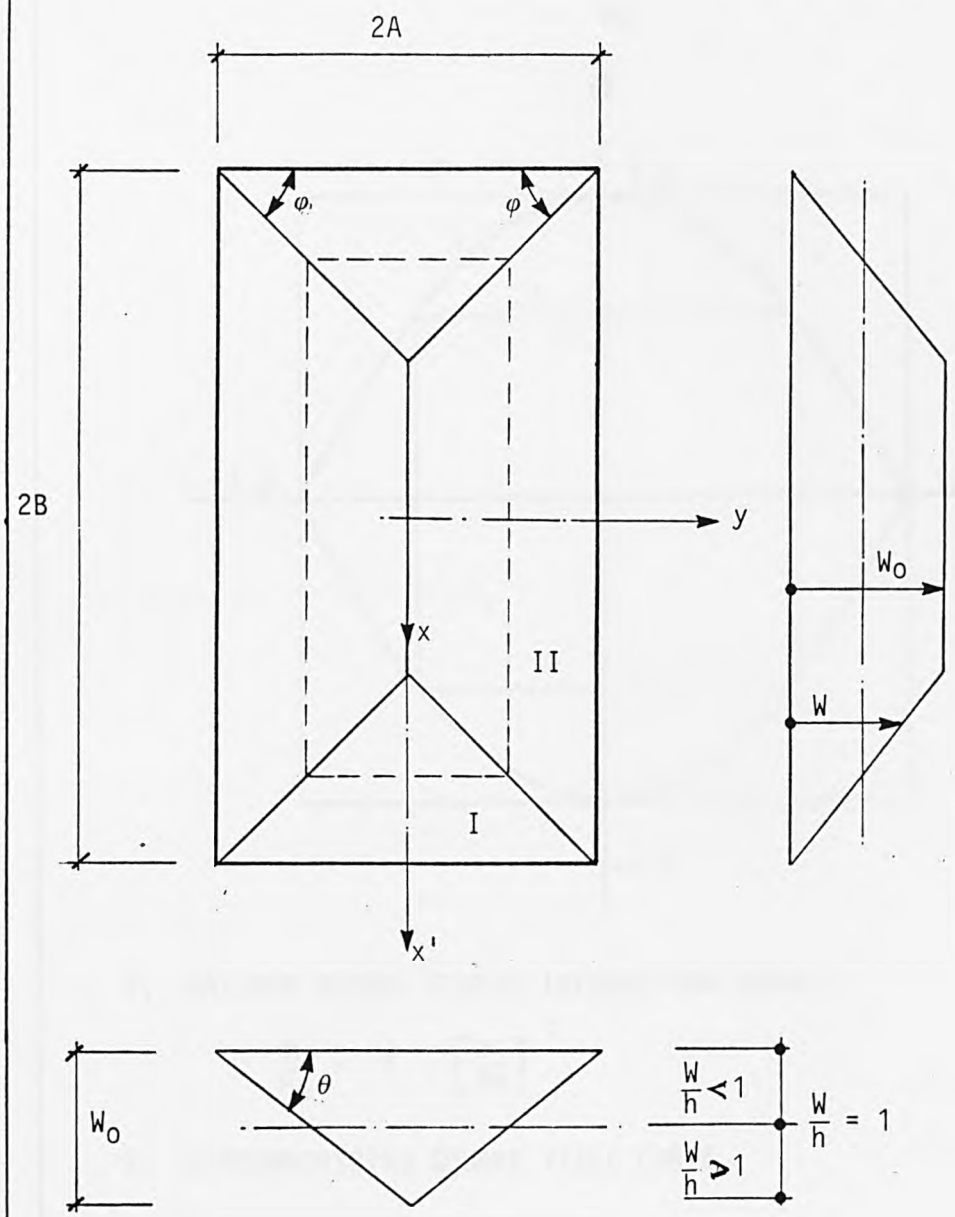

GEOMETRICAL RELATIONSHIPS:

REGION I : $W = \frac{W_o\ (A \tan\varphi - x')}{A \tan\varphi}$

REGION II : $W = \frac{W_o\ (A - y)}{A}$

FIGURE 3.4 U.D.L. COLLAPSE MECHANISM [60]

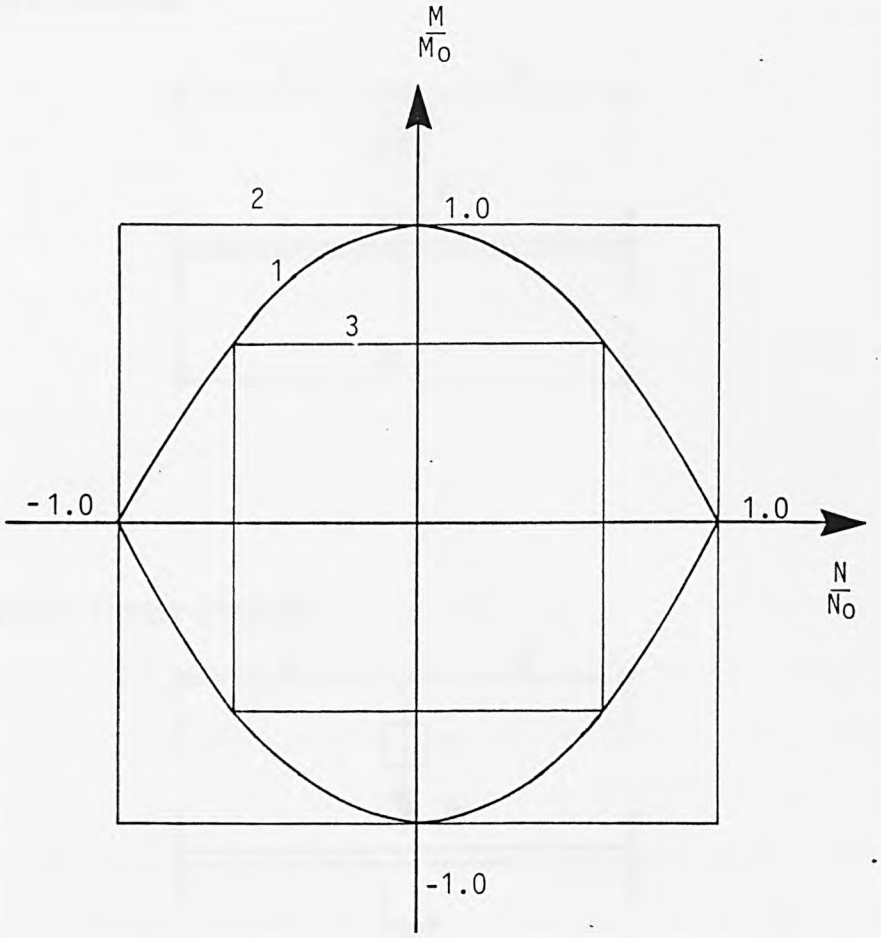

1. MAXIMUM NORMAL STRESS INTERACTION CURVE

$$\frac{M}{M_o} = 1 - \left[\frac{N}{No}\right]^2$$

2. CIRCUMSCRIBING SQUARE YIELD CURVE

3. INSCRIBING SQUARE YIELD CURVE

FIGURE 3.5 YIELD CURVES

a) STATIC LOADING

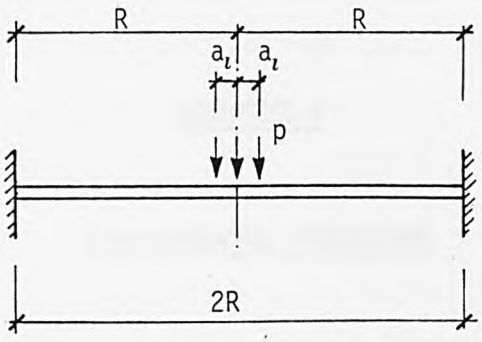

b) MISSILE IMPACT LOADING

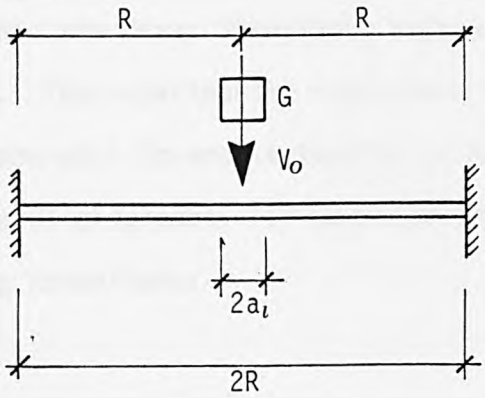

c) COLLAPSE PROFILE

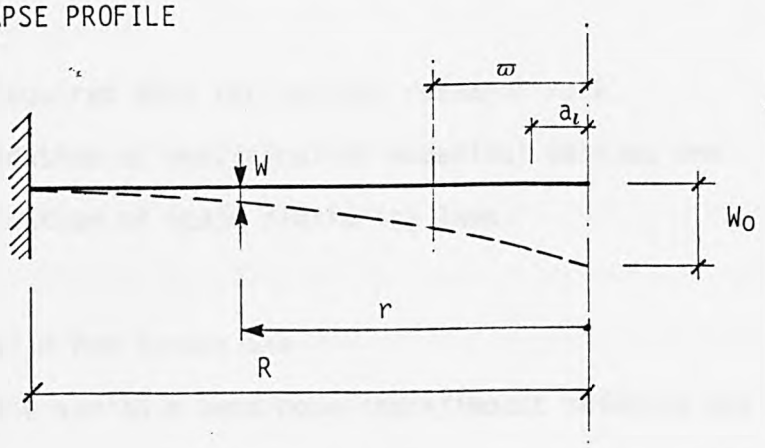

FIGURE 3.6 CIRCULAR PLATE IDEALISATION

CHAPTER 4

EXPERIMENTAL PROGRAMME

4.1 Introduction

This Chapter describes the design and construction of an impact testing facility within the Heavy Structures Laboratory of the Department of Civil Engineering. The experimental requirement was the design and construction of an apparatus to enable testing within the time available for the current research programme. In addition the apparatus needed to satisfy the following conditions:

i) Laboratory space
   a) Height restriction imposed by overhead crane and
   b) Ground area allocation for each research programme.

ii) Provide required data for current research work
   a) Validation of analytical or numerical methods and
   b) Validation of scale similarity laws.

iii) Be versatile for future use
   a) Enable variable mass/nose shape/impact velocity and
   b) Enable variable specimen size/shape/support condition.

iv) Satisfy safety requirements

a) Not endanger personnel within the laboratory and

b) Not transfer damaging shock or vibration to the laboratory environment.

The following sections describe the apparatus designed to satisfy the above requirements and the instrumentation associated with this test facility. Two series of tests comprising of 59 specimens in all and the testing procedure adopted are also described.

4.2 Drop Hammer Apparatus

The drop hammer apparatus is shown in figures 4.1 and 4.2. The structure consists of a steel frame approximately 5m high and 2m wide, which is tied back at three locations to a central laboratory pillar to provide lateral stability.

4.2.1 Guide System

The two vertical mild steel channels shown in figures 4.1(a) and 4.1(c) are adjustable in the horizontal and vertical planes and support the missile guide system. Figure 4.3 shows a section through the guides, which are machined bright mild steel bars, bolted to the steel channels at 300mm centres. The channels are adjusted so that clearance between missile and guide is 3mm ±1mm in both horizontal planes.

The mild steel channels are adjustable in the vertical plane to enable a variety of specimens and specimen supports to be tested. In a typical test, the guide system may be positioned close enough to the specimen so that no possibility exists of the missile coming out of the guides after the impact has occurred.

Repeated impact will occur for a specimen with post impact elastic strain energy capacity (coefficient of restitution >0). This may be overcome by securing the missile after the first impact. This facility was not installed, however, but results given in the next Chapter show this omission to be unimportant in this study.

4.2.2 Missile (Striker)

Two missiles have been fabricated for the purposes of the current research. The general purpose missile was used in 53 of the 59 tests, and a second missile, having low mass, was used in the remaining 6 tests.

4.2.2.1 General Purpose Missile (GPM)

The GPM, shown in figures 4.4 and 4.5, is a welded construction approximately 0.7m long comprising of bright mild steel guides, mild steel stiffening plates and a hardened central core of EN24T steel.

The missile needed to be fairly short to enable the theoretical analyses, developed in Chapter 3, to consider a 'rigid' striker. This is a valid assumption provided the stress wave transit time over the length of the missile is short compared to the impact duration. The resulting force-time history of a typical impact event will exhibit significant 'noise' due to the constantly varying contribution of mass, caused by elastic stress waves within the missile. Since the impact duration is long compared to the elastic stress wave transmission time filtering to a smooth wave form is justified.

The GPM weighs approximately 20kg without addition of weights which can, at present, increase the total mass up to 200kg approximately. The largest mass used in the current tests was 185.92kg. The GPM can be dropped from any height within the frame and the missile nose is detachable to allow variation in contact shape and area. Figure 4.5 shows the GPM with the additional weights available. The markings on the missile are to aid analyses of the high speed film (section 4.4.1.3).

4.2.2.2 Scale Test Missile (STM)

Test series 2 examines the behaviour of mild steel plates at three different scales ($^1/_3$:$^2/_3$:$^3/_3$). From the laws of scale similarity (section 2.6) mass scales according to the scale factor cubed and, therefore, if the full size test has a mass of 200kg, the $^1/_3$ scale test will require a mass of 7.4074kg. The GPM has a mass of approximately 20kg without addition of weights and was thus unsuitable for the $^1/_3$ scale tests.

In view of the above, the STM was built to have a mass of around 7kg. Ultimately the fabricated mass of the STM determined the $^2/_3$ and full scale masses for the scale tests. Figures 4.6 and 4.7 show details of the STM which is of aluminium construction apart from the EN24T hardened steel central core.

4.2.3 Release System

The missile is raised to the required height and released using an electromagnet. The device, which has a lift capacity of approximately 900kg (see figure 4.8), can be seen in figure 4.2. This method was chosen in preference to a mechanical release system as it allowed 'instantaneous' release of the missile from an electronic signal. This satisfies the condition shown in figure 4.28(b) where the time taken for the high speed camera (section 4.4.1.3) to reach operating speed, exceeds the time taken for the missile to reach the specimen after release and, therefore, a signal from the camera is able to release the missile at the required instant of time.

A method, which involved supporting the weight from thin wire and releasing it by passing along the wire a current of sufficient magnitude to burn it through, was also considered. This would have satisfied the 'instantaneous' release requirement, but was discounted for practical and safety reasons.

The electromagnetic release was achieved by reversing the polarity of a 24V D.C. supply to the device. Several problems were encountered during preliminary tests:

i) The lift force generated is proportional to the air gap between magnet and missile top plate (see figure 4.8). The microsecond delay time of release also increases with decreasing air gap. A satisfactory compromise was needed to ensure the magnet released with minimum delay yet safely held the required mass. A machined bright mild steel surface was found to satisfy the requirements.

ii) The reversal of polarity, necessary to release the magnetic field, causes an electro-motive voltage surge to travel through the mains and, to a lesser extent, through the air. This has the effect of triggering other instrumentation in the vicinity or on the same mains system. The problem was significantly reduced by powering the release system from a battery source, but in a few cases, the release system continued to interfere with other apparatus.

4.3 Specimen Support

Different specimen support systems were used for the two test series. At the outset, the lighting requirements for high speed filming of the events were uncertain and the experience gained from Test series 1 resulted in Test series 2 having a more simple and efficient support system.

4.3.1 Test Series 1 Support

The specimen support system used in Test series 1 is shown in figures 4.9 and 4.10. The primary consideration in designing the base was to

provide a fully fixed support for square plates, but at the same time be able to view the deflection-time history of the event using a high speed camera (section 4.4.1.3). The series 1 tests showed that lights placed within the base were just as effective as the arrangement shown in figure 4.9(a) where light shone through side slots in the base. It was necessary to rest the lights on rubber mats to prevent shock breakage on impact when placing them within the base. The lower specimen support plate was bolted to the reinforced concrete base using countersunk bolts.

A 'fixed' edge condition was achieved using 19 high strength friction grip bolts (section 4.3.3). Despite 150mm of the specimen side being effectively unclamped, test results proved this had no significant effect. The base also allowed static testing of specimens on a 'self-reaction' basis. This test set up is shown in figures 4.11(a) and 4.10(b).

4.3.2 Test Series 2 Support

The scale tests in Test series 2 required that three sizes of specimen be tested. In view of the lighting experience gained in test series 1, a single slot in a support would be adequate to view dynamic specimen displacement.

The plate specimens are clamped to massive U.C. steel frames as shown in figures 4.12 and 4.13(a). Three U.C. welded frame constructions were fabricated for the scale tests. Each frame rests on and is clamped to a common reinforced concrete base weighing approximately 4 tonnes. The

number of clamping positions in the reinforced concrete base will allow numerous support frame configurations to be considered.

Edge clamping was again achieved using high strength friction grip bolts, numbering 16, 26 and 35 in the $^{1}/_{3}$, $^{2}/_{3}$ and full size test support frames respectively. Checks on effective clamping were carried out and are discussed in section 4.3.3. Figures 4.11(b) and 4.13(b) show the static test arrangement for Test series 2.

4.3.3 Edge Clamping

The use of high strength friction grip (HSFG) bolts in structural steelwork is documented in BS4604. The bolts are tightened to a predetrermined shank tension so that a clamping force will transmit the force in the connection by friction. The bolts do not act in shear or bearing as in conventional bolted connections since there is no slip or movement between connected parts. The contacting surfaces of the connected parts must be free from oil, grease, burrs, etc.

The bolt pretension requirement is the 'proof load' of the bolt, which is equal to 0.7 times the ultimate load. The pretension can be achieved using torque control methods or load indicating washers (LIW)*. The latter are specifically designed washers having protruding nibs, which are compressed as the bolt is tightened. The suitable compression of these nibs results in the bolt proof load being achieved (see figure 4.14).

* British patent no. 1006452 Messrs. Cooper & Turner, Sheffield.

The correct use of a HSFG bolt and LIW is shown in figure 4.14(a). The LIW should be placed under the stationary component (bolt head) and a hardened steel washer under the moving component (nut). This results in a direct pressure on the nibs plus a very small shear load resulting from the tendency of the bolt to rotate.

Due to the arrangement of the structural support frames only one side of the connection is accessible. The arrangement is shown in figure 4.14(b) and results in a somewhat higher shear load on the nibs. Consequently, the recommended torque for the M20 bolts used (576Nm) is probably too small. For this reason the bolts were tightened to a torque of approximately 600Nm using the LIW visual check and a hand wrench with torque multiplier. Significant clamping is achieved in the specimen connections as no tensile load is applied at the joint and therefore the interface load is equal to the applied bolt load.

The use of HSFG bolts provided excellent clamping in all tests. Dial gauges monitored any slippage of the plates in static tests, figure 4.15. A slight movement was discernable on the gauges which have graduations of 0.01mm. In dynamic tests, once the plates had been fixed, lines were lightly scribed at eight locations around the plate edge, using a special flat edge scriber, figure 4.16. No movement was detectable when checking the scribe lines after each test.

4.3.4 Shock Isolation

Two criteria had to be satisfied in isolating the reinforced concrete block and specimen support frames.

i) The laboratory floor and surrounding environment had to be protected from potentially harmful shock transients and

ii) The behaviour being studied had to be unaffected by support damping.

Isolation was achieved using "TICO CV/LF/B"* low frequency bearings. A typical bearing cross-section and the technical details of bearing properties are shown in figure 4.17.

The principles of shock isolation involve the incorporation of suitable isolators to reduce the shock severity by storage of the shock energy within the isolators and its subsequent release, over a much longer period of time, in a 'smoother' form.

A given shock pulse may contain frequency components ranging from zero to infinity and it is often not possible to avoid excitation of the isolator resonance. If the duration of the shock pulse is short in comparison with one half period of the isolation system resonant frequency, however, the response of the system will be unaffected.

* Manufactured by Tico Ltd., Woking, Surrey.

The combined mass of the concrete base, specimen support and specimen, give a required area of isolating pad ($0.732m^2$) and a pad frequency of approximately 12 Hz if a mean stress of 60 kN/m^2 is assumed. Typical pulse durations in the tests were in the order of 10ms and were, therefore, substantially less than the half period of the isolation system.

The principles of vibration isolation involve the reduction of force transmissibility which may be achieved by selecting an isolation layer whose natural frequency is considerably lower than the lowest frequency of the forcing function. If the duration of the shock pulse is taken as one half period of the lowest frequency component, then this criterion is satisfied. Alternatively if vibration is transferred through elastic vibration of the specimens, the lowest frequency of the plates tested is 41 Hz, table 4.1, and the criteria is once more satisfied. Table 4.1 refers to the plates in undeformed condition. The natural frequencies are likely to increase with permanent deflection as the structure stiffens. Figure 4.1.8 shows the arrangement of isolation pads beneath the concrete base.

4.4 Instrumentation

The following sections describe the instrumentation associated with dynamic and static testing of plate specimens.

4.4.1 Impact Tests

Two types of data are of interest in impact testing and these are

i) Static measurements which involve physical measurements of a system state before and after impact has occurred. Generally these measurements provide no significant data handling difficulties.

ii) Dynamic measurements which involve the histories of system state over every short periods of time. These measurements may often require sophisticated expensive instrumentation.

It is considered important to obtain as much information as possible during an impact experiment. Once plastic deformation or failure has taken place, the experiment cannot be repeated.

Electronic data retrieval methods are usually chosen to satisfy economic as well as practical requirements. During dynamic measurement each transducer will require conditioning and recording before data analysis is carried out.

4.4.1.1 Static Displacement Profile

The permanent deflection profile of each specimen was measured using the depth gauge shown in figures 4.19 and 4.20. The instrument incorporates a 'horizontal travel' vernier gauge with resolution of 0.1mm. The bar is of sufficient length to measure the profile across any section of the test specimens.

4.4.1.2 Missile Velocity

The velocity of the missile was measured just prior to impact for all tests. Two different schemes were tried for this purpose:

i) Mechanical reed switches.

Two reed switches were placed at a known distance apart near the lower end of the guide system. The lower switch was positioned so that the magnet attached to the missile triggered the switch just before the missile hit the plate. The upper switch was positioned relative to the lower switch. The upper and lower switches started and stopped an electronic timer with a resolution of 10^{-5} seconds. The ratio of the distance between the two switches and the time recorded gave the mean value of the missile speed for the distance. This value was taken as the impact speed of the missile.

ii) Photocells.

A set of photocells, one a source of light and the other a receiver, were placed across the guide system to form a light beam. The passage of the missile cut the beam and triggered the timer. The timer stopped when the missile had passed completely and the light beam was restored. The length of missile 'cutting' the beam divided by the time taken gave a measure of impact velocity.

In preliminary tests both systems gave almost identical estimates of missile velocity. The reed switches were finally selected because

the photocells were sensitive to the light of the environment as well as the light required for the high speed filming which was to be used in several of the tests. The reed switch arrangement can be seen in figure 4.21.

4.4.1.3 Dynamic Displacement

The displacement time history of the missile and specimen motions were obtained using a Hadland high speed rotating prism camera capable of filming at speeds up to 10000 frames per second. In order to capture the event at the required framing speed, allowance has to be made for the time taken for the camera to reach operating speed (see figure 4.28).

Figure 4.22 shows the position of the camera in relation to the specimen and figure 4.23 shows how the camera was set up to ensure horizontal alignment of the line of sight. The quality of film was found to be superior when the underside of the test specimens was painted white with a black background.

For real time correlation of the film, an electronic pulse generator deposited timing marks on the film at a pre-set rate (e.g. 1000/sec). For subsequent analysis of each film, various datum points and markers were placed on the rig, missile and base.

A film analysis facility is required to efficiently obtain accurate information from high speed film. The system shown in figure 4.24 was used for this purpose. The apparatus consists of a pin registered analysis projector with frame counter and single frame advance operation. The film is projected onto a screen, above which a sonic

digitiser is situated. The digitiser, which measures coordinate positions anywhere on the screen is interfaced with a BBC microcomputer. The complete system allows fast, efficient digitising of up to ten points on each frame. Graphical output options include particle displacement, velocity and acceleration.

The information obtained from the current test series films, included missile velocity (as a further check to systems described in section 4.4.1.2), plate displacement, missile bounce height and time between missile bounces.

4.4.1.4 Dynamic Strain

The time histories of strain at various locations across the plate surface was measured on most specimens. Two types of wire resistance strain gauge were used

Standard: Gauge Factor 2.14 Resistance 120 $\Omega \pm 0.3$

High Yield: Gauge Factor 2.11 Resistance 120 $\Omega \pm 0.3$

The use of high yield gauges was only necessary in regions close to the impact. The standard gauges give 0.1% accuracy up to 4000 $\mu\varepsilon$, 1% accuracy up to 10000 $\mu\varepsilon$ and have a breaking strain of about 25000 $\mu\varepsilon$.

The signal from each strain gauge requires a separate channel for amplification and recording during the short event time involved. The recording equipment will, therefore, determine the number of transducers which may be used in any one test.

The analogue signal from each gauge may be recorded in analogue form, or converted "on-line" to digital form before recording. Two systems were considered to record dynamic strain gauge data:

i) Compulog IV 16 channel analogue to digital converter linked to PDP-11 minicomputer and a

ii) RACAL 14 channel magnetic tape recorder.

The Compulog system sequentially scans data channels with a 25 kHz maximum scan rate for dual channels. When more channels are used and impact times are of the order of 10ms, this system is clearly not fast enough to obtain meaningful transducer signals.

The strain signals were, therefore, recorded in analogue form using the multi-channel magnetic tape recorder. The recorder incorporates frequency modulation recording and can produce a signal bandwidth of D.C. to 40kHz at a tape speed of 60 in/sec. Eight different tape speeds are available resulting in the ability to record at one speed and playback at another and, therefore, expand or contract the data time scale.

The recorded strain gauge signals were subsequently output using a "Bryan IV" dual channel X-Y plotter.

The strain measuring system (gauge, amplifier, recorder, plotter), was calibrated using cantilever beams cut from the specimen material. The procedure for each cantilever beam (two beams for each gauge type) was to incrementally load the cantilever and, at each increment, record

the signal on tape and take a direct reading of strain. This was carried out for several amplifier settings, tape record levels and plotter output settings. A typical calibration chart and details of the calibration beams, is shown in figure 4.25. Table 4.2 shows the chart for Y-axis interpretation of plotter output, incorporating variables of amplifier setting, tape record level and plotter output level.

The time scale calibration was carried out using a signal generator. The resulting chart for X-axis interpretation of plotter output is shown in table 4.3 where the variables are tape record speed, tape playback speed and the paper speed through the plotter.

Problems were encountered with the gauges placed closest to the impact in regions of highest strain. On several occasions the gauge adhesive failed as a result of the local strain level or, alternatively, signal amplifier overload occured for the same reason. Most gauge readings, however, were obtained successfully. The information available from each gauge includes maximum strain, maximumm permanent strain, number of missile impacts, time between impacts, initial strain rate and elastic vibration frequency.

4.4.1.5 Acceleration Measurements

The acceleration time-history of the impact was measured using a piezoelectric accelerometer. Such an instrument outputs a charge signal proportional to the acceleration to which it is subjected for frequencies from D.C. up to approximately one third of its resonant frequency. The

selected transducer could measure accelerations up to 10000g and had a resonant frequency of 50 kHz. The accelerometer and coaxial connecting cable can be seen in figure 4.21.

The charge signal is converted to voltage using a charge amplifier with two low impedence outputs available simultaneously, both producing voltage proportional to acceleration. The voltage signal was subsequently recorded on a 'Gould 4035' dual channel digital storage osciloscope. This instrument incorporated pre-trigger, signal magnification and filtering facilities and was interfaced with a BBC microcomputer to obtain printout and disc storage of the suitably filtered signal. The set up is shown in figure 4.26.

In test series 1 the accelerometer was mounted at the far end of the missile and away from the point of impact (see figure 4.4). Initially problems were encountered with the trace exhibiting 'zero shift' characteristics, due to either the transducer retaining charge after the impact, or the high frequency components in the signal overloading the charge amplifier. The problem was solved by changing the sensitivity setting of the transducer on the charge amplifier i.e. for a transducer with 7.71 pc/g sensitivity, setting the charge amplifier to 77.1 pc/g will effectively decrease the sensitivity by a factor of 10. Good results were obtained for all test series 1 specimens apart from three occasions when the magnetic release device (section 4.2.3) triggered the oscilloscope.

The basic signal is extremely 'noisy' due to stress waves within the missile. The signal was filtered using the facility incorporated in the

digital oscilloscope and, therefore, peak values of acceleration associated with the impact were lost. These are unimportant, however, if they do not cause material failure. From the filtered acceleration time history, an estimation of force-time history can be obtained by assuming the missile to be rigid and using Newton's 2nd Law. This is a valid assumption provided the stress wave transit time within the missile is short compared to the impact duration. This was the case in all tests in the current research.

In test series 2 an attempt was made to mount the accelerometer beneath the specimens since it was thought that the effects of noise might be reduced, figure 4.27. A number of difficulties arose as a result of the change of accelerometer position.

An attempt was made to overcome these difficulties by observing the signal direct from the accelerometer. It was concluded that the charge amplifier was continuously overloading. This was due to the high frequency content in the signal caused by the short distance between impact and transducer. In an attempt to overcome this, a resistor was placed 'on-line' to filter the signal before it passed through the charge amplifier. This arrangement caused the charge amplifier to retain charge and so exhibit a zero shift on output. The problem was not fully solved and sensible readings were obtained only when the transducer was returned to its original missile location.

4.4.1.6 Instrumentation Synchronization

In experimental work involving impact, accurate synchronization

between various pieces of equipment is vital due to the short durations involved. It should be noted that the film time (for the high speed camera) is split into the time it takes the camera to reach operating speed and the time remaining when the film runs at constant speed. It is desirable that the impact event occurs during the latter period.

Figures 4.28(a) and 4.28(b) show schematically the required interlinking between the photographic equipment, the release mechanism and the recording equipment for the case when the missile drop time exceeds the camera time to reach constant speed and vice versa.

4.4.2 Static Tests

The support frames which were used allowed static testing of specimens by loading plates from the underside, figure 4.11. Depending on specimen thickness, either a 10 ton or a 30 ton hydraulic jack was used. Jack specifications are given in table 4.4.

The fully clamped edge condition was monitored using dial gauges, figure 4.10. Strains at various locations across the specimen surface were measured using the gauges described in section 4.4.1.4. The value of strain from the "TDS digital strain meter" recording system is converted to actual strain using the formula:

$$\epsilon = \frac{2.00}{Kg} \cdot \epsilon r_e$$

where K_g = gauge factor of strain gauge.

ϵr_e = recorded strain value.

ϵ = actual strain value.

The strain gauge configurations used are shown in figures 4.29.

4.5 Description of Tests

4.5.1 Test Series 1

Thirty six fully clamped square mild steel plates, with 0.6m x 0.6m clear opening, were tested using the base shown in figures 4.9 and 4.10. Thirty were impact tests and six were static tests. Six different plate thicknesses were impacted with various mass configurations dropped from heights up to 3m. The missile nose shape was flat cylindrical in all cases. The test series details are shown in table 4.5 and strain gauge configurations are shown in figure 4.29.

4.5.2 Test Series 2

Twenty three fully clamped square mild steel plates, at three different scales ($\frac{1}{3}, \frac{2}{3}, \frac{3}{3}$), were tested using the support system shown in figures 4.12 and 4.13. Fifteen were impact tests and eight were

static tests. The full size test specimen had a 0.9m x 0.9m clear opening. The loaded area was also scaled using the hardened steel plate arrangement shown in figure 4.27. The mass was constant for each scale, while the drop height was varied. Details of series 2 tests and strain gauge configurations used, are shown in table 4.6 and figure 4.29, respectively.

4.5.3 Material Tests

The properties of the plate material were determined by conducting tensile tests on specimens fabricated in accordance with BS18 Parts 2 and 3. In each case the specimens were cut from the same sheet as the plates. For each thickness, two tensile tests were carried out for series 1 plates and three tensile tests for series 2 tests.

The yield stress for each thickness was taken as the average of values obtained from each specimen. The yield stress was defined as the load at which significant strain occurred, divided by the original cross sectional area of the section thus the "lower" yield stress value. Table 4.7 gives a summary of the test results.

The density of each material was determined from the rectangular specimens cut for the purposes of tensile tests i.e. before cutting to shape. Each specimen was carefully measured and weighed to enable calculation of density. The results are shown in table 4.8.

4.6 Test Procedure

4.6.1 Impact Tests

The drop tests were carried out in the following manner

i) Assemble appropriate mass onto missile.

ii) Ensure accelerometer seating is tight.

iii) Raise missile to above safety bar.

iv) Align high speed camera and load film.

v) Rest specimen in position and wire strain gauges.

vi) Clamp down specimen by sequential tightening of bolts.

vii) Measure undeformed profile of specimen.

viii) Select instrumentation settings i.e. oscilloscope, tape recorder, etc.

ix) Raise weight to required height, check all equipment, remove safety bar and drop, and finally

x) Measure permanent profile of deformed specimen.

Readings from strain gauges were taken at steps v) and vi). It was concluded that strains induced due to clamping of the specimen were insignificant.

4.6.2 Static Tests

The static test procedure varied slightly depending on whether

load-deflection or load-permanent deflection was being measured. In the former case step vi) is omitted.

i) Place jack beneath specimen so that minimum gap exists with jack in fully depressed condition i.e. enabling maximum jack travel.

ii) Rest specimen in position and wire gauges.

iii) Clamp down specimen with sequential bolt tightening.

iv) Position dial gauges, take initial readings.

v) Apply increment of load, read dial gauges, take strain readings.

vi) Release load, read dial gauges and take strain readings.

vii) Apply next increment of load and repeat.

Strain readings taken at steps ii) and iii) again showed that strains induced through clamping of the plate were insignificantly small.

TABLE 4.1 PLATE NATURAL FREQUENCIES

TEST SERIES 1

Thickness (mm)	Size (mm)	ρ (kg/m^3)	w_n (rads/sec)	f (Hz)	T (ms)
1.638	600 x 600	7688	258.99	41.22	24.3
2.045	600 x 600	7761	321.82	51.22	19.5
2.466	600 x 600	7798	387.15	61.62	16.2
3.107	600 x 600	7761	488.94	77.82	12.8
4.02	600 x 600	7787	631.56	100.52	9.9
5.111	600 x 600	7765	804.1	128.0	7.8

TEST SERIES 2

Thickness (mm)	Size (mm)	ρ (kg/m^3)	w_n (rads/sec)	f (Hz)	T (ms)
2.0	300 x 300	7682	1265.41	201.4	5.0
3.95	600 x 600	7624	627.17	99.82	10.0
6.03	900 x 900	7677	424.05	67.49	14.8

NOTE:

All edge conditions fully clamped.

TABLE 4.2 STRAIN GAUGE OUTPUT INTERPRETATION

PLOTTER Y-AXIS (STRAIN MAGNITUDE)

Amplifier Setting	Tape Record Level (volts peak)	Strain Values ($\mu\epsilon$) for Plotter Settings: (mv/cm)				
		100	50	10	5	2
30	1	195	97.5	19.5	9.75	3.9
	2	390	195	39.0	19.5	7.8
	5	975	487.5	97.5	48.75	19.5
	10	1950	975	195.0	97.5	39.0
36	1	390	195	39	19.5	7.8
	2	780	390	78	39	15.6
	5	1950	975	195	97.5	39.0
	10	3900	1950	390	195	78.0
42	1	780	390	78	39	15.6
	2	1560	780	156	78	31.2
	5	3900	1950	390	195	78
	10	7800	3900	780	390	156
48	1	1560	780	156	78	31.2
	2	3120	1560	312	156	62.4
	5	7800	3900	780	390	156
	10	15600	7800	1560	780	312
54	1	3120	1560	312	156	62.4
	2	6240	3120	624	312	124.8
	5	15600	7800	1560	780	312
	10	31200	15600	3120	1560	624

TABLE 4.3 STRAIN GAUGE OUTPUT INTERPRETATION

PLOTTER X-AXIS (TIME)

Tape Record Speed (in/sec)	Tape Playback Speed (in/sec)	Plotter Paper Speed (sec/mm)	Real Time Output	
			sec/cm	ms/cm
60	15/16	0.5	0.078125	78.125
		0.2	0.03125	31.25
		0.1	0.015675	15.625
60	15/8	0.5	0.15625	156.25
		0.2	0.0625	62.5
		0.1	0.03125	31.25
60	15/4	0.5	0.3125	312.5
		0.2	0.125	125.0
		0.1	0.0625	62.5
60	15/2	0.5	0.625	625.0
		0.2	0.250	250.0
		0.1	0.125	125.0
30	15/16	0.5	0.15625	156.25
		0.2	0.0625	62.5
		0.1	0.03125	31.25
30	15/8	0.5	0.3125	312.5
		0.2	0.125	125.0
		0.1	0.0625	62.5

TABLE 4.4 STATIC TEST JACK DATA

JACK SPECIFICATIONS:

10 Ton: Capacity - 99KN, 22360 lbs.
Stroke - 6.12 ins
Eff. Area - 2.24 in^2, 14.45 cm^2

30 Ton: Capacity - 321KN, 72160 lbs.
Stroke - 2.5 ins
Eff. Area - 7.22 in^2. 46.58 cm^2

Pressure Dial Reading (lb/in^2)	10 Ton Jack		30 Ton Jack	
	Load (lbs)	Load (N)	Load (lbs)	Load (N)
500	1120	4981.8	3610	16057.3
1000	2240	9965.5	7220	32114.6
1500	3360	14945.3	10830	48171.8
2000	4480	19927.0	14440	64229.1
2500	5600	24908.8	18050	80286.4
3000	6720	29890.6	21660	96343.7
3500	8740	34872.3	25270	112400.7
4000	8960	39854.1	28880	128458.2
4500	10080	44835.8	32490	144515.5
5000	11200	49817.6	36100	160572.8
5500	12320	54799.4	39710	176630.1
6000	13440	59781.1	43320	192687.4
6500	14560	64762.9	46930	208744.6
7000	15680	69744.6	50540	224801.9
7500	16800	74726.4	54150	240859.2
8000	17920	79708.2	57760	256916.5
8500	19040	84689.9	61370	272973.8
9000	21280	94653.4	68590	305088.3
10000	22400	(99635.2)	72200	(321145.6)

TABLE 4.5 TEST SERIES 1 DATA

Test Type: S - Static
D - Dynamic

Strain Gauge ref: see Figure 4.29.

Test	Type	Mass (kg)	Height (m)	Strain Gauge ref	High Speed Film	Jack Capacity
A1	D	27.4	1.5	E	Yes	-
A2	D	27.4	0.5	E	No	-
A3	D	27.4	1.0	E	Yes	-
A4	D	27.4	2.0	D	No	-
A5	D	54.8	0.5	D	No	-
A6	S	-	-	C	-	10T
A1-A6: h = 1.638mm			σ_y = 340N/mm^2 ρ = 7688kg/m/^{3}			
B1	D	32.8	1.5	D	No	-
B2	D	32.8	2.0	D	Yes	-
B3	D	32.8	2.5	E	No	-
B4	D	32.8	1.0	E	Yes	-
B5	D	32.8	0.5	D	No	-
B6	S	-	-	C	-	10T
B1-B6: h = 2.045mm			σ_y = 240N/mm^2 ρ = 7761kg/m^3			
C1	D	37.5	2.75	E	No	-
C2	D	32.1	2.75	E	No	-
C3	D	25.7	2.75	F	Yes	-
C4	D	22.0	2.75	E	No	-
C5	D	41.2	2.75	F	Yes	-
C6	S	-	-	C	-	10T
C1-C6: h = 2.466mm			σ_y = 290N/mm^2 ρ = 7798kg/m^3			

ALL PLATES: Clamped Edge Condition
900mm x 900mm (Overall specimen size)
600mm x 600mm (dimensions 2A x 2B)

(Contd.)

TABLE 4.5 (Contd.)

Test	Type	Mass (kg)	Height (m)	Strain Gauge ref.	High Speed Rim	Jack Capacity
D1	D	43.9	2.0	D	No	-
D2	D	43.9	1.5	E	No	-
D3	D	43.9	1.0	E	Yes	-
D4	D	43.9	2.5	F	No	-
D5	D	43.9	2.75	E	Yes	-
D6	S	-	-	B	-	30T
D1-D6: h = 3.107mm				σ_y = 300N/mm^2 ρ = 7761kg/m^3		
E1	D	51.3	3.0	F	No	-
E2	D	51.3	2.5	E	Yes	-
E3	D	51.3	2.0	E	No	-
E4	D	51.3	1.5	E	Yes	-
E5	D	76.5	2.0	F	No	-
E6	S	-	-	A	-	30T
E1-E6: h = 4.02mm				σ_y = 314N/mm^2 ρ = 7787kg/m^3		
F1	D	51.3	3.0	D	No	-
F2	D	40.5	3.0	E	Yes	-
F3	D	62.1	3.0	F	No	-
F4	D	72.9	3.0	E	Yes	-
F5	D	79.4	3.0	D	No	-
F6	S	-	-	C	-	30T
F1-F6: h = 5.111mm				σ_y = 280N/mm^2 ρ 7765kg/m^3		

ALL PLATES: Clamped Edge Condition.
900mm x 900mm (Overall specimen size)
600mm x 600mm (dimensions 2A x 2B)

TABLE 4.6 TEST SERIES 2 DATA

Test Type: S - Static
D - Dynamic

Strain Gauge ref:
See Figure 4.29

Test	Type	Mass (kg)	Height (m)	Strain Gauge ref.	High Speed Film	Jack Capacity
S1	D	6.886	1.0	D	No	-
S2	D	6.886	1.5	D	No	-
S3	D	6.886	2.0	D	No	-
S4	D	6.886	2.5	D	Yes	-
S5	D	6.886	3.0	D	Yes	-
S6	S	-	-	-	-	10T
S1-S6:	h = 2.0mm $2A \times 2B$ = 300mm x 300mm β = 1/3			σ_y = 285N/mm^2 ρ = 7682kg/m^3		
M1	D	55.09	1.0	D	No	-
M2	D	55.09	1.5	D	No	-
M3	D	55.09	2.0	D	No	-
M4	D	55.09	2.5	D	Yes	-
M5	D	55.09	3.0	D	Yes	-
MS31	S	-	-	C	-	30T
MS32	S	-	-	C	-	30T
MS41	S	-	-	C	-	30T
MS42	S	-	-	C	-	30T
MS51	S	-	-	C	-	30T
MS52	S	-	-	C	-	30T
MS61	S	-	-	C	-	30T
MS62	S	-	-	C	-	30T
M1-M5: MS41,MS42	h = 3.95mm $2A \times 2B$ = 600mmm x 600mm β = 2/3			σ_y = 260N/mm^2 ρ = 7624kg/m^3		
MS31,MS32:	h = 3.04mm			σ_y = 293N/m^2 ρ = 7722kg/m^3		
MS51,MS52:	h = 5.07mm			σ_y = 306N/m^2 ρ = 7700kg/m^3		
MS61,MS62:	h = 6.03mm			σ_y = 255N/m^2 ρ = 7677kg/m^3		

...(Contd.)

TABLE 4.6 (Contd.)

Test	Type	Mass (kg)	Height (m)	Strain Gauge Ref.	High Speed Film	Jack Capacity
L1	D	185.92	1.0	D	No	-
L2	D	185.92	1.5	D	No	-
L3	D	185.92	2.0	D	No	-
L4	D	185.92	2.5	D	Yes	-
L5	D	185.92	3.0	D	Yes	-
L6	S	-	-	-	-	30T
L1-L6:		$h = 6.63mm$ $2A \times 2B = 900mm \times 900mm$ $\beta = 1$		$\sigma_y = 255N/mm^2$ $\rho = 7677kg/m^3$		

TABLE 4.7 MATERIAL TENSILE TESTS

TESTS CARRIED OUT ACCORDING TO BS18, Parts 2 and 3.
MILD STEEL SPECIMENS TO BS4360 Grade 43a and BS1449 HRI5

SPECIMEN:

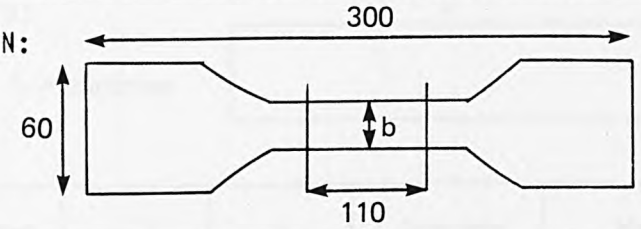

Dimensions in mm.

Test	Average b (mm)	Average h (mm)	Yield Load (N)	Yield Stress (N/mm^2)	Ult. Load (N)	Ult. Stress	σ_y AV.
Series 1							
1	15.0	1.642	8305	338	9986	406	
							340
2	15.0	1.633	8403	342	10088	411	
3	15.0	2.04	7393	241	9585	312	
							240
4	15.0	2.049	7331	239	9964	325	
5	14.97	2.465	10521	285	13566	367	
							290
6	14.97	2.467	10890	295	13592	368	
7	14.98	3.107	13688	294	19883	427	
							291
8	14.98	3.108	13407	288	20105	432	
9	15.05	4.01	19179	317	25932	429	
							314
10	15.05	4.03	18816	311	25531	422	
11	15.05	5.127	22223	288	30335	394	
							280
12	15.0	5.095	20788	272	29768	387	
Series 2							
1	14.9	6.05	23219	258	37808	419	
2	14.9	6.02	23130	256	38164	423	255
3	14.9	6.02	22676	251	38342	425	
4	14.95	5.07	23708	312	31447	414	
5	15.0	6.07	23218	305	32026	421	305
6	14.9	5.07	22663	298	31092	409	
7	14.95	3.95	15590	264	22507	381	
8	14.9	3.95	15591	264	22240	377	260
9	14.9	3.95	14881	252	21706	368	
10	16.0	3.05	13498	296	19689	432	
11	15.1	3.02	13776	301	19617	430	293
12	15.0	3.05	13133	288	19971	438	
13	15.0	2.0	8490	283	10939	365	
14	15.02	2.0	8490	283	11035	368	285
15	14.95	2.0	8670	289	11021	367	

TABLE 4.8 MATERIAL DENSITY DATA

MILD STEEL SPECIMENS TO BS4360 Grade 43A and BS1449 HR15

SPECIMEN:

h = thickness

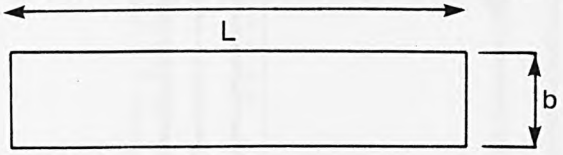

Specimen	L (mm)	b (mm)	Average h (mm)	Mass (g)	ρ (kg/m^3)	ρ_{AV}
Series 1						
1	500.8	60.0	1.642	378.5	7666	
						7687
2	501.0	60.1	1.633	378.5	7709	
3	501.2	60.1	2.04	476.0	7762	
						7761
4	501.0	60.0	2.049	478.0	7760	
5	501.1	59.9	2.465	576.0	7774	
						7798
6	501.0	60.0	2.467	580.0	7822	
7	501.0	59.8	3.107	724.0	7753	
						7761
8	500.8	59.9	3.108	726.0	7770	
9	500.9	60.1	4.01	936.0	7765	
						7787
10	501.0	60.0	4.03	946.0	7809	
11	500.9	60.1	5.127	1194.0	7748	
						7765
12	500.9	60.0	5.095	1192.0	7783	
Series 2						
1	401.7	46.23	6.05	858	7637	
2	401.6	46.1	6.02	857	7689	7677
3	401.5	46.02	6.02	857	7705	
4	401.3	46.4	5.07	728	7678	
5	401.0	46.55	5.07	730	7714	7700
6	400.8	46.6	5.07	730	7709	
7	401.7	46.75	3.95	566	7630	
8	401.4	46.65	3.95	563	7612	7624
9	401.2	46.8	3.95	566	7631	
10	400.5	46.52	3.05	439	7725	
11	401.0	46.42	3.02	434	7720	7722
12	400.7	46.52	3.05	439	7722	
13	400.7	44.0	2.0	271	7685	
14	400.7	44.05	2.0	272	7705	7682
15	399.7	44.28	2.0	271	7656	

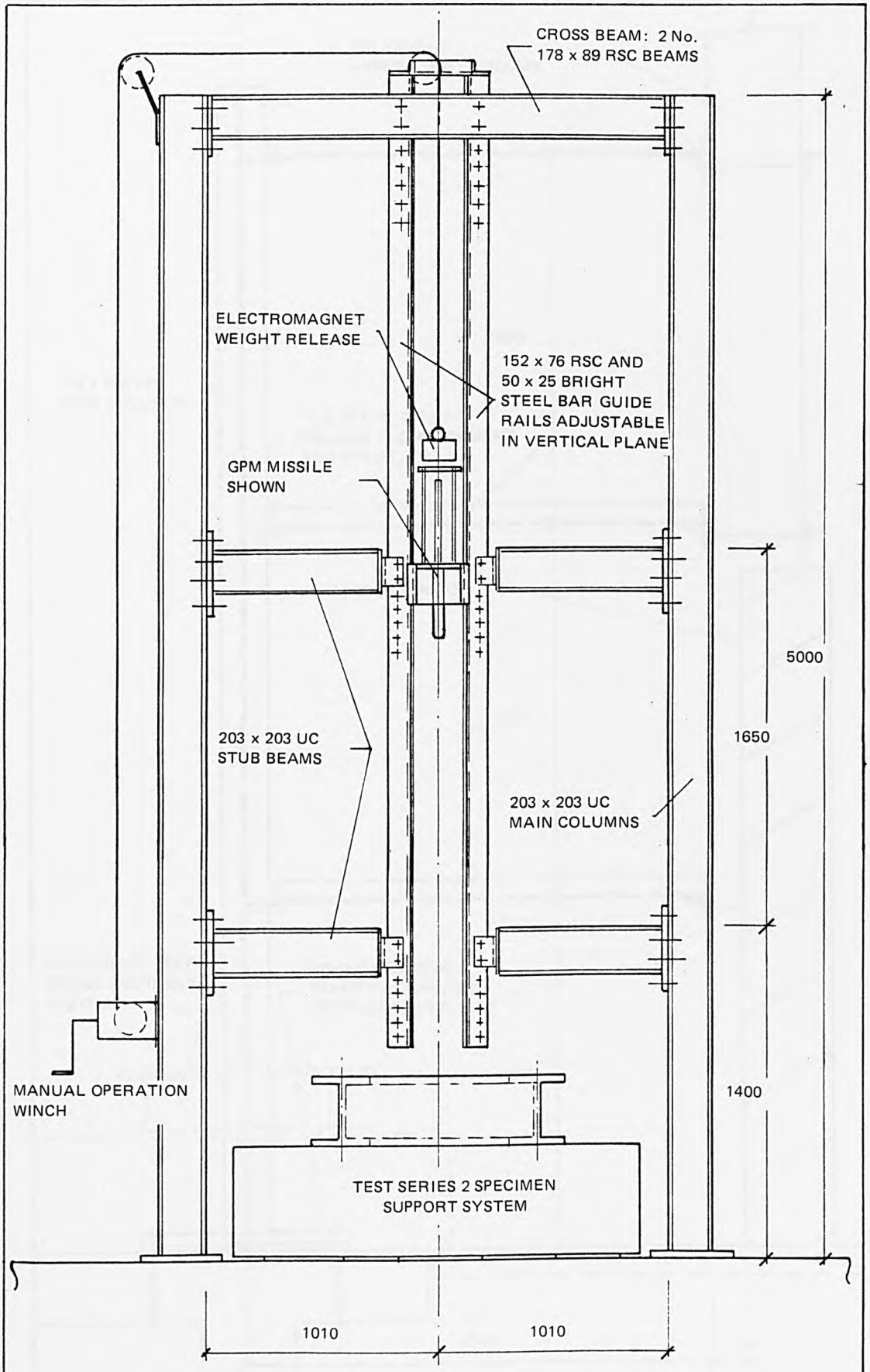

FIGURE 4.1(a) FRONT ELEVATION TO DROP RIG

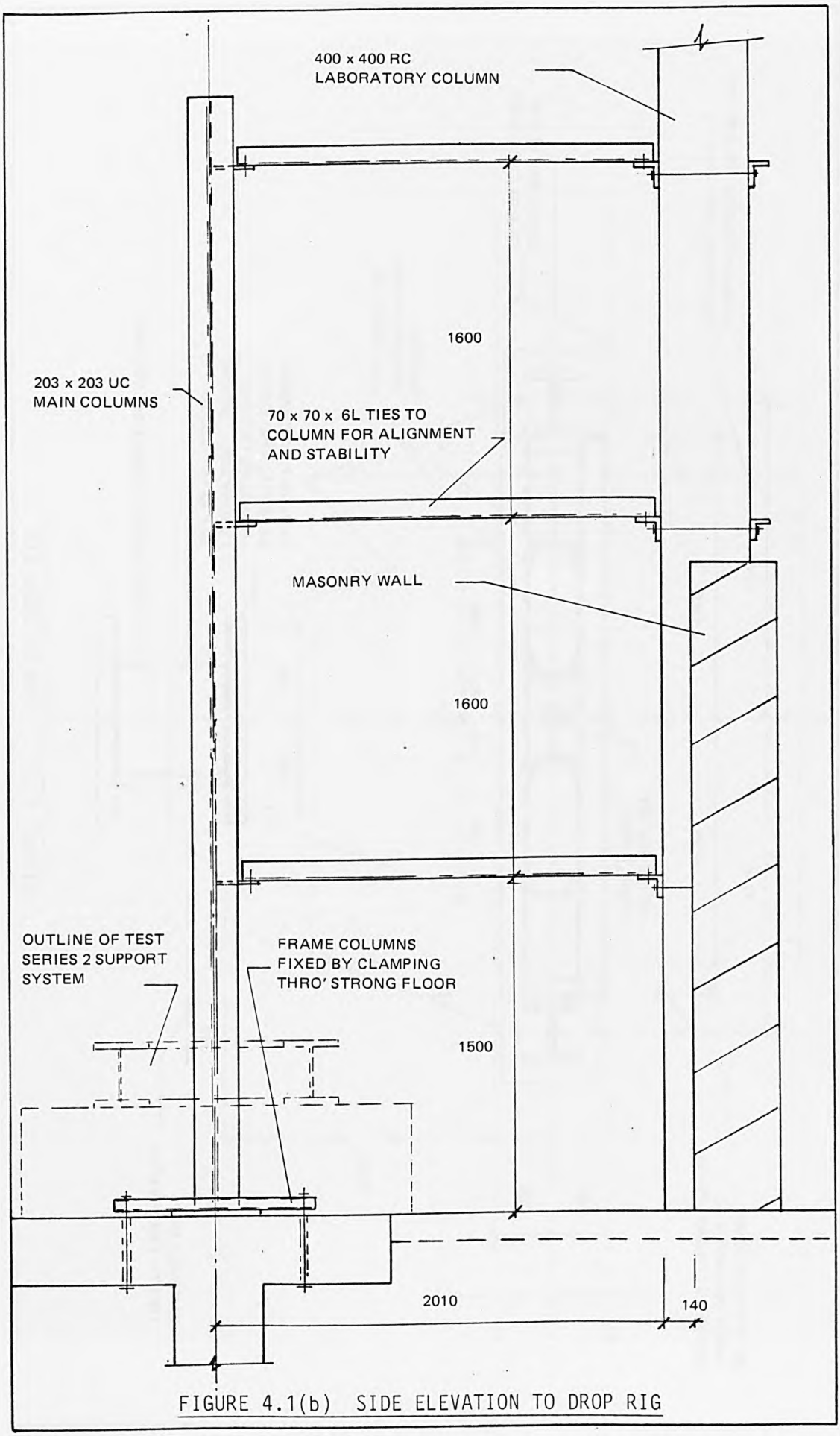

FIGURE 4.1(b) SIDE ELEVATION TO DROP RIG

FIGURE 4.1(c) PLAN ON DROP RIG

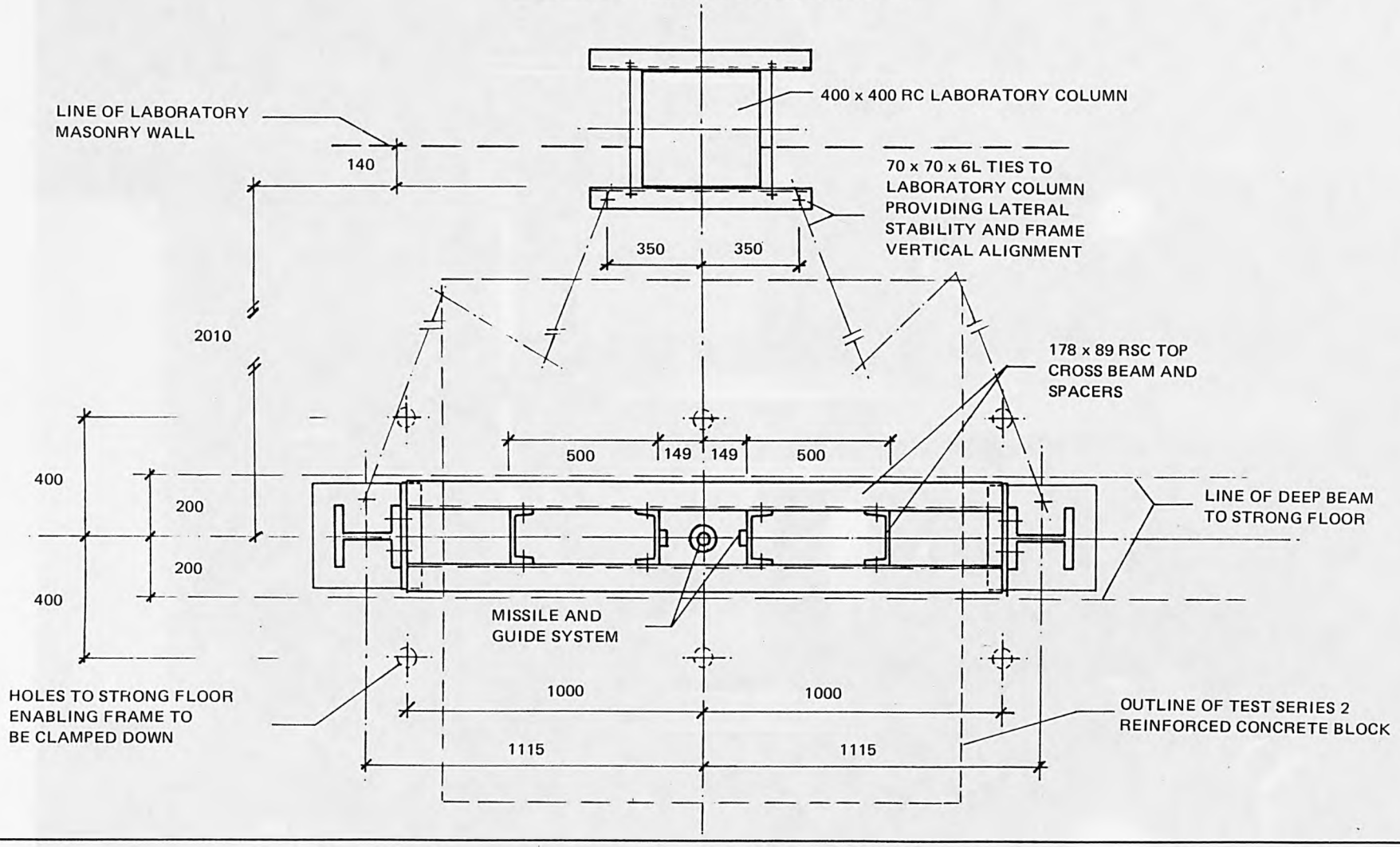

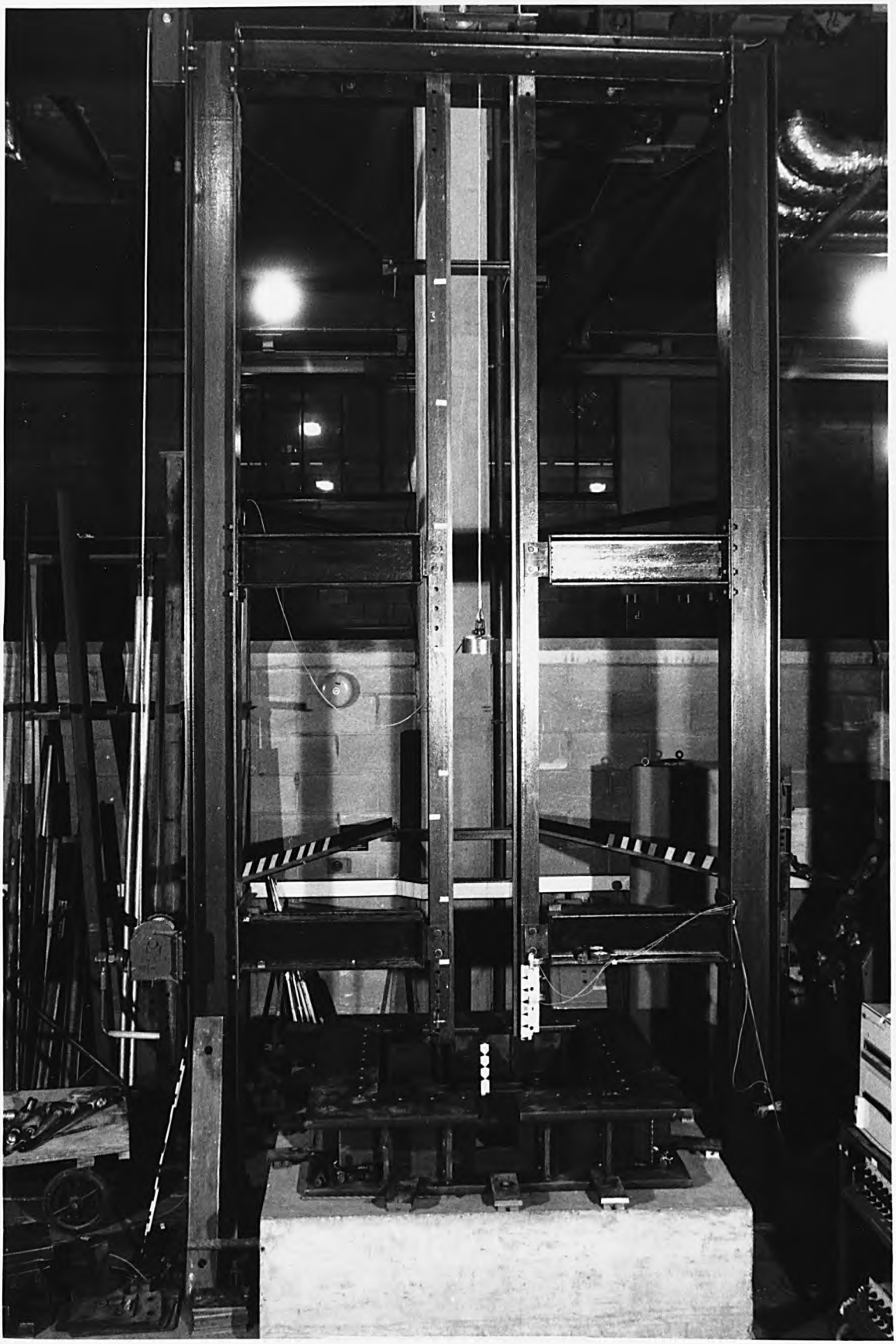

FIGURE 4.2.

EXPERIMENTAL DROP
RIG

FIGURE 4.3 SECTION THROUGH MISSILE GUIDE SYSTEM

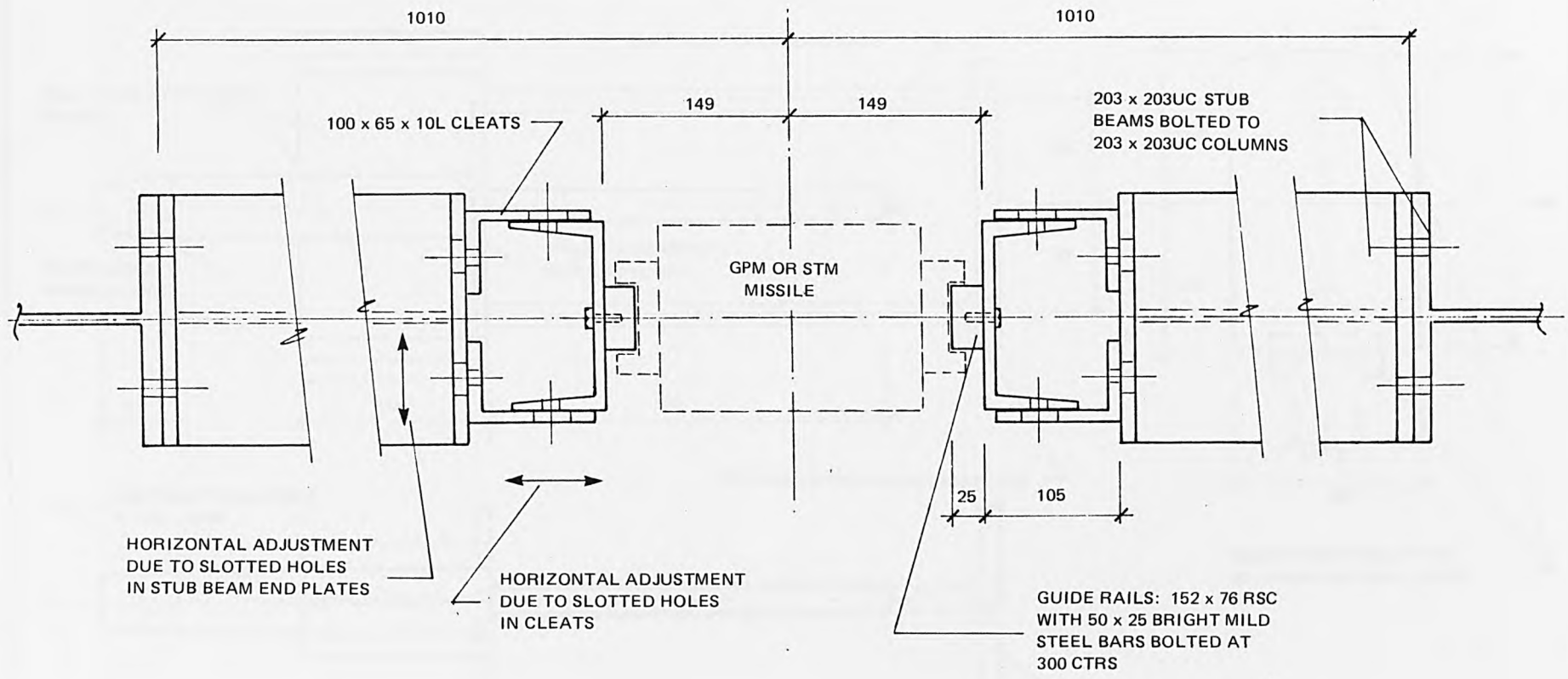

M16 BOLTS USED IN ALL BOLTED CONNECTIONS

FIGURE 4.4 GENERAL PURPOSE MISSILE (GPM)

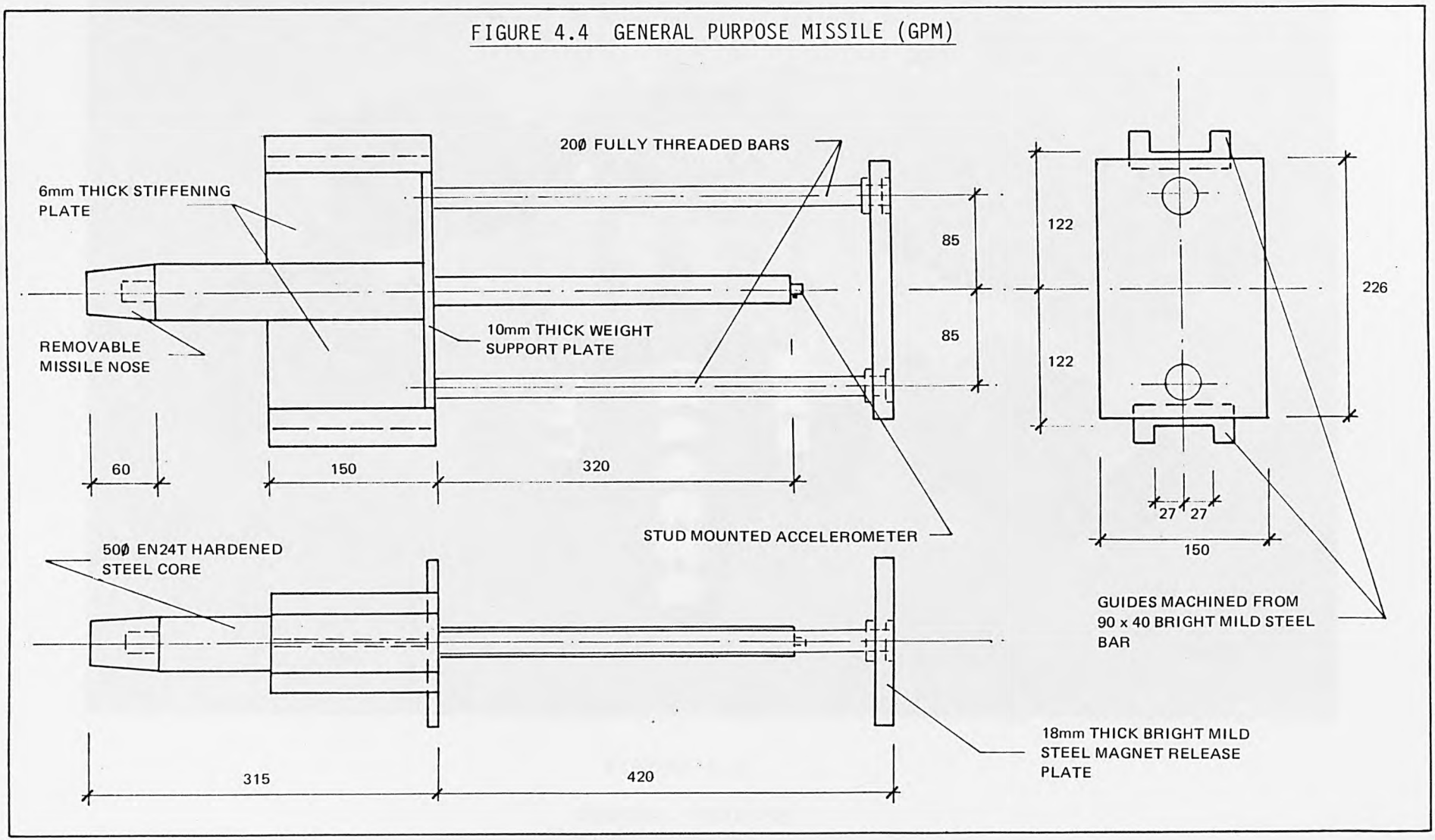

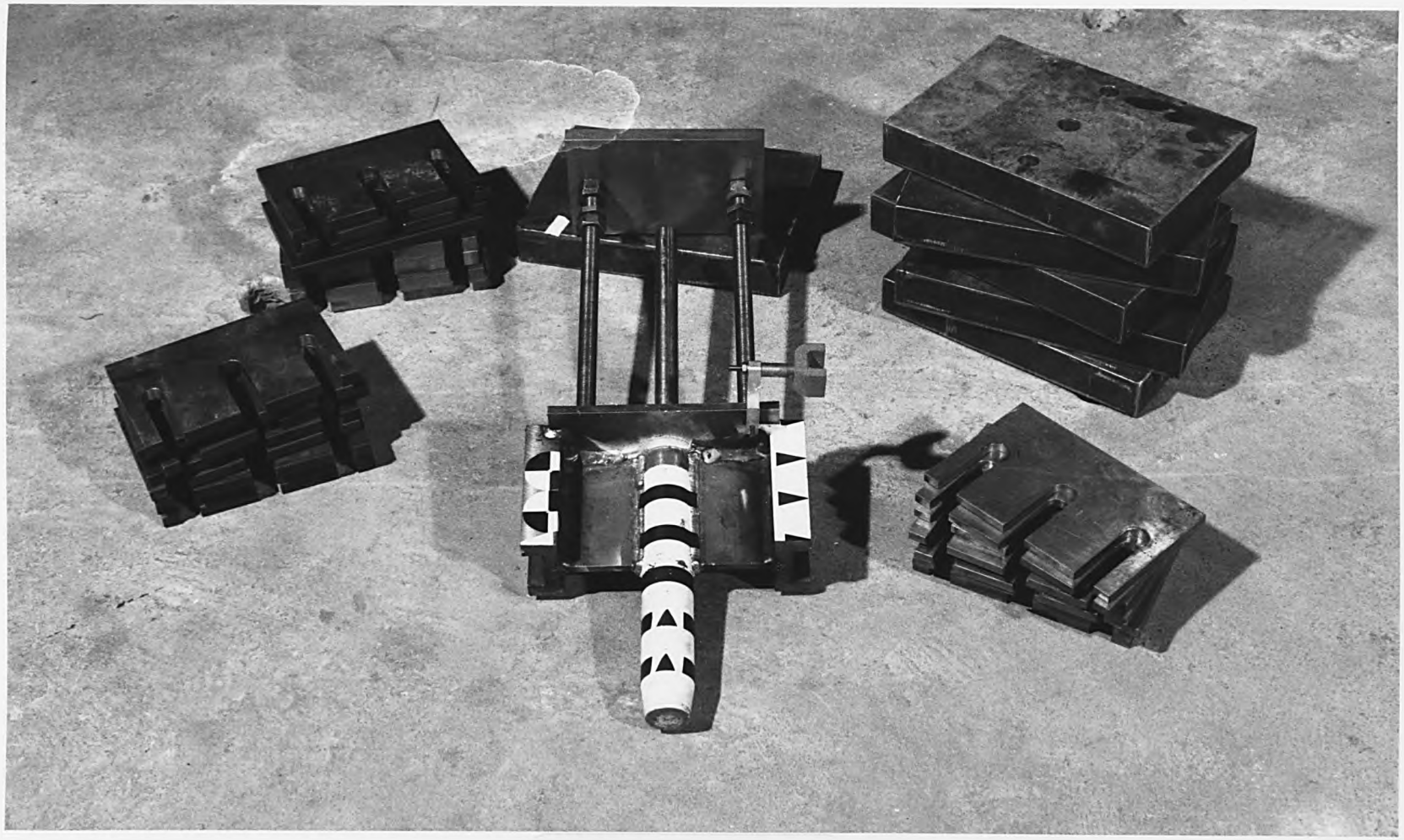

FIGURE 4.5

GENERAL PURPOSE
MISSILE WITH
ADDITIONAL WEIGHTS

FIGURE 4.6 SMALL SCALE TEST MISSILE (STM)

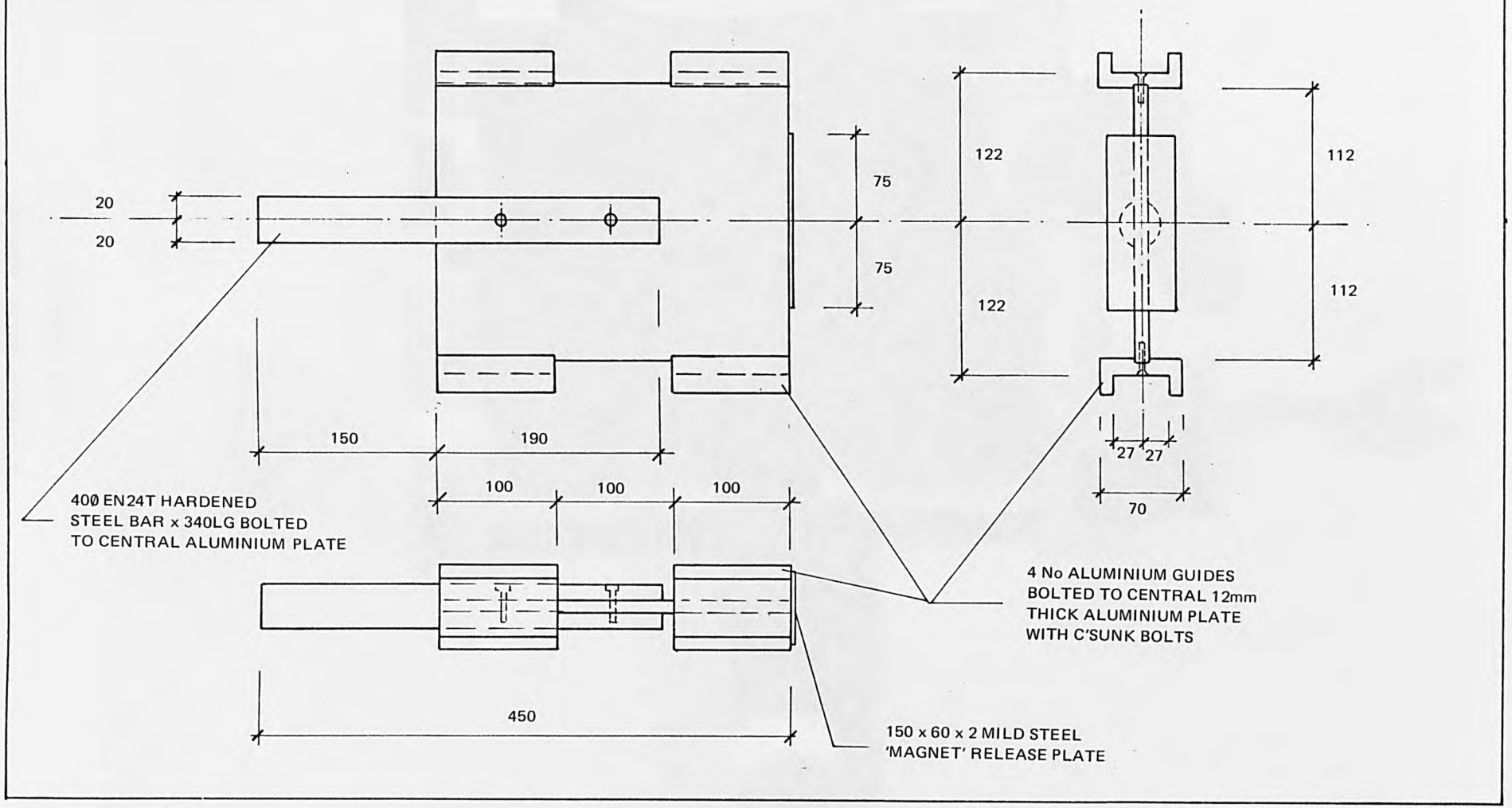

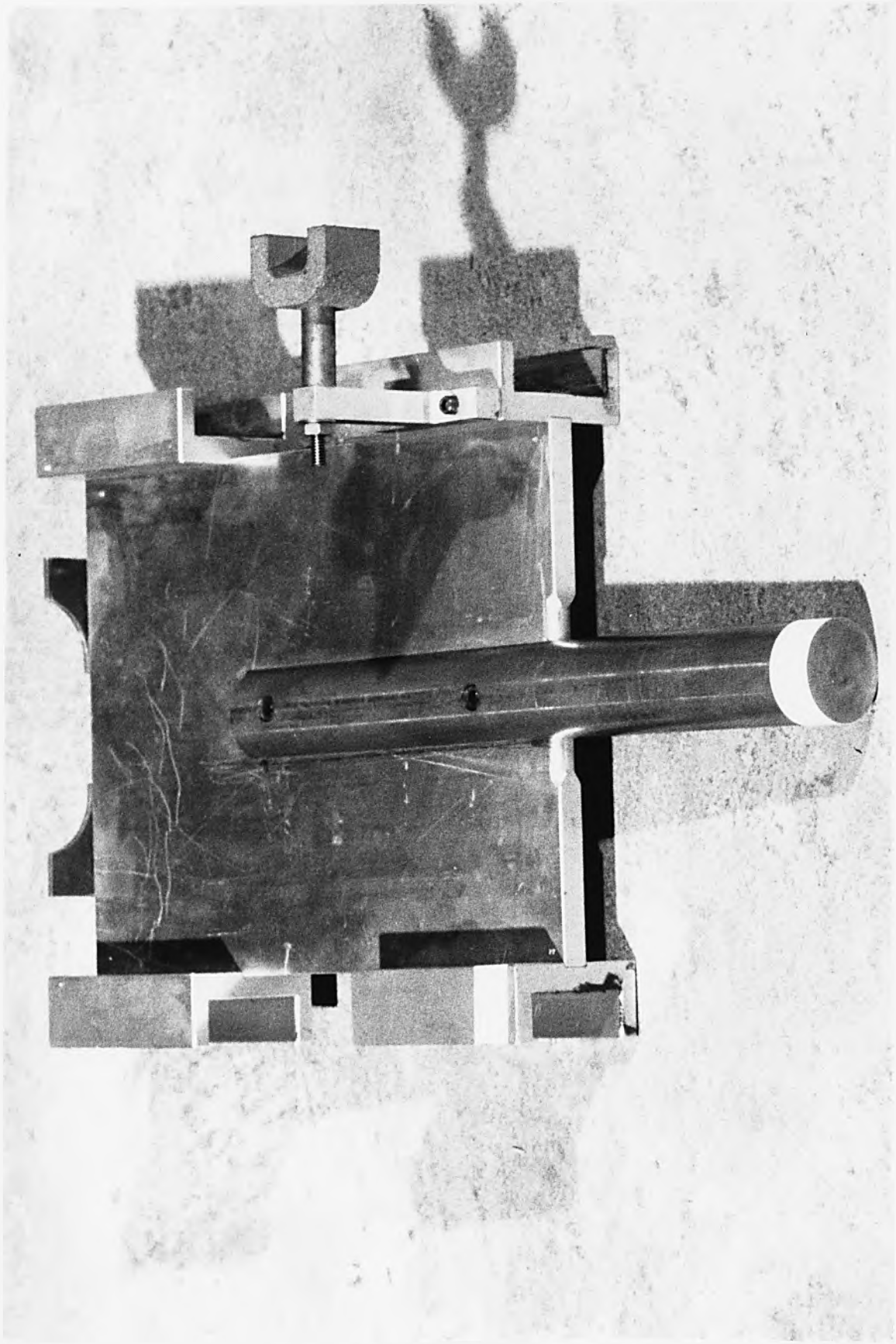

FIGURE 4.7

SCALE TEST MISSILE

FIGURE 4.8 ELECTROMAGNETIC RELEASE PROPERTIES*

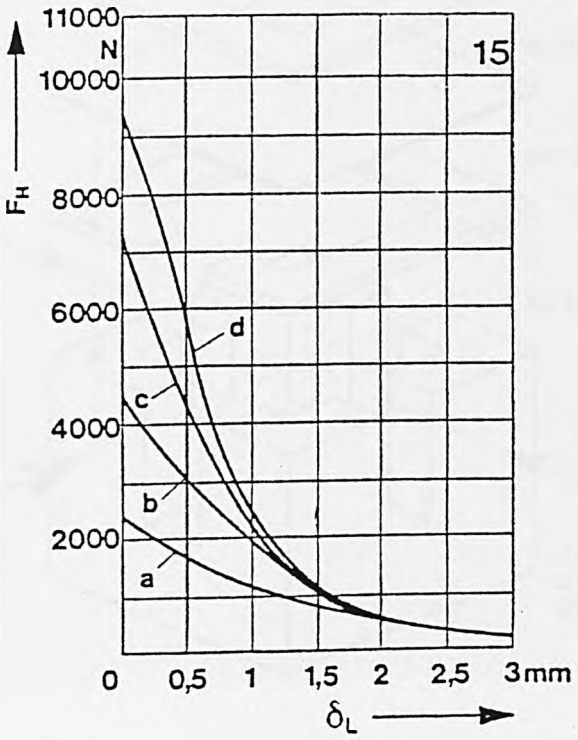

Eff. Material Thickness

a = 5 mm c = 12 mm

b = 8 mm d = 17 mm

HOLD FORCE CAPABILITY, F_H IS DEPENDANT UPON THE SIZE OF OPERATING AIR GAP, δ_L, BETWEEN THE MAGNET HOLDING FACE AND THE WORKPIECE, COUPLED WITH THE EFFECTIVE MATERIAL THICKNESS. THE FORCES OUTLINED RELATE TO WORKPIECES MANUFACTURED IN St37 (En2) MATERIAL WHICH FULLY COVER THE MAGNET HOLDING FACE, WITH THE MAGNETS OPERATING AT 90% OF THEIR NOMINAL WORKING VOLTAGE AND AT NORMAL WORKING TEMPERATURE (60°C ABOVE AMBIENT WITHOUT HEAT SINK)

* Above copied from BINDER data sheets, BINDER MAGNETE EmbH, W. Germany.

FIGURE 4.9 TEST SERIES 1 BASE

a) EXPLODED VIEW

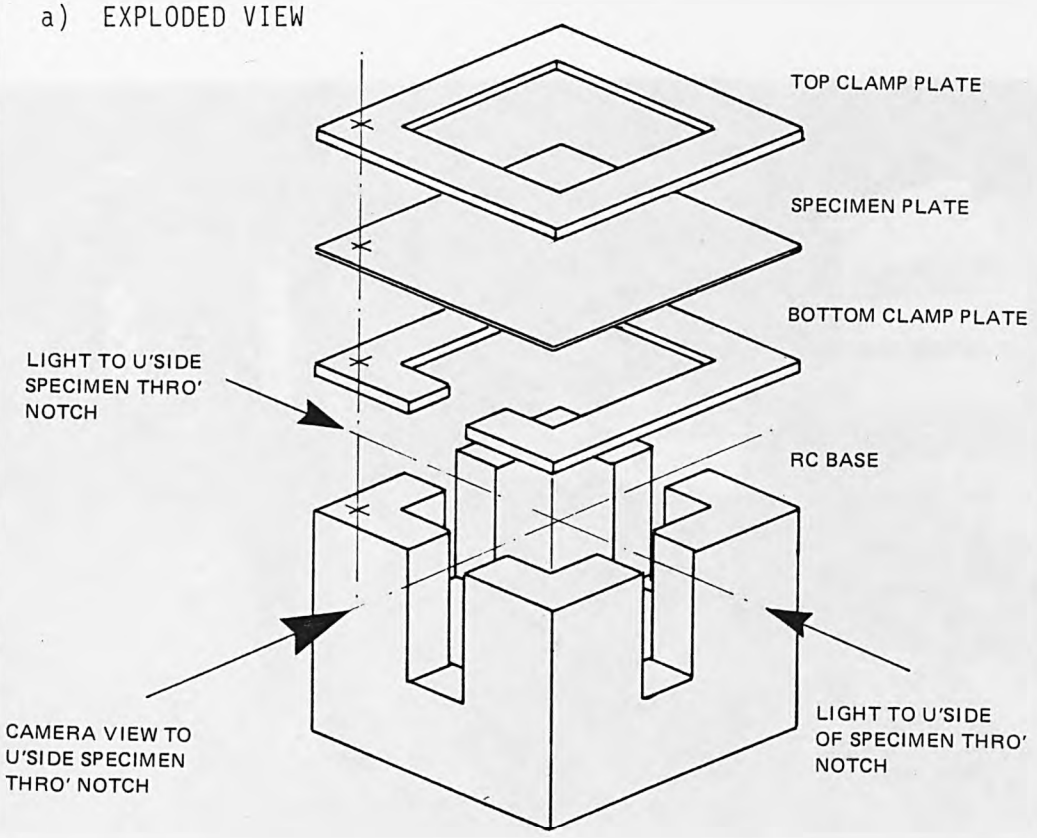

b) FIXING DETAIL

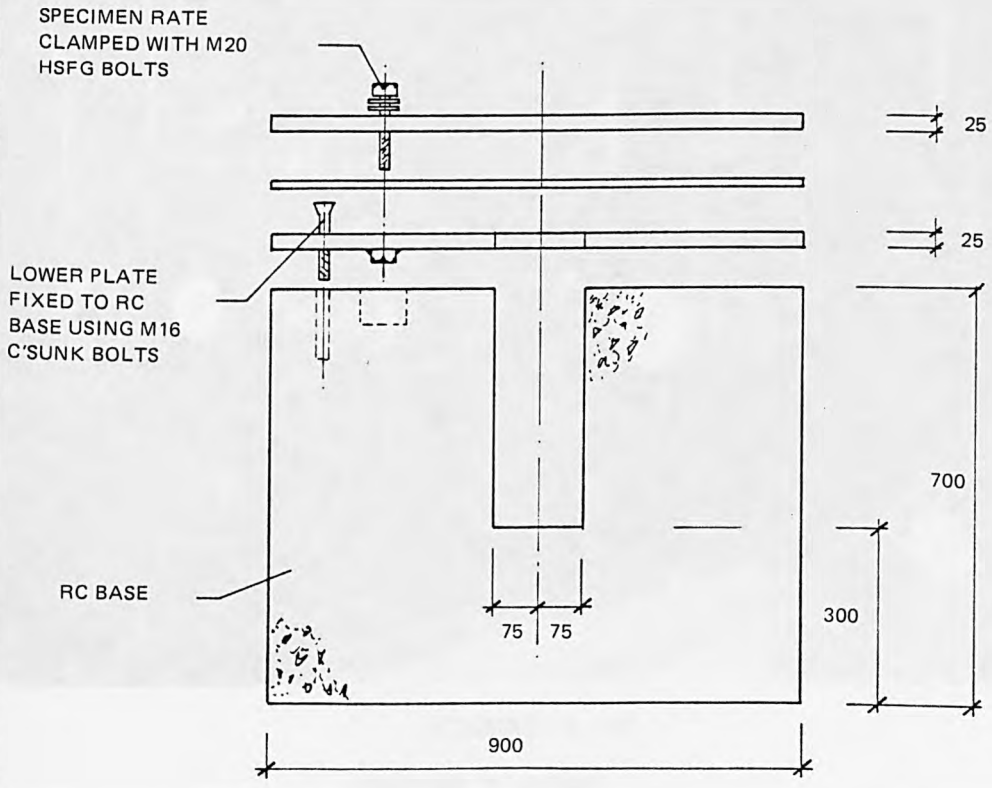

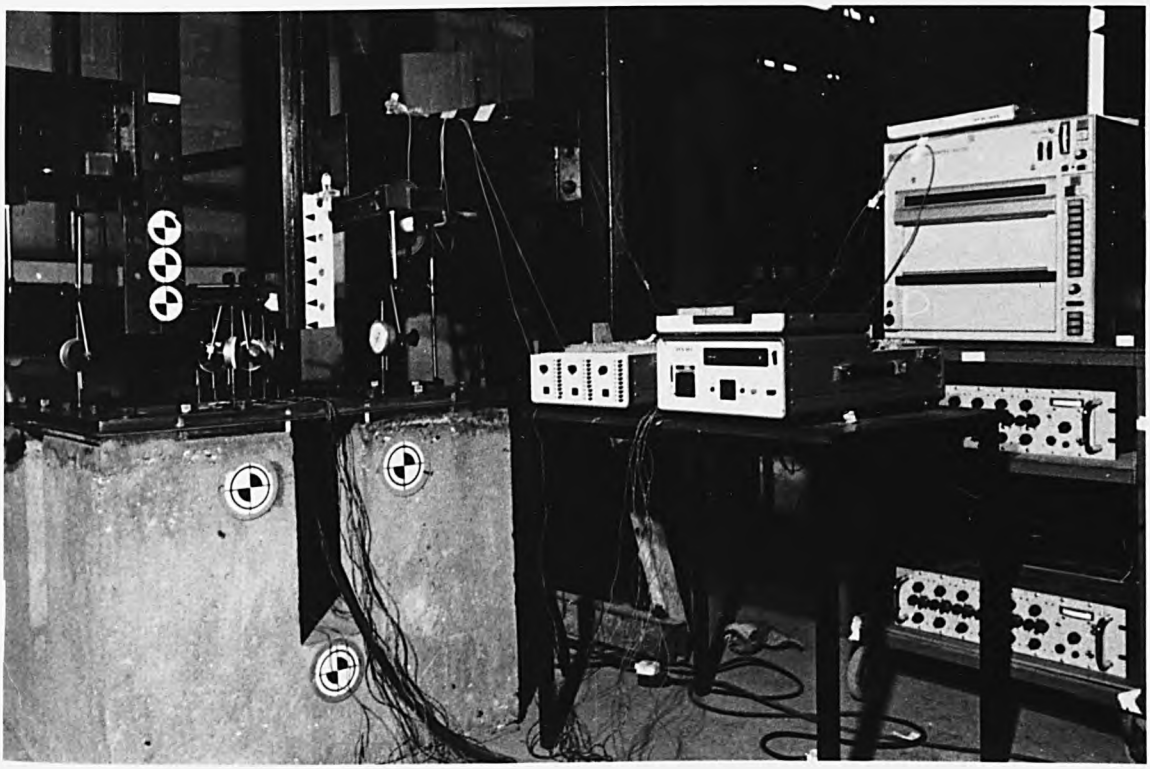

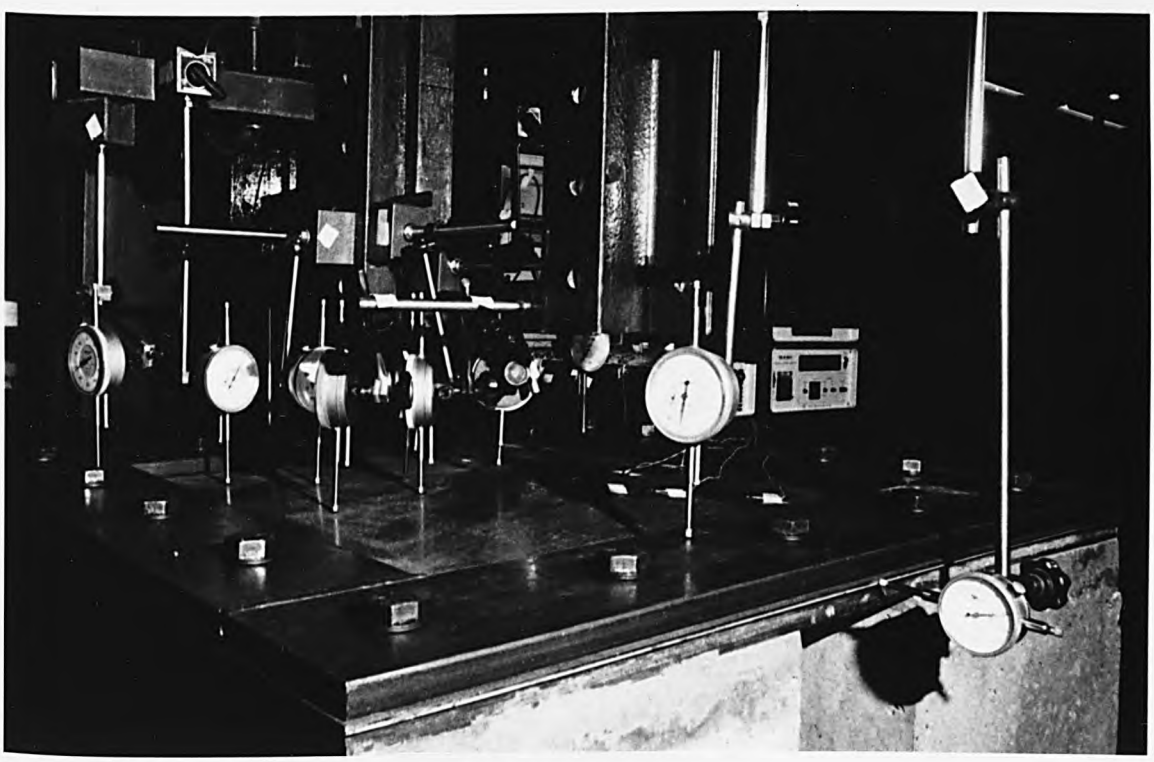

FIGURE 4.10

SERIES 1 BASE
(STATIC TEST SET-
UP)

FIGURE 4.11 STATIC TEST ARRANGEMENT

a) TEST SERIES 1

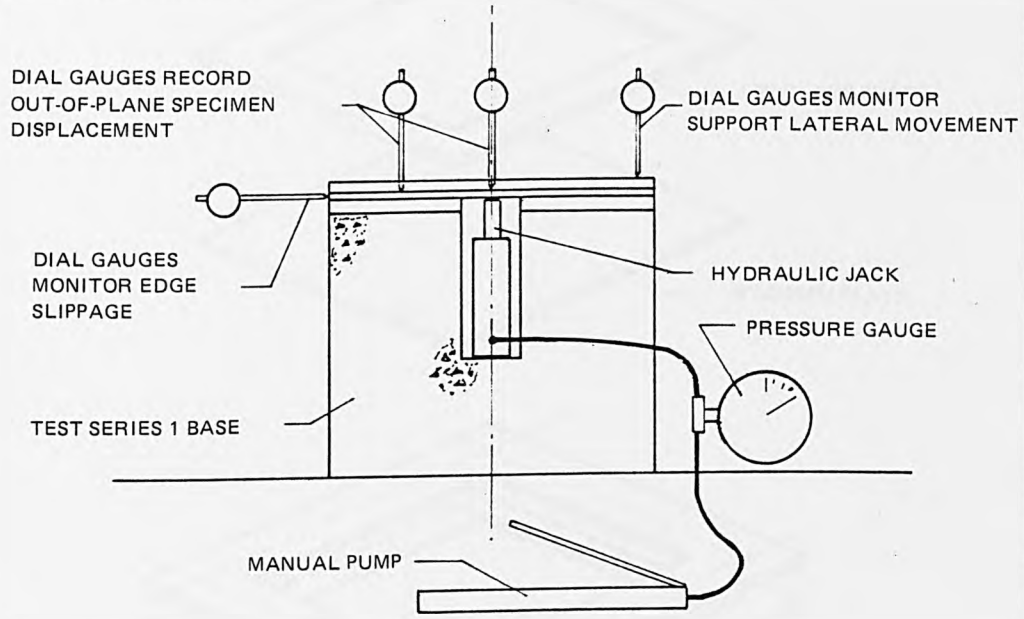

b) TEST SERIES 2

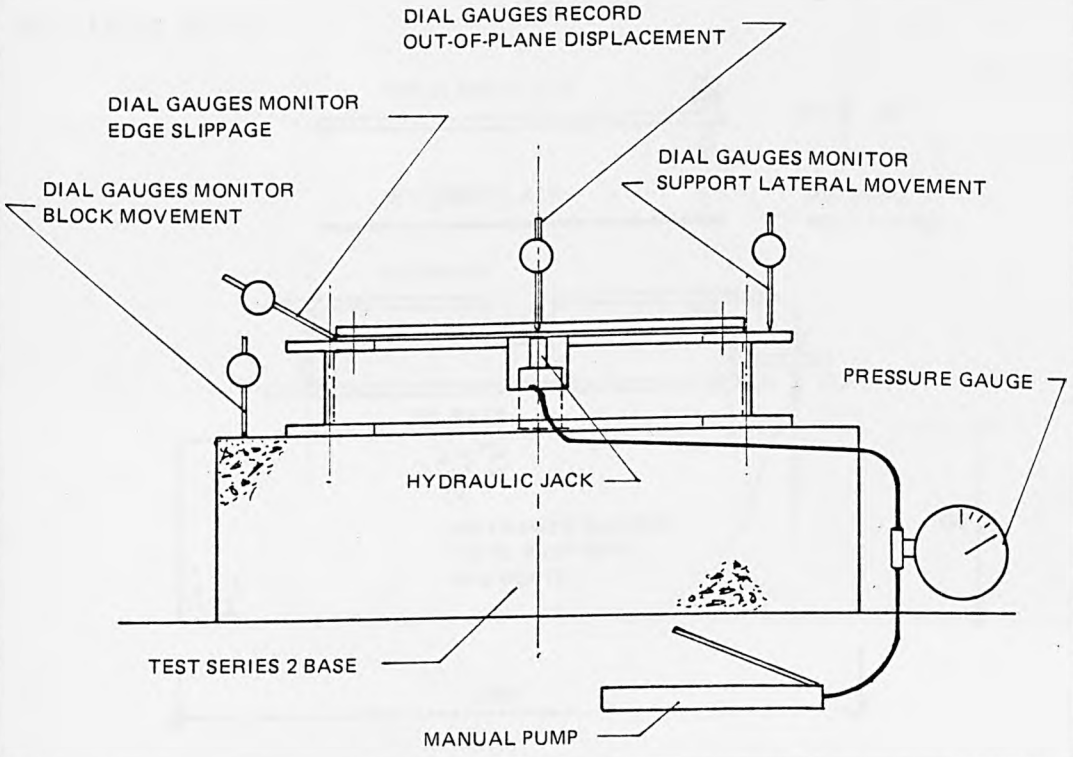

FIGURE 4.12 TEST SERIES 2 BASE

a) EXPLODED VIEW

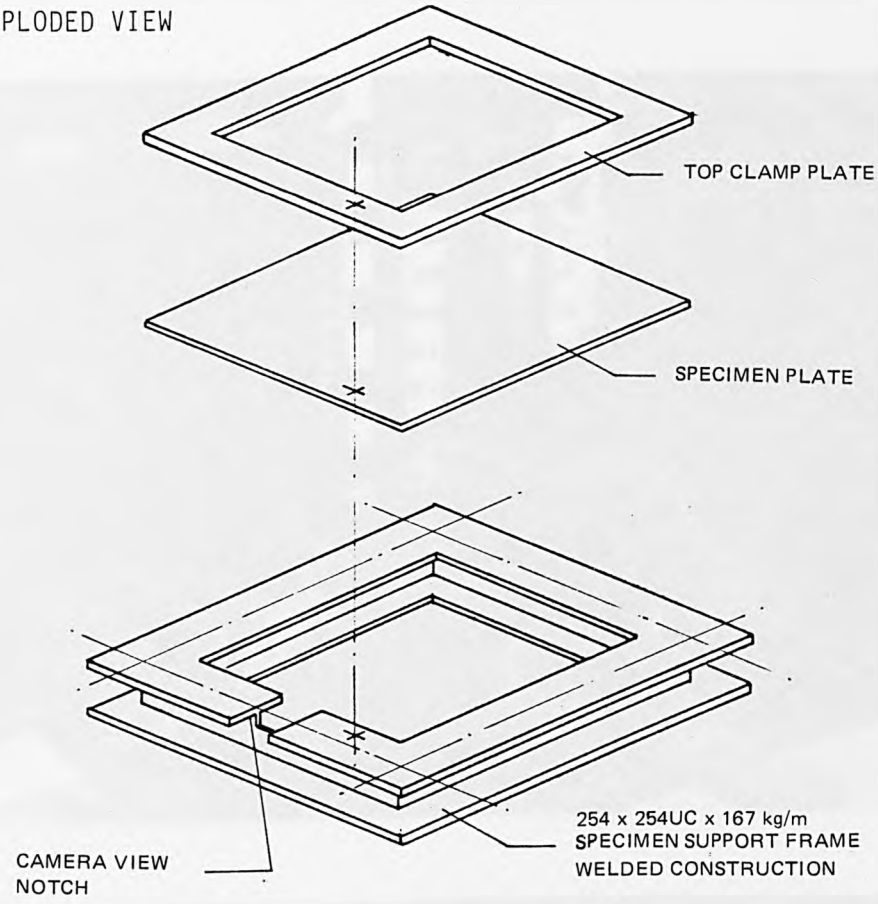

b) FIXING DETAIL

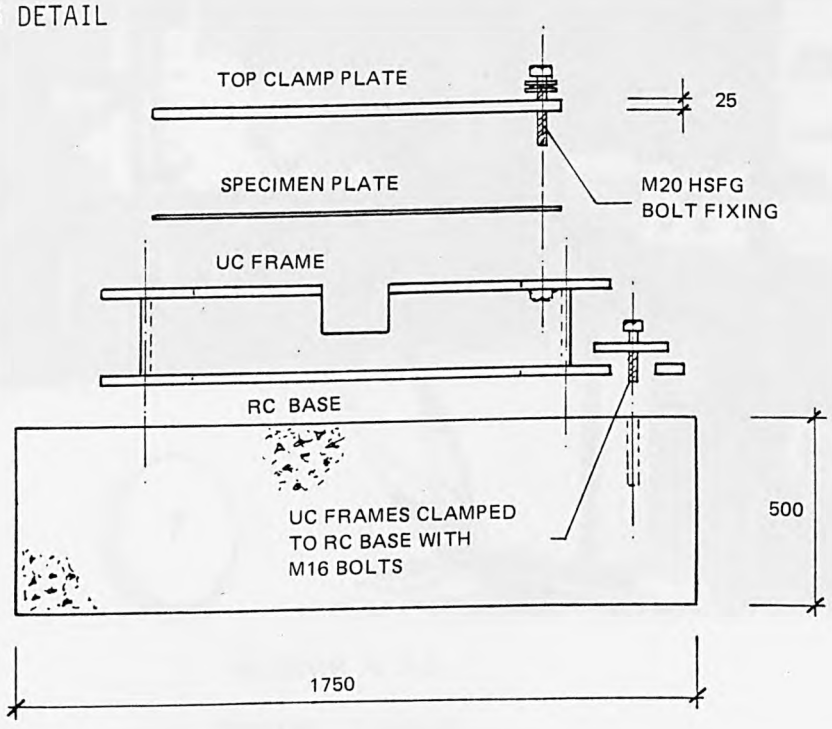

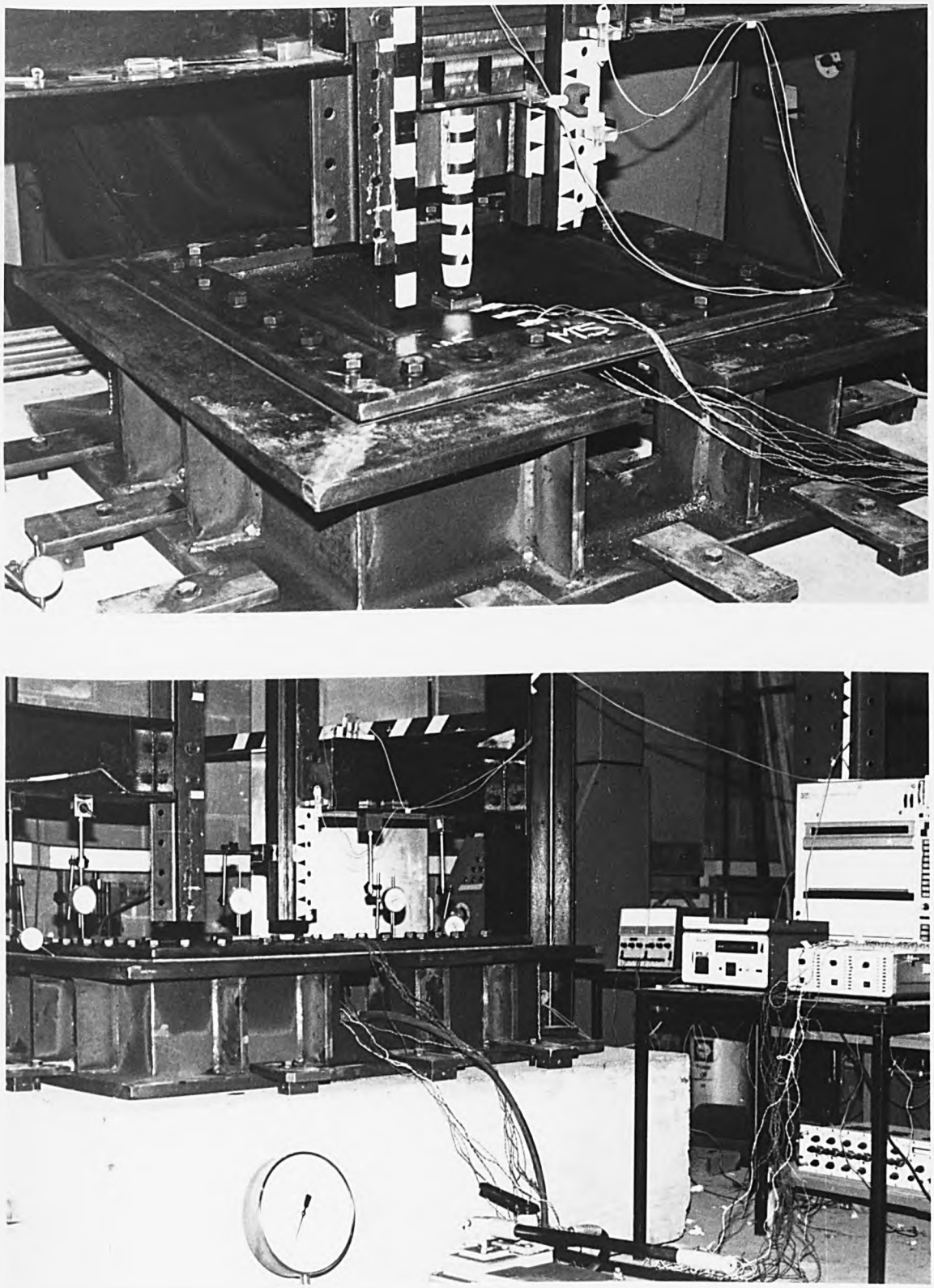

FIGURE 4.13

SERIES 2 BASE

FIGURE 4.14 USE OF HSFG BOLTS

a) CORRECT USE

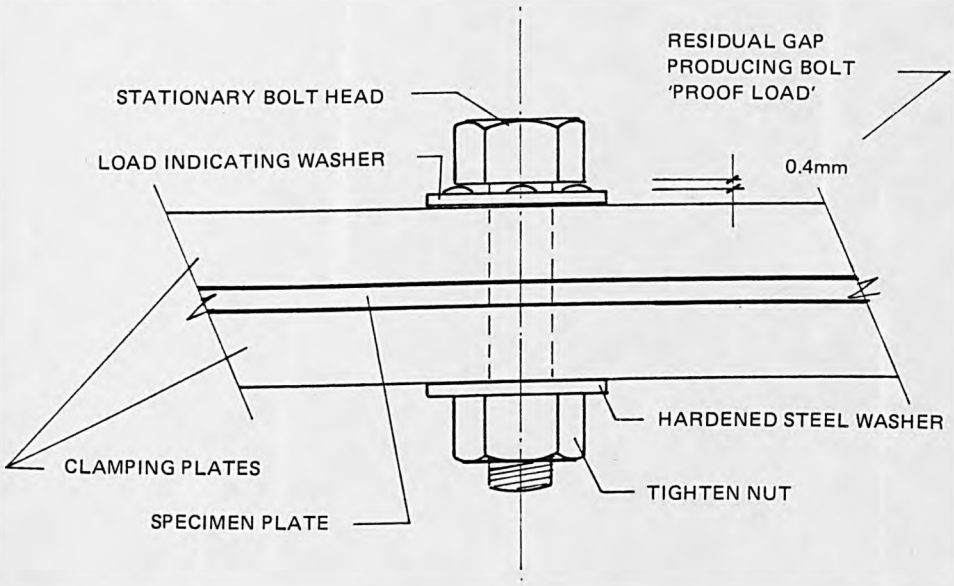

b) CURRENT USE

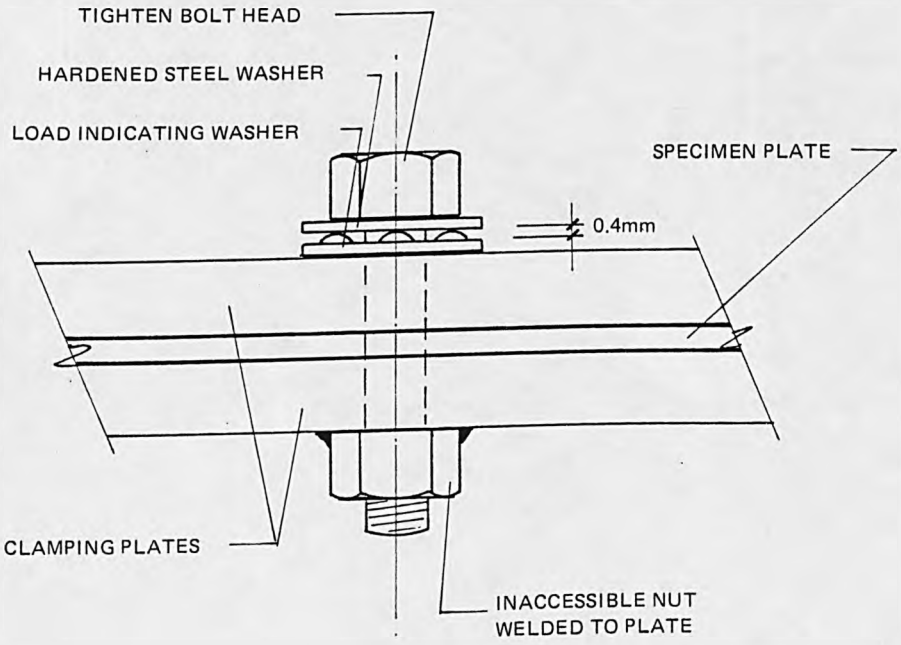

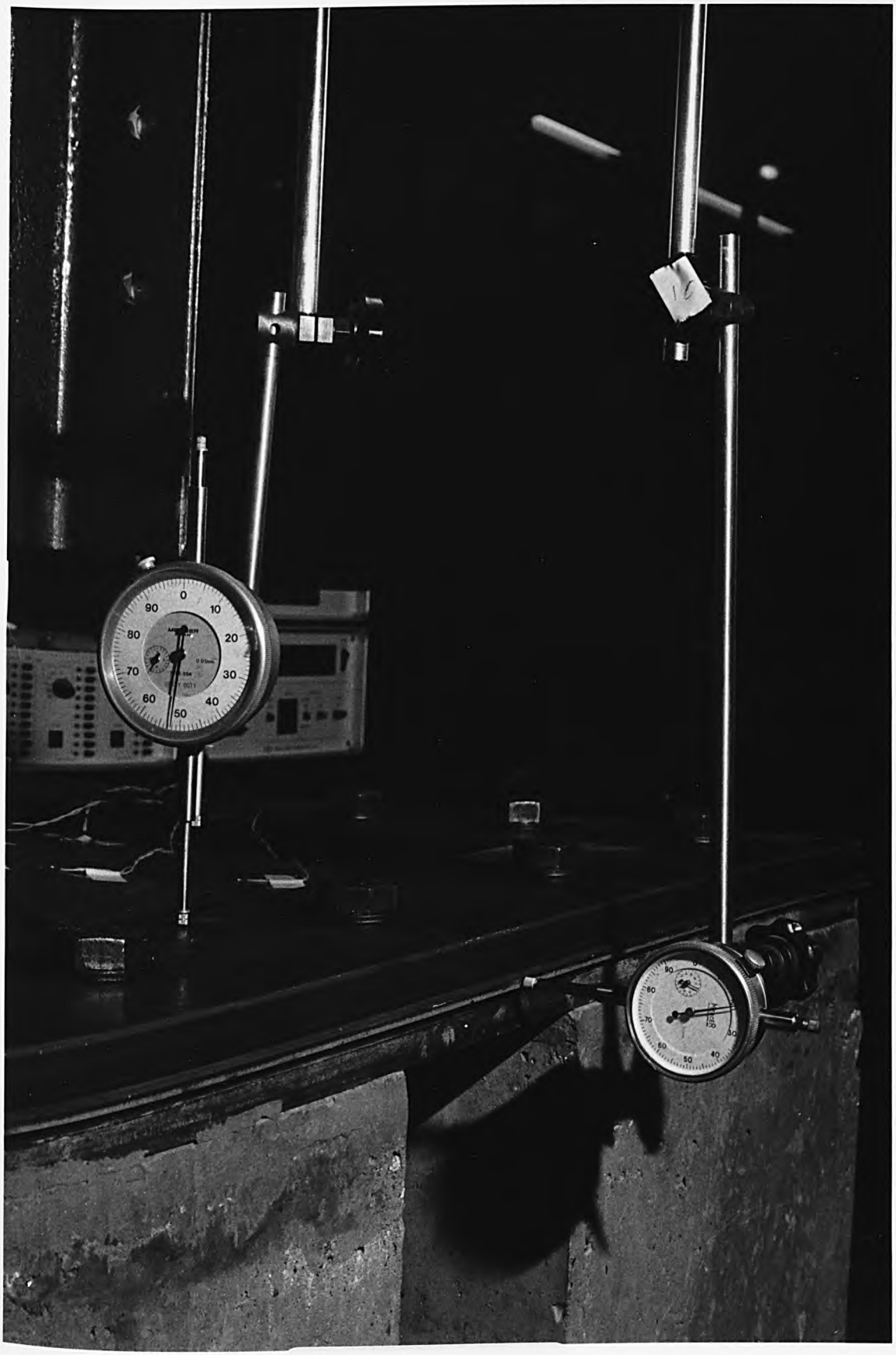

FIGURE 4.15

STATIC TEST EDGE
SLIPPAGE CHECK

FIGURE 4.16 DYNAMIC TEST SUPPORT SLIPPAGE CHECK

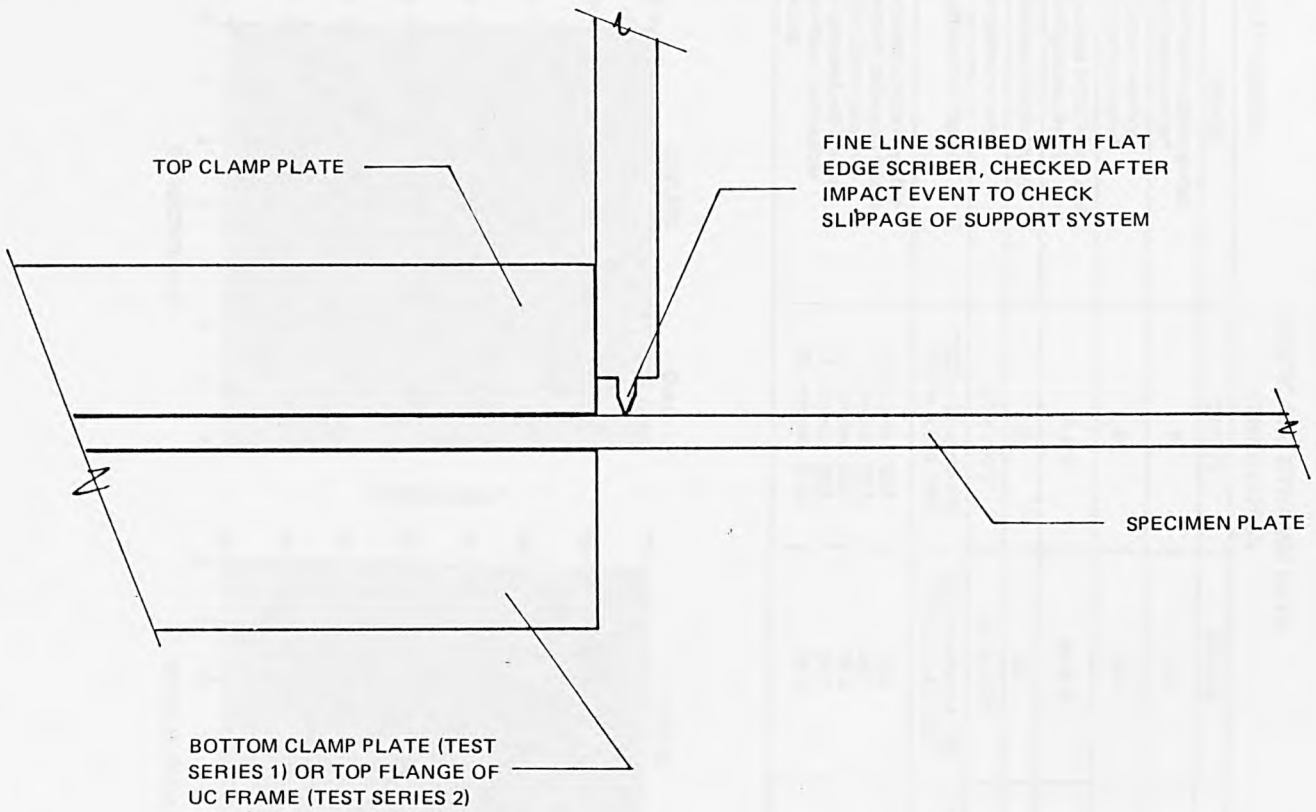

FIGURE 4.17 ISOLATION LAYER TECHNICAL DETAILS*

a) SECTION THROUGH CU/LF/B PAD

b) STATIC AND DYNAMIC DETAILS

* ABOVE COPIED FROM TICO DATA SHEETS, TICO MANUFACTURING LTD., WOKING, SURREY.

FIGURE 4.18 SHOCK ISOLATION

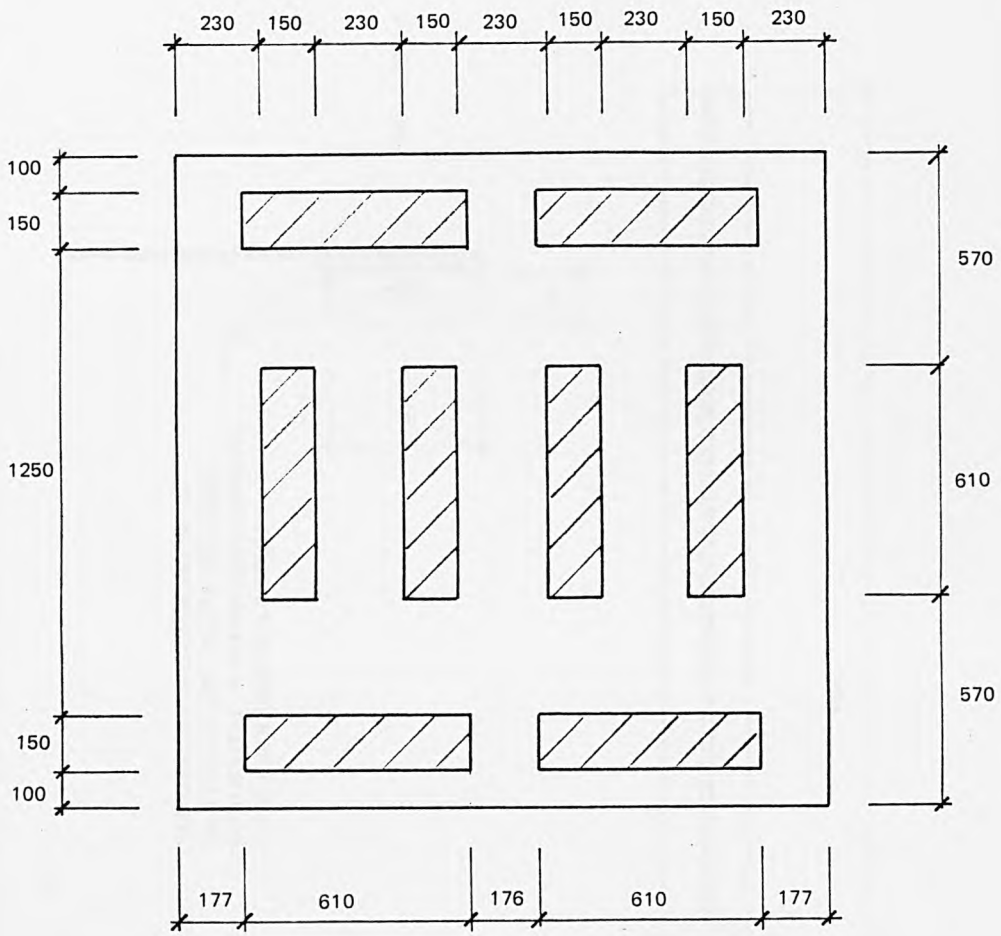

ARRANGEMENT OF 610mm x 150mm TICO
CV/LF/B LOW FREQUENCY BEARING
PADS BENEATH 1750mm x 1750mm REINFORCED
CONCRETE BLOCK

FIGURE 4.19 SPECIMEN PROFILE DEPTH GAUGE

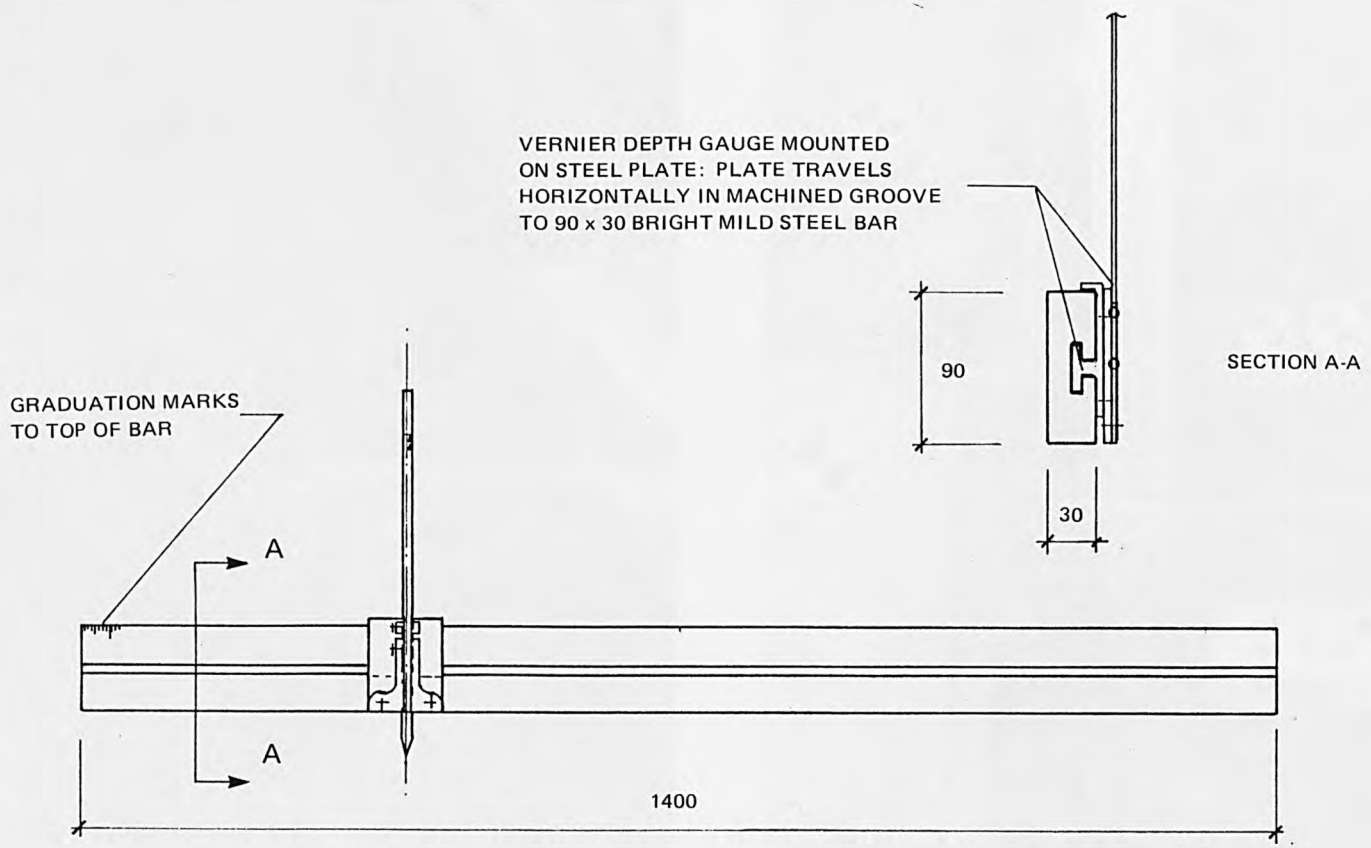

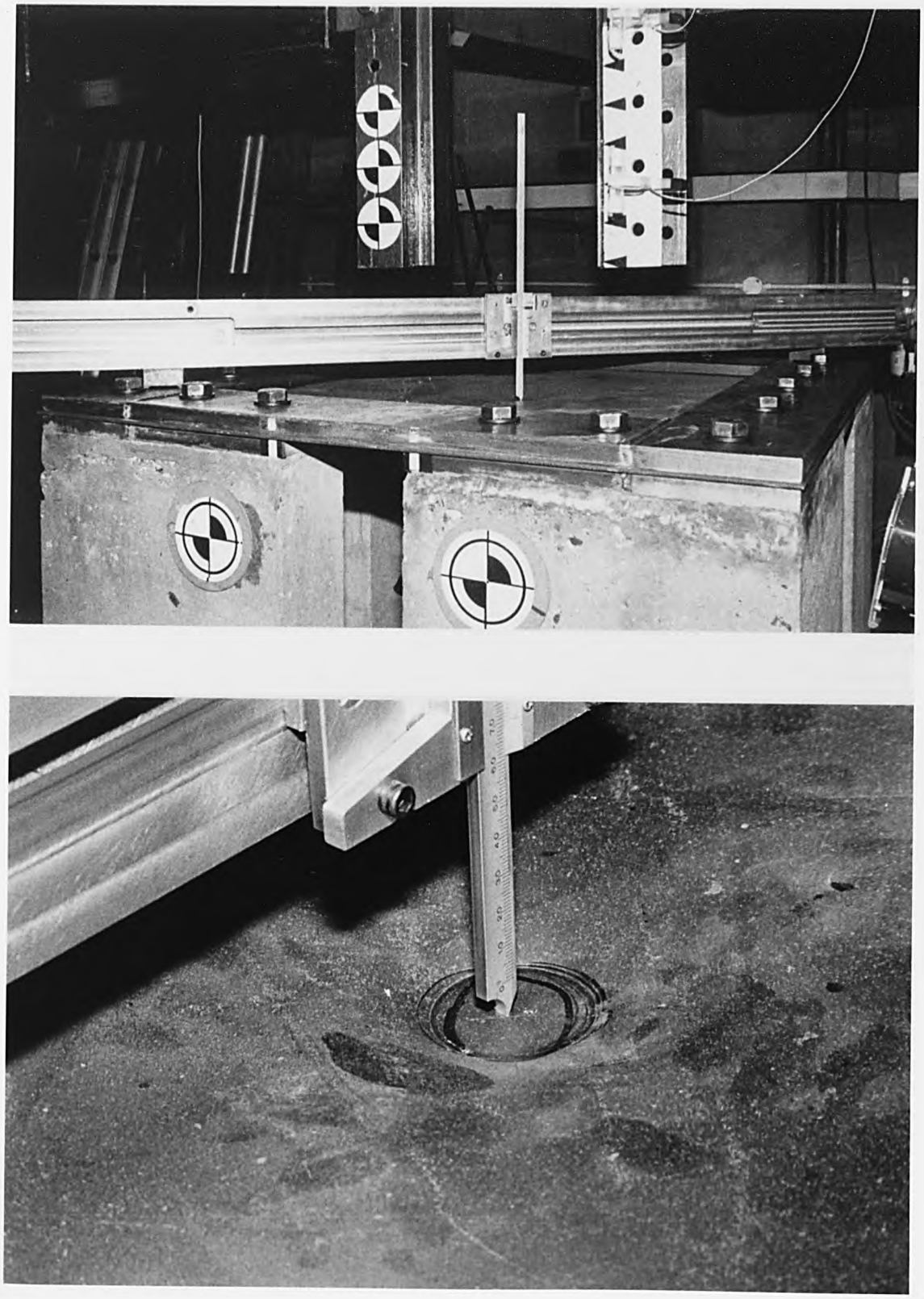

FIGURE 4.20

STATIC PROFILE
VERNIER DEPTH GAUGE

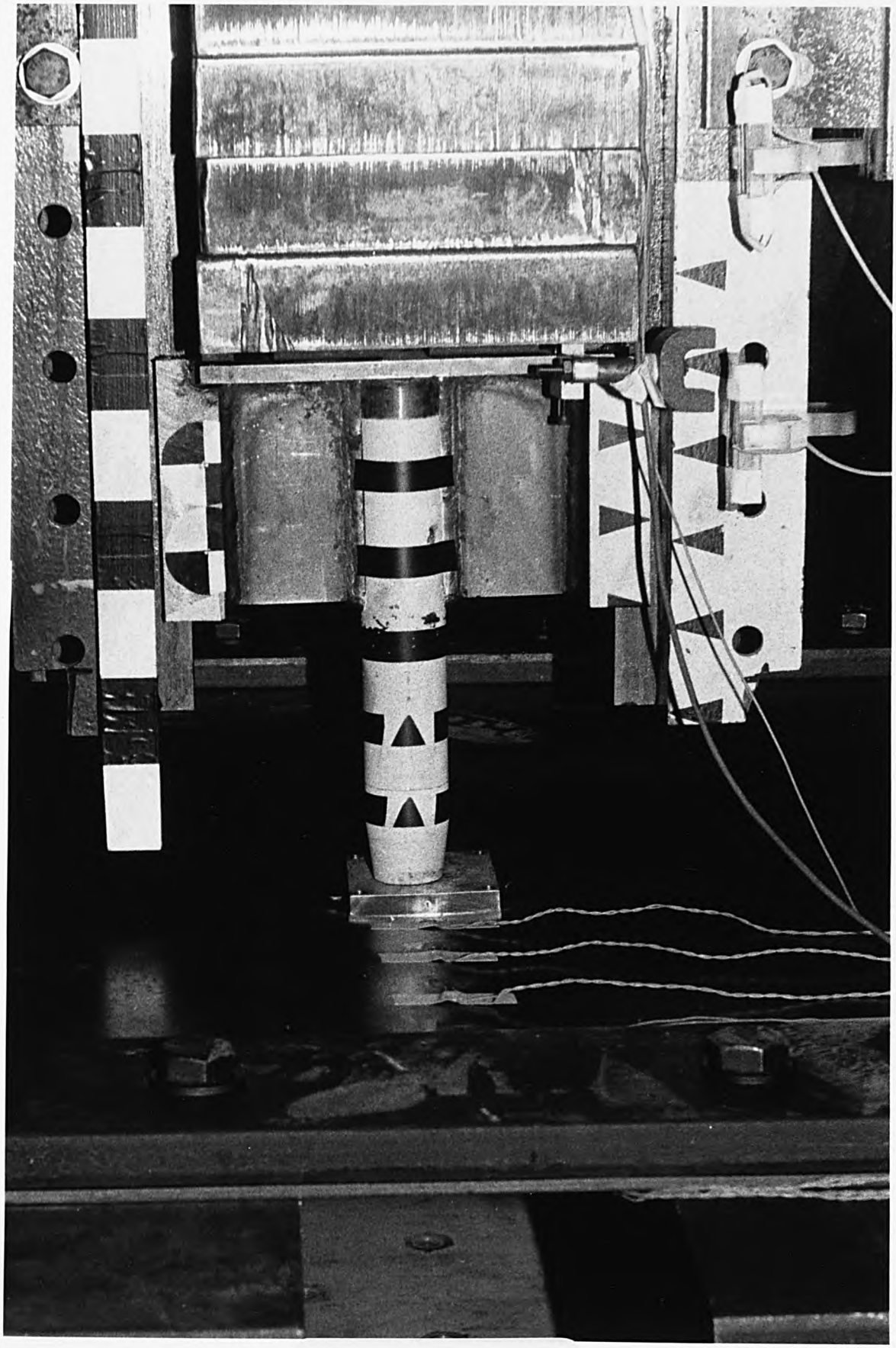

FIGURE 4.21

VELOCITY REED
SWITCHES

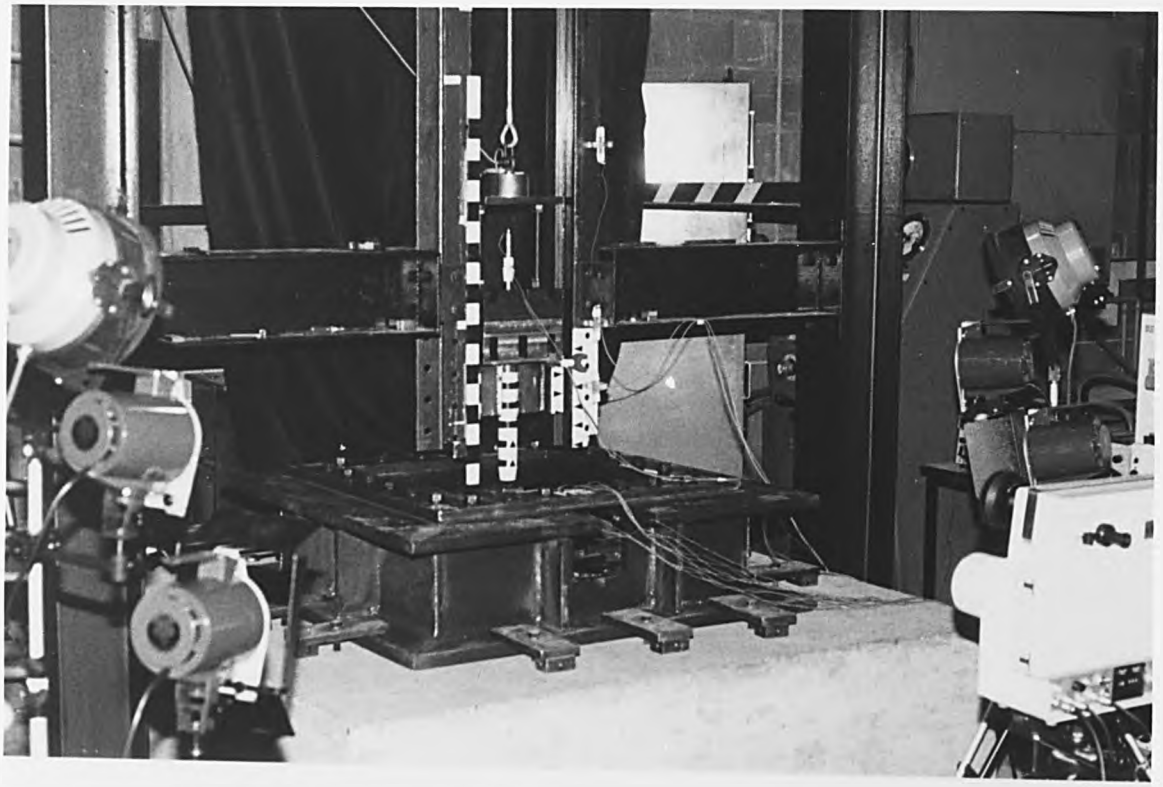

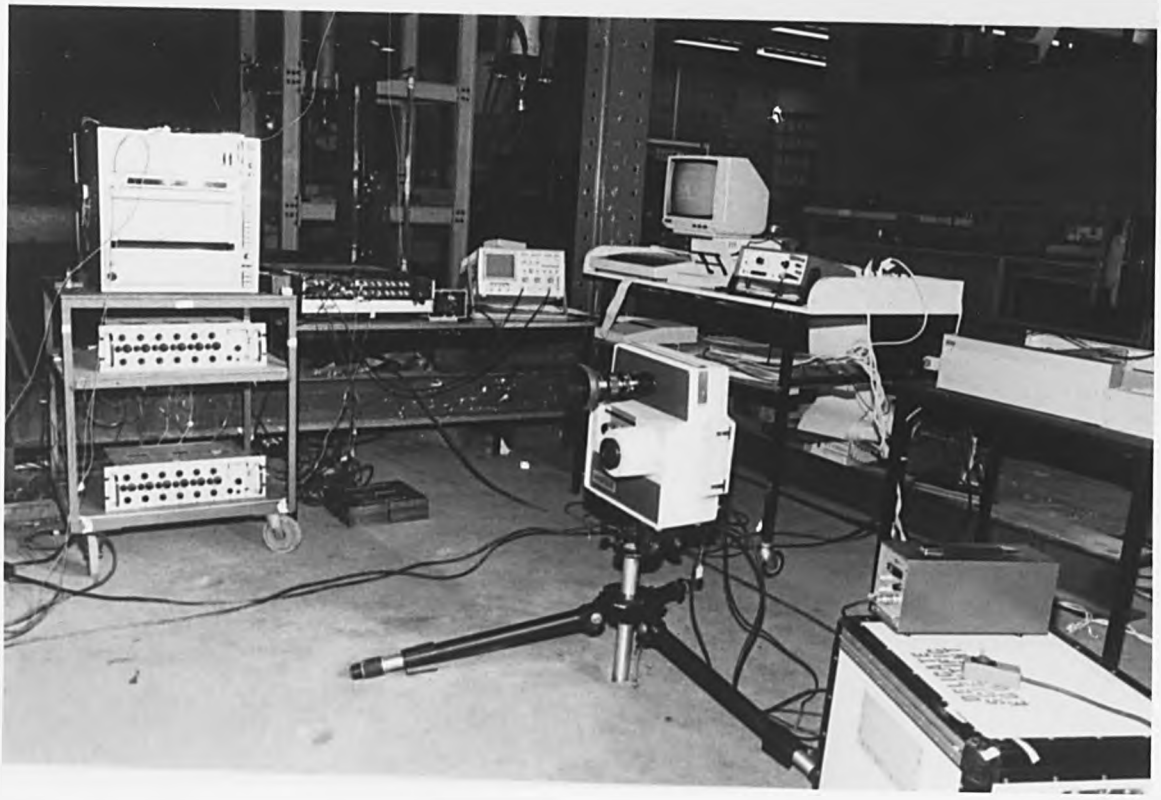

FIGURE 4.22

HIGH SPEED CAMERA
AND LIGHTING

FIGURE 4.23 HIGH SPEED CAMERA ALIGNMENT

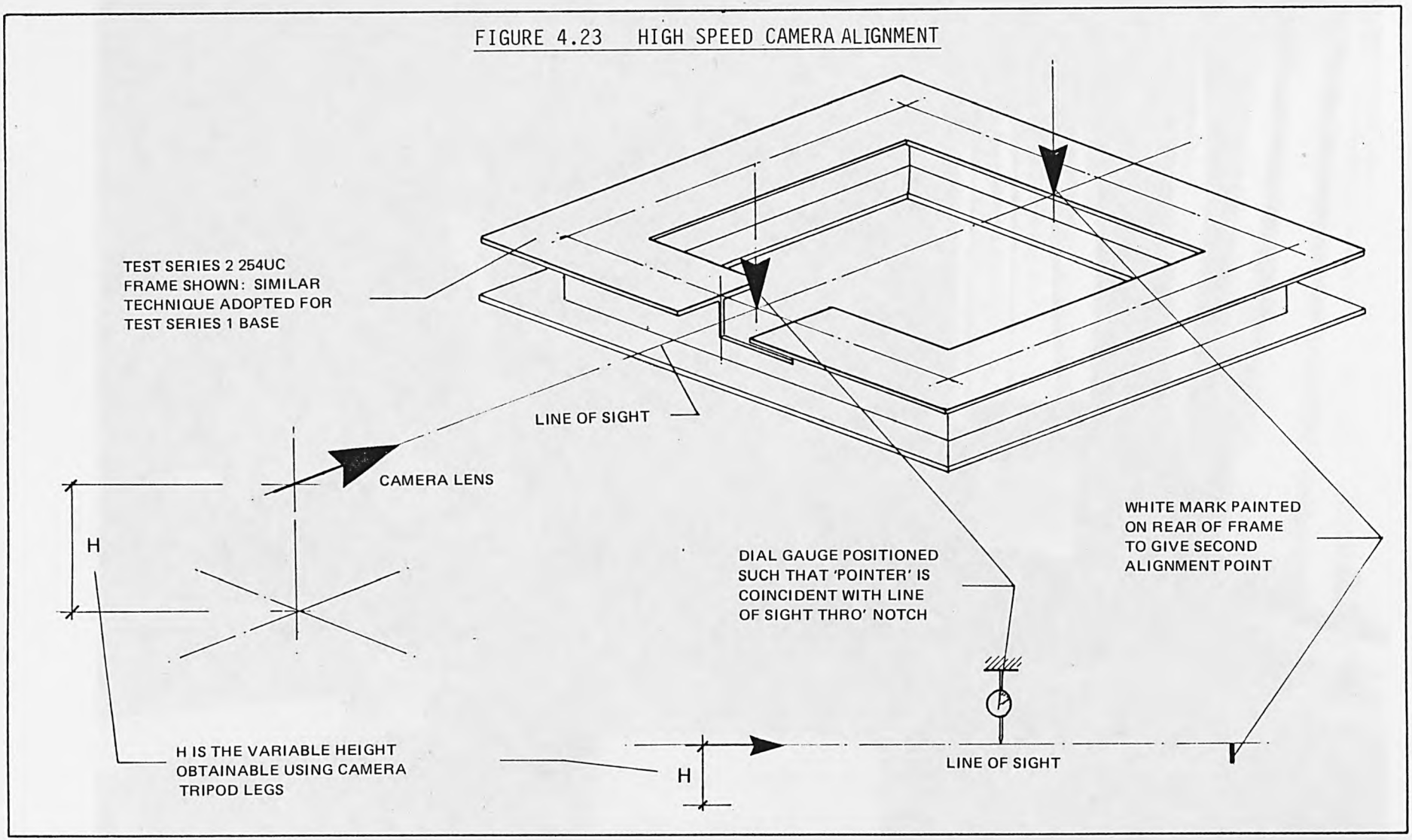

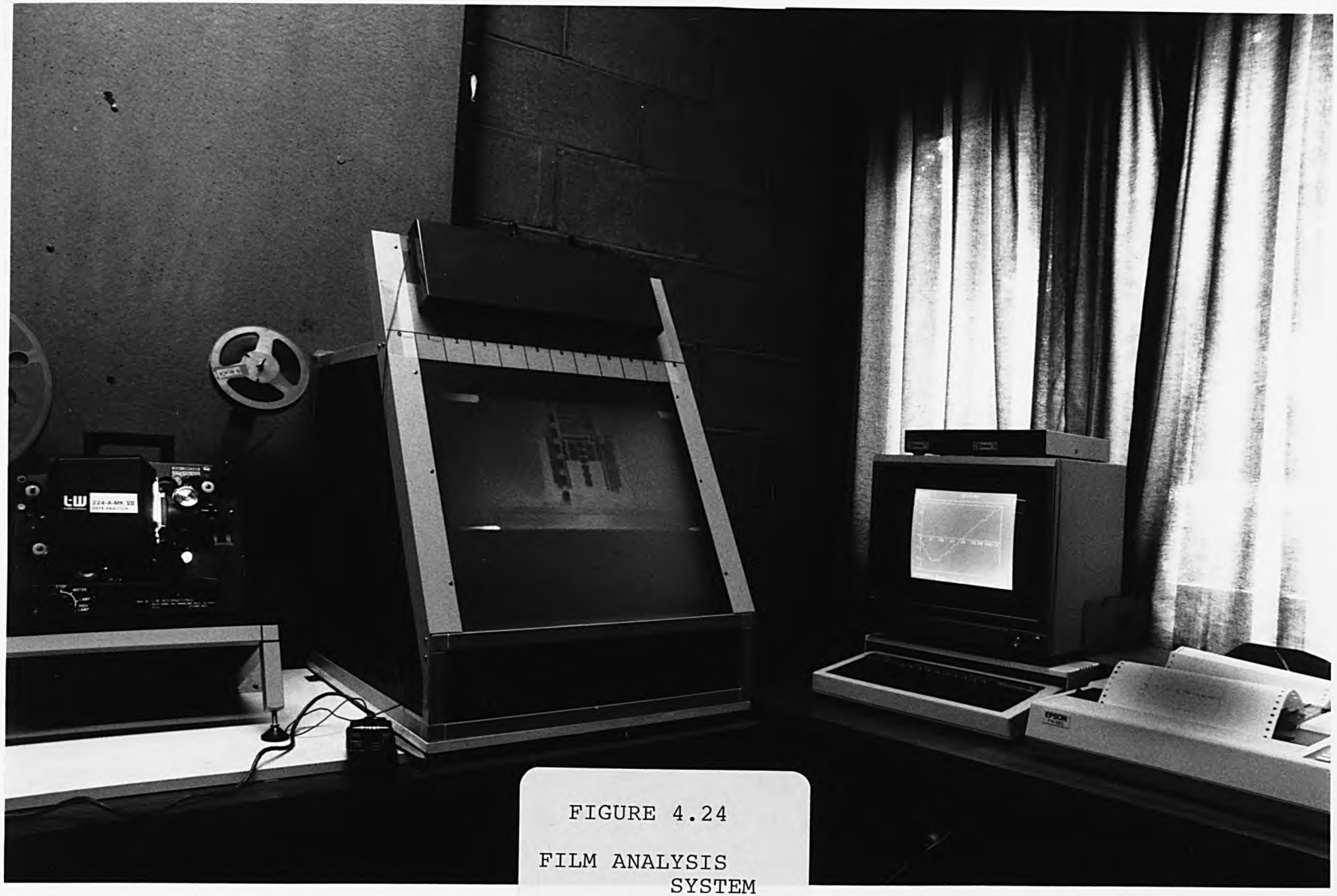

FIGURE 4.24

FILM ANALYSIS SYSTEM

FIGURE 4.25 STRAIN GAUGE CALIBRATION

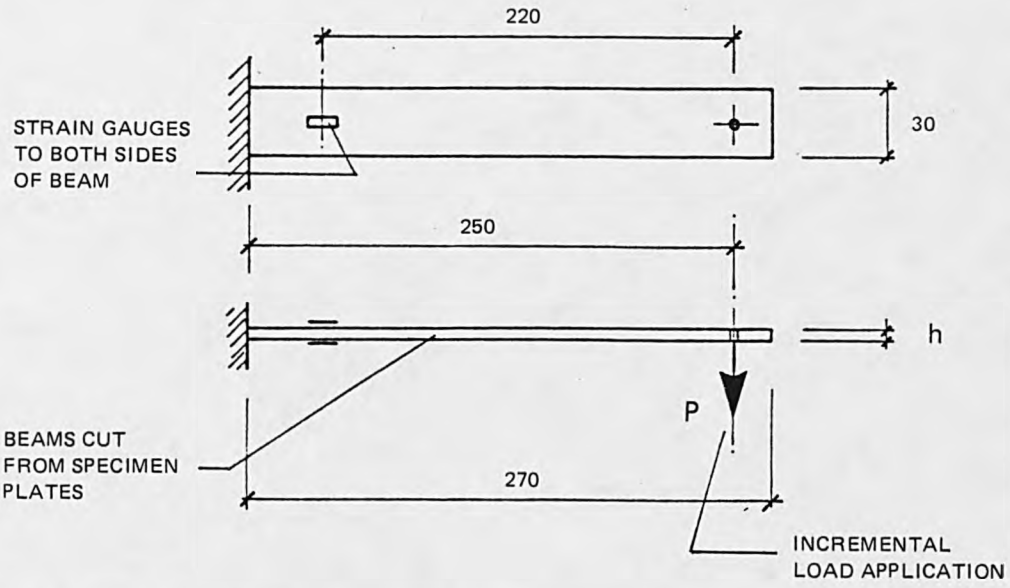

a) CALIBRATION BEAM

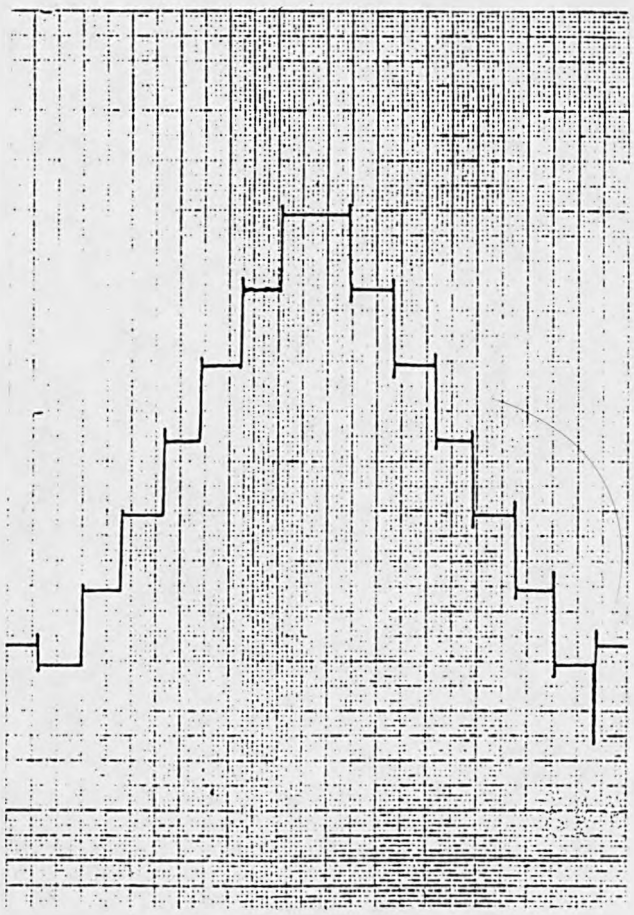

b) TYPICAL CALIBRATION CHART

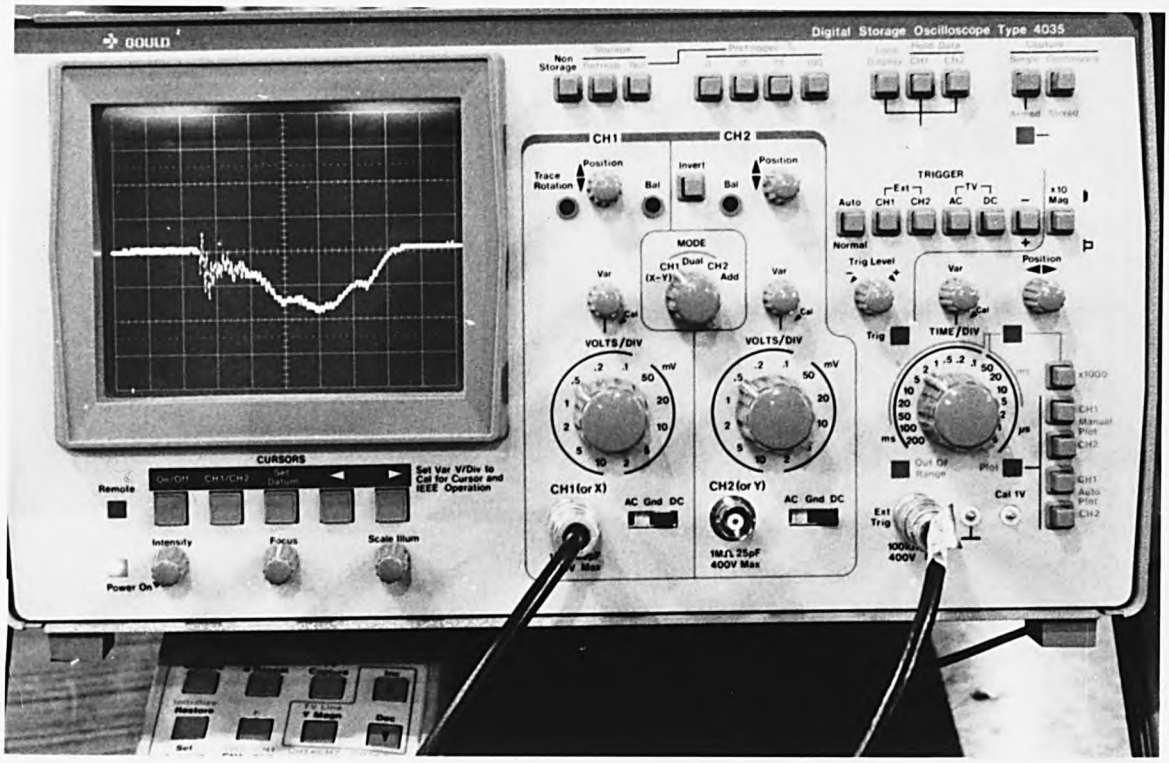

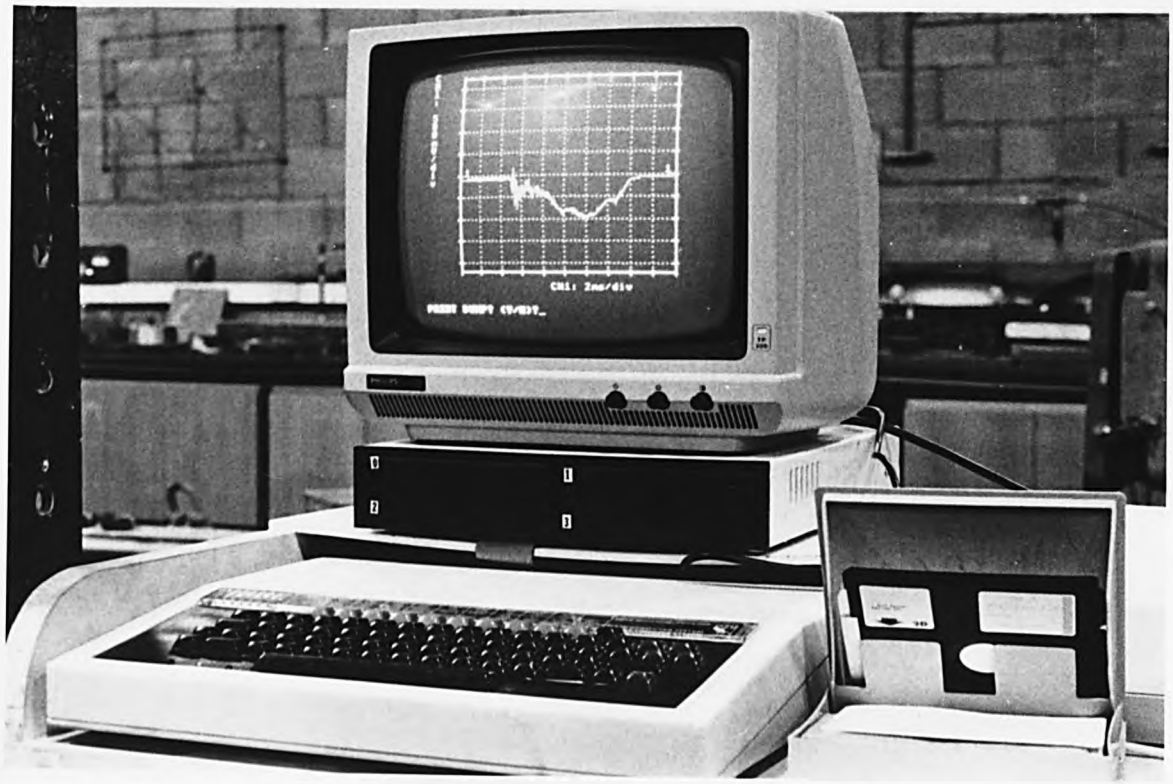

FIGURE 4.26

ACCELERATION
MEASUREMENTS

FIGURE 4.27 SERIES 2 LOADED AREA AND ACCELEROMETER

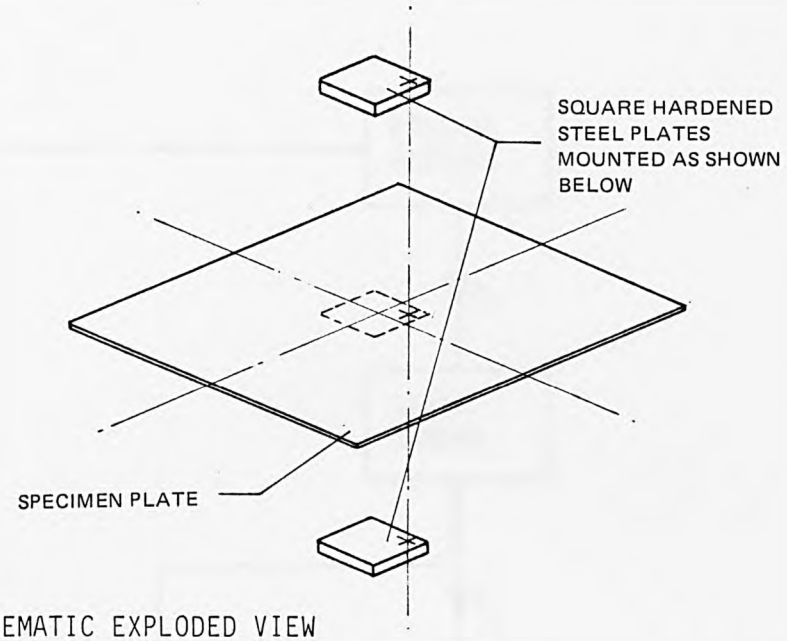

a) SCHEMATIC EXPLODED VIEW

b) FIXING DETAIL

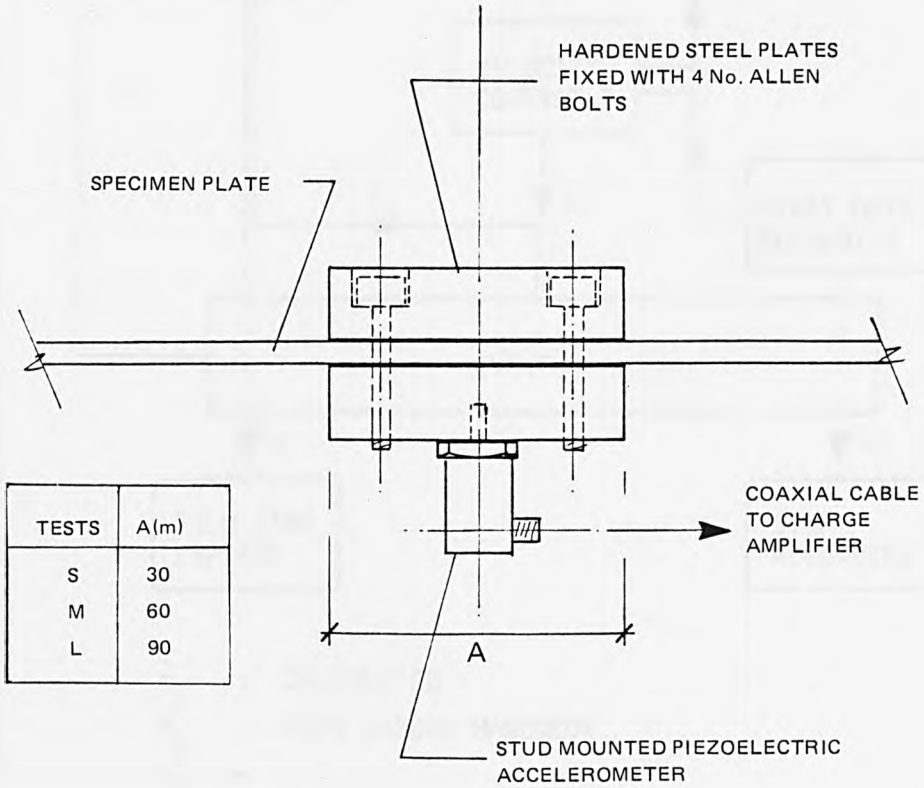

TESTS	A(m)
S	30
M	60
L	90

FIGURE 4.28(a) INSTRUMENTATION SYNCHRONIZATION

MISSILE DROP TIME > CAMERA UP TO SPEED TIME

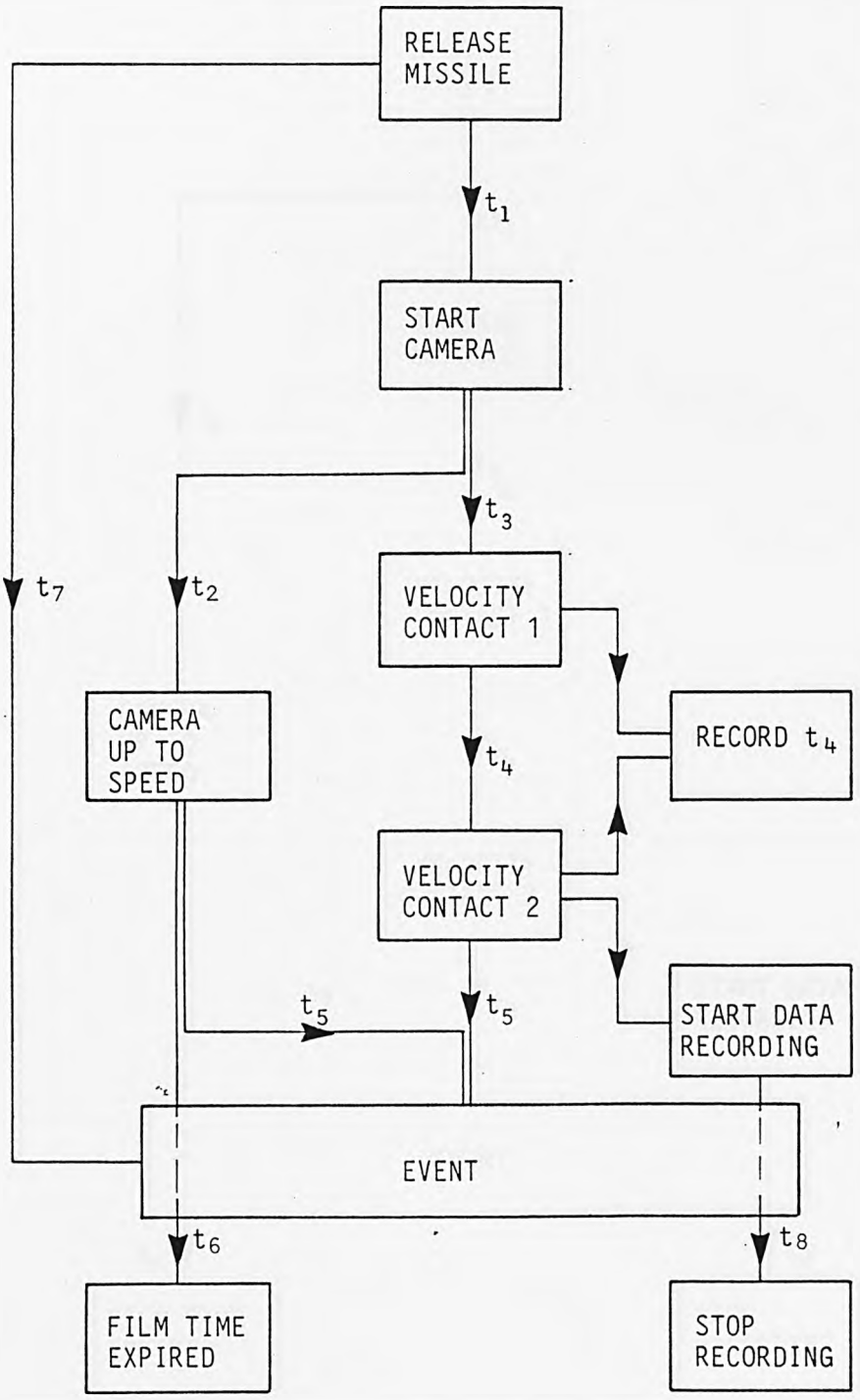

t_1 : CALCULATED

t_2 : FROM CAMERA HANDBOOK

t_5 ≈ 0

FIGURE 4.28(b) INSTRUMENTATION SYNCHRONIZATION

MISSILE DROP TIME < CAMERA UP TO SPEED

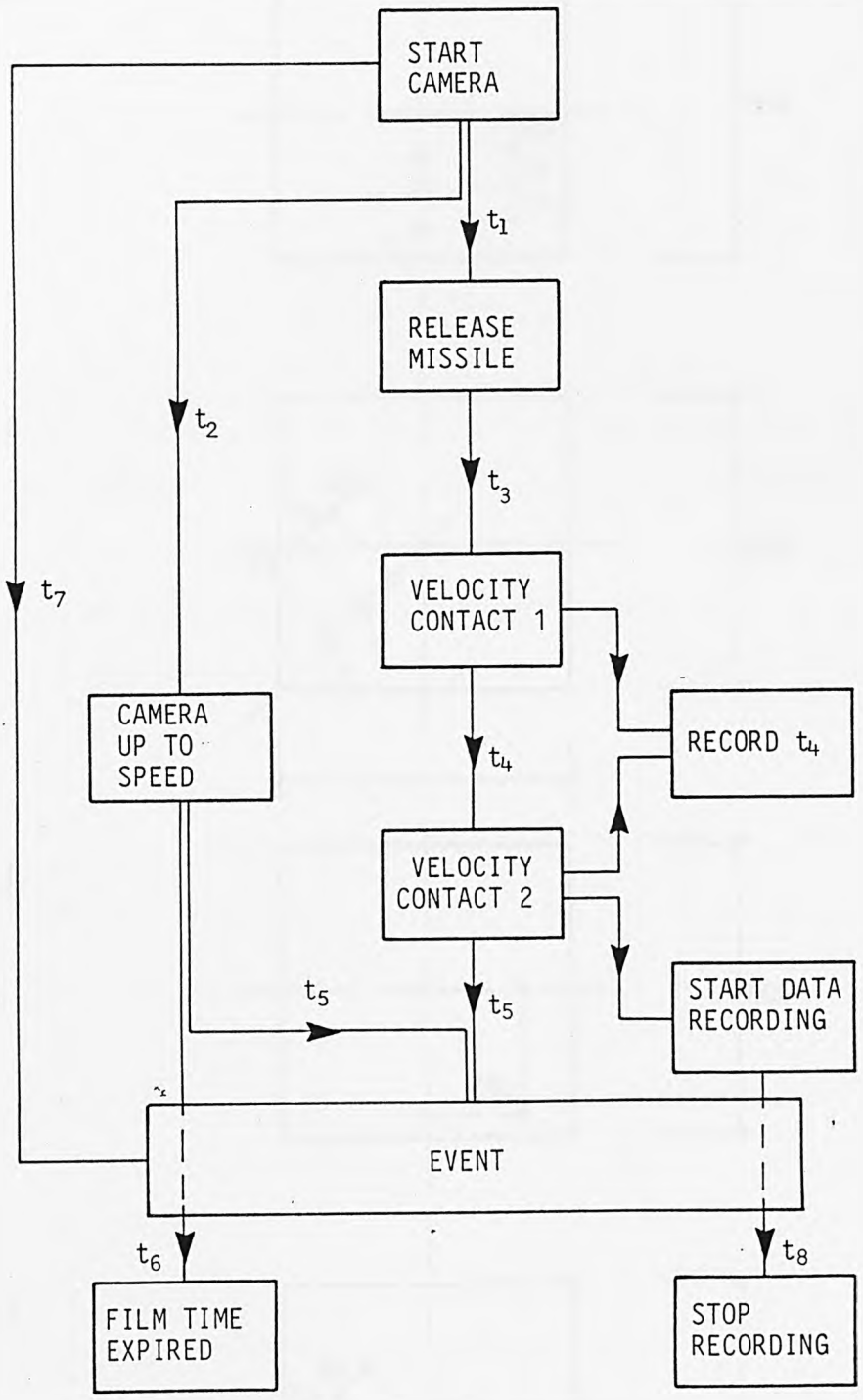

t_1 : CALCULATED

t_2 : FROM CAMERA HANDBOOK

$t_5 \approx 0$

FIGURE 4.29 STRAIN GAUGE CONFIGURATIONS
(ALL GAUGES SHOWN TO BOTH SIDES OF SPECIMENS)

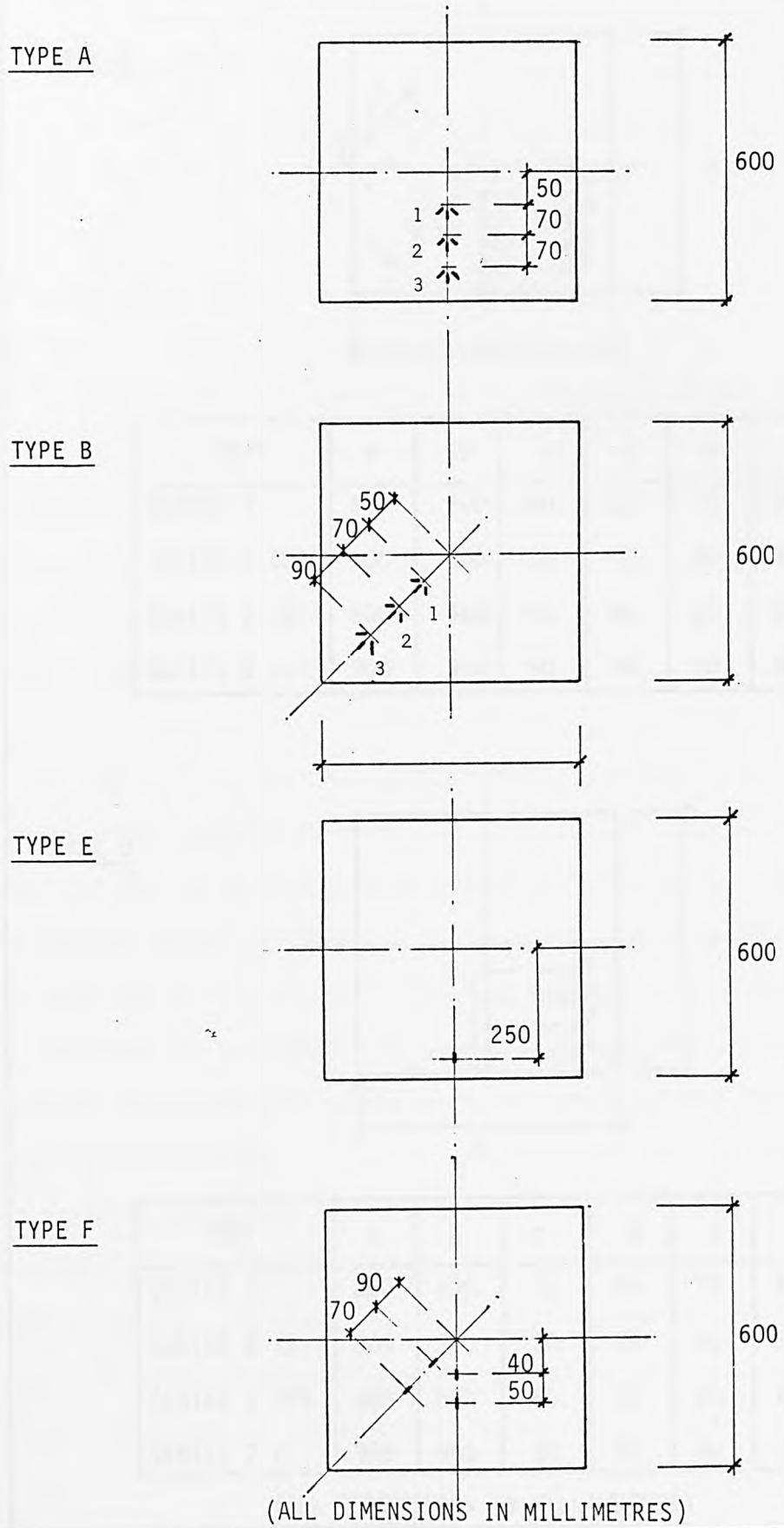

FIGURE 4.29 (CONT'D)

(ALL GAUGES SHOWN TO BOTH SIDES OF SPECIMENS)

TYPE C

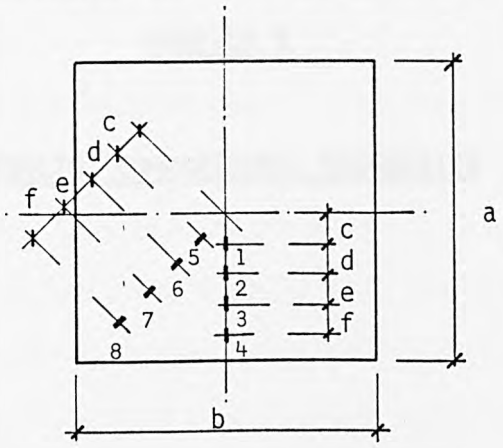

TEST	a	b	c	d	e	f
SERIES 1	600	600	40	50	70	90
SERIES 2 (S)	300	300	30	30	30	30
SERIES 2 (M)	600	600	60	60	60	60
SERIES 2 (L)	900	900	90	90	90	90

TYPE D

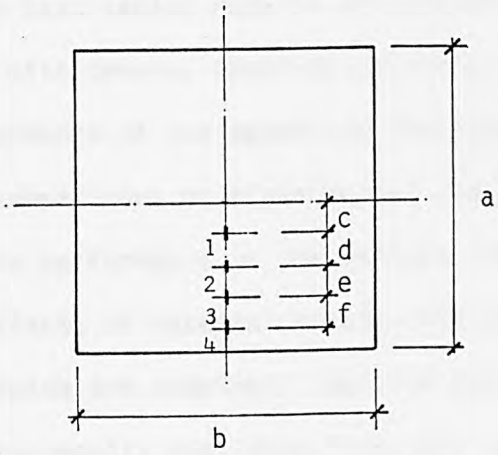

TEST	a	b	c	d	e	f
SERIES 1	600	600	40	50	70	90
SERIES 2 (S)	300	300	30	30	30	30
SERIES 2 (M)	600	600	60	60	60	60
SERIES 2 (L)	900	900	90	90	90	90

(ALL DIMENSIONS IN MILLIMETRES)

CHAPTER 5

RESULTS, COMPARISONS, DISCUSSION

5.1 Introduction

In this Chapter the results from the two experimental test series are presented and compared with predictions from the various theoretical procedures described in Chapter 3. In accordance with the research objectives, the results from test series 2 also examine the validity of using scale models to predict the behaviour of prototypes subject to impact loading.

In section 5.2, the test series results are presented in summarised tabular form, together with general observations relating to the target behaviour and the performance of the apparatus instrumentation. Section 5.3 presents detailed comparisons of experimental and theoretical results from test series 1. The performance of the various theoretical methods is discussed and the effects of material strain rate sensititivity and the yield criterion adopted are examined. Section 5.4 examines and discusses the similarity results available from test series 2 and section 5.5 presents an alternative method for the determination of plate displacement estimation. The method is based on assumed final deflection profiles of the specimens. Finally, section 5.6 presents three case studies from the literature indicating how the proposed methods from the current research work perform in these situations.

5.2 Results and Observations

The theoretical procedures presented in sections 3.4 and 3.6 require the calculation of the kinetic energy available to cause structural damage. This calculation uses the velocity of the projectile immediately prior to impact, together with the assumed velocity profile of the target and the assumption that missile and target remain in contact throughout response. In addition, all theoretical procedures presented in Chapter 3 assume rigid perfectly plastic material behaviour.

It is evident from the tests that none of these assumptions are strictly valid. The kinetic energy possessed by the striker just prior to impact may be dissipated in the following manner

i) Plastic deformation of the target.

ii) Plastic deformation of the striker.

iii) Elastic vibrations of the target.

iv) Elastic vibrations of the striker.

v) Minor losses (heat, noise, etc).

If the available kinetic energy was calculated using theoretical velocity, instead of actual velocity, further dissipation would occur due to losses in the guide system.

It is evident when the energy ratio is high, that the major part of the available kinetic energy is dissipated by plastic deformation of the target. The energy ratio is defined as the kinetic energy possessed by the missile divided by the maximum elastic strain energy capacity of the

target. The elastic vibration in the target becomes increasingly significant as a dissipation mechanism as the energy ratio decreases. Indeed, there will exist a critical missile energy for a given target, below which the specimen response will be entirely elastic.

Plastic deformation of the missile nose tip was discernable after all tests had been completed, but was considered insignificant as an energy dissipation mechanism. The role of the elastic strain energy possessed by the target and the striker throughout response is discussed further in the following sections.

Tables 5.1 and 5.2 give a summary of series 1 and series 2 impact test results. The values of kinetic energy are calculated using the actual velocities of the striker immediately prior to impact.

5.2.1 Deflection Profiles

It was immediately obvious from the test results that the major part of target plastic deformation occurred in continuous deformation fields and the collapse profile which was assumed in section 3.4 and shown in figure 3.2, does not develop in practice, at least for the range of parameters examined here.

The permanent deformed profile of the target was measured in each test using the depth gauge shown in figure 4.19. Measurements were taken across two lines of plate symmetry, from corner to corner and from midside to midside. Measurements from four tests are plotted in figure

5.1 from which it is apparent that, for all thicknesses of plate tested, the deformation is essentially axisymmetric. All specimens exhibited this relationship and those shown in figure 5.1 have been chosen at random.

The theoretical methods developed in sections 3.4 and 3.6 require the dynamic plate response during impact tests to be quasi-static. Figure 5.2 shows the normalised deflection profiles from three impact tests (again chosen at random) plotted with profiles from static tests of corresponding plate thickness. The agreement is extremely good for both profiles measured which confirms the assumption of quasi-static behaviour. It is apparent from figure 5.2, that as the specimen thickness decreases, the curvature of the final deflected profile increases, so producing a more localised target response.

The latter observation is even more apparent in figure 5.3 where equation 3.43 is plotted together with the normalised deflection profiles from three randomly selected tests. Equation 3.43 is the velocity profile assumed in section 3.6, where axisymmetric idealisation of the problem is proposed. It is evident from figure 5.3, that for the range of parameters examined here, equation 3.43 provides a good approximation to the actual specimen profile (except in the region of impact) as plate thickness increases.

Figure 5.4 shows the normalised 'midside to midside' final deflection profiles from tests A, C, E and F. In all tests visual observations confirmed the existance of plastic hinges around the plate edge and at the point where the missile impacted the specimen. Rotation at the

latter location is significantly greater than at the target edge and is coupled with shear deformation, especially in high energy impact events. This shear deformation, which is ignored in the theoretical developments of Chapter 3, will eventually lead to plate failure as the energy ratio increases, by removal of a shear plug [121]. In all tests the central impacted area appeared to have moved vertically as a rigid body. Although the crude 'edge slippage check' described in section 4.3.3 detected no edge movement, it is unlikely that a true encastre support condition was maintained at all locations throughout the duration of response.

Figure 5.4 once again shows the increase in curvature associated with decreasing specimen thickness, but also suggests that it is, to some extent, dependent on missile kinetic energy. The curvature becomes less with increasing missile energy as the specimen response becomes less localised around the point of impact. This was true for all thicknesses of plate tested although as the specimen thickness increases, its profile appears more uniform with variation in available missile energy.

The velocity profile shown in figure 3.2 was not apparent in any of the tests, even when the loaded area was square (test series 2). In fact, preliminary tests on two identical specimens, one of which had a circular loaded area and one with a square loaded area, gave virtually identical, axisymmetric deflection profiles across both lines of symmetry. This is contrary to tests reported by Kling [9] and Samuelides and Frieze [79], where yield line collapse profiles similar to figure 3.2 were experimentally observed under conditions of projectile impact loading.

5.2.2 Acceleration Measurements

An attempt was made to measure the acceleration time history of each impact test. In test series 1, the transducer was mounted at the far end of the missile, figure 4.5 and in test series 2 it was mounted beneath the specimen, figure 4.27.

Table 5.3 gives a summary of the acceleration data from test series 1. The velocity given is the actual velocity of the missile measured immediately prior to impact. The remaining data in the table is obtained from the accelerometer signals which were recorded, via a charge amplifier, on a digital oscilloscope. Typical examples are shown in figure 5.5, which also demonstrate the advantages of filtering and magnification facilities available with the oscilloscope.

The initial signal is extremely noisy since it represents a superposition of the rigid body accelerations of the striker and the multitude of various high frequency stress waves traversing the member on which the transducer is mounted.

The energy absorbed by stress wave propogation in the missile is small compared with the energy required to deform the specimen plastically, since the fundamental vibration period of the striker is short compared with the impact duration. Consequently, force calculations obtained from the product of the missile mass and recorded accelerations should give reasonable estimates of contact force magnitudes. The impact durations are typically of the order of specimen natural frquencies and therefore force-time histories are not significantly influenced by target vibration.

The impact duration can be read directly from the oscilloscope trace, which incorporates a pretrigger facility on the time sweep. Acceleration magnitudes are calculated from settings of Y-axis mv/div on the oscilloscope and the output sensitivity setting (mv/g) on the charge amplifier appropriate to the given test. The electromagnetic release device triggered the acceleration recording system where no values are given in table 5.3.

Several general observations can be made from table 5.3:

i) For a given mass, as the drop height (hence velocity) increases, the duration of impact decreases and the average impact force increases. The available energy is dissipated by a larger force over a shorter time period.

ii) As the mass increases at a given drop height, the duration of impact increases and the average force increases. The available energy is dissipated by a larger force over a longer time period.

iii) For mass-height combinations with identical theoretical kinetic energy capacity (eg A3 and A5), the heavier mass at the lower height will dissipate the energy with a smaller force over a longer time period.

The above observations are trends for a structure having a load-deflection curve which strengthens with increasing displacement, i.e increasing stiffness. Different behaviour would be expected from an unstable structure where, in particular,the impact duration in the

section above (i) would be expected to increase and the impact force decrease, with increasing drop height [109].

Acceleration measurements in test series 2 were marred by equipment malfunctions and breakages, although the new transducer location was partly to blame. The small distance between transducer and the point of impact produced very high frequency stress waves, which continually overloaded the charge amplifier and may have been responsible for the breakage of one accelerometer. Examination of the signal direct from the transducer confirmed that the charge amplifier was incapable of conditioning the signal. An attempt was made to rectify the problem by incorporating an on-line resistor between transducer and amplifier. The selection of a suitable resistor for this purpose is largely a trial and error process which, in view of the nature of the tests, is difficult to incorporate. In addition, resistors were found to cause 'zero shift' problems due to retention of charge in the transducer. Although limited success was achieved using this technique, it is unfortunate that sufficient results were not obtained to compare force-time histories of the events at the three different scales.

An additional problem, which was common to all instrumentation, but particularly troublesome on acceleration measurements, was superficial noise caused by equipment ground loops. The problem was rectified during preliminary tests when it was found necessary to earth all instrumentation, including the accelerometer itself, to a common ground.

5.2.3 Strain Measurement

Time histories of strain at various locations on the surface of targets were measured and recorded in analogue form on magnetic tape. Figure 5.6 shows examples of strain signals from test F1. Interpretation of strain magnitudes and real time durations is achieved using tables 4.2 and 4.3 respectively.

Estimations of maximum strain, maximum permanent strain, initial strain rate and post deformation elastic vibration frequencies can be obtained from output such as figure 5.6(a). In this particular case, it is apparant that plastic deformation is complete within about 5ms after which time elastic vibration of the target dissipates the remaining energy at the supports. The period of elastic vibration is around 7ms, which is slightly less than the fundamental period of vibration of the plate in an undeformed state. This is not entirely surprising since the plate is assumed to be vibrating in its fundamental mode and by undergoing plastic deformation, the plate has assumed a new stiffer profile. The information provided by this strain gauge, however, gives the behaviour of a single 'point' on the surface of the specimen. The point measurement of strain by a small number of gauges provides only an approximate strain distribution.

The estimation of strain rate from signals such as figure 5.6(a) is approximate, but nevertheless useful. A correction for strain rate is presented in section 5.3.1 and it is apparent that these theoretical strain rates are of the correct order of magnitude. Examination of the strain rates obtained from strain gauges across the plate show that

strain rate magnitudes vary significantly across the plate surface in a manner not dissimilar to permanent deformation magnitudes.

Signals such as figure 5.6(b) enable the number of missile impacts and the time between them to be determined. It is also apparent from the figure that secondary impacts are unimportant in this case since no permanent strain results after initial impact. This may not always be the case. Goldsmith [84] reports on situations where secondary impacts have greater effect than initial impacts due to the upward velocity of the target in elastic vibration making the approach velocity greater for second impact than for initial impact.

The curvature of a given deforming specimen is constantly changing and hence the contribution of plastic bending strain and plastic membrane strain varies significantly in position and time throughout the plate. Apart from the obvious bending contribution at plastic hinge locations, bending is most evident in regions of high curvature which develop with elastic recovery.

Figures 5.18(a) and 5.18(b) show strain gauge signals from opposite sides of test series 2 specimens. On the loaded face a high tensile strain occurs during load application, which remains in part as a permanent tensile strain, about which elastic plate vibration occurs when loading has ceased. Conversely, the gauge beneath initially exhibits tensile strain during load application, but at this particular location, the removal of the loading and elastic recovery of the specimen results in a permanent strain of compressive nature. Furthermore, in this particular case, it is evident that the resultant permanent membrane

strain is compressive. This situation was not common to most of the locations examined. The tests have shown that most plastic strain, hence energy absorbtion, takes place locally around the impact region ($r/R < 0.3$ say). At this location strains of between 4% and 5% were measured in some cases and permanent tensile strains generally exist on both faces after elastic recovery has occurred.

These trends can be confirmed by observing the more detailed strain data available from static tests. All specimen locations monitored by strain gauges under static load stretch in radial tension and corresponding radial locations along the two lines of plate symmetry exhibit similar strain once more confirming the axisymmetric idealisation. Strain magnitudes are generally higher on the loaded face. The plate will assume a minimum energy configuration when the load is released and certain areas of the specimen may revert to compression. This will depend on the local curvature assumed and the original strain magnitudes due to the applied load.

It is worth mentioning that strain magnitudes from static and dynamic tests with similar permanent displacements agree well. This is not entirely surprising considering the similarity of deflection profiles shown in figure 5.2.

Several general observations can be made from the strain data retrieved and these are.

i) As drop height increases for constant mass, the time between bounces, hence rebound velocity, increases.

ii) Shorter impact durations are associated with higher rates.

iii) Strain and strain rate magnitudes along the two lines of plate symmetry are approximately equal at a corresponding radial distance and

iv) The magnitude of strain for tests having identical theoretical kinetic energy capacity (eg E1 and E5) are approximately equal, although strain rate magnitudes are greater for the lower mass at greater impact velocity.

In general, signals obtained from all strain gauges were excellent although a few problems were encountered with gauges close to the impact region. In a number of cases the signal amplifier overloaded and in two cases the adhesive fixing the gauges to the specimen failed. It must also be stressed that the employment of a limited number of strain gauges at various surface locations provides an approximate strain profile of a highly complex, three dimensional dynamic strain field.

5.2.4 Velocity Measurements

Tables 5.1 and 5.2 show theoretical and actual velocity measurements from each test. It is evident that the apparatus could not have been calibrated to obtain velocity simply as a function of drop height and measurement is required in each case. The actual velocity approached the theoretical velocity as drop height increased for a given mass and as mass increased from a given drop height.

5.2.5 Displacement Time History

A check on the velocity of missile prior to impact and an estimation of missile rebound velocity can be obtained from analysis of the high speed film. Figure 5.7 shows graphical output from the film analysis system shown in figure 4.24, for tests A3, C2 and F2. In each case the datum on the graphs is the point where the missile initially contacts the target. The top graph shows the motions of the underside of the plate and of the missile, while the lower graph indicates the motion of the target in greater detail. Estimates of maximum permanent deflection obtained by assuming subsequent elastic vibrations about w_o agree well with measured values. The graphs also provide estimates of maximum deflection before elastic unloading on cessation of plastic straining and estimates of post deformation elastic vibration frequencies.

It is evident from figures 5.7 that the elastic vibration amplitude and the ratio of maximum deflection to maximum permanent deflection increases with decreasing plate thickness. This is partly due to the increased stiffness of the thicker targets and partly due to the higher value of energy ratio generally associated with thicker targets e.g. E2 (6.38) and A3 (2.14). The calculation of elastic strain energy capacity for this purpose is given in Appendix 3.

Analysis of high speed films also allow the calculation of time between missile impacts and the determination of the number of impacts. The analysis also confirms that in these tests secondary impacts have no effect on permanent deformation. The 'bounce' times between subsequent missile impacts, obtained from high speed film agreed with those

calculated from strain gauge signals such as figure 5.6(b).

For a particular test configuration the target permanent deflection will increase with increasing missile velocity until some critical velocity when penetration of the target will occur. At still higher velocities, the permanent deflection will decrease with increasing missile velocity and the missile will perforate the target and continue motion with residual velocity. The severity of target damage thus ranges from indentation to perforation to penetration. Although perforation is not considered theoretically in this research, test C5 exceeded the critical velocity and, therefore, proved the apparatus to be capable of studying penetration phenomena. Figure 5.8(a) shows high speed film from test C5 up to time t = 16ms, when the missile has continued through the target and the latter has recovered elastically. Figures 5.8(b) and 5.8(c) show high speed film from tests E2 and L5 respectively; the latter shows motion up to second impact at time t = 587.5ms. All three tests were filmed at 2000 frames per second. Figures 5.8 should be read in conjunction with table 5.4.

During preliminary tests many lighting and target marking configurations were tested. The quality of processed film was best when the underside of the target was painted white and all background was black. Lights within the base together with free standing spotlights provided adequate illumination. Films were generally run at 2000 frames per second with real time correlation achieved using a pulse generator depositing timing marks on the film at the rate of 1000 per second.

5.3 Theoretical and Experimental Correlation

The graphs presented in figure 5.9 show missile velocity plotted against target central permanent deflection for test series 1. Experimental data is compared with up to five theoretical predictions using equations presented in Chapters 2 and 3.

The above mentioned equations generally incorporate mass as a variable and therefore all experimental data points from tests where mass remains constant and drop height varies, may be plotted on a single graph. Tests A, B, D and E generally satisfy this condition and are shown in figure 5.9, where data is effectively represented at two different scales, with and without inclusion of equation 2.8. For tests C and F, where mass is varied from a constant drop height, similar graphs would contain only one experimental data point. An alternative representation, which can include all experimental data for a given set of tests, is shown in figure 5.10. Two theoretical predictions, equations 3.27 and 3.45, are plotted for the appropriate mass variations and, therefore, each theoretical line is associated with one experimental data point. In all cases the velocity coordinate of experimental data is the actual striker velocity just prior to impact.

A useful graphical presentation is achieved by plotting dimensionless deflection against the dimensionless kinetic energy parameter λ . The theoretical predictions of Chapter 3 generally involve the calculation of system kinetic energy at the moment of impact. As noted in section 3.4, for low values of χ (plate-striker mass ratio), the initial value for system kinetic energy approaches the value of initial striker energy just

prior to impact. The striker has always been significantly heavier than the target in the current research and theoretical values of w_o/h for values of λ will, therefore, display insignificant variation with striker mass values used. Consequently, all experimental data points for tests C and F can be plotted on single graphs. Figure 5.11 shows theoretical predictions (excluding equation 2.8) with experimental data points from test series 1. It is worth mentioning that, if all specimen thicknesses had possessed common yield stress value, the experimental data from tests A to F inclusive could have been plotted on a single graph.

5.3.1 Strain Rate Correction

An approximation to allow for material strain rate sensitivity can be made by using an approach outlined for single degree of freedom systems by Hobbs [134].

The strain at yield (σ_{yd}/E), is a measure of strain at the first yield point in a specimen. The time required to reach this yield point (assuming elastic-perfectly plastic material behaviour) is calculated by dividing the maximum elastic deflection by the initial impact velocity of the striker. The maximum elastic deflection (w_e) is found by replacing P with P_L in the formula for elastic plate central deflection which has been discussed in Chapter 3. In quantitative terms this calculation is meaningless since the fundamental definition of limit load does not apply because of strengthening membrane effects within the plate. The estimated strain rate ($\dot{\varepsilon}$) is then found by dividing the strain at yield ($\dot{\varepsilon}_y$) by the time required to reach it.

For circular plates under central concentrated loading:

$$w = \frac{PR^2}{16\pi D} \qquad \ldots.(5.1)$$

where $D = \dfrac{Eh^3}{12(1-\upsilon^2)}$

$$P_L = 4\pi M_o \qquad \ldots.(5.2)$$

where $M_o = \dfrac{\sigma_{yd}\, h^2}{4}$

Using equations 5.1 and 5.2,

$$w_e = \frac{3}{4} \cdot \frac{\sigma_{yd} \cdot R^2 (1-\upsilon^2)}{Eh} \qquad \ldots.(5.3)$$

and

$$t_e = \frac{w_e}{V_o} \qquad \ldots.(5.4)$$

which gives

$$\dot{\epsilon} = \frac{4h}{3R^2(1-\upsilon^2)} \cdot V_o \qquad \ldots.(5.5)$$

Substituting $\dot{\epsilon}$ from equation 5.5 into equation 2.9 gives a value of dynamic yield stress (σ_{yd}) for a given initial striker velocity.

A correction for strain rate can effectively be incorporated by calculating updated striker velocities using strain rates calculated from

equation 5.5 and dynamic yield stress values calculated from equation 2.9. Table 5.5 lists updated striker velocities for test series 1 and figure 5.12 shows velocity permanent deflection graphs for tests A, B, D and E with strain rate corrections applied to equations 3.45 and 3.48.

5.3.2 Bound Solutions

The theoretical procedures derived in Chapter 3 use the yield curves shown in figure 3.5. Upper and lower bounds to the solution obtained using the parabolic interaction yield curve, can be found using inscribing and circumscribing yield curves. Figures 5.13 and 5.14 show bound solutions to equation 3.27 (equation 3.29) and equations 3.42a (equation 3.40a) respectively, for tests A, B, D and E.

5.3.3 Discussion

It is evident from the experimental data presented in figure 5.9 that a linear relationship exists between missile velocity and target permanent deflection for the range of parameters examined. For very thin plates a projected line through experimental data will intercept the origin. As plate thickness hence stiffness, increases, the projected line makes a positive intercept on the velocity axis, indicating the existence of an impact velocity at which no permanent deflection takes place.

It is clear that predictions using equation 2.8 are inaccurate and

unsafe for the complete range of test parameters. Equation 3.27 gives good predictions for very thin plates (6.7% maximum error tests "A") but these predictions progressively become worse as plate thickness increases, until a maximum error of 22% occurs for test F4. For test C and F, where drop height is constant, the predictions of equation 3.27 become worse as mass, hence available kinetic energy, increases. For all tests, equation 3.27 underestimated plate deflection, and as such provides a potentially 'unsafe' solution.

Conversely, equations 3.45 always predicted an overestimate of plate deflection and thus provides a safe solution. The predictions of equations 3.45 and equation 3.48 become more accurate as plate thickness increases. For tests C and F, the theoretical predictions become more accurate as mass, hence available kinetic energy, increases.

For a given target the ratio of initial available kinetic energy to strain energy capacity of the target (the energy ratio), increases as mass is increased from a constant drop height. For the current tests this ratio also increased with increasing plate thickness. It is, therefore, apparent that equations 3.45 predict increasingly accurate results with increasing energy ratio while the converse is true of equation 3.27. The difference in predictions using equations 3.45 and 3.48 are evident, but not too significant in the context of the current analyses. It is apparent that, in this case, the inclusion of bending provides the more accurate predictions.

Figures 5.1 and 5.2 show plate deformation to be approximately axisymmetric and quasi-static. Furthermore, figure 5.3 show deformation

profiles to agree well with equations 3.43 (the velocity profile in the derivation of equations 3.45), especially for increasing plate thickness. The latter observation may well explain the improvement in accuracy of equations 3.45 with increasing plate thickness.

The deformation profile shown in figure 5.2 was not observed in any of the tests and there would, therefore, seem to be no reason why equation 3.27 should predict accurate results. The velocity profile of figure 3.2, however, has been experimentally observed by Kling [9] and Samuelides and Frieze [79] which indicates that the profile assumed by deforming structures is to some extent dependant on the parameters of the individual problem. Notwithstanding these comments, it is evident that both equations 3.27 and 3.45 provide useful engineering estimates of permanent plate deflection and collectively always bound the true solution.

Equation 3.42 underestimated plate deflection in all tests. This equation is derived on the basis of rigid plastic dynamic behaviour which requires impulse durations which are short compared to target fundamental periods. It is evident from table 5.3 that this is not the case for the current tests and so inaccurate predictions using equation 3.42 are hardly surprising. In section 5.6, equation 3.42 is employed with more success to study published experimental data.

The dimensionless plots presented in figure 5.11 are simply an alternative representation of figure 5.9 and, therefore, the above comments on theoretical predictions are equally applicable to figure 5.11. Equation 2.8 is not represented in these figures in order to

clarify the behaviour of the other equations.

The dimensionless presentation is particularly useful for design purposes if, say, a thickness of material of given yield stress, is to be determined for a given impact energy and maximum permanent deflection restriction. Furthermore, a single graph is also applicable to various mass-drop height kinetic energy combinations provided that the mass of the striker is always significantly heavier than the target.

The effect of material strain rate sensitivity is to increase the yield stress and hence decrease the permanent deflection for a given impact energy. In redundant structures this increase may be 'smoothed out' due to a re-distribution of strain as discussed in section 3.2.3. It is evident from figure 5.9 that a correction for strain rate is only appropriate for predictions using equations 3.45 and equation 3.48.

Figures 5.12 show that strain rate corrections applied to equations 3.45 and equation 3.48 improve permanent deflection predictions, especially for the plates with higher stiffness values. Also, as the energy ratio increases, the rate corrected predictions increase in accuracy. Predictions for tests E and F show only a small percentage error in permanent deflection when correction for rate sensitivity is applied to equations 3.45.

It is evident that the accuracy of predictions from the various approximate theories are dependant upon the parameters of the individual problems. Equation 3.27 has predicted good results for plates with low stiffness and impact events of low energy ratio, while the converse is

true for equations 3.45. Equation 3.42 has predicted good results for impact events where impact duration is short compared to the plate fundamental period as discussed in section 5.6. Figures 5.13 and 5.14 show equations 3.27 and 3.45 together with their respective upper and lower bound solutions for test series 1 data. If more experimental data were available, it is probable that good engineering estimates of permanent deflection could be obtained using bound solutions, when the appropriate parameter range applicable to a given equation is known.

In view of the assumptions used in the theoretical derivations, encouraging results have been obtained. All analyses use rigid plastic material idealisation and assume the angular change across a hinge line is small enough to replace tan θ by θ radians. Rigid plastic analyses are generally expected to increase in accuracy with increasing energy ratio and equations 3.45 behaved accordingly. Furthermore, by inspecting figure 5.3 it would be expected that the accuracy of equations 3.45 would increase with increasing target thickness. In view of the deformation profiles presented in figures 5.1 to 5.4 it is surprising that equation 3.27 predicts answers which are at worst only 22% in error. It seems likely that the plastic hinge energy, associated with the velocity profile of figure 3.2, which is dissipated in deforming a plate to a given permanent deflection is of the same order as that expended in a continuous deformation field. The influence of bending increases as plate thickness increases and as rates of curvature become less in continuous deformation fields, the plastic hinge energy predictions underestimate the final deflection. It is nevertheless useful to note that, predictions from equations 3.27 and 3.45 have always bounded the true solution.

It is likely that the assumption of a fully fixed edge condition was partially violated but it is also probable that this is the case in most practical situations where analyses presume encastre supports. This uncertainty is unfortunate from an analytical point of view, as Jones [73] has shown that very small movements of edge supports can significantly effect the structural behaviour being studied.

5.4 Scale Similarity Tests

A summary of test series 2 results have been given in table 5.2. The final deformed profiles of series 2 tests displayed similar characteristics to series 1 tests, and previous discussions of figures 5.1 to 5.4 are equally applicable here. The main objective of test series 2 was to examine the effects of specimen scale on impact loaded structures. In pursuing this aim, however, further information was obtained to compare missile velocity versus target permanent deflection data, with the formulae of Chapter 3. Figure 5.15 shows the experimental data from the three scales of test plotted with four of the equations from Chapter 3. It is evident that equation 3.27 provides good estimates of permanent deflection for these test cases.

Table 5.5 shows permanent central deflection data from the 15 impact tests. It can be seen from table 2.1 that linear dimensions in structural models should scale in direct proportion to the scale factor. Permanent deflections which are normalised with respect to the smallest scale, will have values of 1.0, 2.0 and 3.0 for tests S, M and L respectively if the results can be predicted from similarity principles.

It is evident from column four of table 5.6 that this is not the case. It is also quite clear, however, that perfect scale conditions do not exist prior to missile impact. In particular, material properties are not common for all three scales, and individual velocity measurements show that velocity is not constant for different masses dropped from the same height. Accordingly, two attempts are made in table 5.5 to improve scale similarity by allowing for these discrepancies. Figure 5.16 shows test results plotted with results obtained from a theoretical scale analysis. Significant improvement is achieved when allowance is made for material yield stress and missile velocity variations, although it is unlikely that permanent displacement depends linearly on either of these two parameters.

Figure 5.17 shows the permanent deformed profiles from the highest and lowest energy tests, measured from plate midside to midside. Scale similarity is again improved when allowance is made for the imperfection of initial test conditions. In every case the displacement scale similarity of the three tests agree within 10%. It is noticable that discrepancies for the higher energy test are more or less uniform across the plate, whereas the low energy test displays a scale discrepancy at the plate centre, but good agreement away from the centre.

Figure 5.18 shows dynamic strain information from strain gauges on opposite sides of the plate on the three suffix 4 tests. The strain history at this location exhibits the behaviour noted in section 5.2.3. Permanent tensile strain results on the loaded face and initial tensile strain is reversed to a permanent compressive value on the far side of the target when elastic recovery occurs. Values of permanent strain

agree fairly well, but test S4, not unexpectedly, exhibits slightly less permanent strain due to the increased value of material yield stress.

It can be seen from table 2.1 that time is theoretically proportional to the scale factor and events should happen faster in small scale models. The strain signals demonstrate this relationship, it being particularly noticeable from figure 5.19, that post deformation elastic vibration frequencies are greater at small scale. This fact is further confirmed by undeformed natural frequency values given in table 4.1. The time to reach maximum strain is, therefore, faster in small scale models and it is this scale discrepancy which is often thought to be the cause of 'scale effect' i.e. small scale models appearing to be stronger than prototypes [122,123]. In [122] Calladine suggests an experimental technique specifically designed to alter theoretical scale relationships so that strain rate sensitivity is faithfully scaled in model and prototype.

Despite the strain rate effects encountered in the current tests, the permanent displacements measured were found to scale reasonably well. This may be due to the redundant nature of the problem causing re-distribution of strain, or it may simply be that strain rate magnitudes are not sufficient to be of importance in this case. It is evident that tests from the literature which have reported discrepancies in scale similarity [e.g. 122,123], invariably involve buckling, tearing or fracture in structural response.

It is unfortunate that equipment problems prevented the collection of adequate data to compare acceleration, force and impact duration at

different scales. Since gravitational acceleration will obviously not scale, the time between missile impacts was approximately the same for all three scales. This is, however, unimportant in the current tests as no permanent strain resulted after initial impact.

Figure 5.19 shows strain data from the static tests S6, M6 and L6. The data plotted is strain on the surface of the specimen during load application, before the removal of load has allowed elastic recovery. Consequently both sides of the plate are in tension but, at this particular location, removal of this load was to cause the unloaded face of the specimen to revert to compression. Even after a correction for material yield stress discrepancies, test S6 results are consistently different from the results of tets M6 and L6. After completion of test S6 the hydraulic jack was found to be leaking and it is thought that this may account for the discrepancy displayed in figure 5.19.

Figure 5.20 shows load-permanent deflection data for static tests S6, M6 and L6. It is apparent once again, that tests M6 and L6 agree well, while test S6 exhibits a marked shift from similarity. It is likely that the faulty hydraulic jack was the cause of this phenomena.

Figure 5.21 show the results from figure 5.20 in greater detail. The predictions of up to four equations from Chapter 3 are compared with experimental data. Equation 2.6 is seen to predict inadequate and unsafe results. Equation 3.12 gives good predictions at low values of wo/h for tests M6 and L6 while the results from test S6 must be treated with some caution following observations from figures 5.19 and 5.20.

5.5 Displacement Estimation Based on Final Deformed Shape

An approximate procedure for calculating the central permanent displacement of a thin, plastic, linearly strain hardening circular plate subjected to projectile impact, is developed in reference [105]. In common with the developments of Chapter 3, the procedure requires that the plate deformation profile be assumed, but here it is the final deformed shape which is of interest irrespective of how this was achieved. The procedure is an energy balance which assumes that internal membrane energy dissipation in the plate is entirely responsible for dissipation of the initial kinetic energy of the projectile.

The actions of flexural work and transverse shear energy absorption are therefore ignored and, in addition, radial mid-surface strains are approximated for large deflections as

$$\epsilon_r = \frac{1}{2}\left(\frac{\partial w}{\partial r}\right)^2 \qquad \ldots.(5.6)$$

which ignores radial displacement. Furthermore, tangential strain is assumed negligible.

In [124] Duffey et al have numerically assessed the implications of the above assumptions and concluded that tangential strain (ϵ_θ) is responsible for less than 3% of plastic work and the radial displacement component of ϵ_r contributes somewhat less than 12% to plastic energy absorption.

In [124] it is shown that, for a perfectly plastic material, the energy

balance of [105] reduces to

$$C_o \pi \sigma_y h w_o^2 \left[\int_o^R \left(\frac{\partial f}{\partial r} \right)^2 r \, dr \right] - K.E = O \qquad \ldots.(5.7)$$

where C_o is a function of Poisson's ratio and is numerically equal to 1.125 if $\nu = 0.3$. K.E is the kinetic energy of the missile.

Furthermore $w(r) = w_o f(r)$

where $f(r)$ = normalised transverse plate deflection.

This procedure has also been used by Miyamoto et al [118] and Corren et al [121]. The value of C_o is ultimately dependant on the yield criterion assumed and is given as $2/\sqrt{3}$ and 1.0 respectively in the above references, if the influence of bending dissipation is ignored in [121].

It is evident that equation 5.7 can be solved for w_o if f(r) is known or assumed.

In [118] f(r) is approximated as

$$f(r) = a_o e^{-b_o \cdot r} \qquad \ldots.(5.8)$$

where a_o, b_o are empirically determined shape functions.

In [124] two different deflection profiles are assumed:

i) hyperbolic

$$f(r) = 1 \qquad \text{for} \quad O \leqslant r \leqslant a \qquad \ldots.(5.9a)$$

$$f(r) = 1 - \left(\frac{r^2 - a^2}{R^2 - a^2}\right) \qquad \text{for} \quad a \leqslant r \leqslant R \qquad \ldots.(5.9b)$$

ii) sinusoidal

$$f(r) = 1 \qquad \text{for} \quad O \leqslant r \leqslant a \qquad \ldots.(5.10a)$$

$$f(r) = 1 - \sin\left(\frac{\pi}{2} \cdot \frac{r - a}{R - a}\right) \quad \text{for} \quad a \leqslant r \leqslant R \qquad \ldots.(5.10b)$$

where r , a and R are defined in figure 3.6.

The above equations are explicit functions which are chosen to fit general experimental data as closely as possible. In the current research, an attempt has been made to improve on accuracy by fitting curves through individual data sets from the experiments.

A least squares technique has been used to fit a cubic polynomial through each set of data consisting of normalised deflection profiles for the tests from each plate thickness. This results in the determination of four unknown coefficients satisfying the following polynomial

$$f(r) = A^1\left(\frac{r}{R}\right)^3 + B^1\left(\frac{r}{R}\right)^2 + C^1\left(\frac{r}{R}\right) + D^1 \qquad \ldots.(5.11)$$

for the correct set of initial and boundary conditions.

Having determined the function f(r), it is differentiated, whence the appropriate integration is carried out and w_o is evaluated from equation 5.7.

Figure 5.22 shows the profiles from 5.9 and 5.10 along with the equation 5.11 curve fit and the experimental data points from tests D of series 1. Table 5.7 shows the resulting displacements calculated using the profiles from figure 5.22 and equation 5.7, along with the actual measured permanent displacements. It is evident that the extra work associated with curve fitting of experimental data does not necessarily improve on the accuracy of permanent displacement estimation.

5.6 Case Studies

Very little experimental data which has direct relevance to the current research exists. In this section the results from three publications have been used to indicate performance of approximate methods for other structural configurations.

i) Samuelides and Frieze [79,80]

The work reported in [79,80] involved determination of critical velocities of perforation in situations of ship collision. The critical

collision case is taken as the normal impact of a wedge shaped bow against side ship plating midway between structural bulkheads. It represents a situation where the striker is substantially heavier than the target. The actual deformation profile which was observed in these tests is similar to figure 3.2 with a = 0.

Since no specific data was available on the mass and velocity of individual tests, equation 3.27 has been used to give coordinates of final deformation as a function of initial striker energy.

The diagram shown in figure 5.23 is reproduced from [80]. The dotted line shows the predictions of equation 3.27. Lines 1-4 show various numerical predictions from [79] and line 5 is the prediction of equation 2.8 (which was used in both [79] and [80].)

The following data was used for equation 3.27:

$2A = 243$ mm

$2B = 255$ mm

$2a = 0$

$2b = 145$ mm

$h = 0.81$ mm

$\rho = 7800$ kg/m^3

$\sigma_y = 217$N/mm^2

It is apparent from figure 5.23 that equation 3.27 agrees more closely with experimental data than either equation 2.8 or the various numerical predictions from [79]. It is also worth noting that this is a situation

where the collapse profile in the experiments resembles closely the assumed profile in figure 3.2.

ii) Miyamoto et al [118]

References [118-120] report on tests carried out over a six year period in conjunction with the japanese nuclear power industry. Steel clamped plates 2m square were impacted centrally by missiles with mass up to 50 kg at velocities up to 150 m/s. This now represents a situation where the target has a significantly greater mass than the missile and therefore, following Parkes [31], a quasi-static response is not expected. Unfortunately detailed results and material properties are not published, but one test involving a 90 degree cone headed missile impacting a 30mm thick target may be examined. The following data is used:

$2A = 2m$

$2B = 2m$

$2a = 0.1m$

$2b = 0.1m$

$h = 0.03m$

$\rho = 7850\ kg/m^3$ (assumed)

$G = 50\ kg$

V_o 150 m/s

It is hardly surprising that equation 3.27 now gives totally inaccurate results (> 100% error). This is a true dynamic event where plate inertia has a great influence on final deformation and where impact

duration is short compared with the target fundamental period. Equation 3.42, as expected, now provides the more expected accurate prediction. Figure 5.24 shows predictions using equation 3.42 with and without a correction for strain rate sensitivity. The results are particularly encouraging considering a conical missile was used in the experiment and some energy was inevitably lost in deforming this shape.

iii) Neilson [113]

Tests carried out at UKAEA have examined, amongst other things, the performance of finite element and finite difference computer codes for large deflection impact situations and the implications of using axisymmetric idealisations for square and triangular plate configurations. The tests reported in [113] represent a situation where missile mass is generally greater than target mass and therefore quasi-static target response may be expected. The following data is used:

$2A = 0.22m$

$2B = 0.22m$

$2a = 0.032m$

$2b = 0.032m$

$h = 0.0012$

$\rho = 7850\ kg/m^3$ (assumed)

$\sigma_y = 186N/mm^2$

$G = 4.295\ kg$

$V_o = 8.8m/s$

Figure 5.25 shows the experimental data point together with predictions using equation 3.27 and equations 3.45 corrected for material strain rate sensitivity. Use of the axisymmetric idealisation is supported by Neilson's experimental results which produced results to within 5% for square and inscribed circular plates.

Both equations 3.27 and 3.45 give good engineering estimates of final plate deflection in this case. The predictions are as good as and in some cases better than the numerical predictions from [113].

5.7 Concluding Remarks

The contents of this Chapter have shown the approximate methods developed in Chapter 3 to be useful methods of analysis. The substantial assumptions associated with these methods have been discussed at length and are sufficient to necessitate careful use of these equations. In addition, it is apparent from the tests reported here, that the accuracy of predictions from the various equations used, depend on the set of parameters defining initial problem conditions. The parametric boundaries, where one equation becomes a superior approximation to another, can never be exactly defined, but with experience and further experimental evidence, it seems that results, which are generally accurate enough for most engineering purposes, may be obtained.

The current tests have produced a certain variation in deformation profiles, although all have been essentially quasi-static and axisymmetric. The yield line collapse profile shown in figure 3.2 has

not occurred, but has been experimentally observed in [9] and [79]. An observation made in reference [135] relates plate collapse mechanisms to plate stiffness. It is stated that increased stiffness 'invites' the formulation of yield lines, while increaed flexibility counteracts their formulation.

It is apparent that many properties of both target and missile will significantly affect response. For the tests here, where the missile is assumed rigid, the energy ratio and the missile-target mass ratio have proved significant. The more flexible targets experiencing relatively low energy ratio impact events were predicted to a good degree of accuracy by equation 3.27, despite the obvious error in velocity profile assumption. Equation 3.45 provided the more accurate prediction as targets became stiffer and the energy ratio increased, particularly when allowance was made for strain rate sensitivity. The dynamic formulation of equation 3.42a has given accurate predictions when the target is substantially heavier than the missile and impact durations are short. This conclusion is, at present, based on a single result.

The tests reported here have considered only central impact of rigid missiles on fully fixed plates. Deflection profiles and plate behaviour would be expected to alter with impact location and support condition. In particular, the exclusion of shear from the yield criterion in the current theoretical procedures, would be expected to become unacceptable as the impact location approached the plate edge, particularly if that edge is fixed.

The only viable alternative to approximate analytical techniques are

numerical methods of the type discussed in section 2.5. It is likely that this approach will be significantly more expensive, particularly if an explicit code is being used. Furthermore, the accuracy of results obtained are not always encouraging especially when assuming quasi-static behaviour [113]. A computer code may accurately predict the static load deflection relationship of a given structure. Equating the initial kinetic energy of the striker to the area beneath this curve, however, will generally not give accurate predictions of permanent deflection. The initial energy of the missile will be dissipated in many other mechanisms, e.g. throwing the missile back from the structure.

The specialised explicit codes are generally based on constant stress element formulations. If bending is to be included, many elements will be required across the thickness of a structure. The codes are consequently extremely expensive to operate and are continuously developed in an attempt to improve on efficiency and speed of calculations without substantial loss in accuracy. The use of constant stress elements mean predictions of strain through the thickness of a plate may be qualitatively good, but quantitatively poor as demonstrated by Neilson [136]. In addition, the voluminous output generated by such codes require the use of post processing facilities which can significantly increase the costs.

In general, the similarity exhibited by the three scales of test in series 2 was very good. Linear displacement was always within 10% despite variations in rate of strain. The theoretical and experimental strain magnitudes agreed well. In the static tests, force-displacement and strain-displacement scaled reasonably well except for the smallest

scale where equipment was thought to be at fault. A major difficulty associated with experimental verification of scaling laws is the initial achievement of perfectly scaled models. Even for the simple structures tested here, material properties and thicknesses, and missile velocities were not scaled faithfully. Further problems are likely to be encountered where tests involve bolted and in particular welded connections.

The method presented in section 5.5 predicted reasonable estimates of permanent deflection. This method assumes a final deformed target profiles. It would appear that choice of a suitable shape function is not particularly critical. It would not, for instance, be worthwhile attempting to find from the current results, relationships between initial conditions and cubic polynomial coefficients for general impact events outside the range studied here.

The use of the limited experimental data available in the literature has produced encouraging results. The case studies have verified that judgement must be employed to select the most appropriate approximate.

It must be remembered that the analytical procedures developed herein assume that angular changes associated with deflections are small enough to replace tan with radians. Further refinement of the methods must be made when deflections reach sufficient magnitudes to produce significant difference in these quantities.

The approximate methods outlined here must always be used with caution if they are to be applied outside the experimental range of

parameters which has been considered. The range of parameters for which each is applicable will become apparent with further experimental work.

It must also be emphasised that no failure criteria are associated with these analyses. Test C5 involved plate failure by perforation, figure 5.8a, which is not indicated by figure 5.10. This consideration highlights a serious drawback associated with all these approximate methods. Strain predictions are highly dependent on the assumed plate velocity profile and since failure criteria are, in general, a function of strain limits, the prediction of failure using these techniques does not seem feasible.

TABLE 5.1 TEST SERIES I RESULTS SUMMARY (IMPACT TESTS)

Test	w_o (mm)	V_A (m/s)	w/h	λ	V_{TH} (m/s)	$\frac{V_A}{V_{TH}}$	K.E (J)
A1	17.9	5.103	10.93	238.4	5.425	0.94	337.3
A2	7.8	2.464	4.76	55.7	3.13	0.79	83.2
A3	13.8	3.918	8.42	140.7	4.43	0.88	210.3
A4	19.9	5.867	12.15	315.6	6.26	0.94	471.6
A5	13.2	2.456	8.06	110.6	3.13	0.78	165.3
B1	20.5	5.1	10.02	251.8	5.425	0.94	426.6
B2	24.0	5.908	11.74	278.9	6.264	0.94	512.4
B3	27.3	6.65	13.3	353.3	7.0	0.95	725.2
B4	16.9	4.105	8.76	134.3	4.43	0.93	255.1
B5	10.25	2.459	5.01	48.3	3.132	0.79	99.2
C1	30.65	6.93	12.43	207.1	7.34	0.94	900.5
C2	22.9	6.53	9.29	157.4	7.34	0.89	684.4
C3	20.5	6.89	8.31	140.3	7.34	0.94	610.7
C4	15.8	6.22	6.41	97.9	7.34	0.85	425.2
C5	PEN.	6.79	-	218.4	7.34	0.93	948.9
D1	21.6	5.92	6.95	88.1	6.26	0.95	769.3
D2	17.9	5.04	5.76	63.9	5.42	0.93	556.9
D3	14.85	4.0	4.78	40.2	4.43	0.9	351.2
D4	24.05	6.51	7.74	106.6	7.0	0.93	930.2
D5	26.2	6.97	8.43	122.2	7.34	0.95	1067.6
E1	25.3	7.09	6.29	63.2	7.67	0.92	1288.3
E2	24.05	6.61	5.98	54.9	7.0	0.94	1122.0
E3	20.0	5.89	4.98	43.6	6.26	0.94	889.9
E4	17.75	5.0	4.41	31.4	5.42	0.92	640.9
E5	25.05	5.84	6.23	63.9	6.26	0.93	1302.7
F1	20.3	7.11	3.97	34.7	7.67	0.93	1296.7
F2	19.6	6.97	3.83	26.3	7.67	0.91	984.6
F3	25.9	7.0	5.1	40.7	7.67	0.91	1521.5
F4	28.7	7.32	5.62	52.2	7.67	0.95	1953.1
F5	14.1	6.67	2.76	17.5	7.67	0.87	653.8

TABLE 5.2 TEST SERIES 2 RESULTS SUMMARY (IMPACT TESTS)

Test	w_o (mm)	V_A (m/s)	$w_{o/h}$	λ	V_{TH} (m/s)	$\frac{V_A}{V_{TH}}$	K.E. (J)
S1	4.9	3.77	2.45	71.5	4.43	0.85	48.9
S2	6.45	4.82	3.225	35.1	5.42	0.89	80.0
S3	8.25	5.66	4.125	48.4	6.26	0.9	110.3
S4	9.55	6.36	4.775	61.1	7.0	0.91	139.3
S1	10.6	7.06	5.3	75.3	7.67	0.92	171.6
M1	12.15	4.19	3.08	30.2	4.43	0.95	483.6
M2	15.75	5.203	3.99	46.5	5.42	0.96	745.7
M3	19.55	6.12	4.95	64.4	6.26	0.98	1031.7
M4	20.6	6.697	5.22	77.1	7.0	0.96	1235.4
M5	23.1	7.35	5.85	92.9	7.67	0.96	1488.1
L1	17.25	4.253	2.86	30.1	4.43	0.96	1681.5
L2	21.3	5.257	3.53	46.0	5.42	0.97	2569.1
L3	26.9	6.135	4.46	62.6	6.26	0.98	3498.9
L4	29.8	6.86	4.94	78.2	7.0	0.98	4374.7
L5	34.15	7.517	5.66	94.0	7.67	0.98	5252.7

TABLE 5.3 ACCELEROMETER TRACE DATA

Test	Mass (kg)	Velocity (m/s)	Impact Duration (ms)	Max. Accel. (g)	Average Accel. (g)	Average Force (KN)	w_o (mm)
A1	27.4	5.103	12.2	140	45	12.1	17.9
A2	27.4	2.464	-	-	-	-	7.8
A3	27.4	3.918	13.0	116	30	8.1	13.8
A4	27.4	5.867	11.9	150	50	13.4	19.8
A5	54.8	2.456	18.9	52	13	7.0	13.2
B1	32.8	51	-	-	-	-	20.5
B2	32.8	5.908	-	-	-	-	24.0
B3	32.8	6.65	10.7	173	61	19.6	27.3
B4	32.8	4.105	13.9	91.5	28	9.02	16.9
B5	32.8	2.459	15.9	60	15	4.8	10.25
C1	37.5	6.93	10.4	108	68	25.0	30.65
C2	32.1	6.53	11.0	200	60	18.9	22.9
C3	25.7	6.89	10.6	216	66	16.6	20.5
C4	22.0	6.22	8.8	210	72	15.5	15.8
C5	41.2	6.79	-	-	-	-	PEN.
D1	43.9	5.92	11.7	162	51	21.9	21.6
D2	43.9	5.04	11.5	133	44	18.9	17.9
D3	43.9	4.0	12.9	110	30	12.9	14.85
D4	43.9	6.51	10.8	170	60	25.8	24.05
D5	43.9	6.97	10.5	180	65	28.0	26.02
E1	51.3	7.09	10.8	200	67	33.7	25.3
E2	51.3	6.61	10.9	180	60	30.2	24.05
E3	51.3	5.89	11.6	250	55	27.7	20.0
E4	51.3	5.0	11.7	160	45	22.6	17.75
E5	76.5	5.84	13.8	150	43	32.3	25.05
F1	51.3	7.11	10.0	230	70	35.2	20.3
F2	40.5	6.97	9.73	417	75	29.8	19.6
F3	62.1	7.0	10.9	220	65	39.6	25.9
F4	72.9	7.32	10.5	367	70	50.1	28.7
F5	29.4	6.67	7.8	435	87	25.1	14.1

TABLE 5.4 FIGURE 8 INTERPRETATION

ALL PICTURES FILMED AT 2000 FRAMES PER SECOND t = 0ms IS THE INSTANT OF INITIAL IMPACT			
Test Figure / Frame	C5 5.8a t (ms)	E2 5.8b t (ms)	L2 5.8c t (ms)
1	-5	-5	-5
2	0	0	0
3	2	2	5
4	4	4	10
5	6	6	20
6	8	8	40
7	10	10	100
8	12	12	200
9	14	14	320
10	16	16	587.5

TABLE 5.5 STRAIN-RATE CORRECTION

Tests	V_o (m/s)	SR	$\dot{\epsilon}$	$\frac{\sigma_{yd}}{\sigma_y}$	V_o^1 (m/s)
A	2	0.0237	0.047	1.26	2.244
	4		0.095	1.30	4.557
	6		0.142	1.323	6.901
B	2	0.0296	0.06	1.271	2.255
	4		0.12	1.31	4.58
	6		0.18	1.34	6.94
C	4	0.0356	0.14	1.32	4.60
	6		0.21	1.351	6.97
	8		0.285	1.371	9.37
D	3	0.045	0.135	1.32	3.45
	6		0.27	1.37	7.02
	9		0.41	1.40	10.64
E	5	0.058	0.291	1.373	5.86
	7		0.41	1.40	8.28
	9		0.52	1.42	10.72
F	5	0.074	0.37	1.39	5.90
	7		0.52	1.42	8.34
	9		0.67	1.44	10.80

TABLE 5.6 TEST SERIES 2 NORMALISED DEFLECTION

Test	w_o (mm)	Normalised W.R.T.S (Theoretical) $\bar{w}_o$	Normalised W.R.T.S (Actual) $\bar{w}_o$	Corrected for σ_Y $\bar{w}_o$	V_A (m/s)	Corrected for $\bar{w}_o$
S1	4.9	1.0	1.0	1.0	3.77	1.0
M1	12.15	2.0	2.48	2.26	4.19	2.23
L1	17.25	3.0	3.52	3.15	4.25	3.12
S2	6.45	1.0	1.0	1.0	4.82	1.0
M2	15.75	2.0	2.44	2.22	5.703	2.26
L2	21.3	3.0	3.30	2.95	5.257	3.03
S3	8.25	1.0	1.0	1.0	5.66	1.0
M3	19.55	2.0	2.37	2.16	6.12	2.19
L3	26.89	3.0	3.26	2.92	6.13	3.01
S4	9.55	1.0	1.0	1.0	6.36	1.0
M4	20.6	2.0	2.16	1.97	6.697	2.05
L4	29.8	3.0	3.12	2.8	6.86	2.9
S5	10.6	1.0	1.0	1.0	7.06	1.0
M5	23.1	2.0	2.18	1.99	7.35	2.09
L5	34.15	3.0	3.72	2.88	7.52	3.02

TABLE 5.7 PERMANENT DISPLACEMENT FROM DIRECT ENERGY BALANCE

Test	w_o (mm)	Eqn.5.9 w_o (mm)	Eqn.5.10 w_o (mm)	w_o (mm)	Equation 5.11 A^1	B^1	C^1	D^1
A1	17.9	18.61	19.41	14.64				
A2	7.8	9.24	9.64	7.27				
A3	13.8	14.7	15.32	11.56	-2.123	5.536	-4.702	1.29
A4	19.9	22.0	22.95	17.31				
A5	13.2	13.03	13.59	10.25				
B1	20.5	22.3	23.25	19.32				
B2	24.0	25.83	26.93	22.37				
B3	27.3	29.07	30.31	25.18	-1.708	4.678	-4.232	1.262
B4	16.9	17.24	17.98	14.94				
B5	10.25	10.75	11.21	9.31				
C1	30.65	26.84	27.99	25.42				
C2	22.9	23.4	24.39	22.16	-1.357	3.953	-3.834	1.239
C3	20.5	22.1	23.04	20.93				
C4	15.8	18.44	19.23	17.46				
D1	21.6	22.06	23.0	21.6				
D2	17.9	18.77	19.57	18.4				
D3	14.85	14.9	15.54	14.6	-1.231	3.691	-3.691	1.230
D4	24.05	24.26	25.29	23.8				
D5	26.2	25.99	27.1	25.5				
E1	25.3	24.166	25.19	24.04				
E2	24.05	22.55	23.51	22.43				
E3	20.0	20.08	20.94	19.98	-1.175	3.576	-3.628	1.226
E4	17.75	17.04	17.77	16.95				
E5	25.05	24.3	25.33	24.17				
F1	20.3	22.76	23.74	23.5				
F2	19.6	19.84	20.68	20.5				
F3	25.9	24.76	25.71	25.5	-1.039	3.295	-3.474	1.217
F4	28.7	27.94	29.13	28.9				
F5	14.1	16.16	16.86	16.7				

FIGURE 5.1(a) TARGET PLATE DEFORMED PROFILE

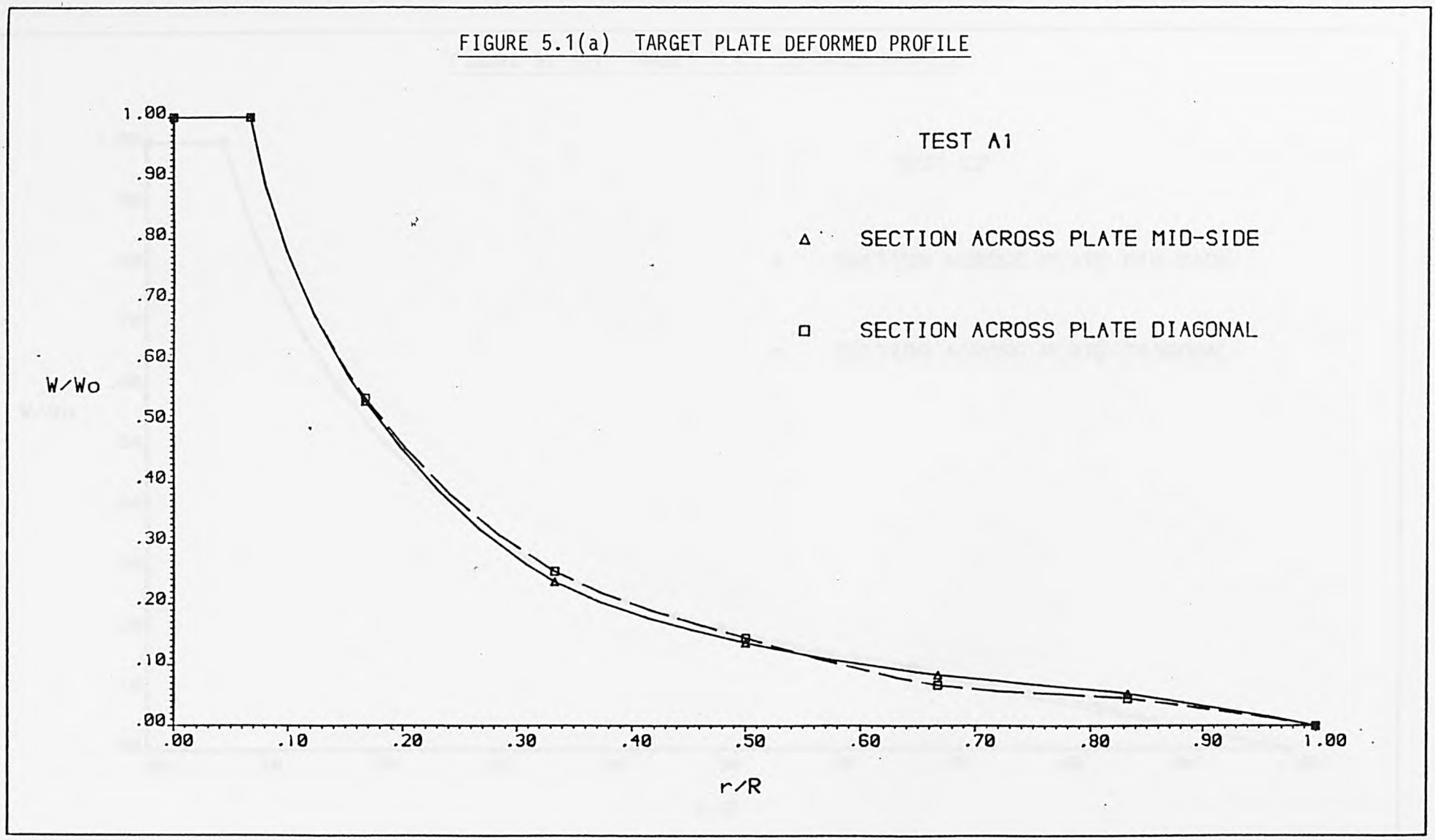

FIGURE 5.1(b) TARGET PLATE DEFORMED PROFILE

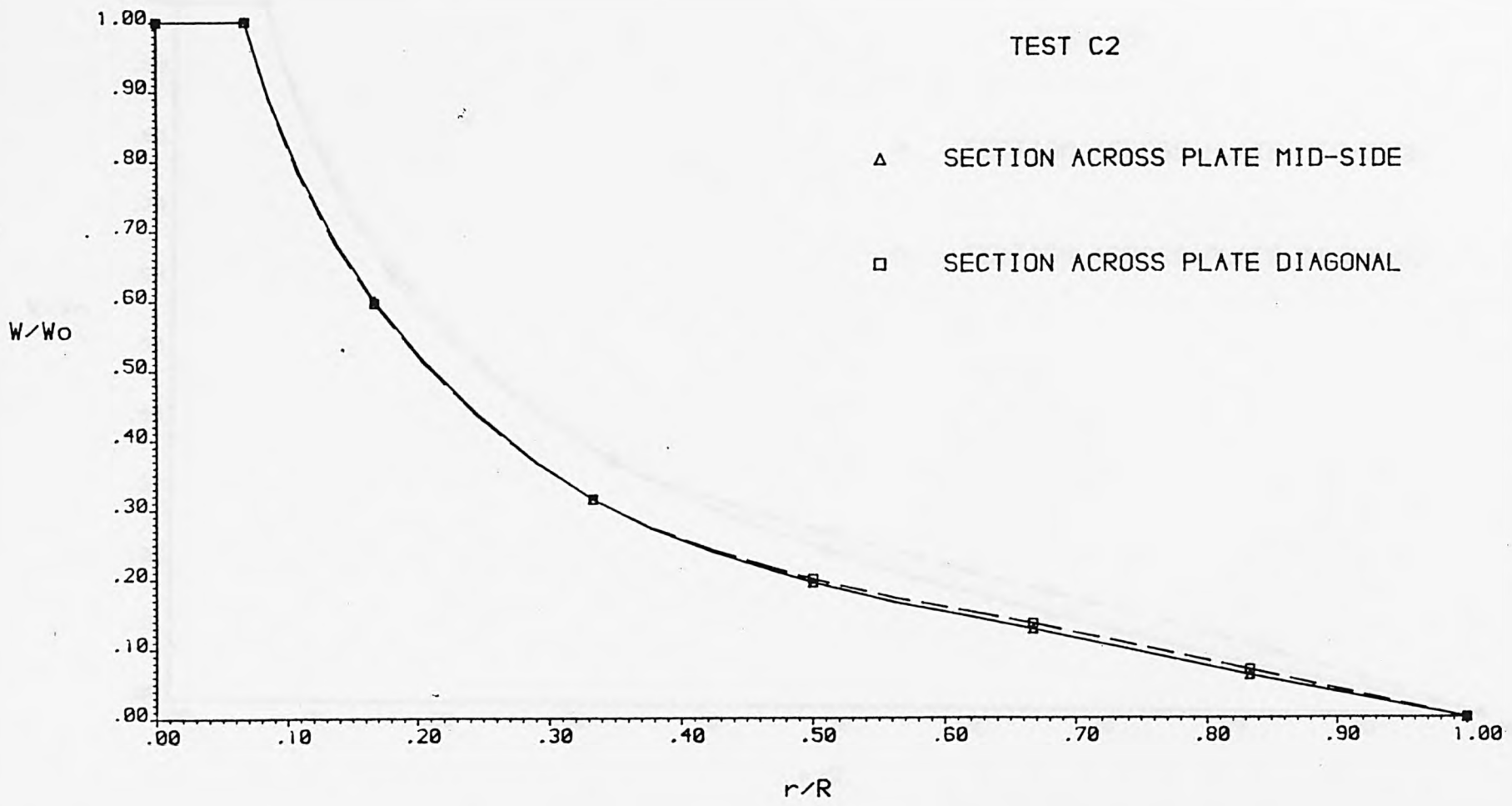

FIGURE 5.1(c) TARGET PLATE DEFORMED PROFILE

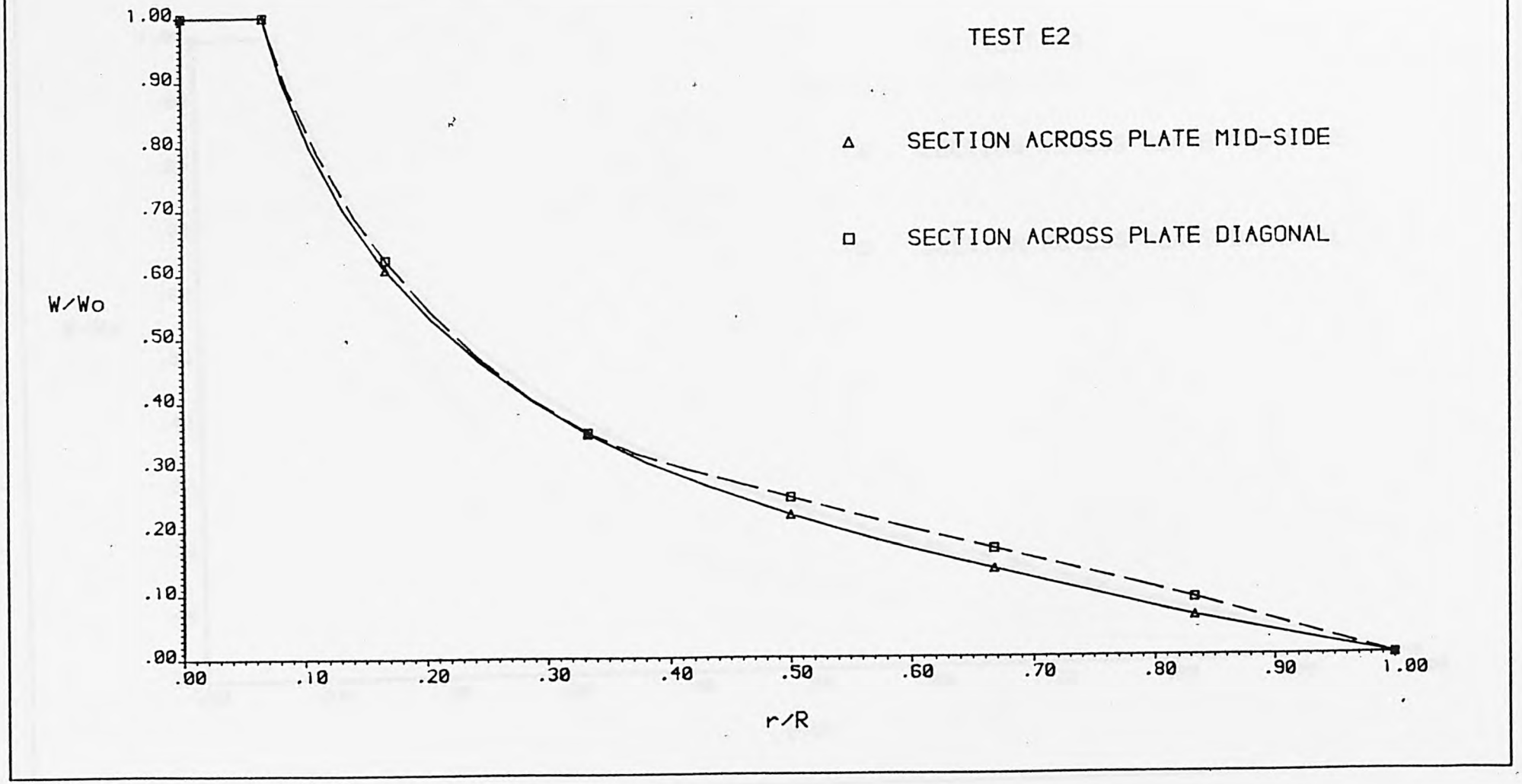

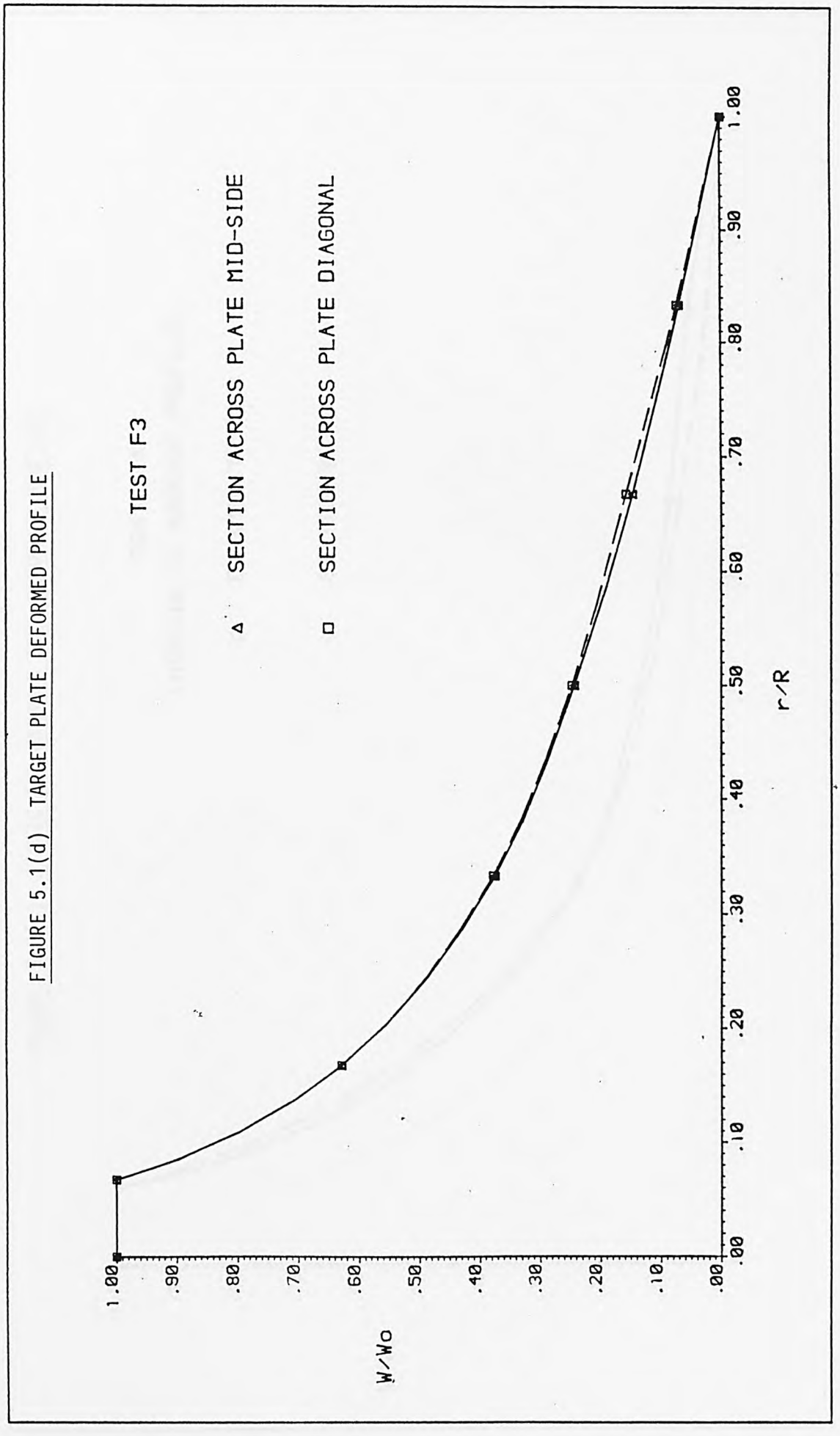

FIGURE 5.1(d) TARGET PLATE DEFORMED PROFILE

FIGURE 5.2(a) STATIC AND DYNAMIC TEST DEFORMED PROFILES

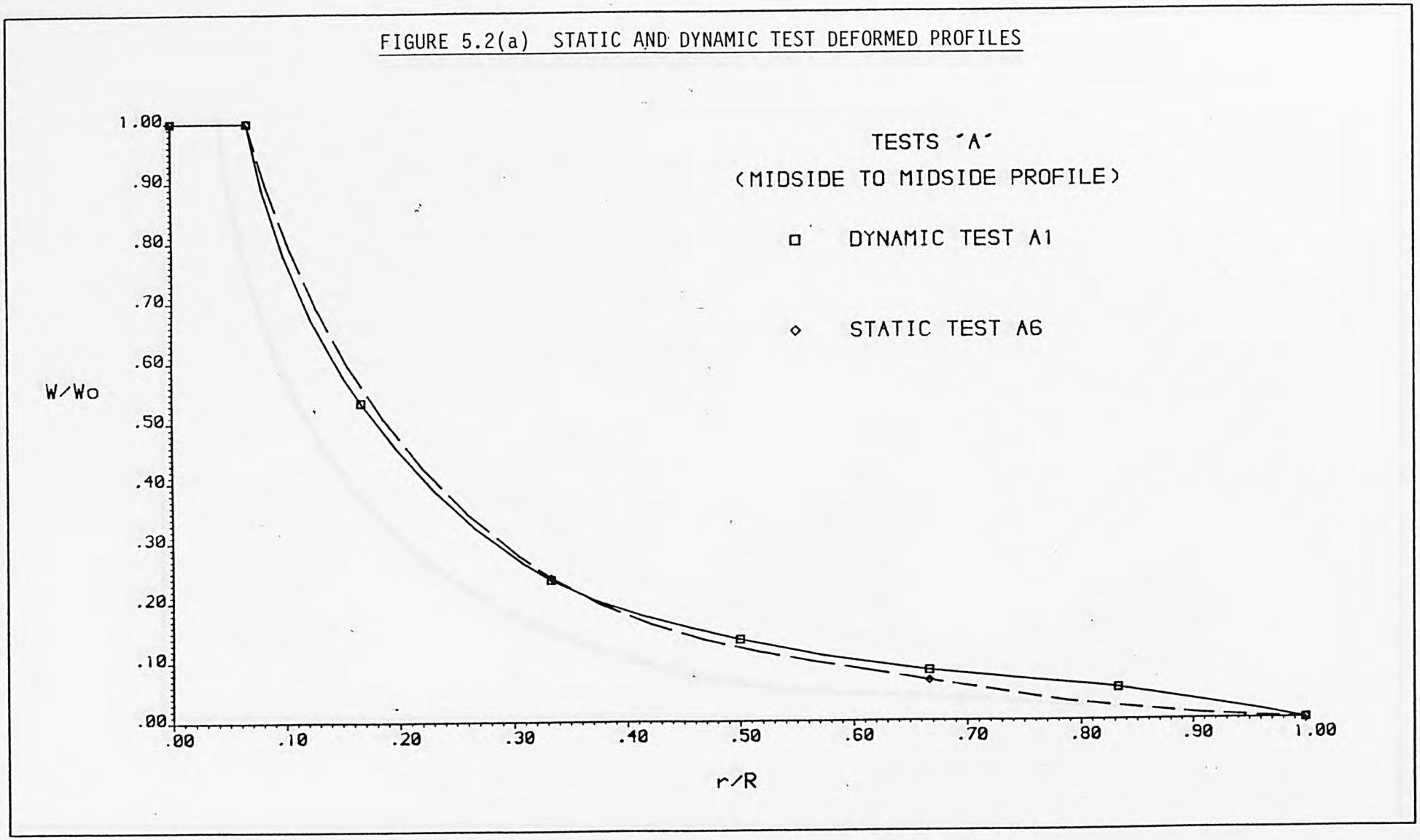

FIGURE 5.2(b) STATIC AND DYNAMIC TEST DEFORMED PROFILES

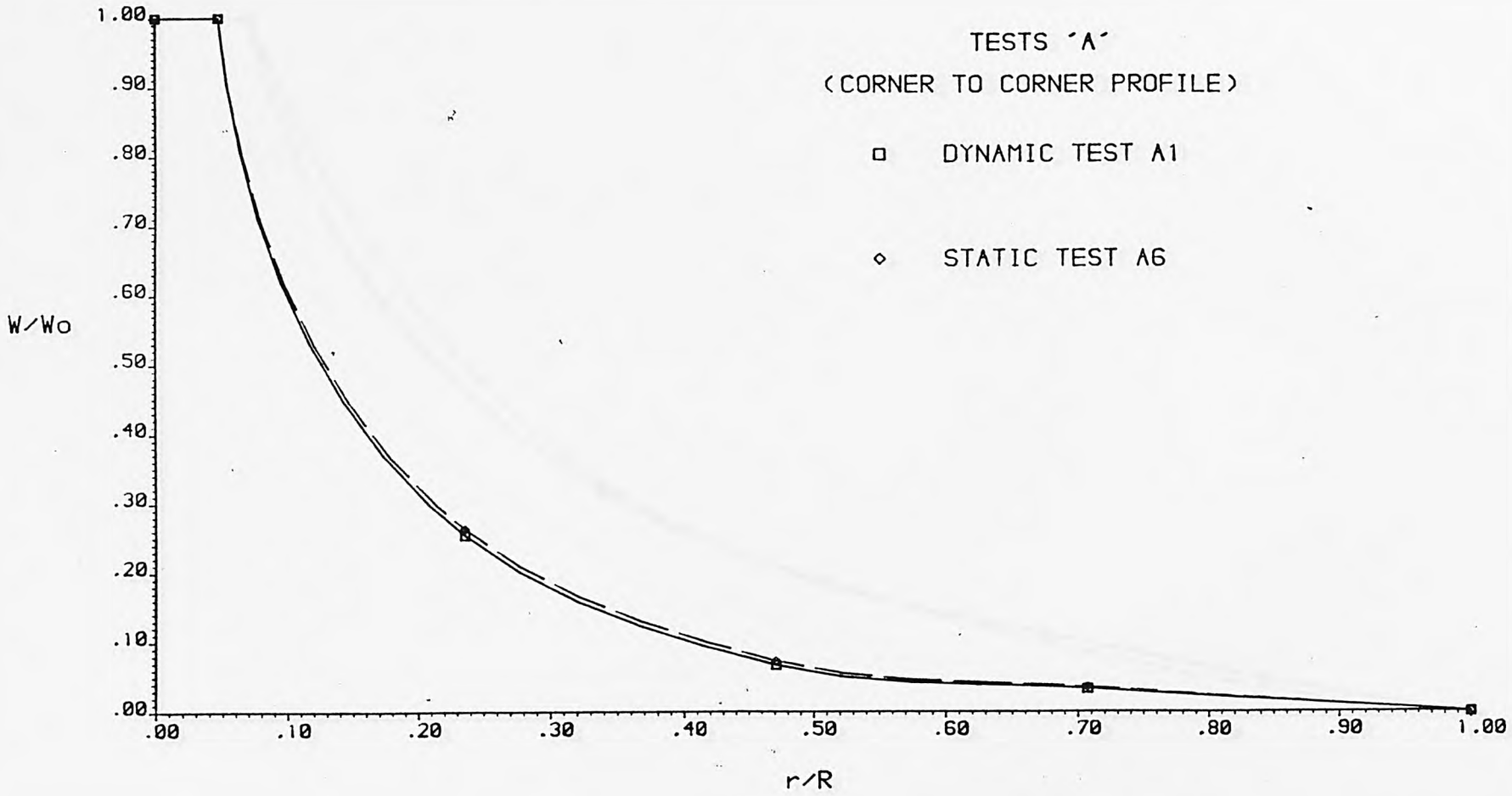

FIGURE 5.2(c) STATIC AND DYNAMIC TEST DEFORMED PROFILES

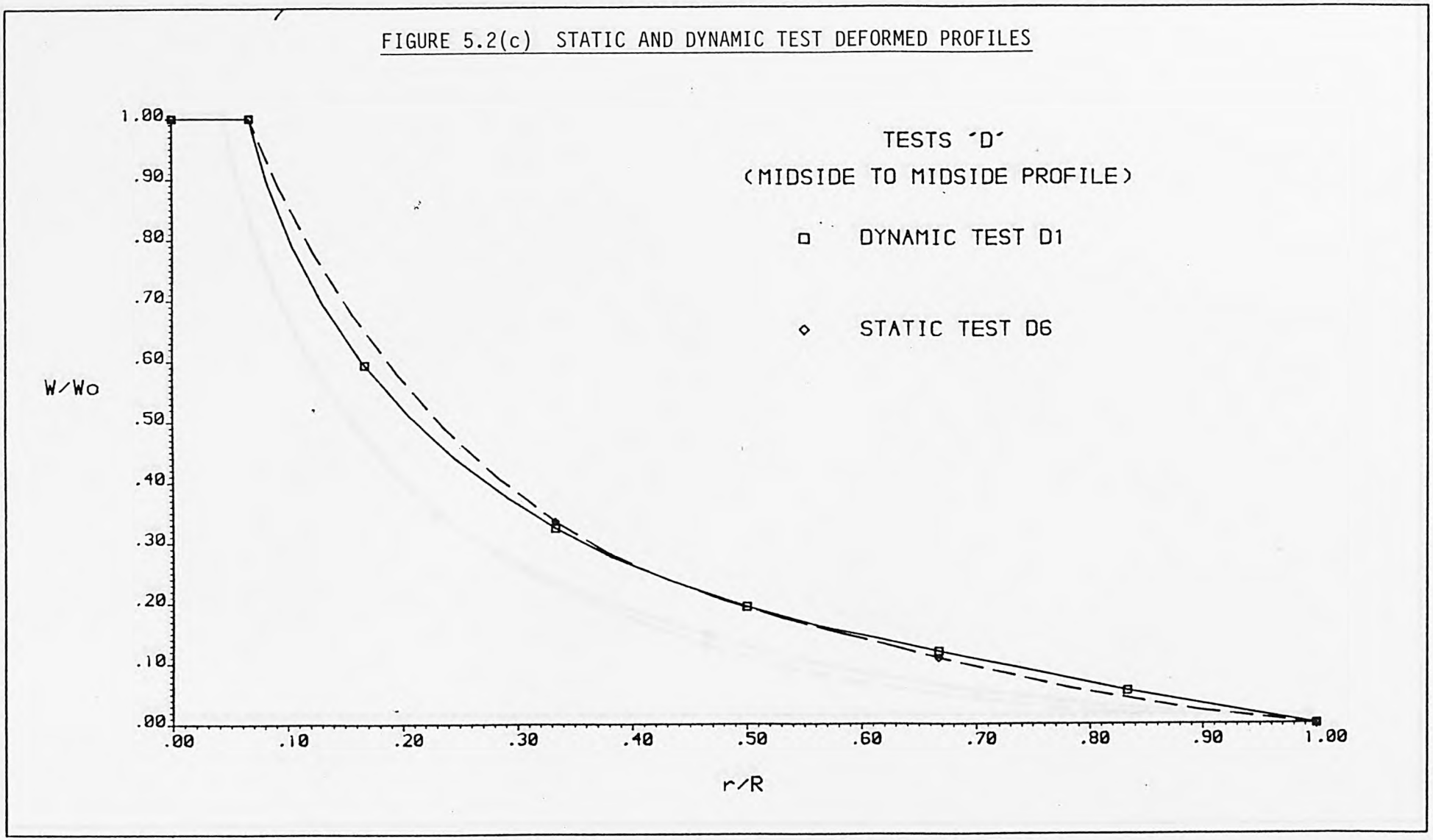

FIGURE 5.2(d) STATIC AND DYNAMIC TEST DEFORMED PROFILES

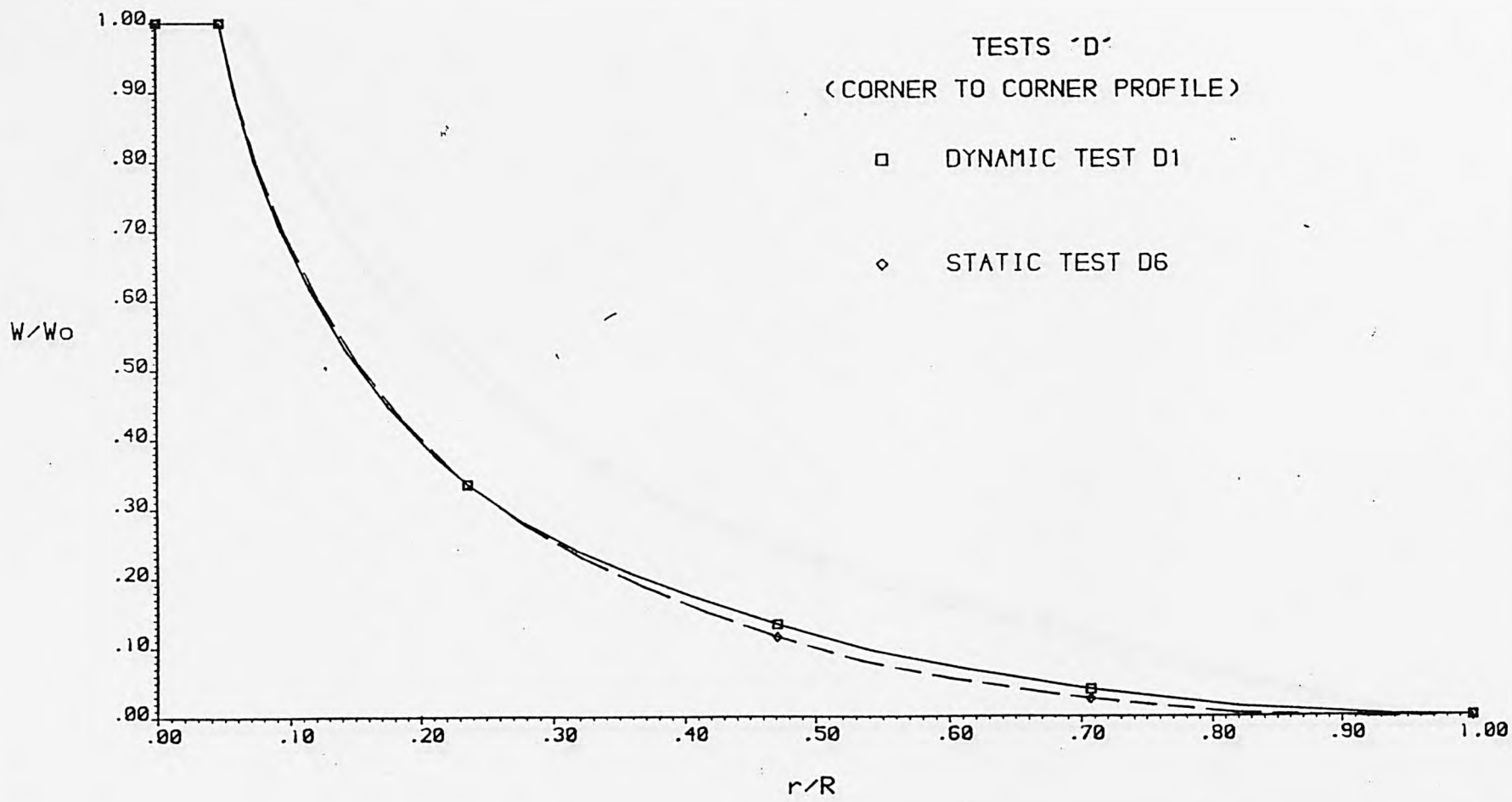

FIGURE 5.2(e) STATIC AND DYNAMIC TEST DEFORMED PROFILES

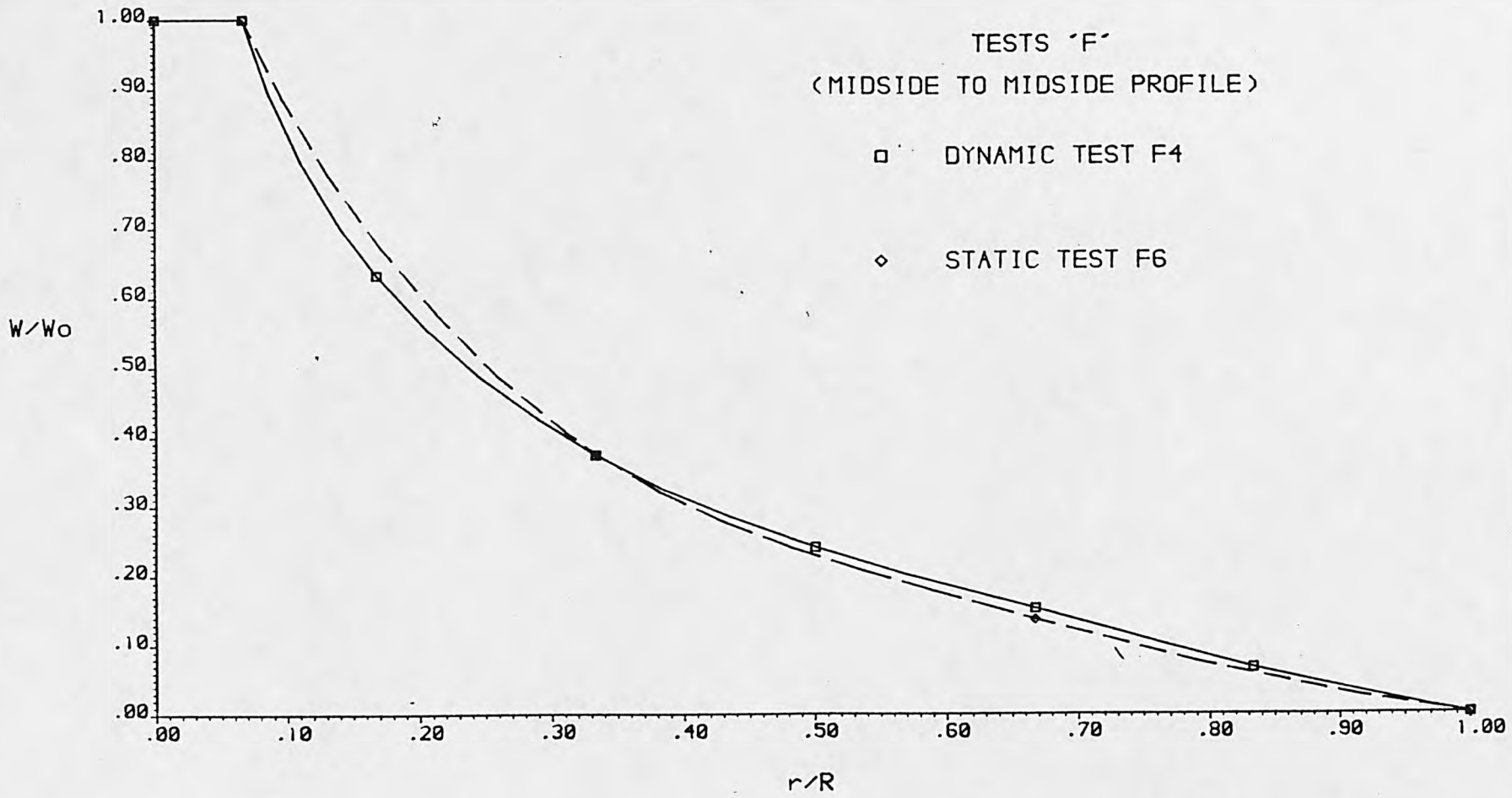

FIGURE 5.2(f) STATIC AND DYNAMIC TEST DEFORMED PROFILES

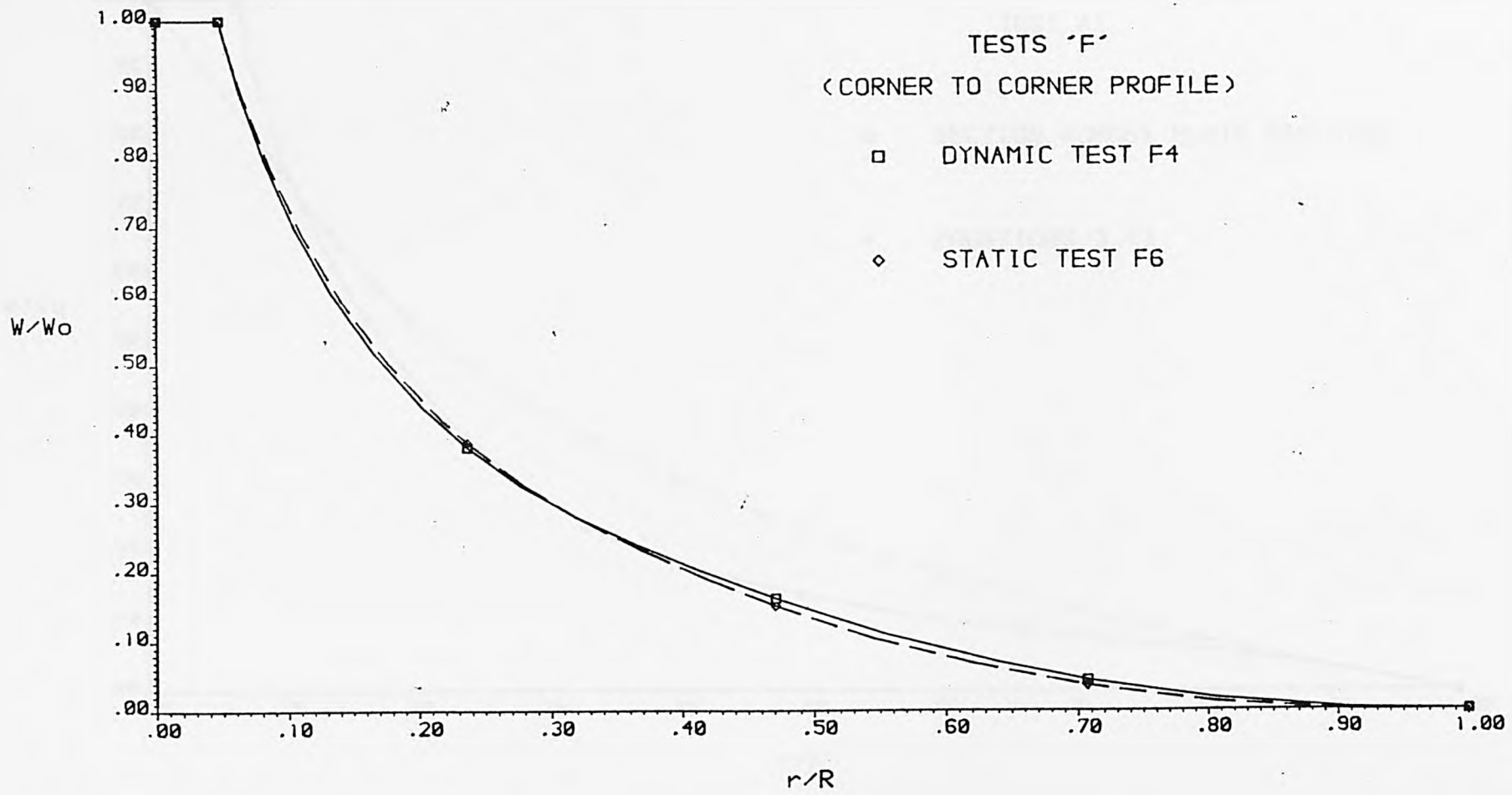

FIGURE 5.3(a) FINAL DEFORMED PROFILE COMPARED WITH ASSUMED PROFILE

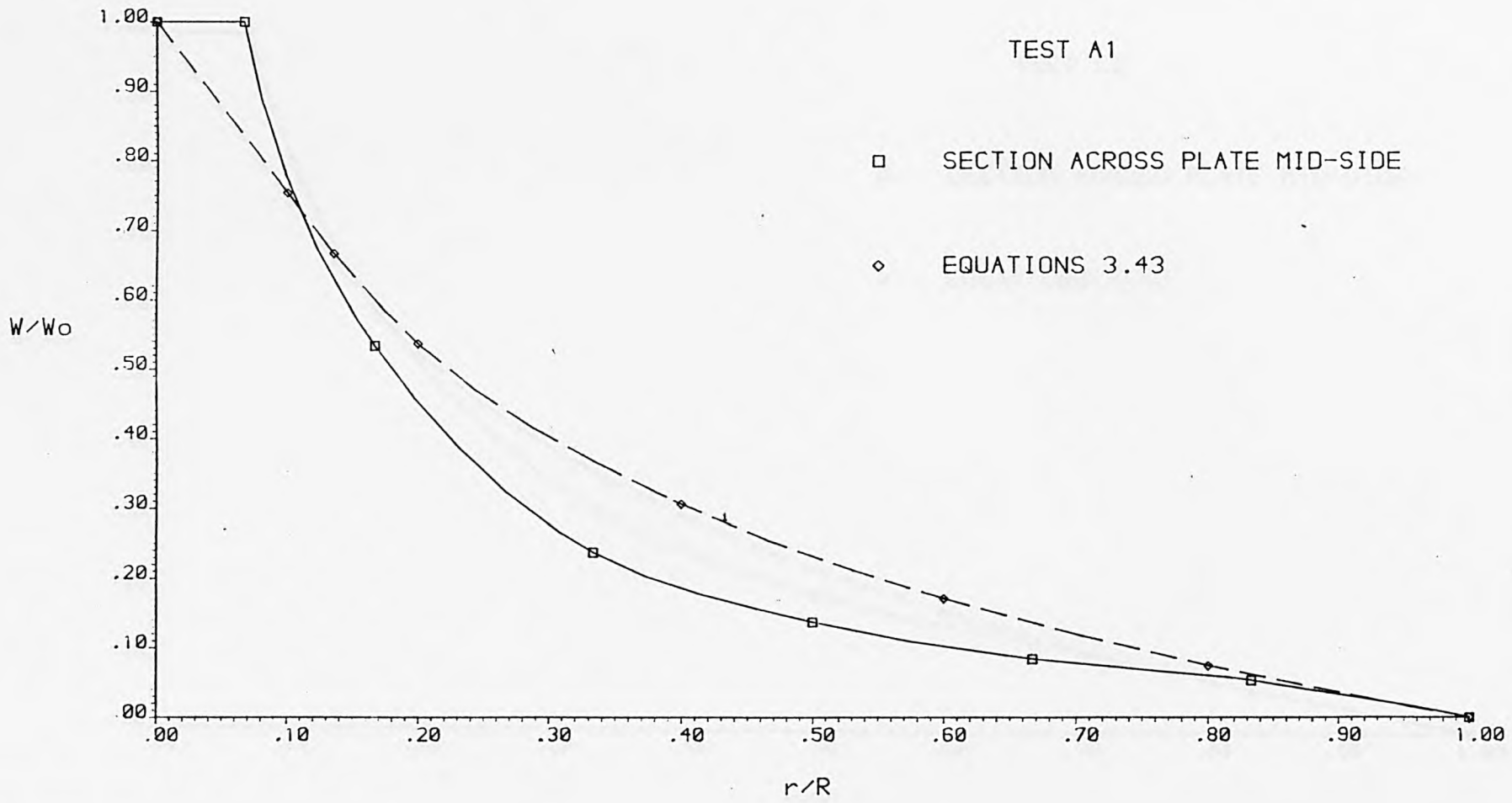

FIGURE 5.3(b) FINAL DEFORMED PROFILE COMPARED WITH ASSUMED PROFILE

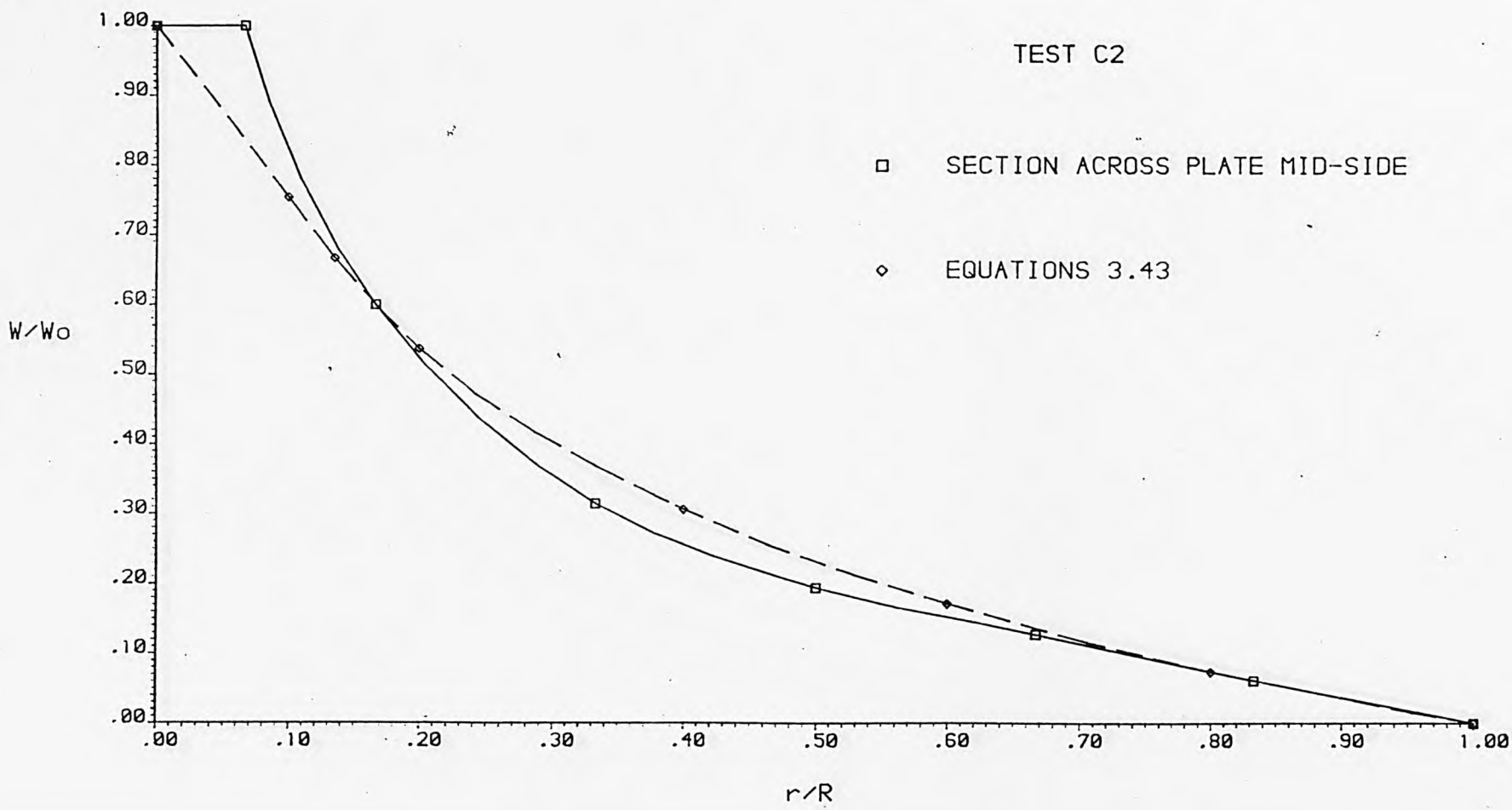

FIGURE 5.3(c) FINAL DEFORMED PROFILE COMPARED WITH ASSUMED PROFILE

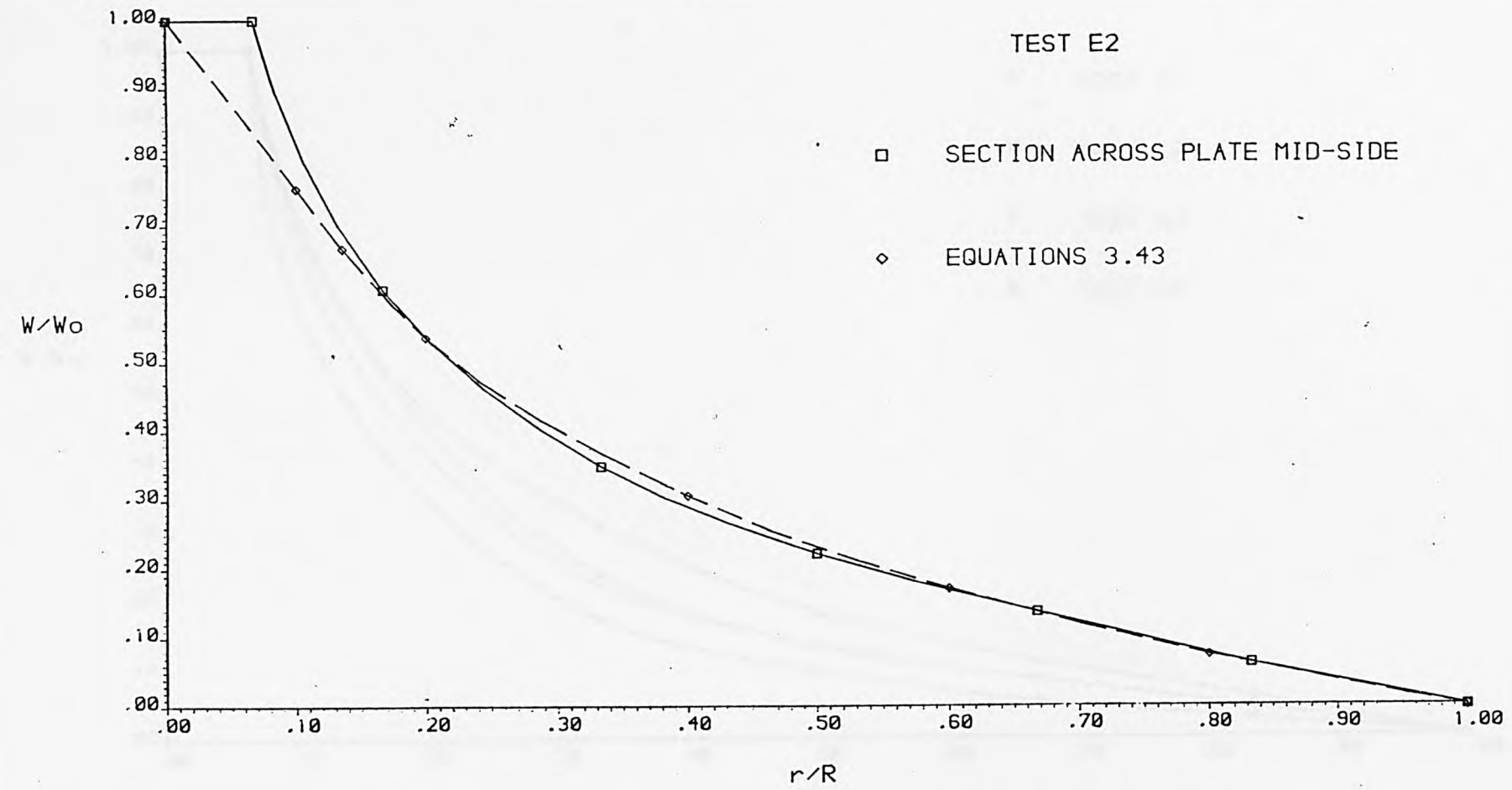

FIGURE 5.4(a) MIDSIDE TO MIDSIDE DEFLECTION PROFILES - TESTS 'A'

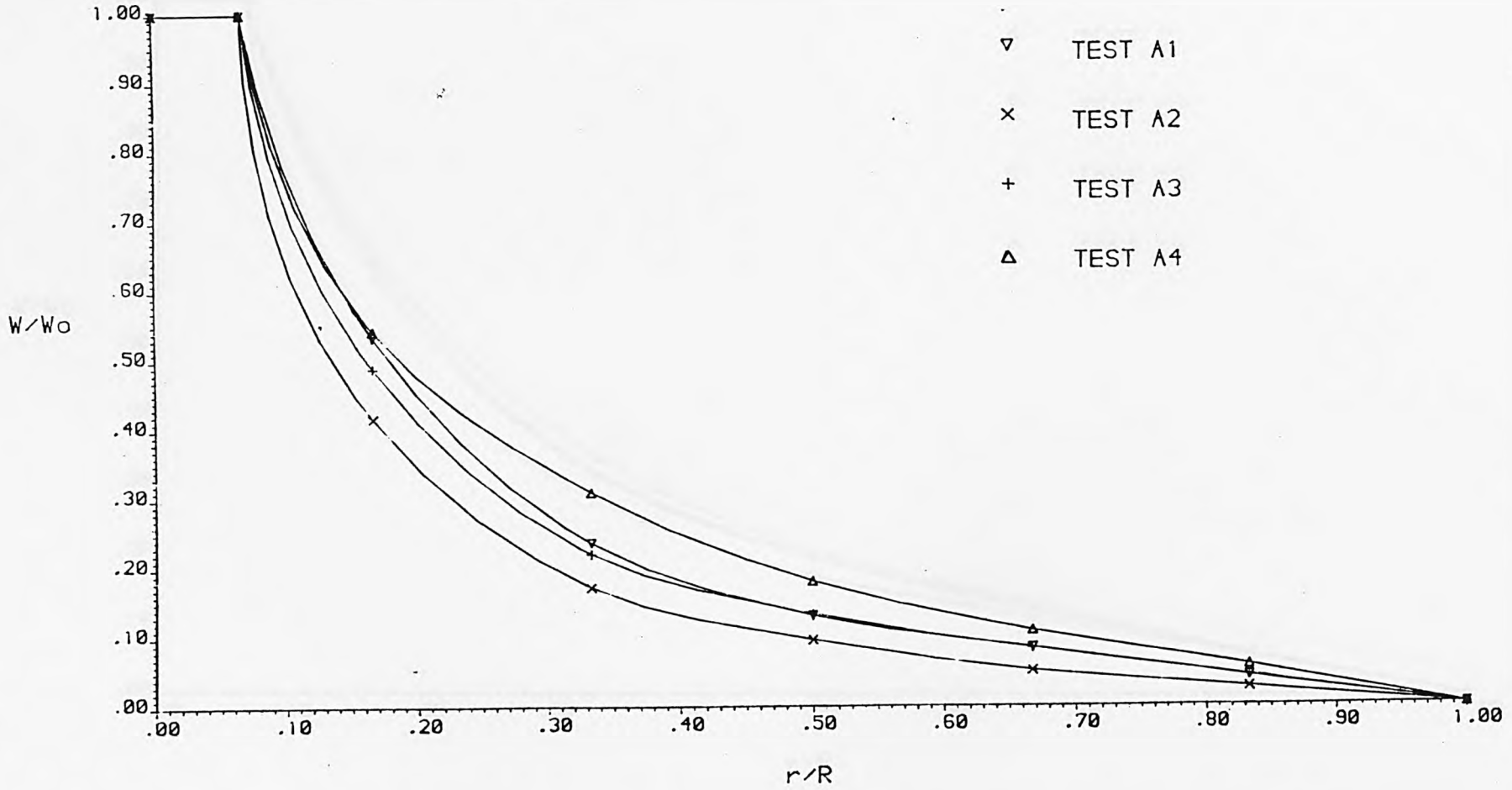

FIGURE 5.4(b) MIDSIDE TO MIDSIDE DEFLECTION PROFILES - TESTS 'C'

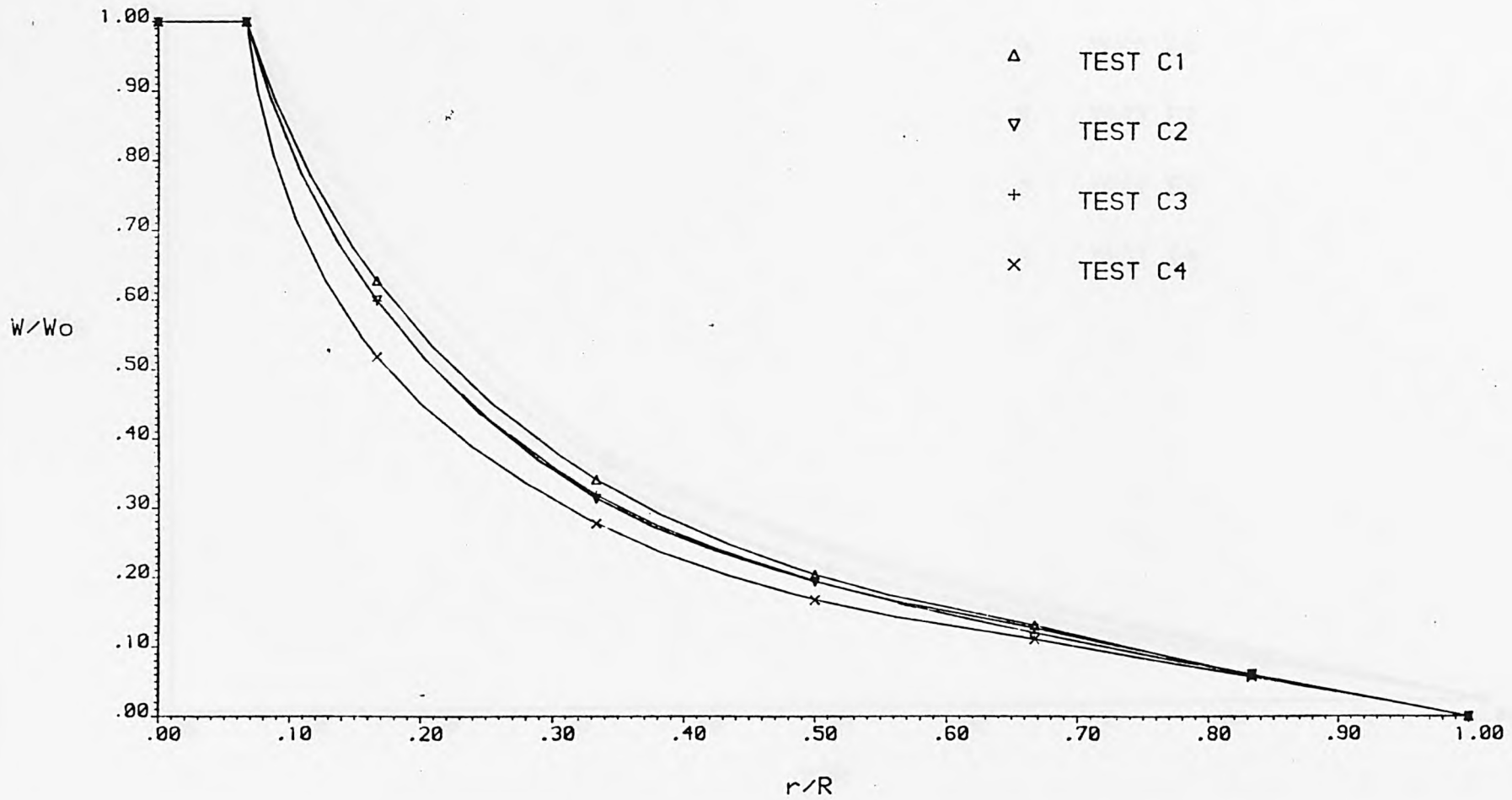

FIGURE 5.4(c) MIDSIDE TO MIDSIDE DEFLECTION PROFILES - TESTS 'E'

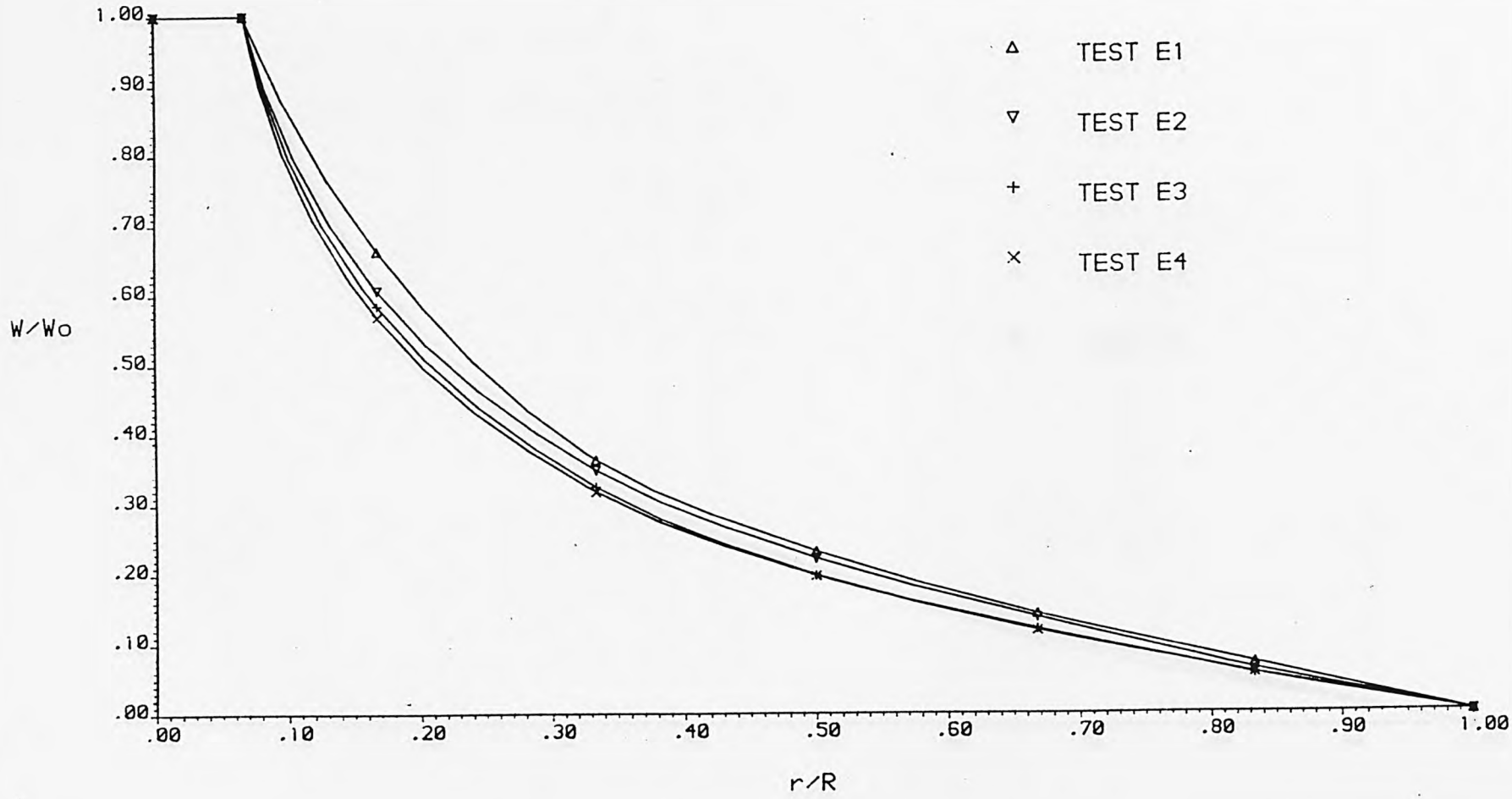

FIGURE 5.4(d) MIDSIDE TO MIDSIDE DEFLECTION PROFILES - TESTS 'F'

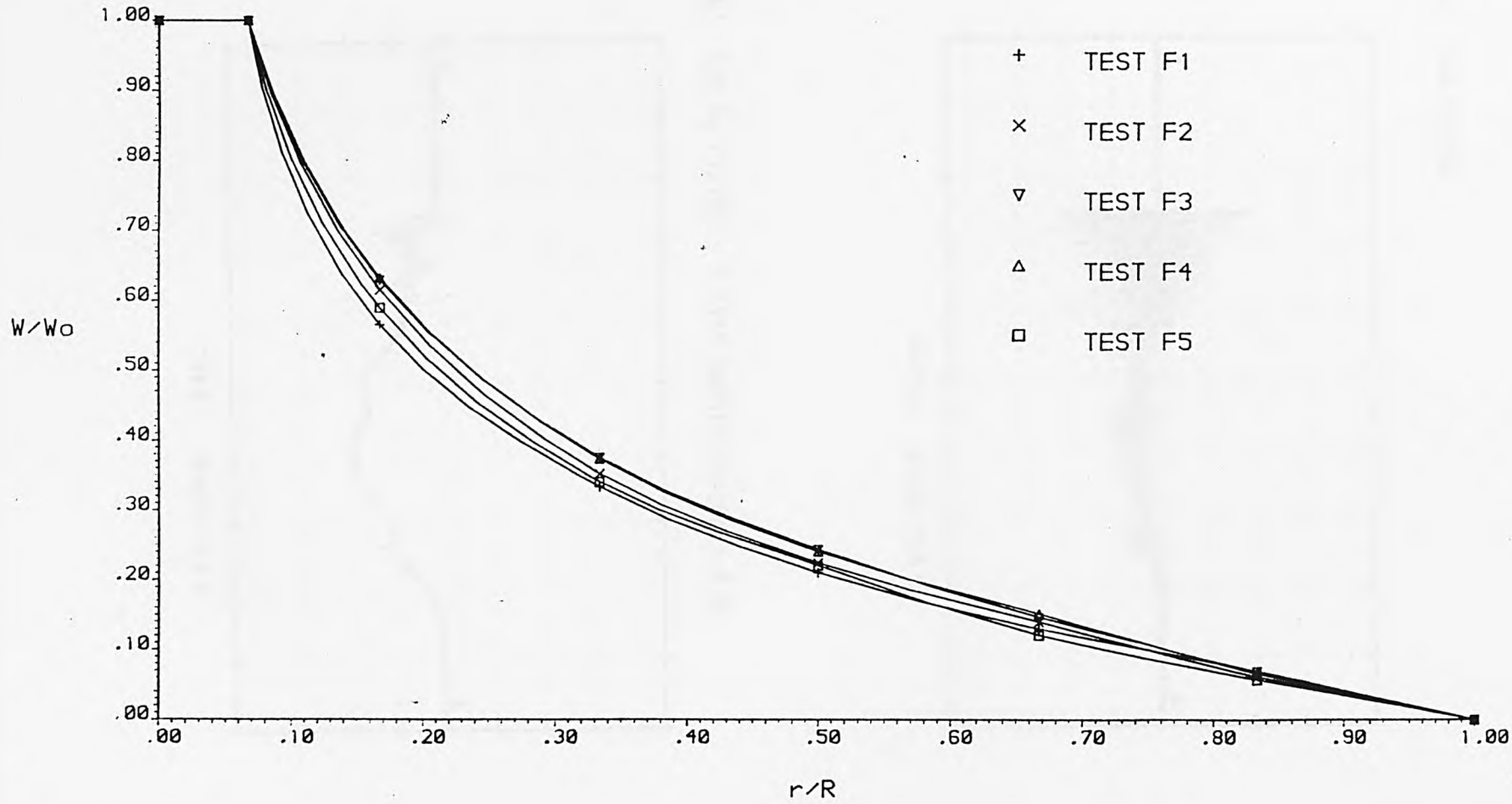

FIGURE 5.5(a) D5 ACCELERATION - TIME HISTORY

a) RAW SIGNAL

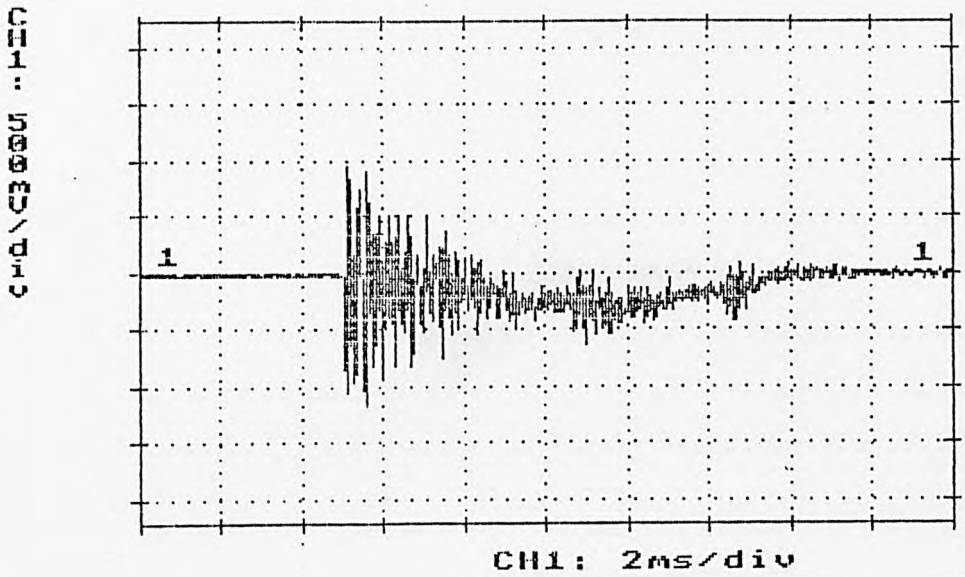

b) 509 Hz FILTER : Y AXIS MAGNIFICATION x 3.0

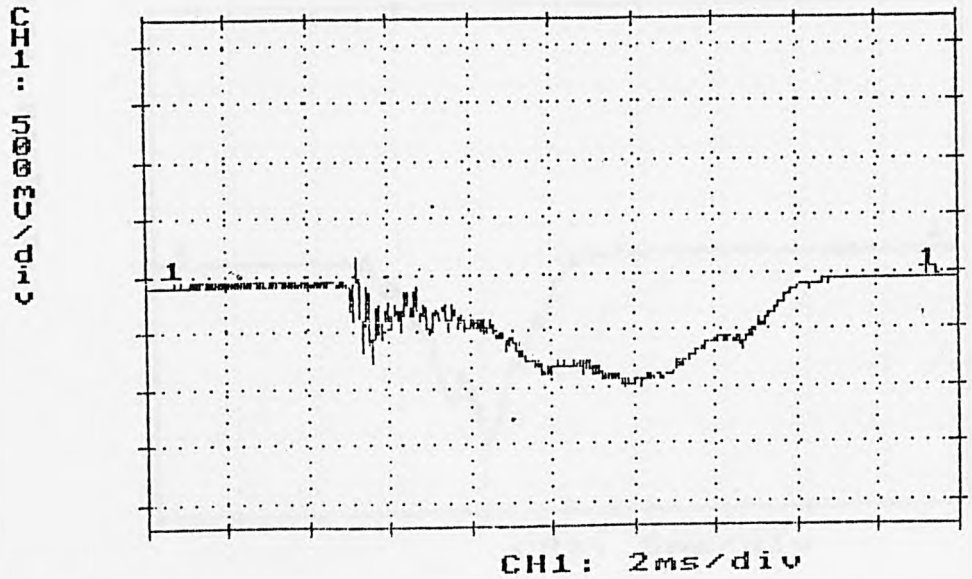

FIGURE 5.5(b) A3 ACCELERATION-TIME HISTORY

a) RAW SIGNAL

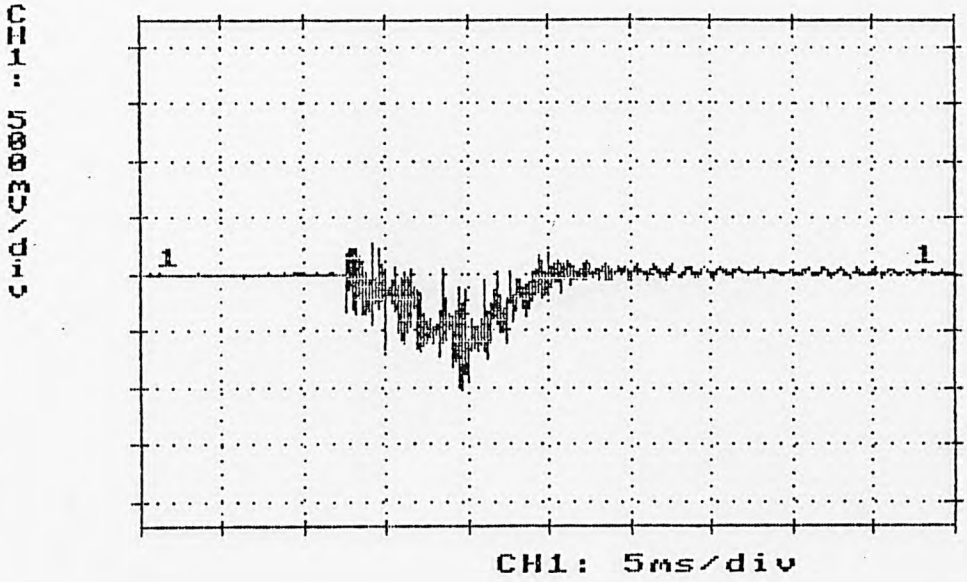

b) 407 Hz FILTER : Y AXIS MAGNIFICATION x 2.5

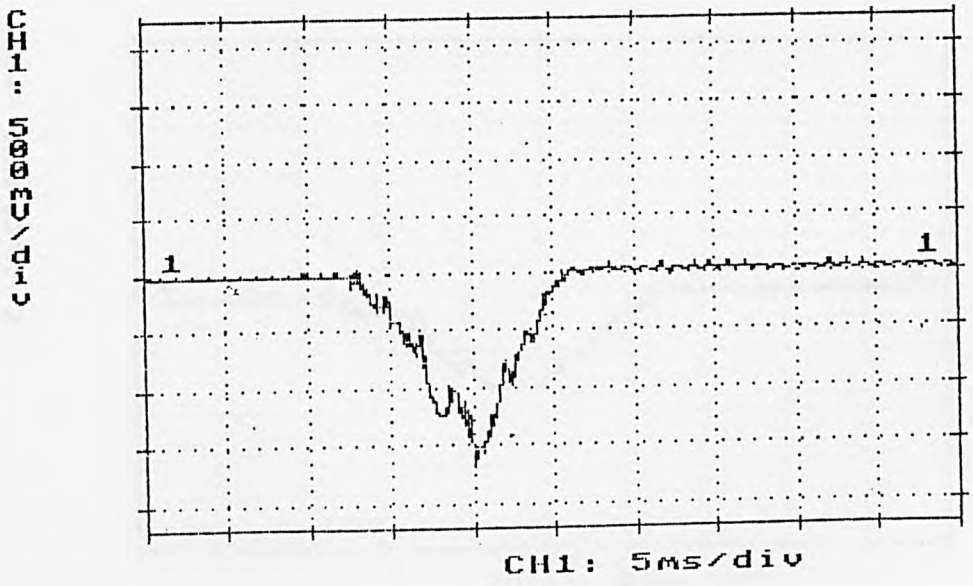

FIGURE 5.5(c) A5 ACCELERATION - TIME HISTORY

a) RAW SIGNAL

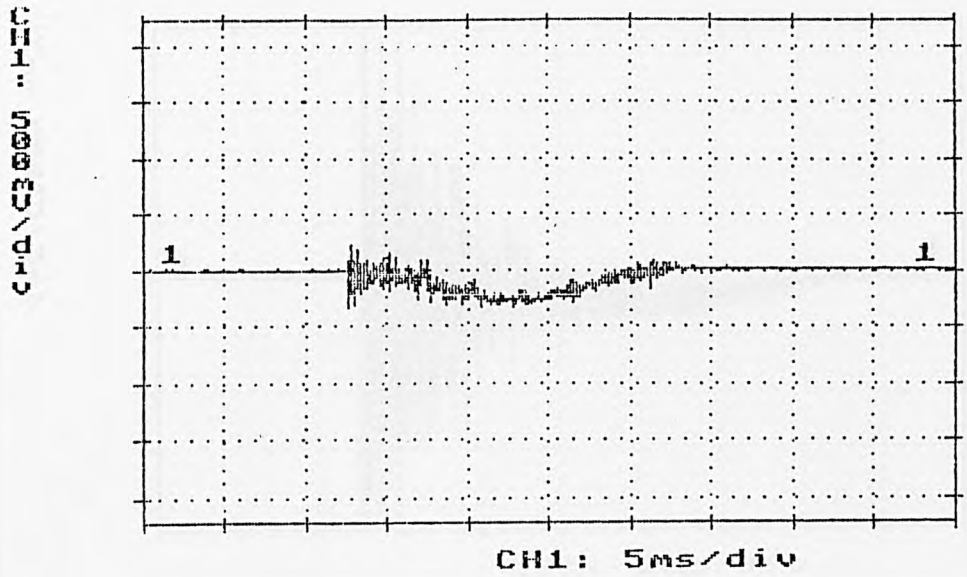

b) 407 Hz FILTER : Y AXIS MAGNIFICATION x 3.0

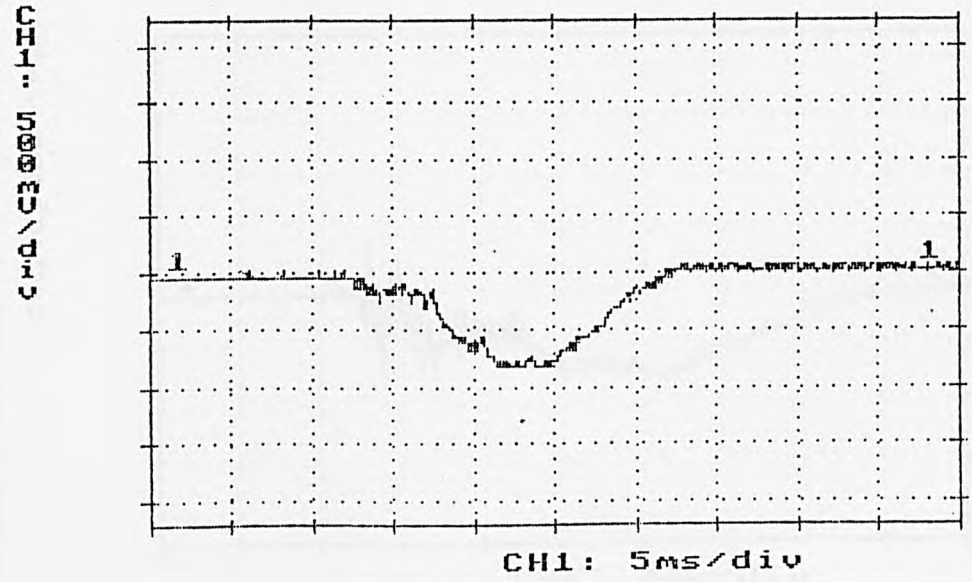

FIGURE 5.5(d) E4 ACCELERATION - TIME HISTORY

a) RAW SIGNAL

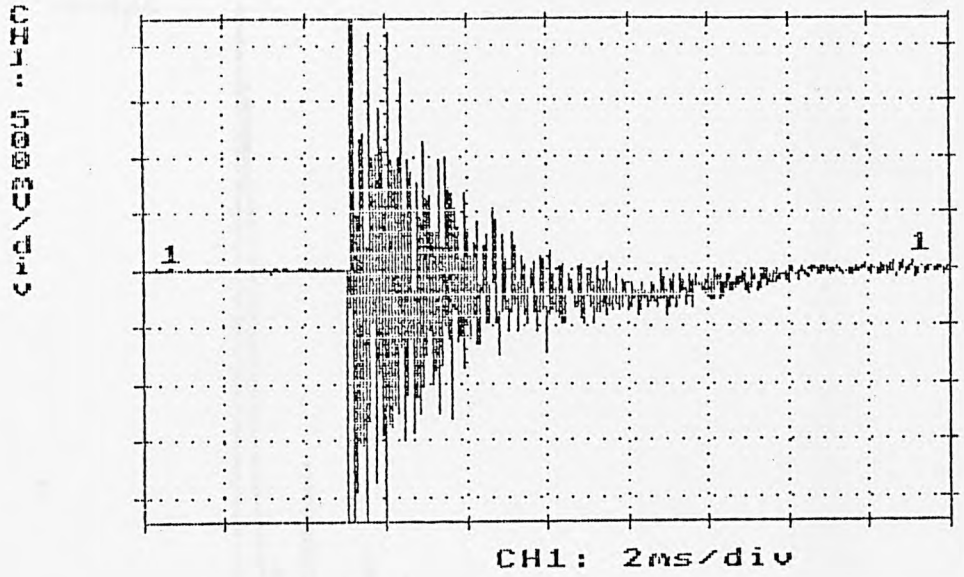

b) 509 Hz FILTER : Y AXIS MAGNIFICATION x 3.0

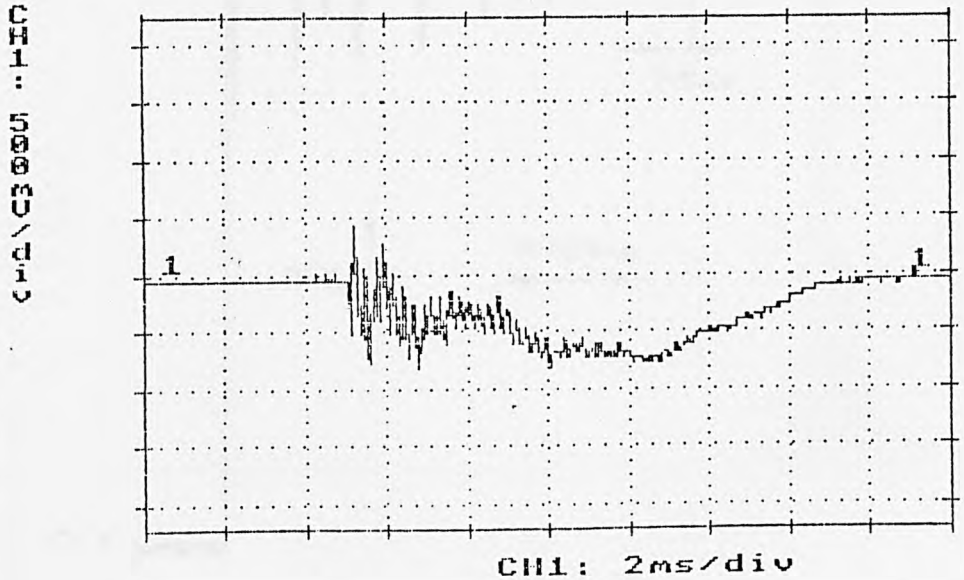

FIGURE 5.6(a) STRAIN GAUGE SIGNAL - TEST F1, GAUGE 2

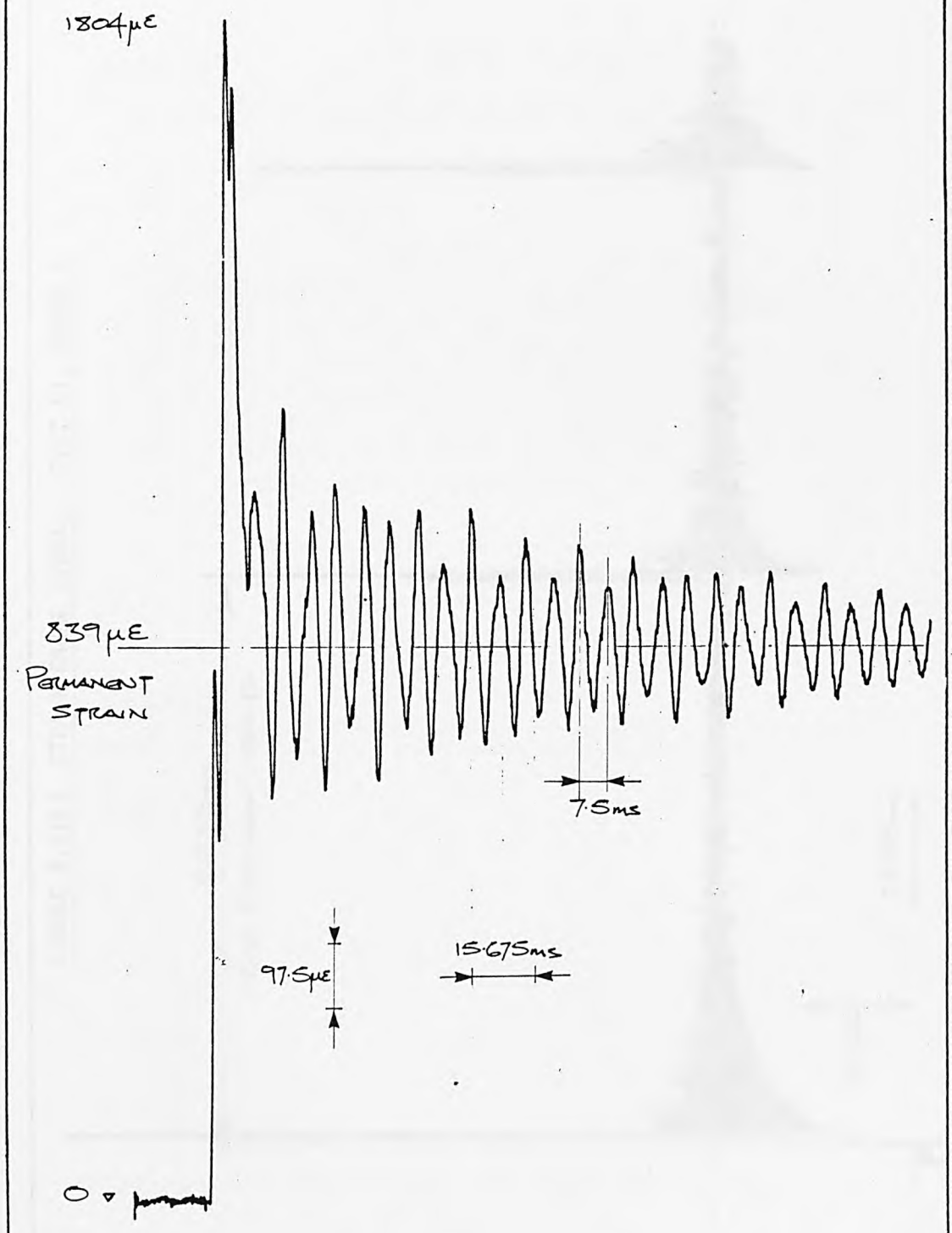

FIGURE 5.6(b) STRAIN GAUGE SIGNAL - TEST F1, GAUGE 1

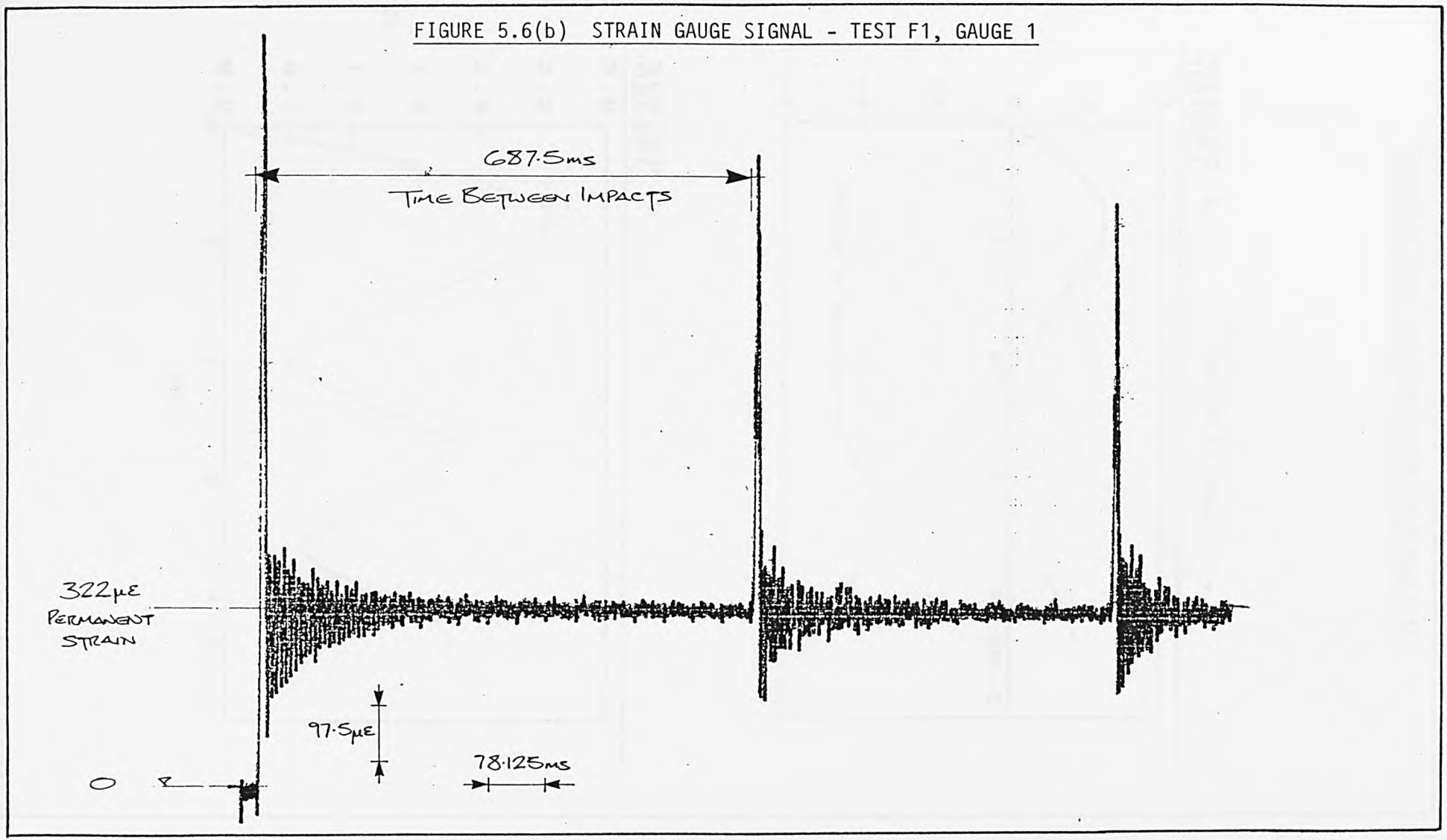

FIGURE 5.7(a) A3 HIGH SPEED FILM ANALYSIS

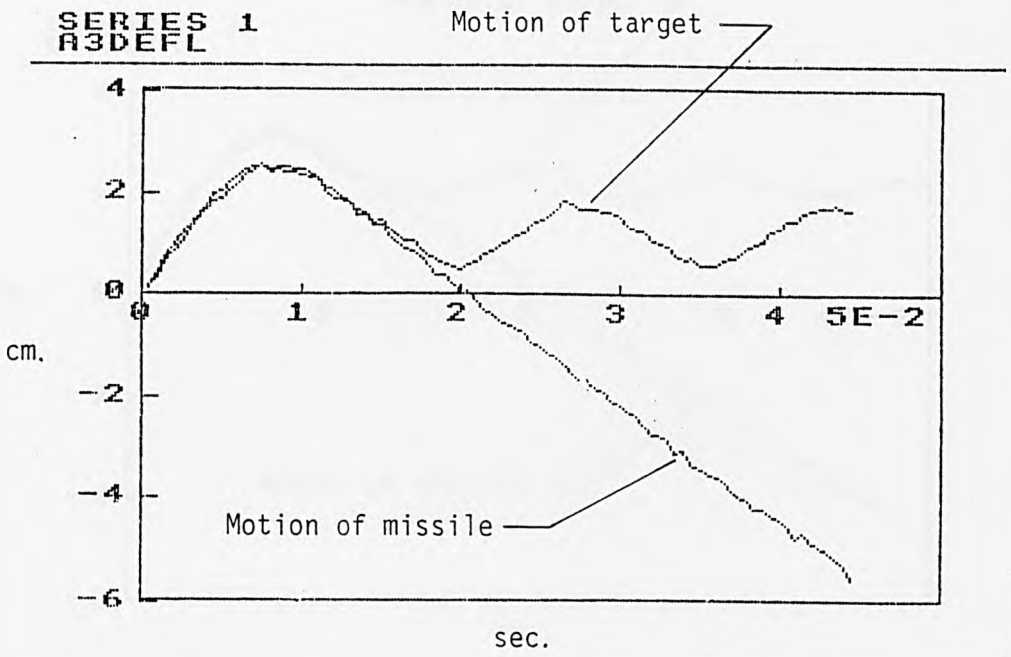

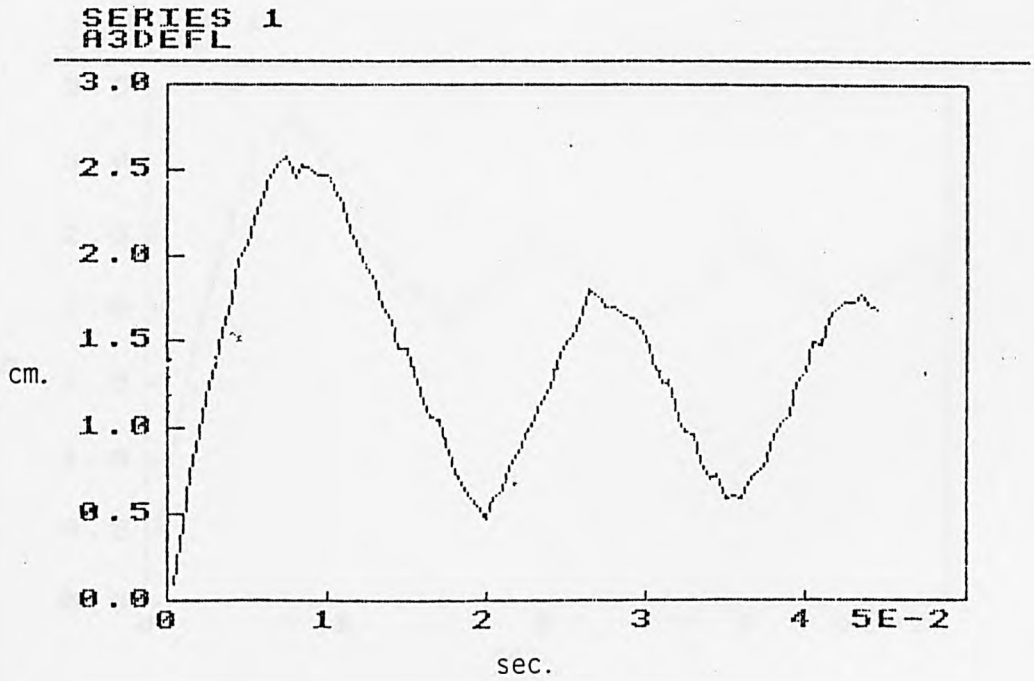

FIGURE 5.7(b) C2 HIGH SPEED FILM ANALYSIS

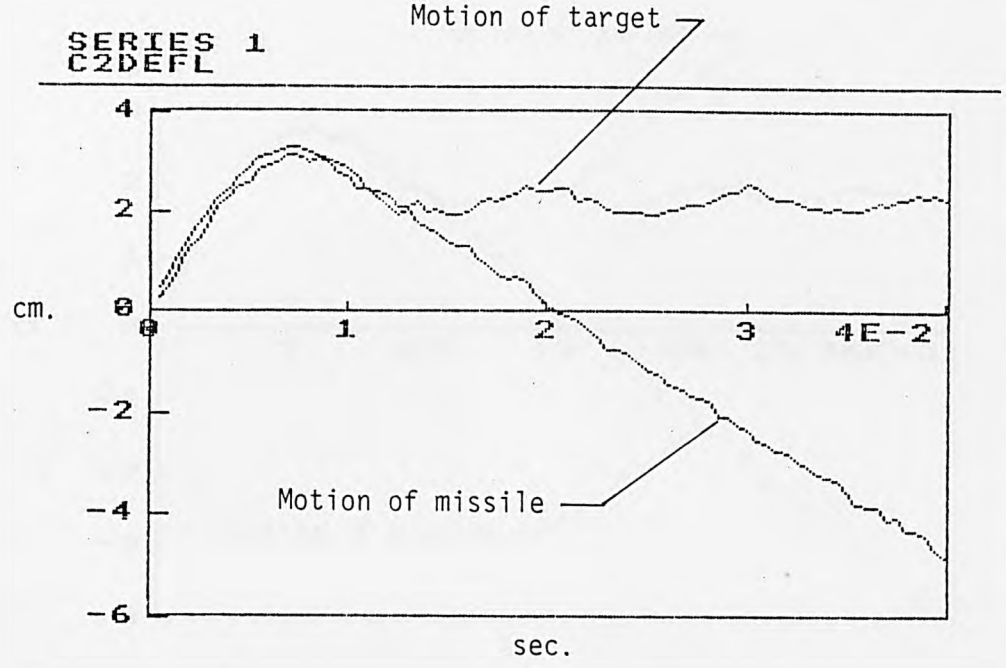

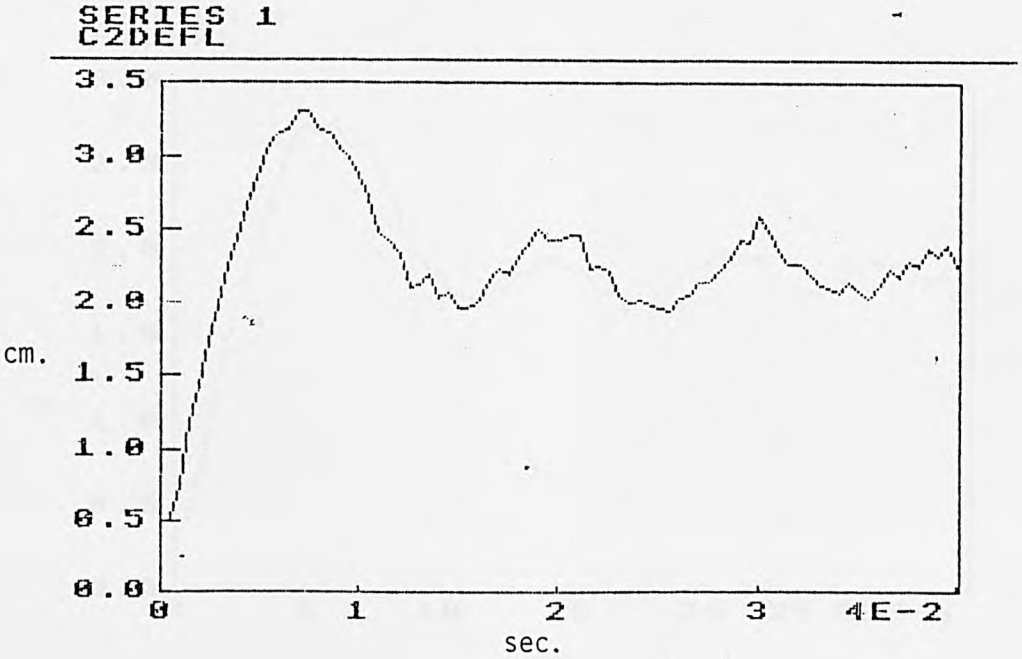

FIGURE 5.7(c) F2 HIGH SPEED FILM ANALYSIS

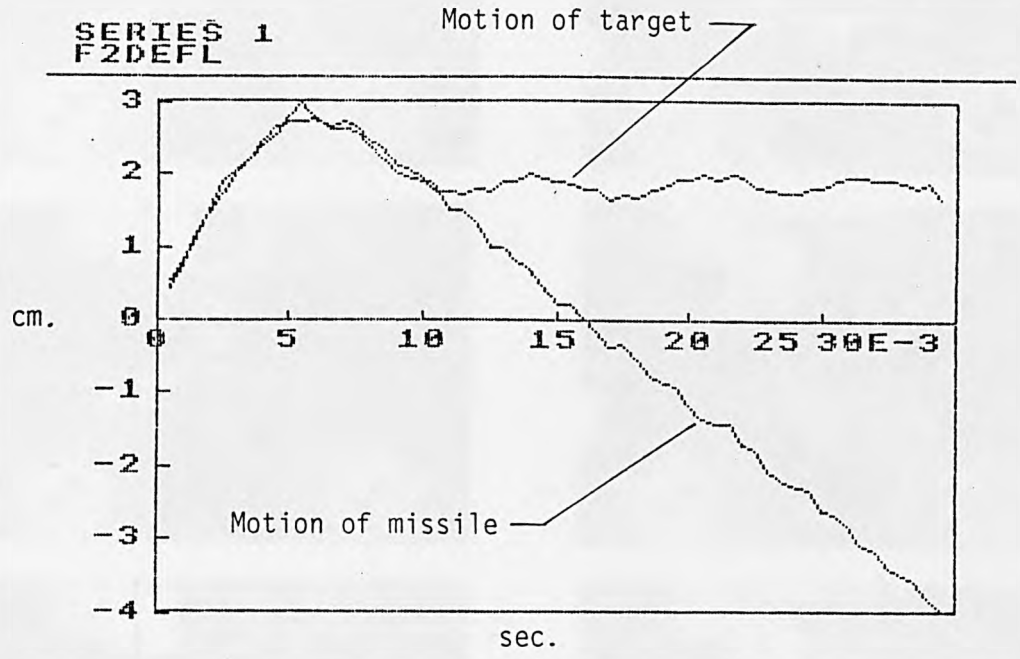

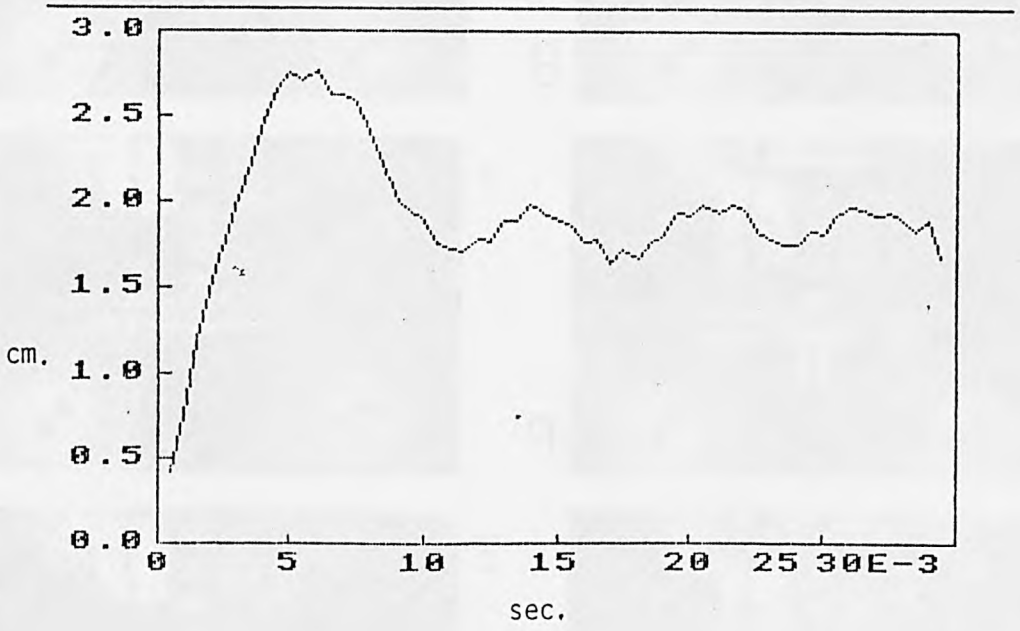

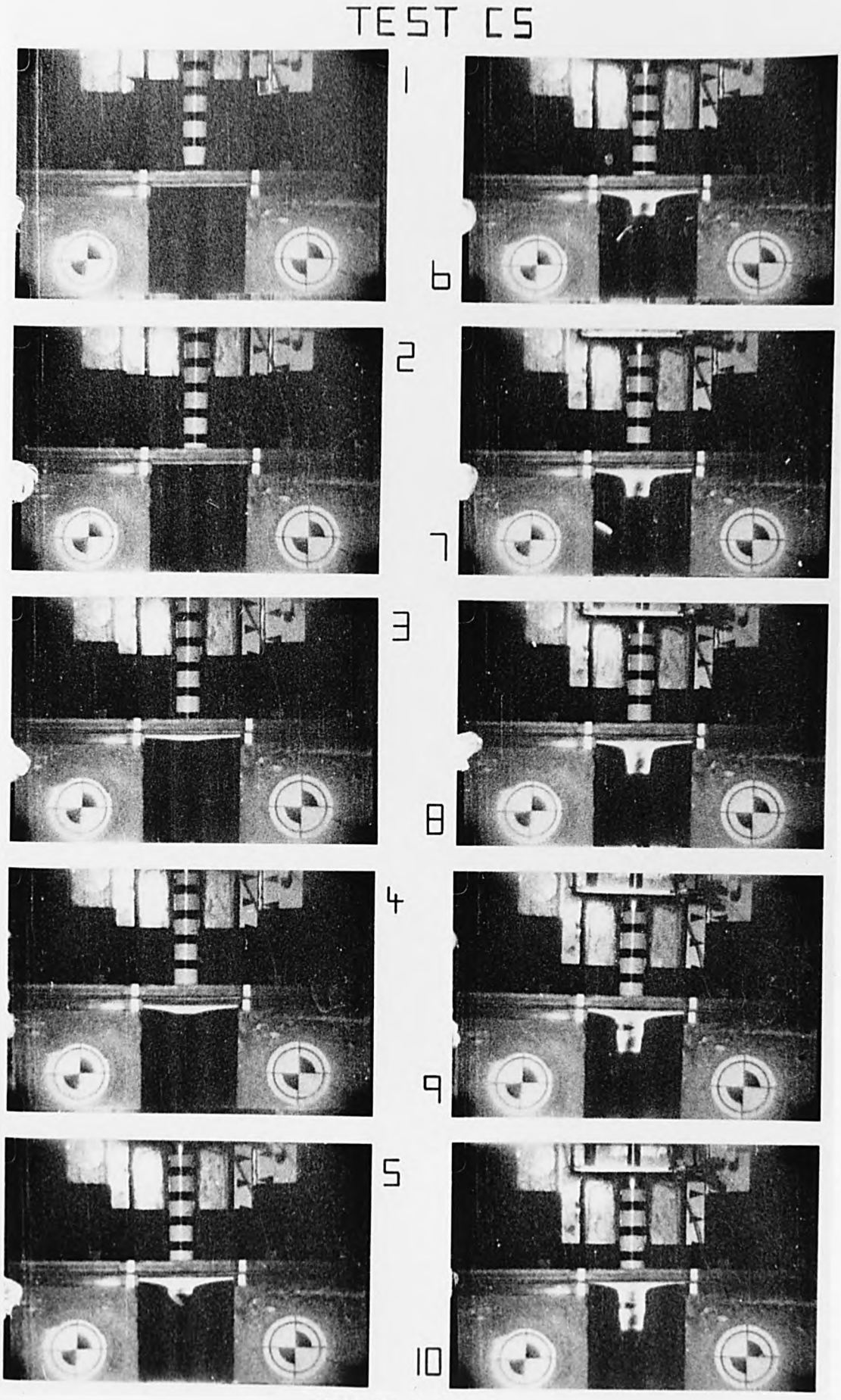

FIGURE 5.8(a)

TEST C5 (SEE TABLE 5.4.)

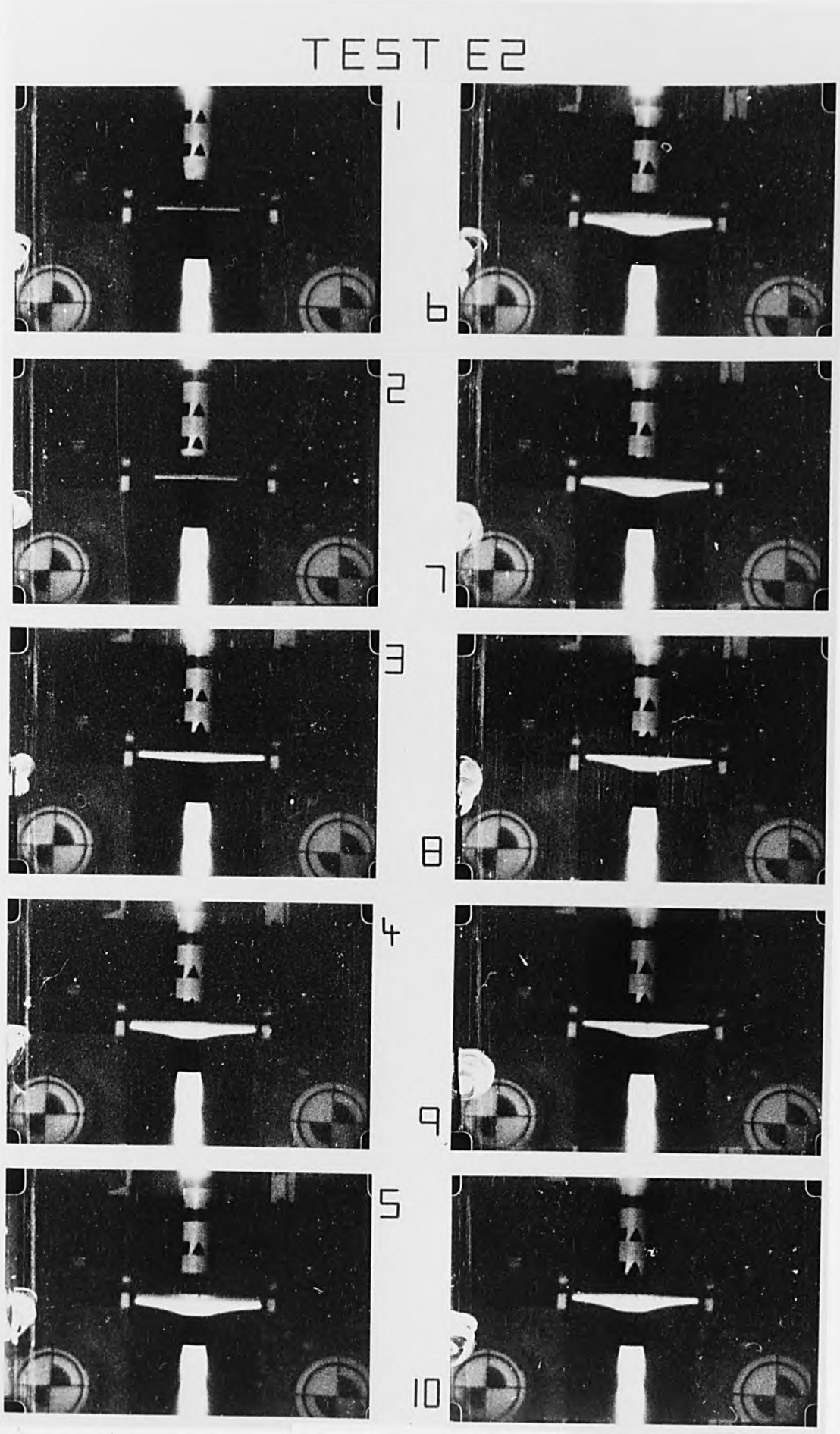

FIGURE 5.8(b)

TEST E2 (SEE TABLE 5.4)

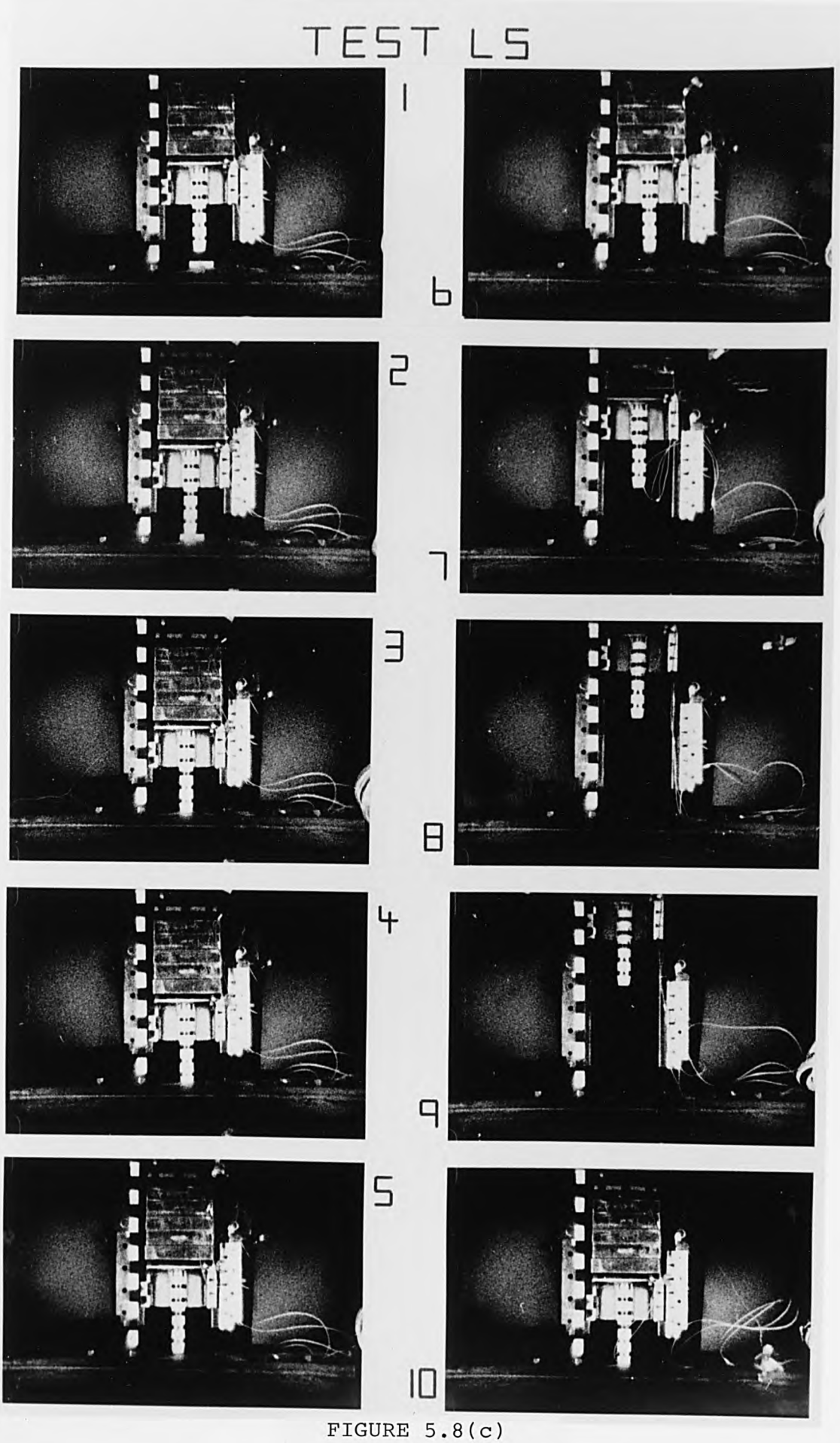

FIGURE 5.8(c)

TEST L5 (SEE TABLE 5.4)

FIGURE 5.9(a) VELOCITY - PERMANENT DEFLECTION TESTS 'A'

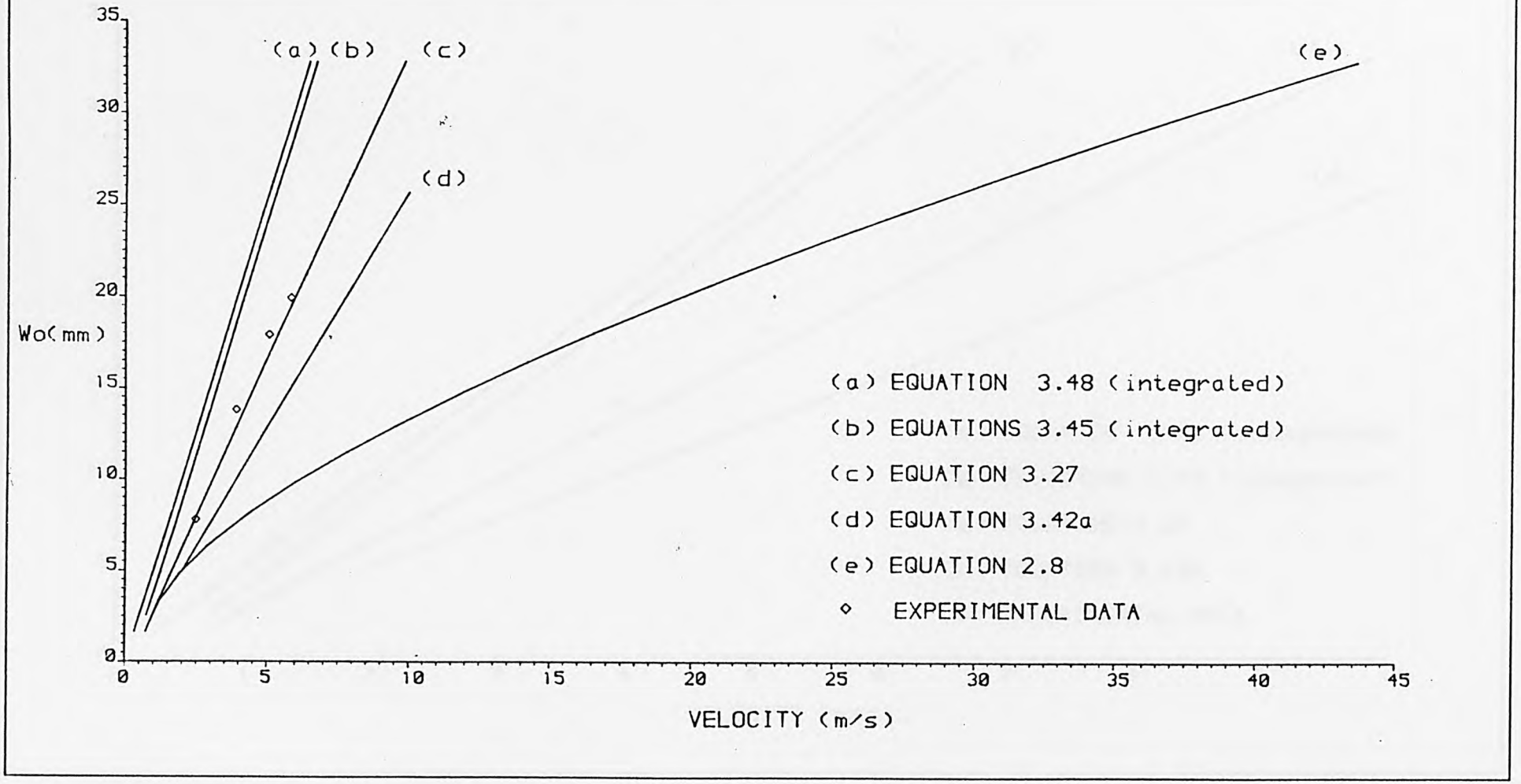

FIGURE 5.9(b) VELOCITY - PERMANENT DEFLECTION - TESTS 'A'

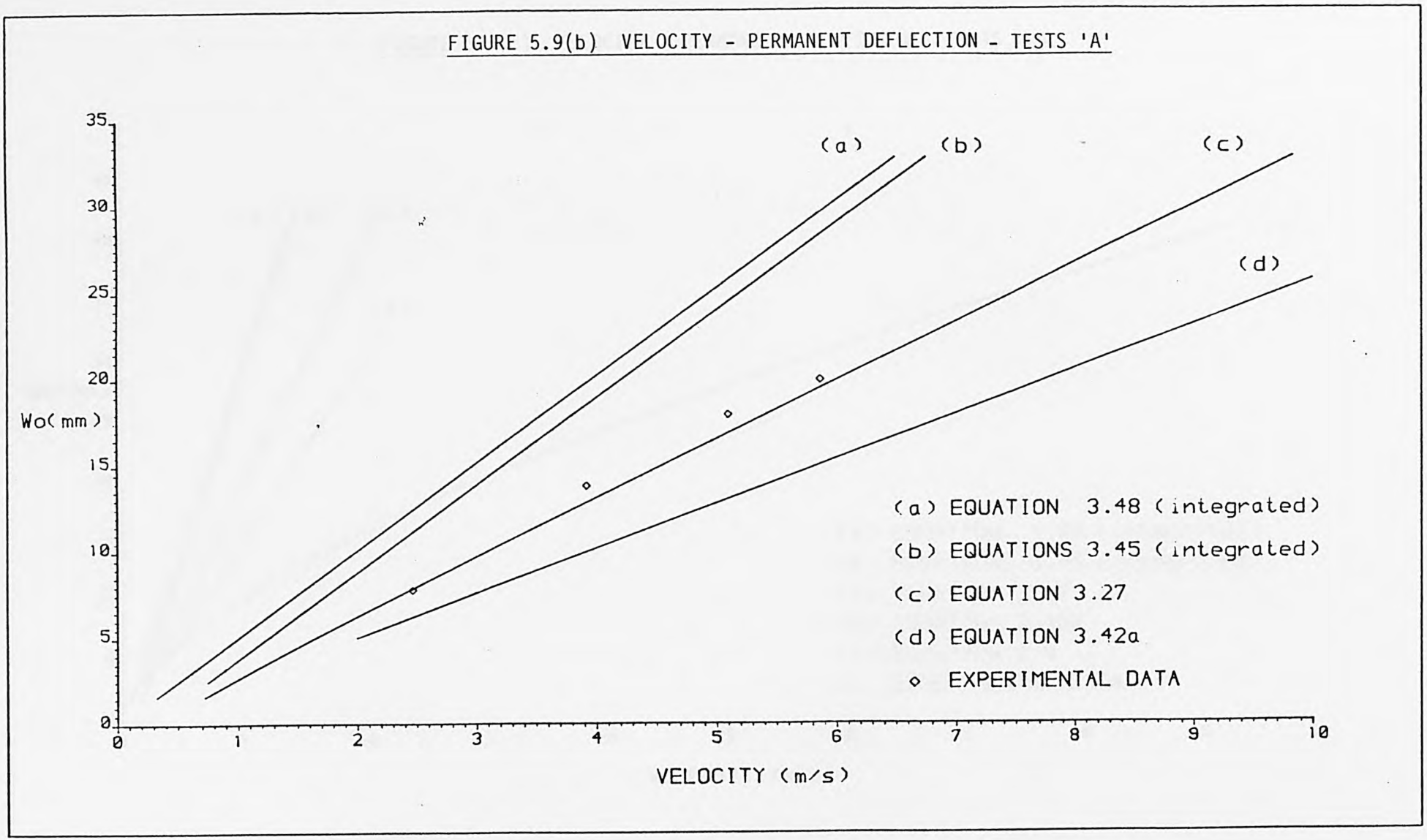

FIGURE 5.9(c) VELOCITY - PERMANENT DEFLECTION TESTS 'B'

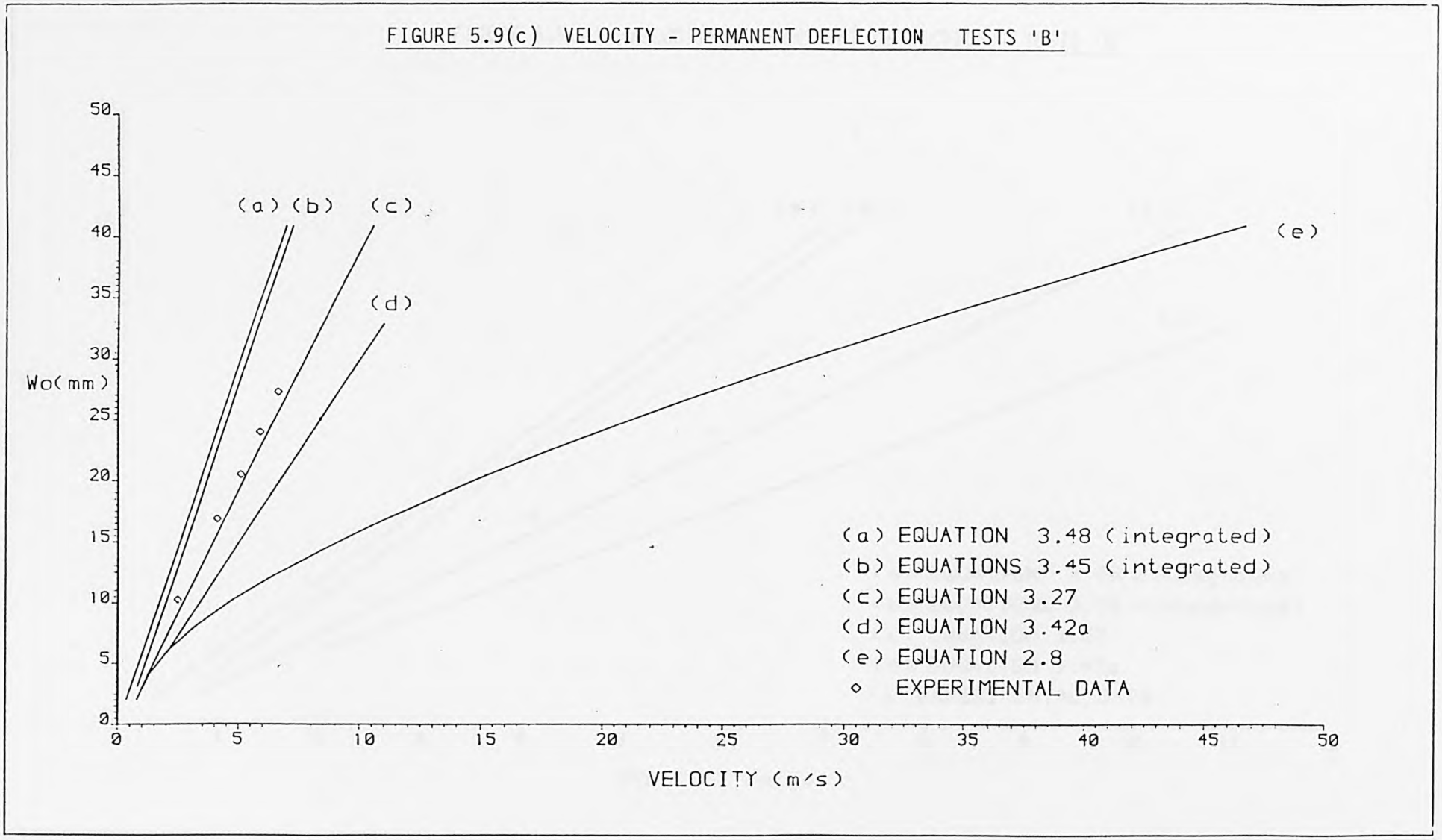

FIGURE 5.9(d) VELOCİTY - PERMANENT DEFLECTION - TESTS 'B'

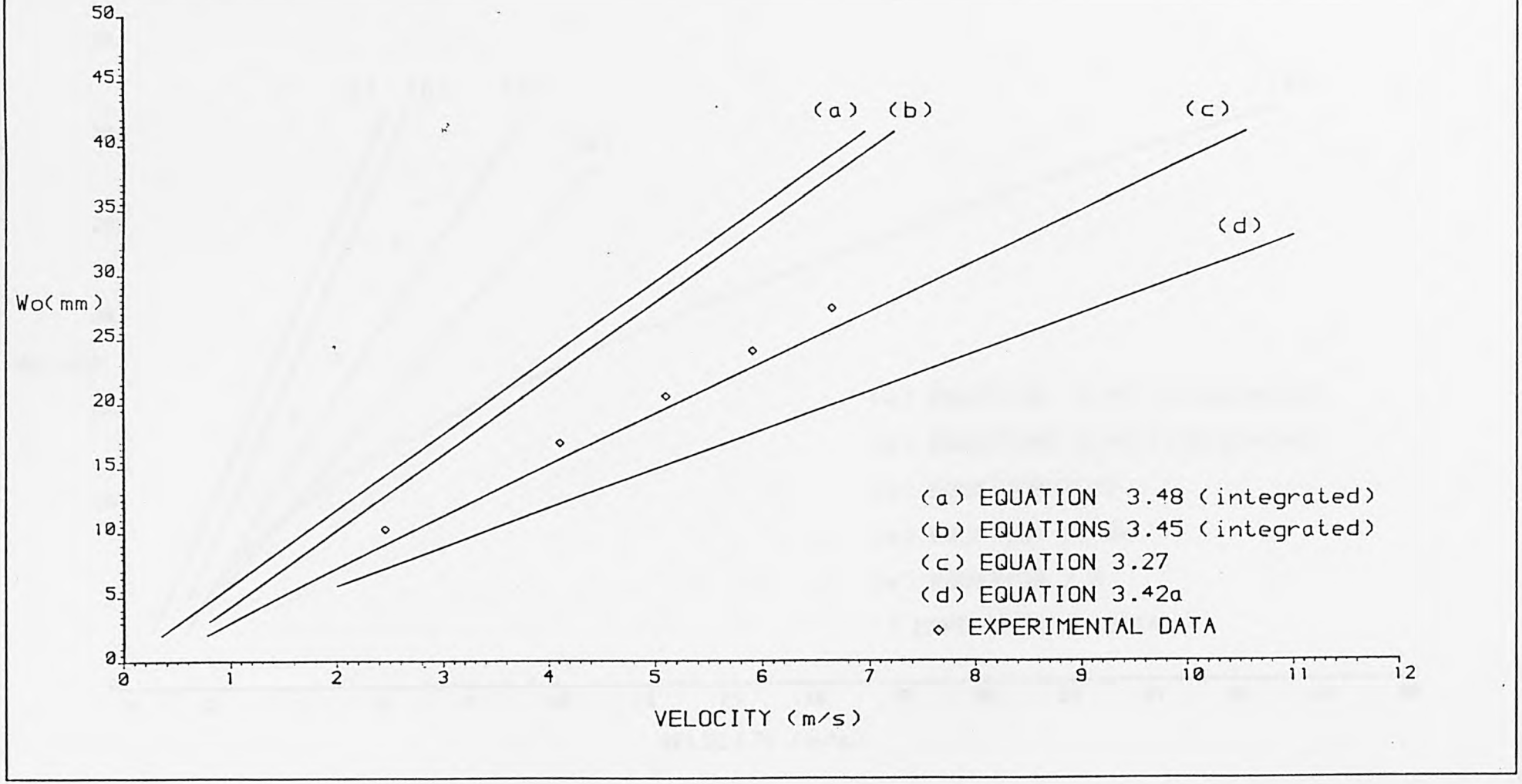

FIGURE 5.9(e) VELOCITY - PERMANENT DEFLECTION TESTS 'D'

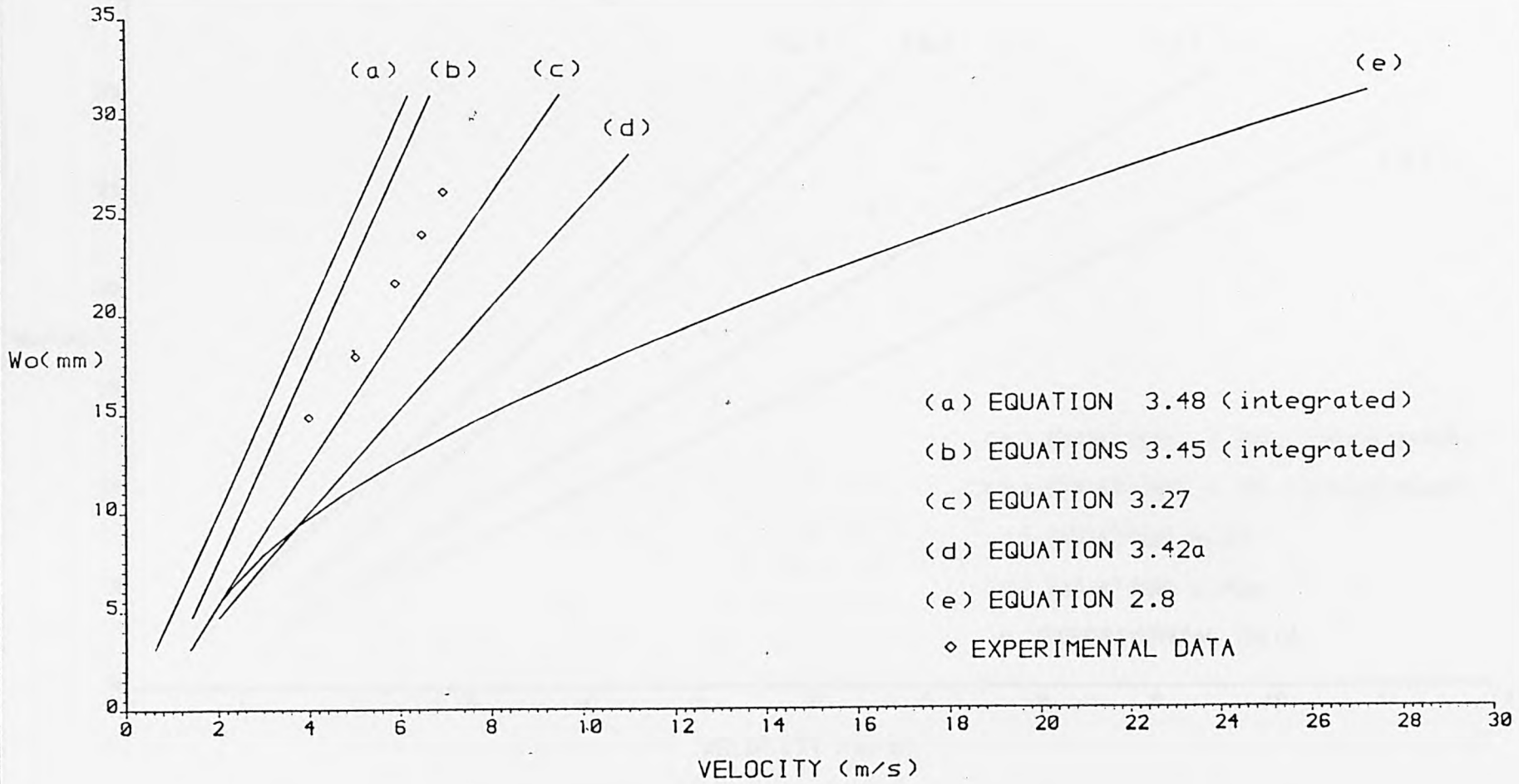

FIGURE 5.9(f) VELOCITY - PERMANENT DEFLECTION- TESTS 'D'

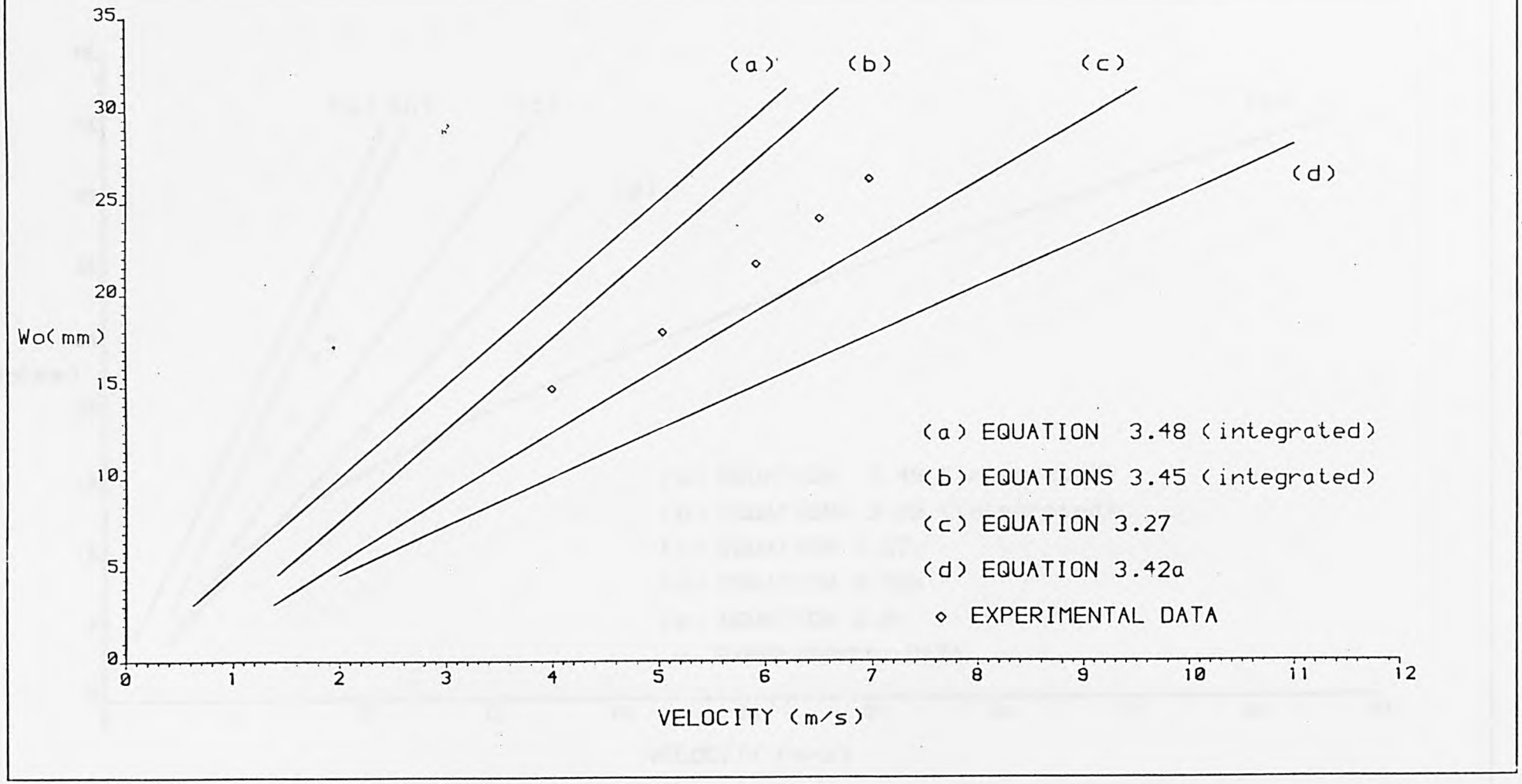

FIGURE 5.9(g) VELOCITY - PERMANENT DEFLECTION TESTS 'E'

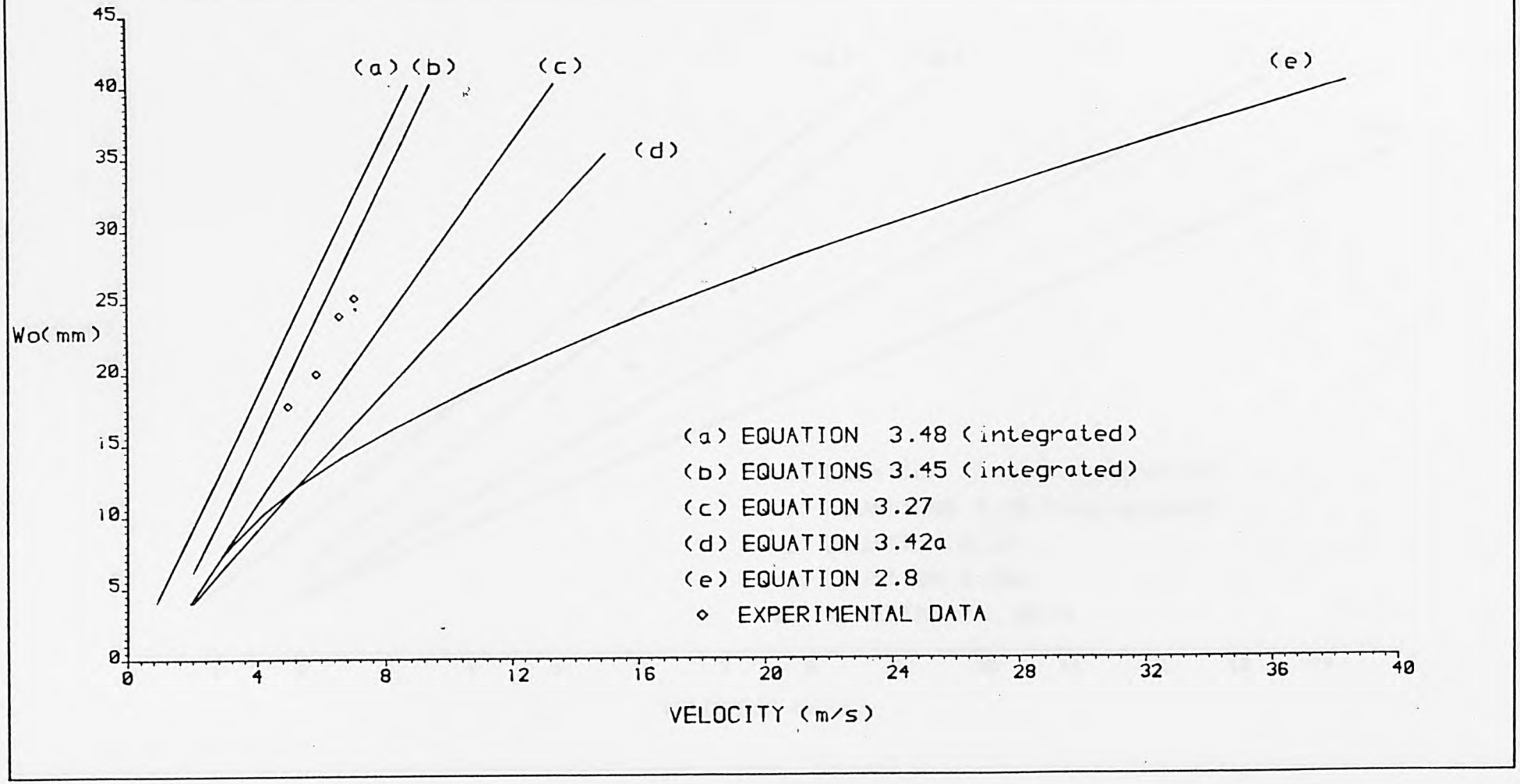

FIGURE 5.9(h) VELOCITY - PERMANENT DEFLECTION - TESTS 'E'

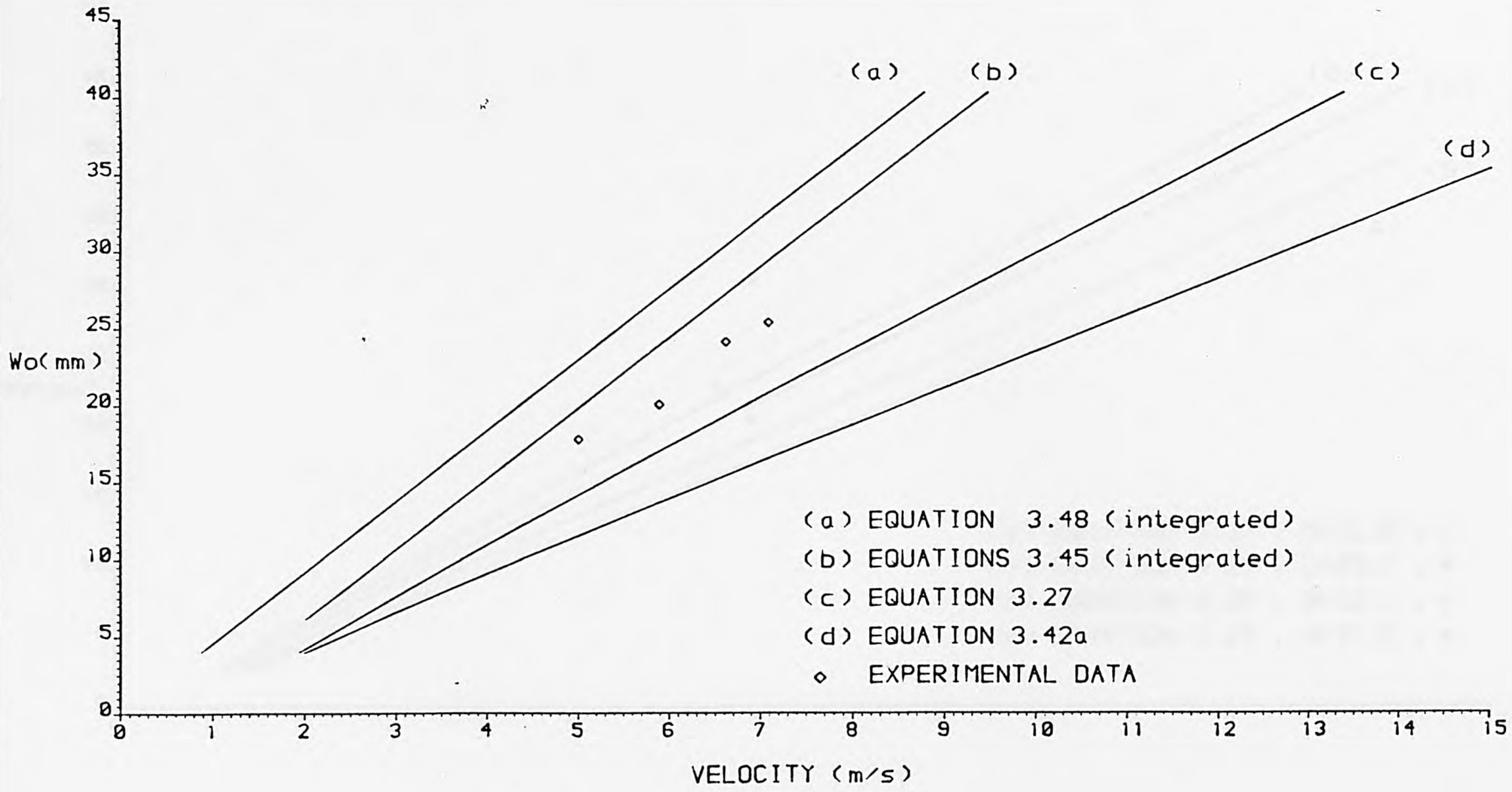

FIGURE 5.10(a) VELOCITY - PERMANENT DEFLECTION TESTS 'C'

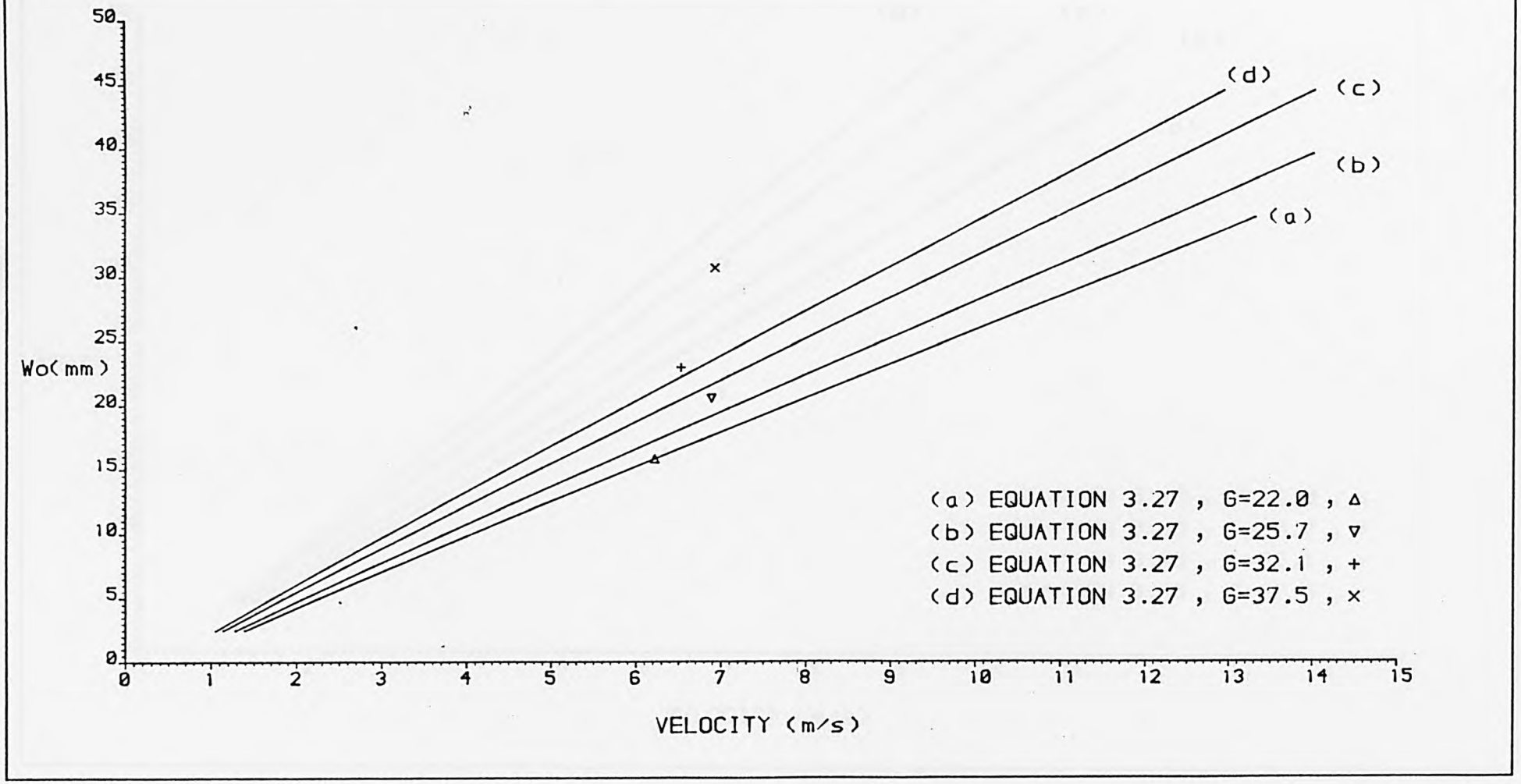

FIGURE 5.10(b) VELOCITY - PERMANENT DEFLECTION - TESTS 'C'

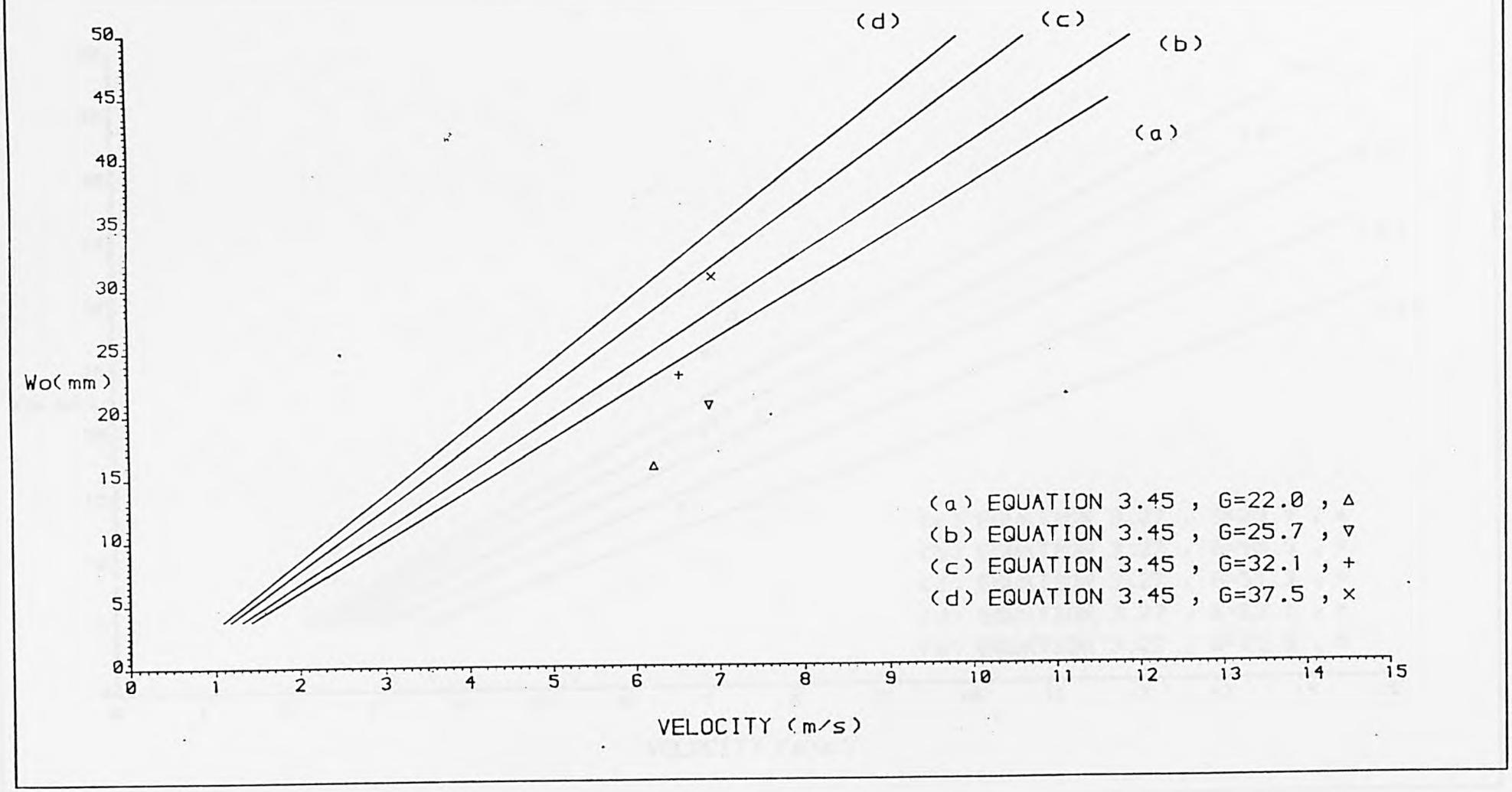

FIGURE 5.10(c) VELOCITY - PERMANENT DEFLECTION TESTS 'F'

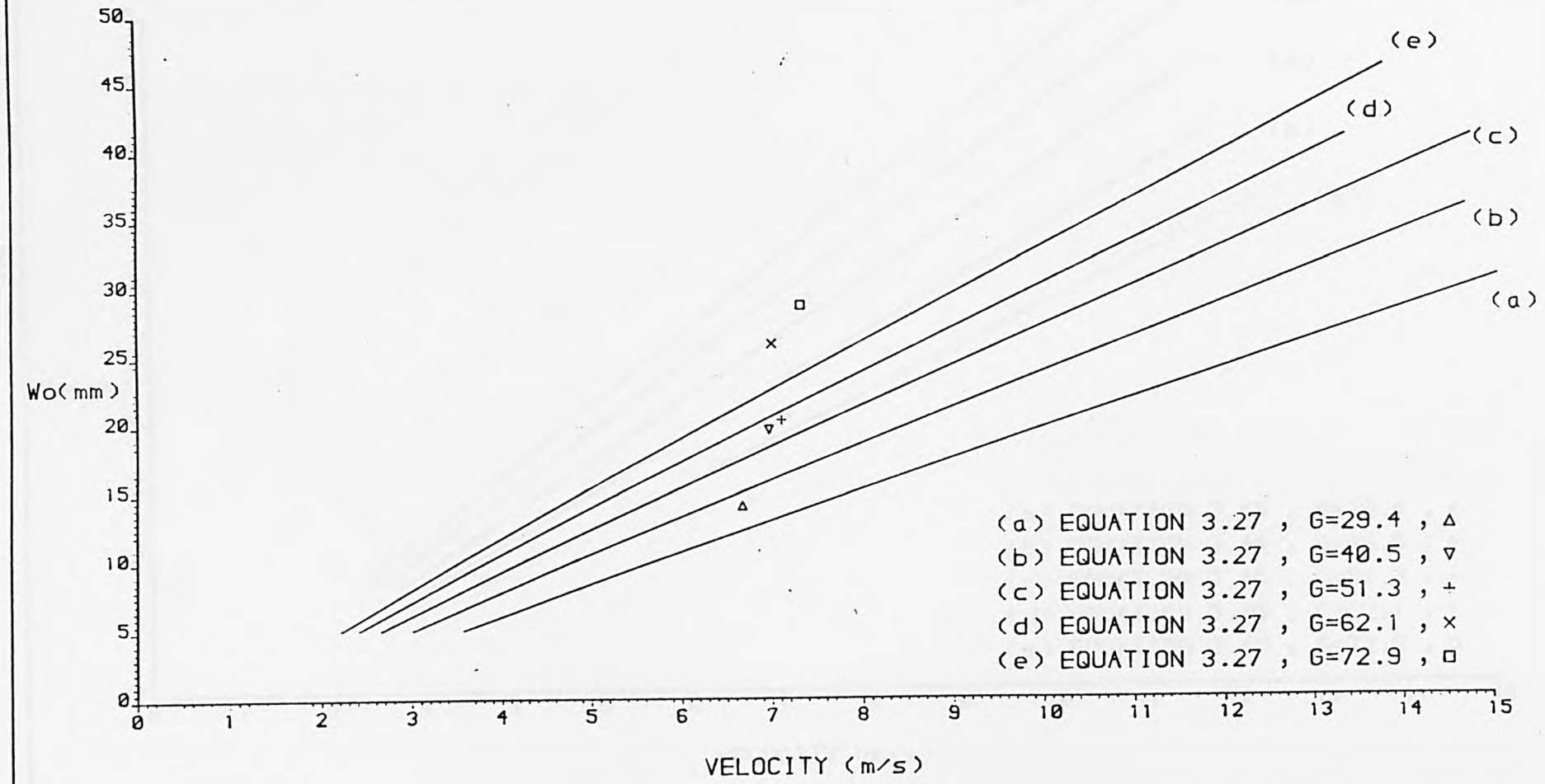

FIGURE 5.10(d) VELOCITY - PERMANENT DEFLECTION - TESTS 'F'

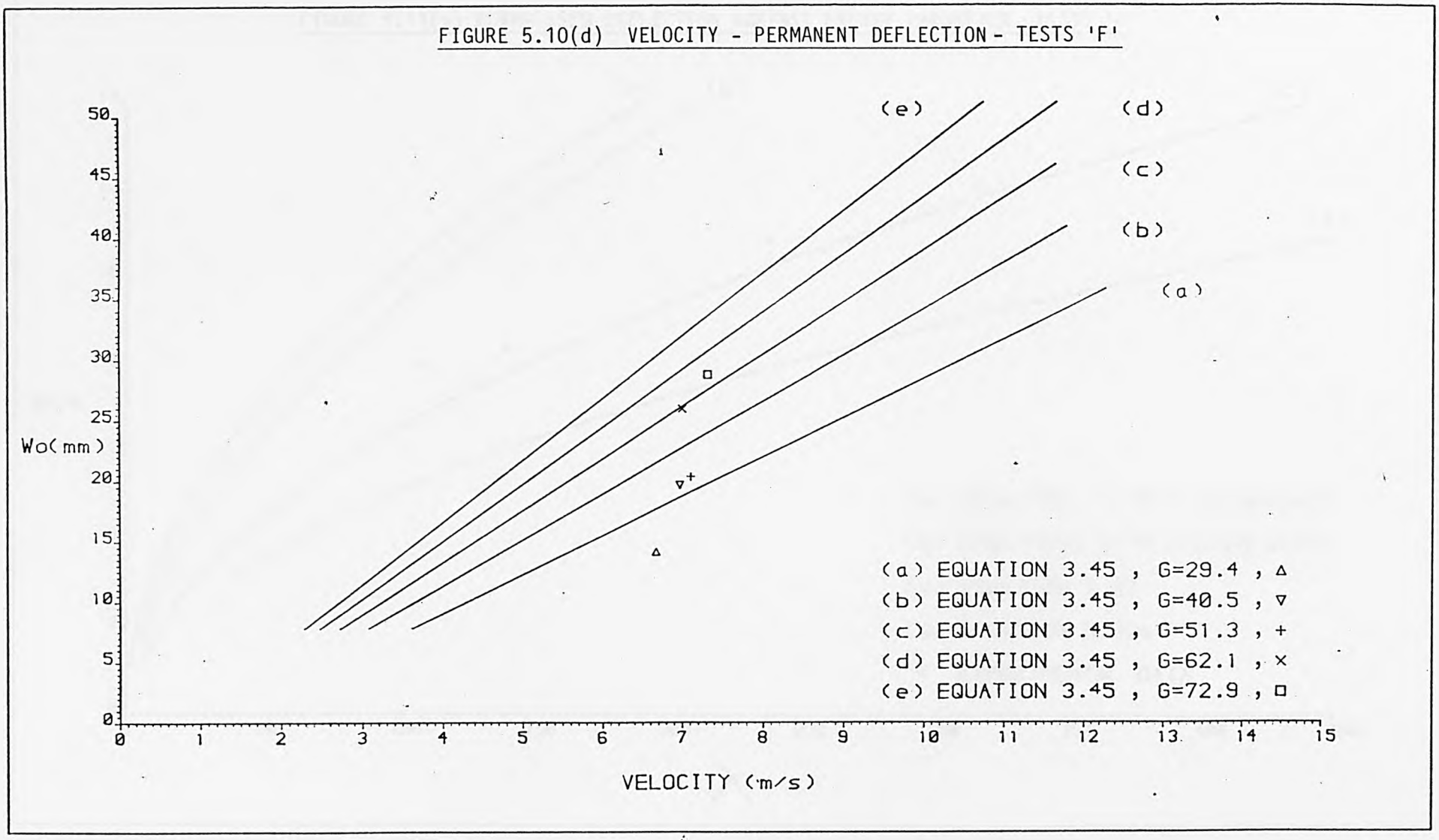

FIGURE 5.11(a) NORMALISED DEFLECTION AGAINST ENERGY PARAMETER TESTS 'A'

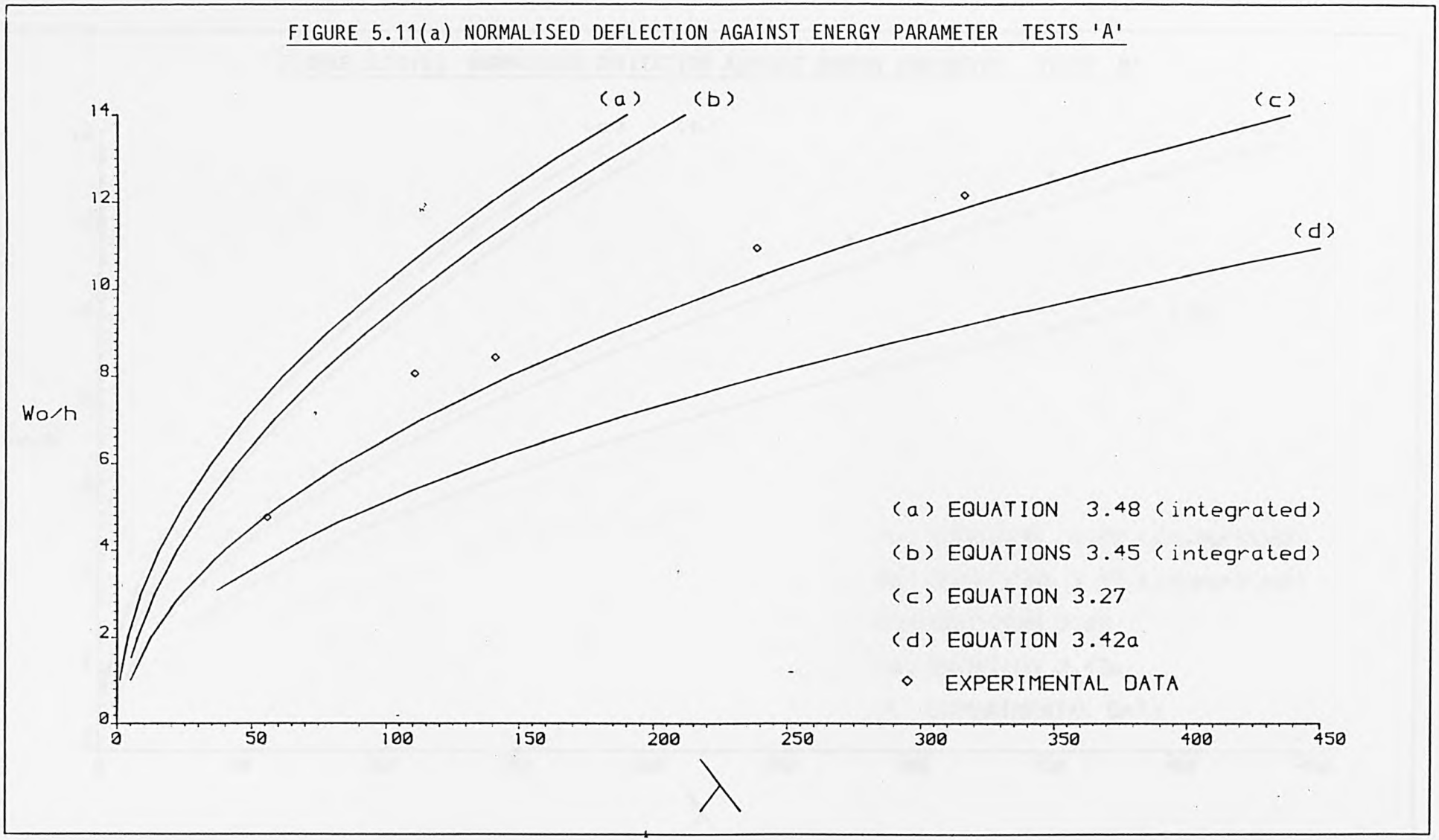

FIGURE 5.11(b) NORMALISED DEFLECTION AGAINST ENERGY PARAMETER TESTS 'B'

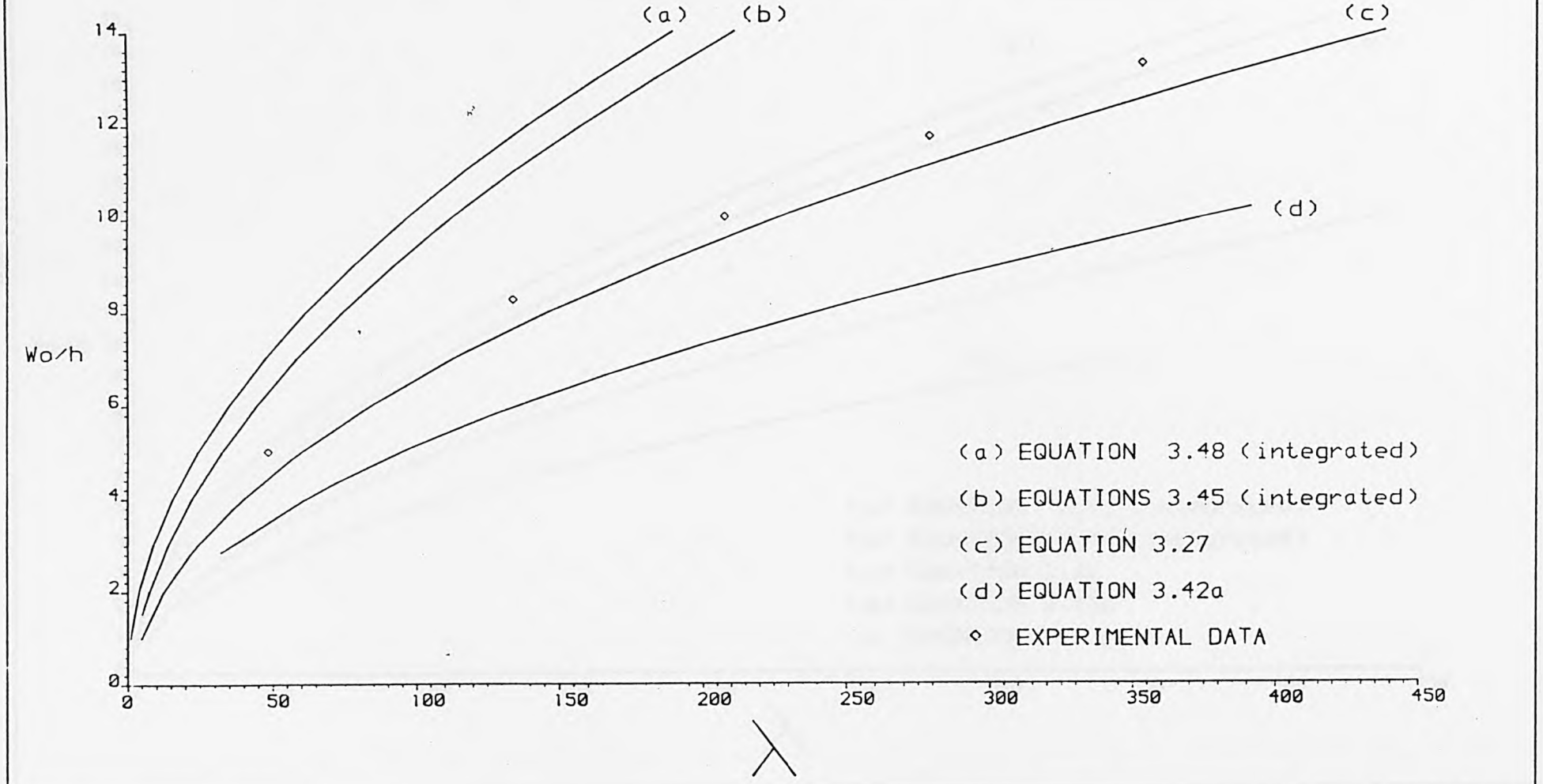

FIGURE 5.11(c) NORMALISED DEFLECTION AGAINST ENERGY PARAMETER TESTS 'C'

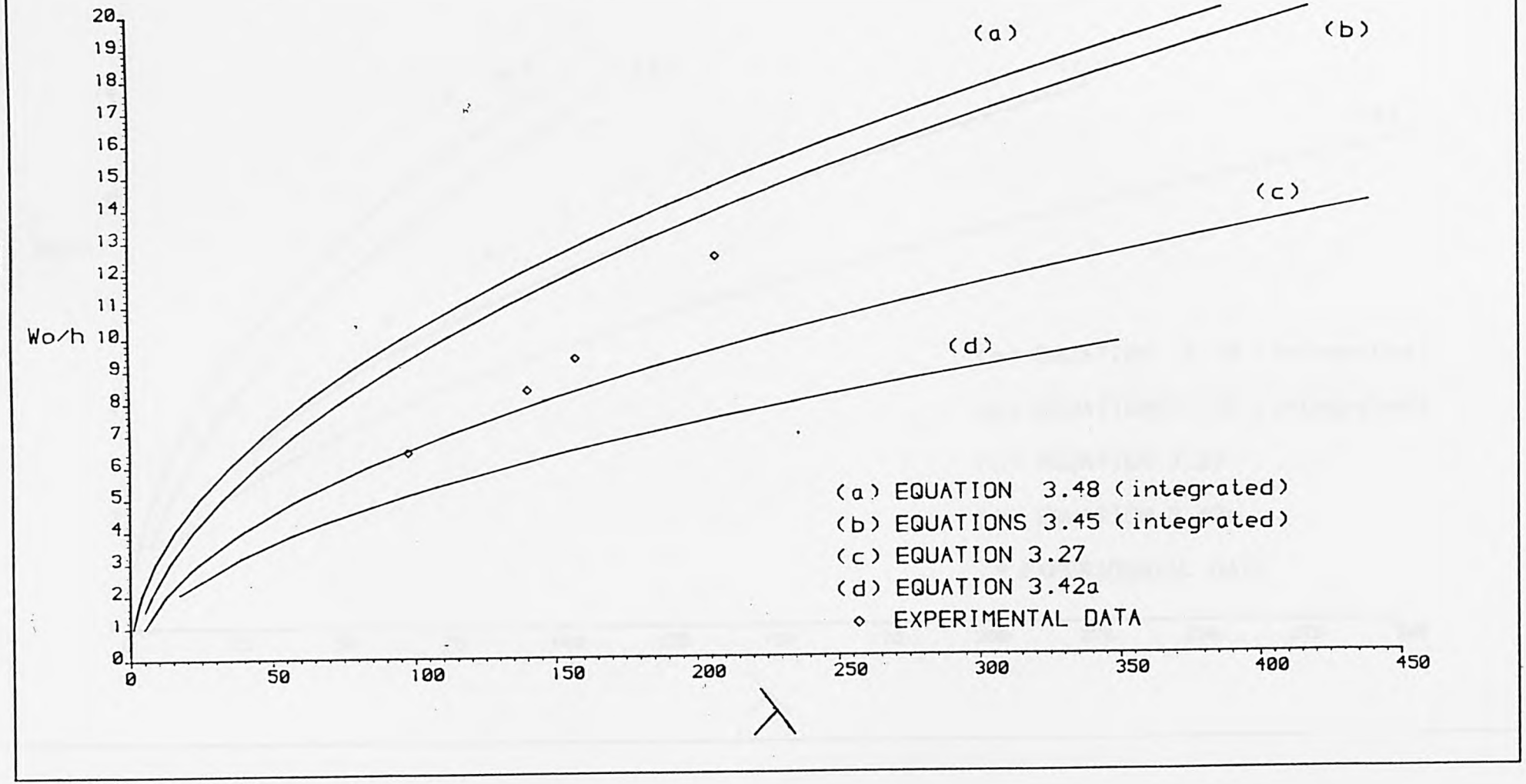

FIGURE 5.11(d) NORMALISED DEFLECTION AGAINST ENERGY PARAMETER TESTS 'D'

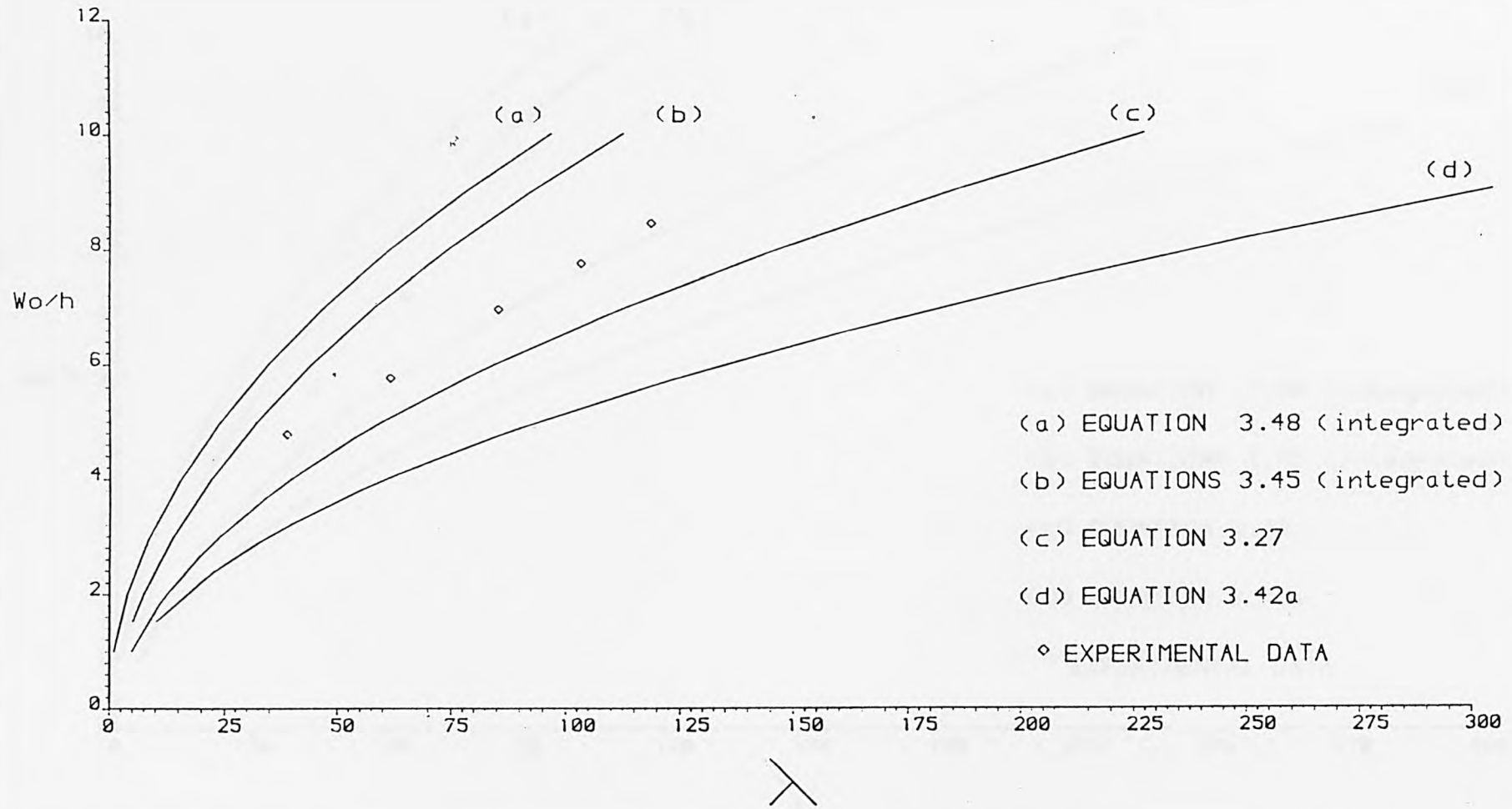

FIGURE 5.11(e) NORMALISED DEFLECTION AGAINST ENERGY PARAMETER TESTS 'E'

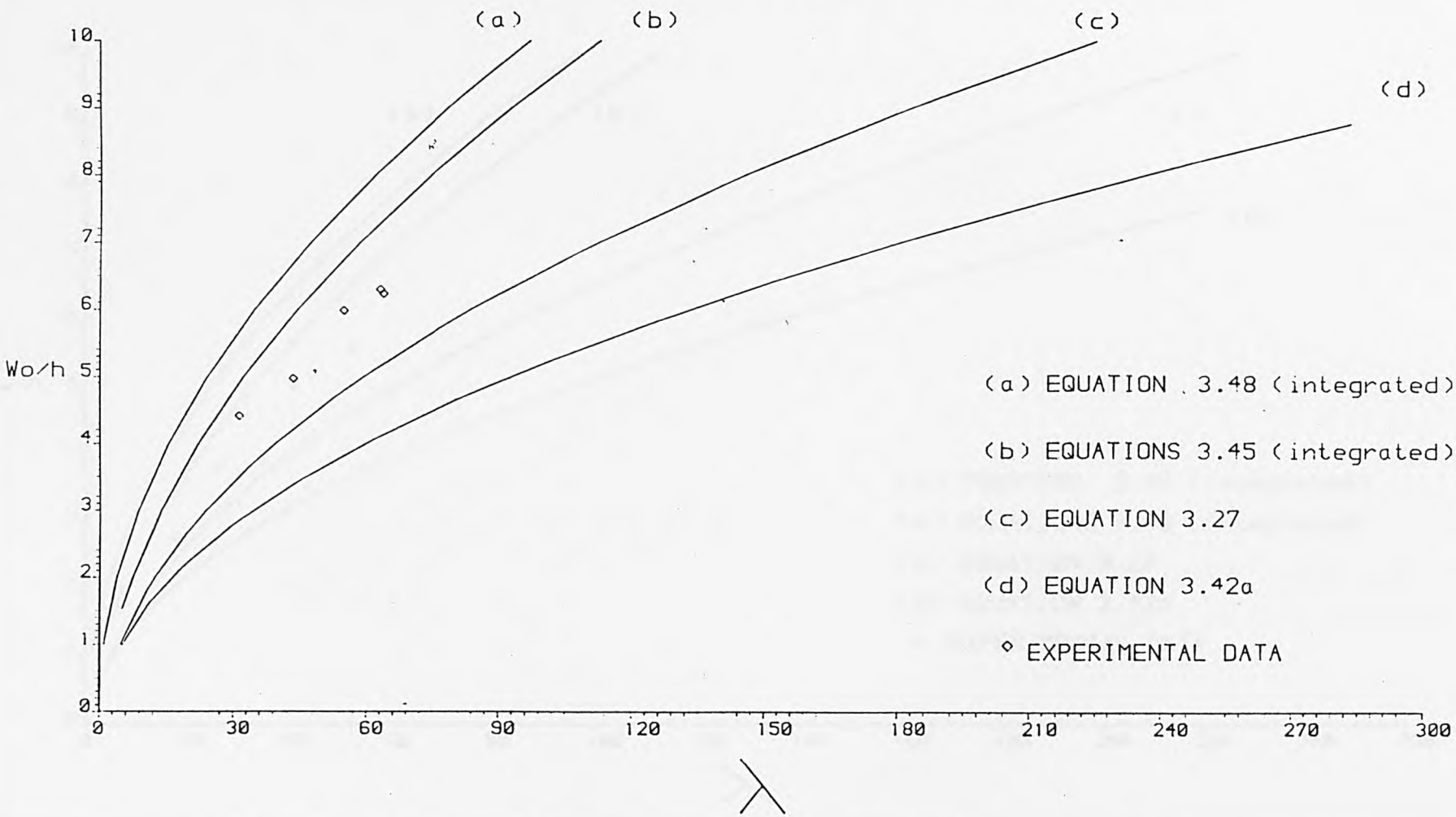

FIGURE 5.11(f) NORMALISED DEFLECTION AGAINST ENERGY PARAMETER TESTS 'F'

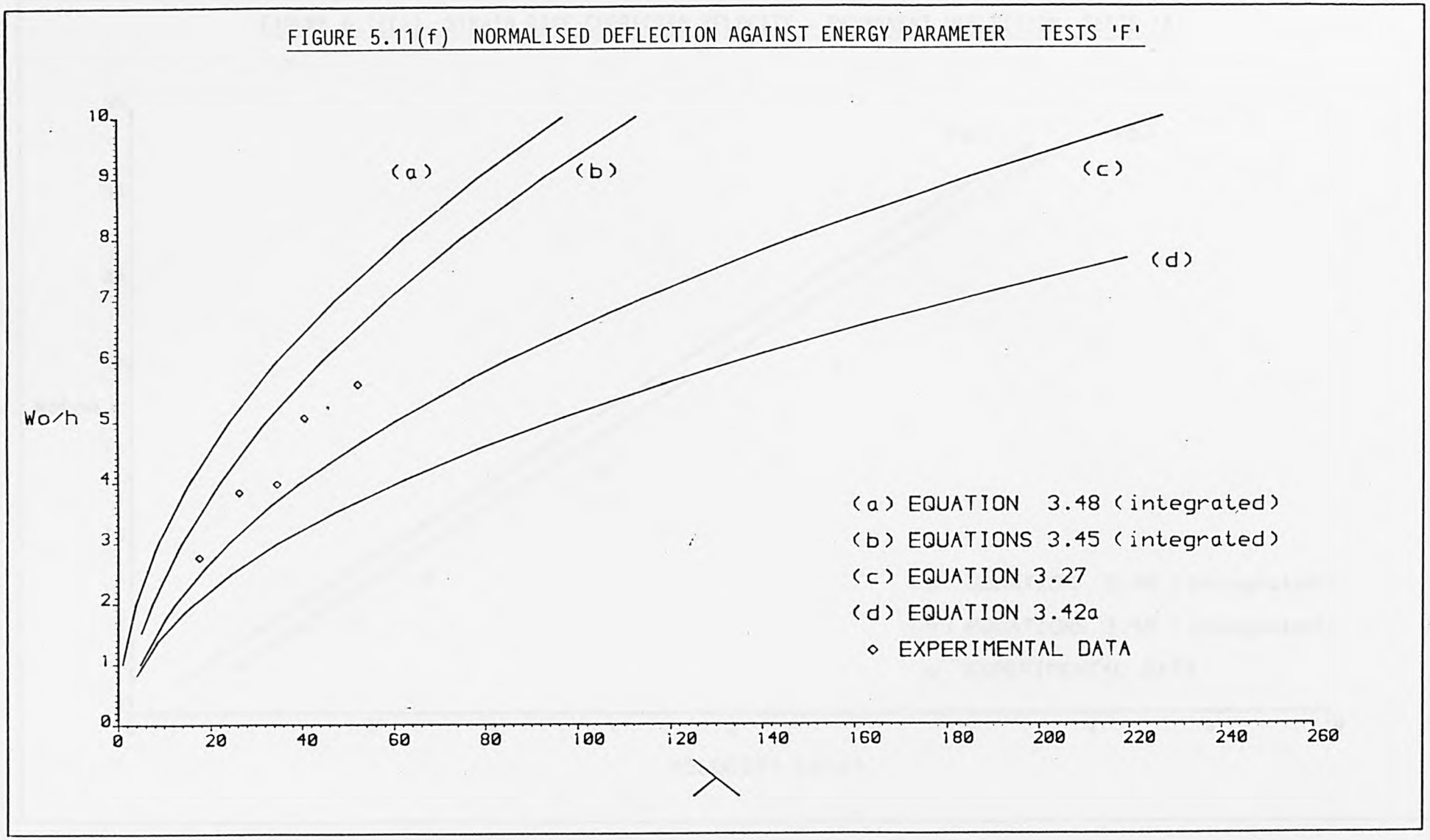

FIGURE 5.12(a) STRAIN RATE CORRECTED VELOCITY - PERMANENT DEFLECTION TESTS 'A'

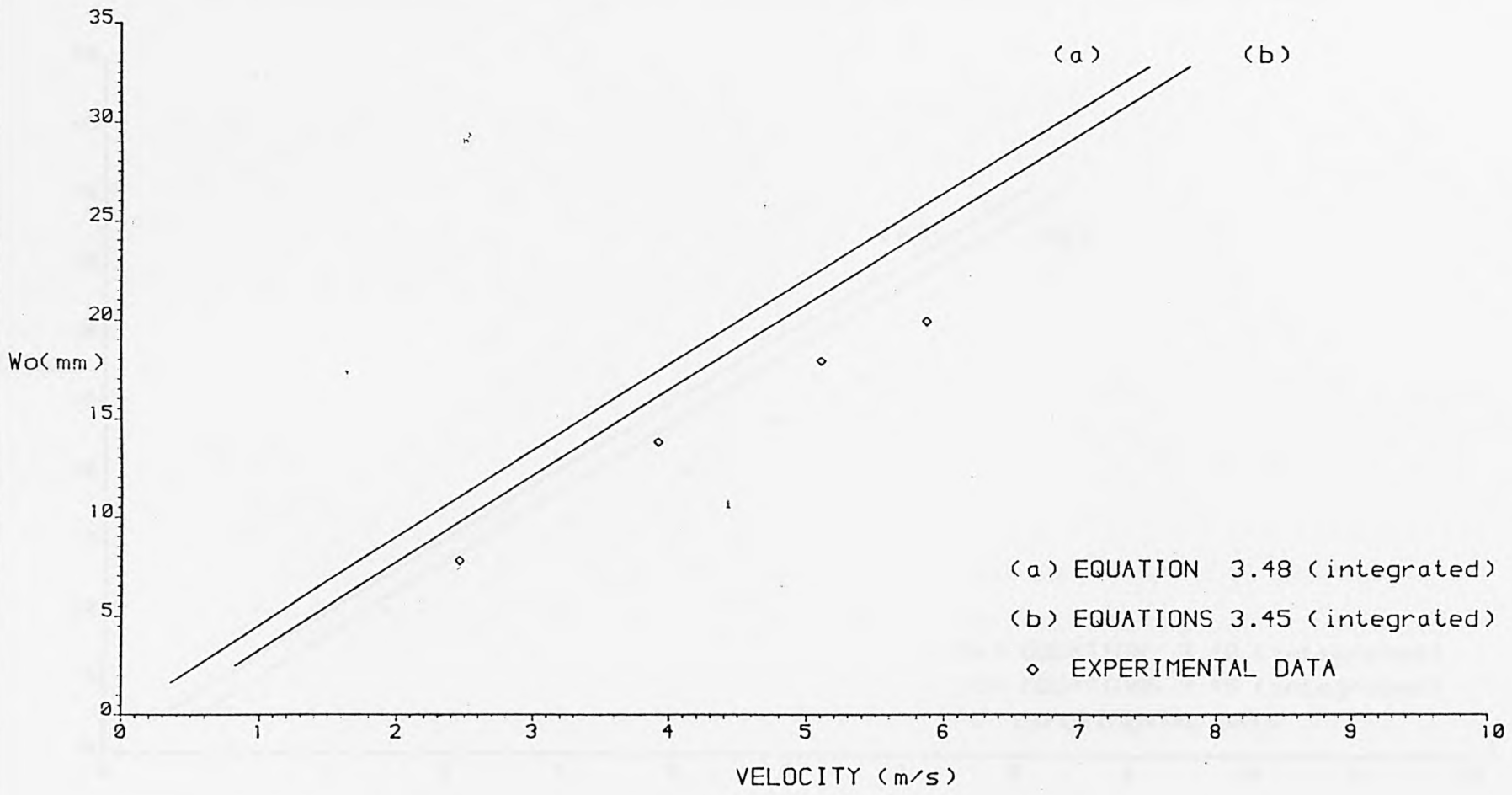

FIGURE 5.12(b) STRAIN RATE CORRECTED VELOCITY - PERMANENT DEFLECTION TESTS 'B'

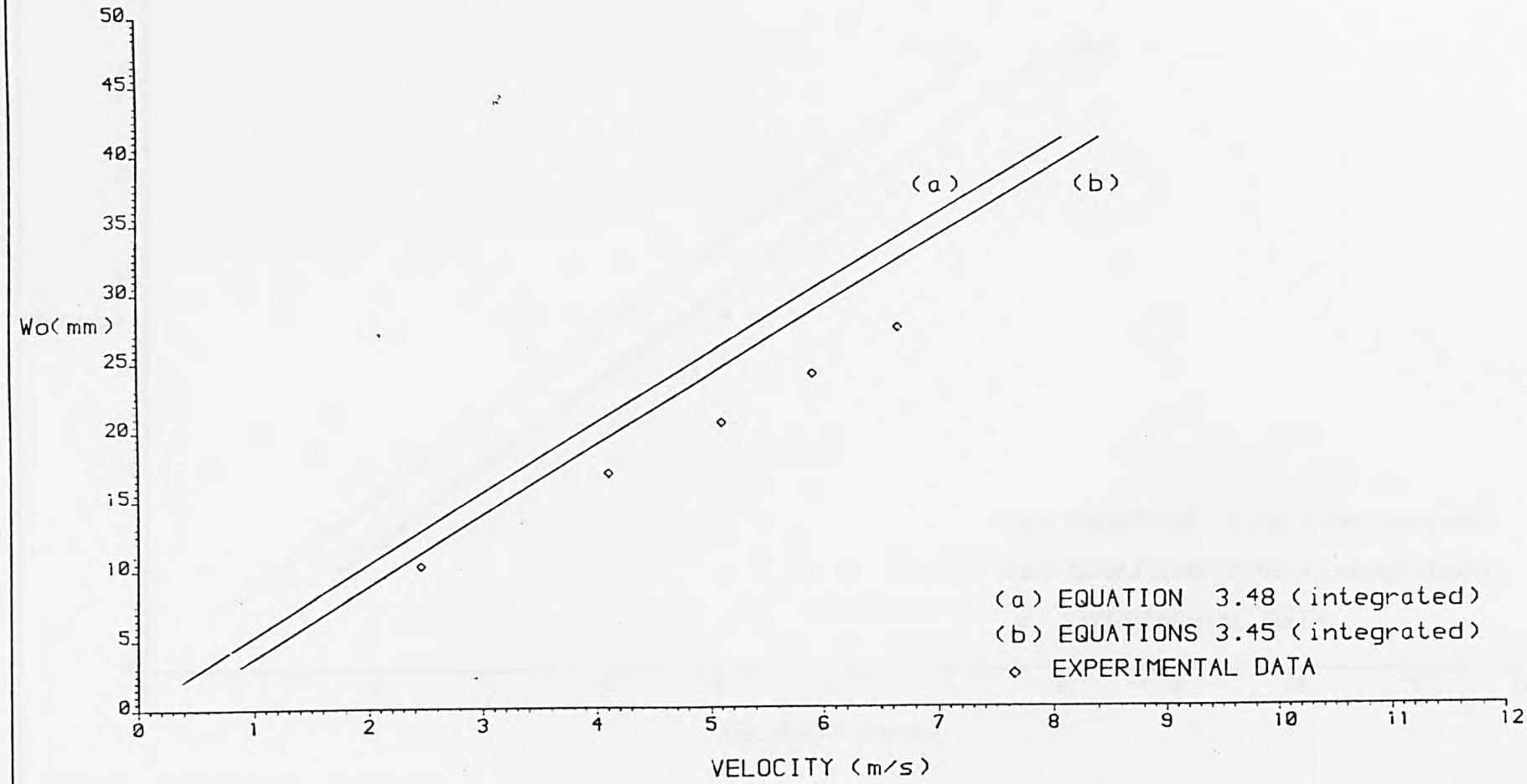

FIGURE 5.12(c) STRAIN RATE CORRECTED VELOCITY - PERMANENT DEFLECTION TESTS 'D'

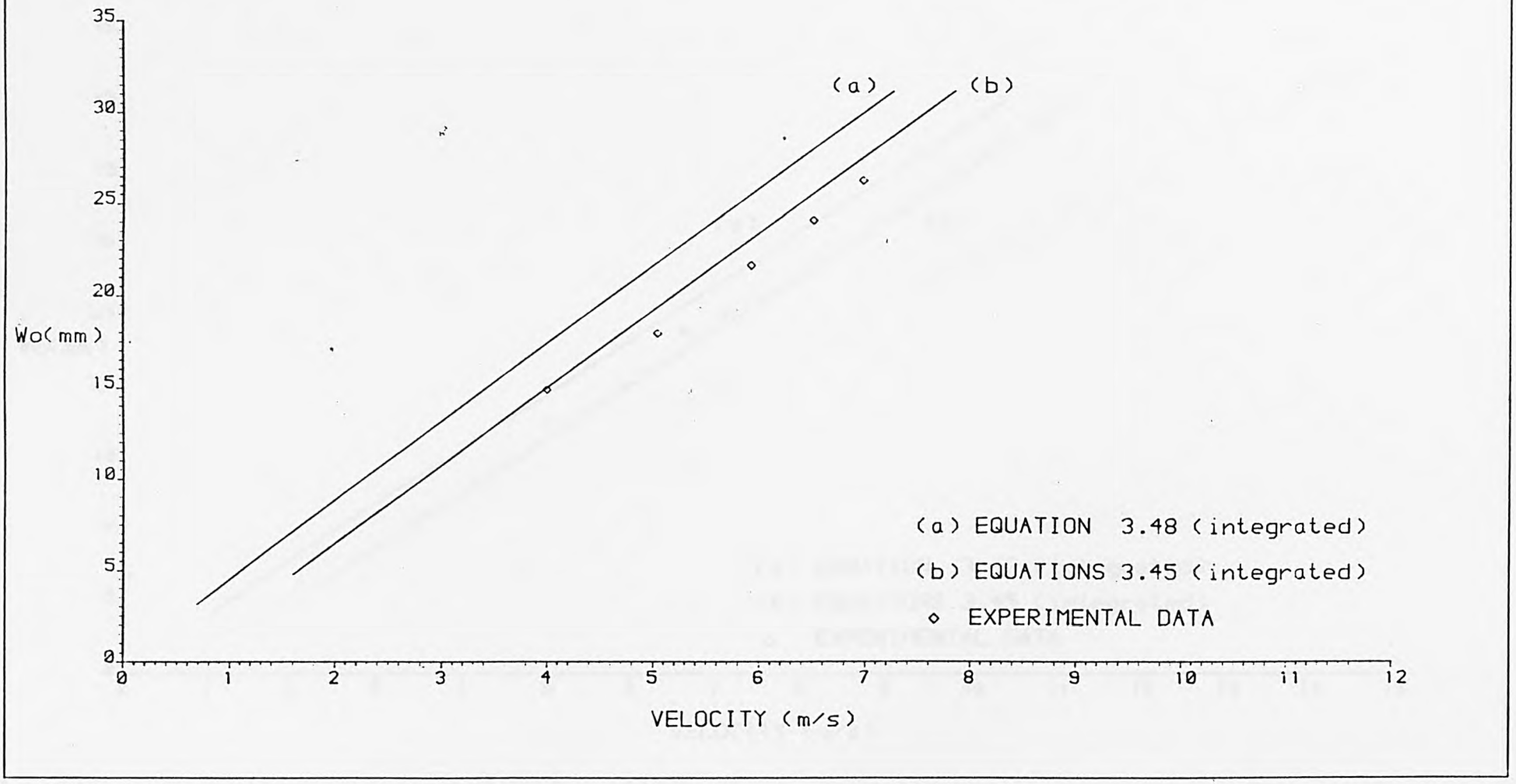

FIGURE 5.12(d) STRAIN RATE CORRECTED VELOCITY - PERMANENT DEFLECTION TESTS 'E'

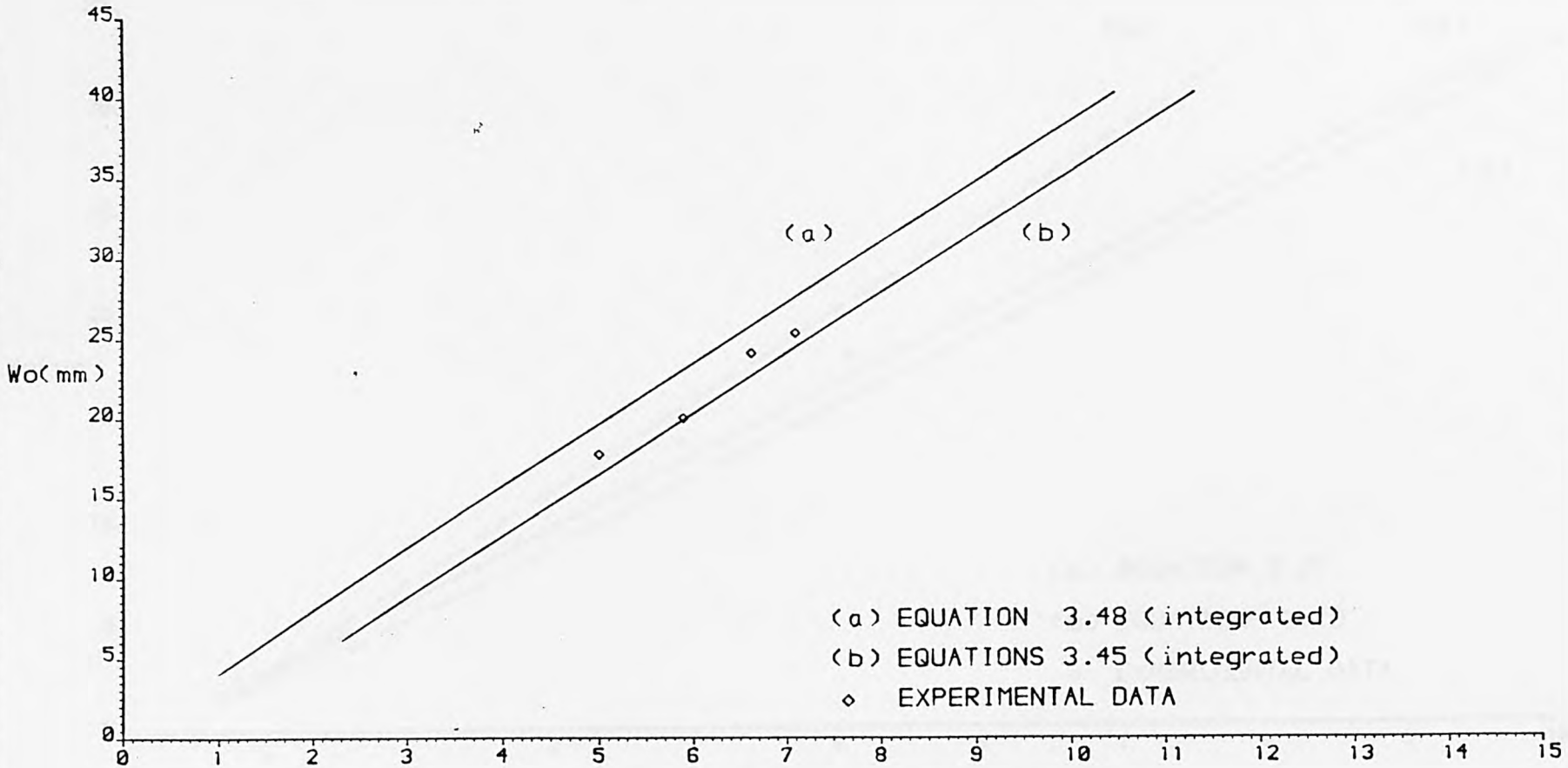

FIGURE 5.13(a) EQUATION 3.27 PLUS BOUND SOLUTIONS - TESTS 'A'

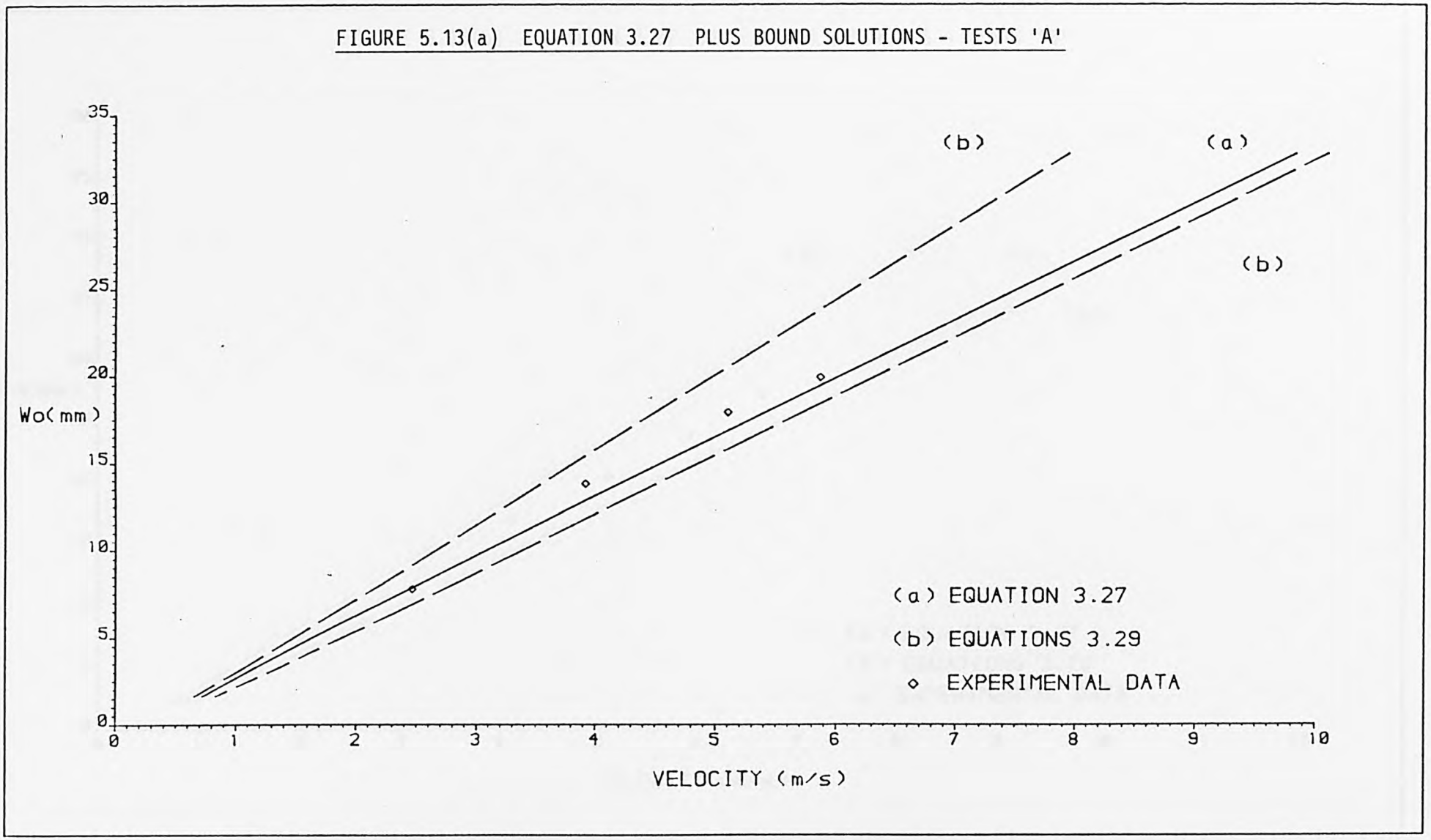

FIGURE 5.13(b) EQUATION 3.27 PLUS BOUND SOLUTIONS - TESTS 'B'

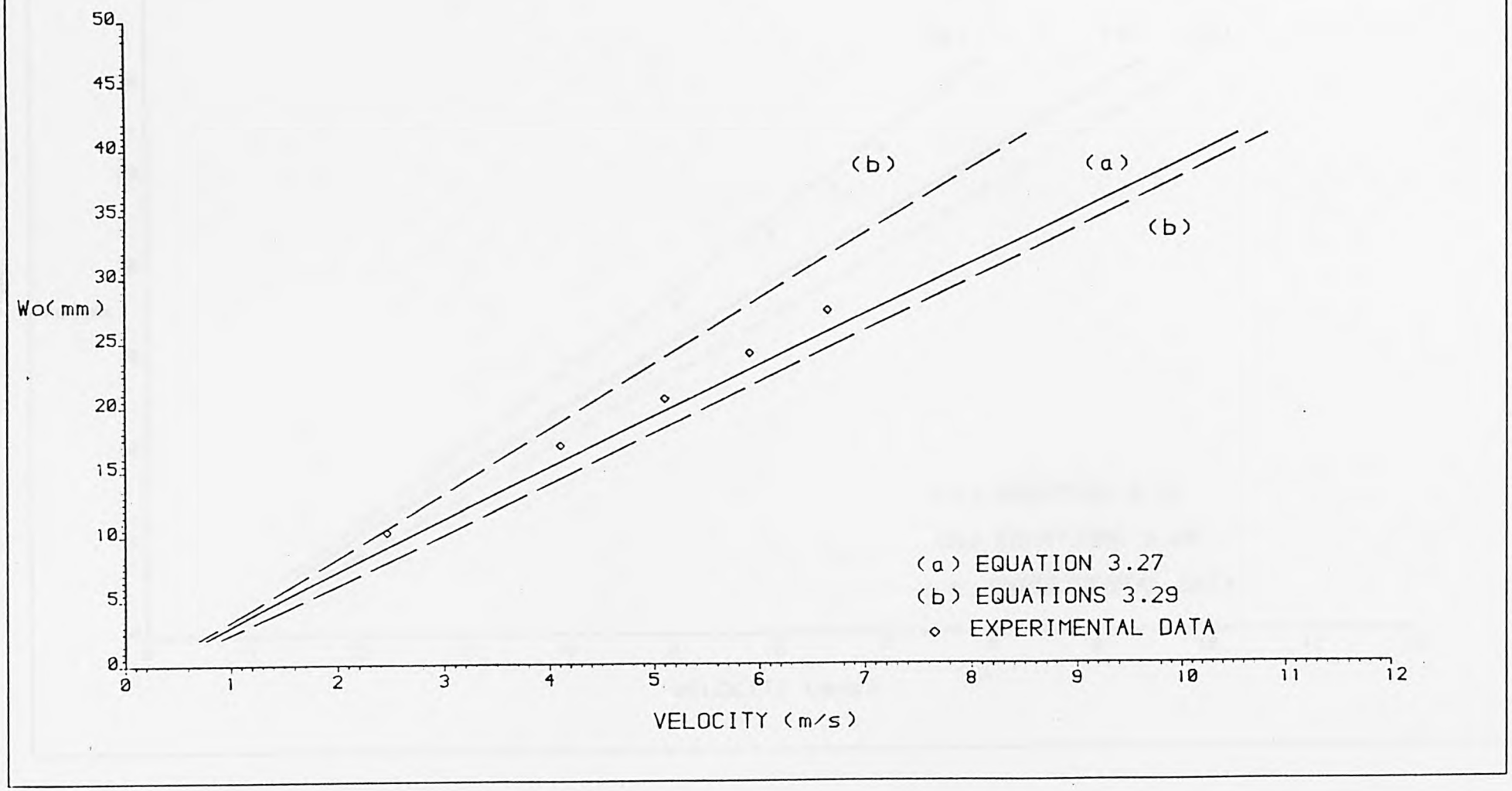

FIGURE 5.13(c) EQUATION 3.27 PLUS BOUND SOLUTIONS - TESTS 'D'

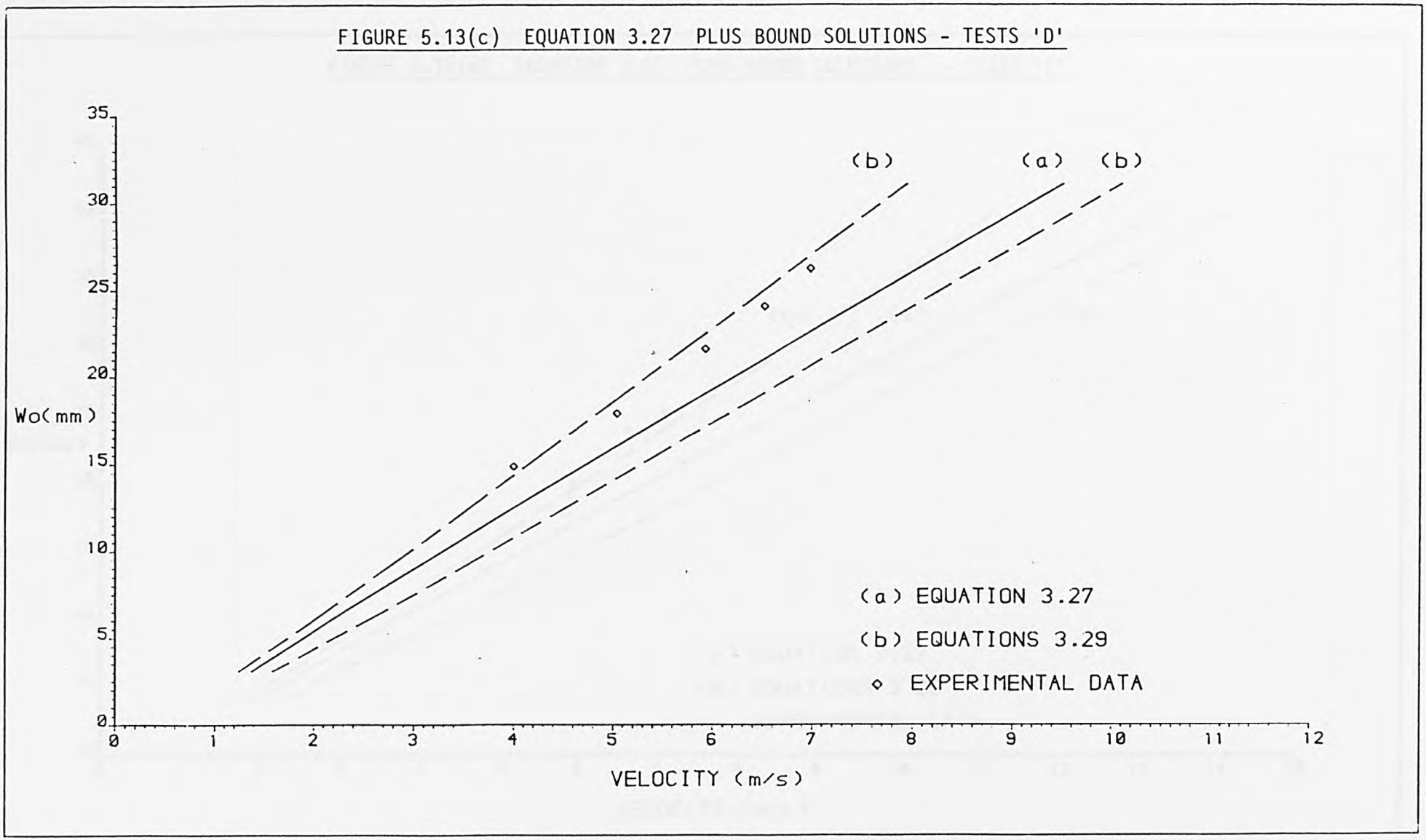

FIGURE 5.13(d) EQUATION 3.27 PLUS BOUND SOLUTIONS - TESTS 'E'

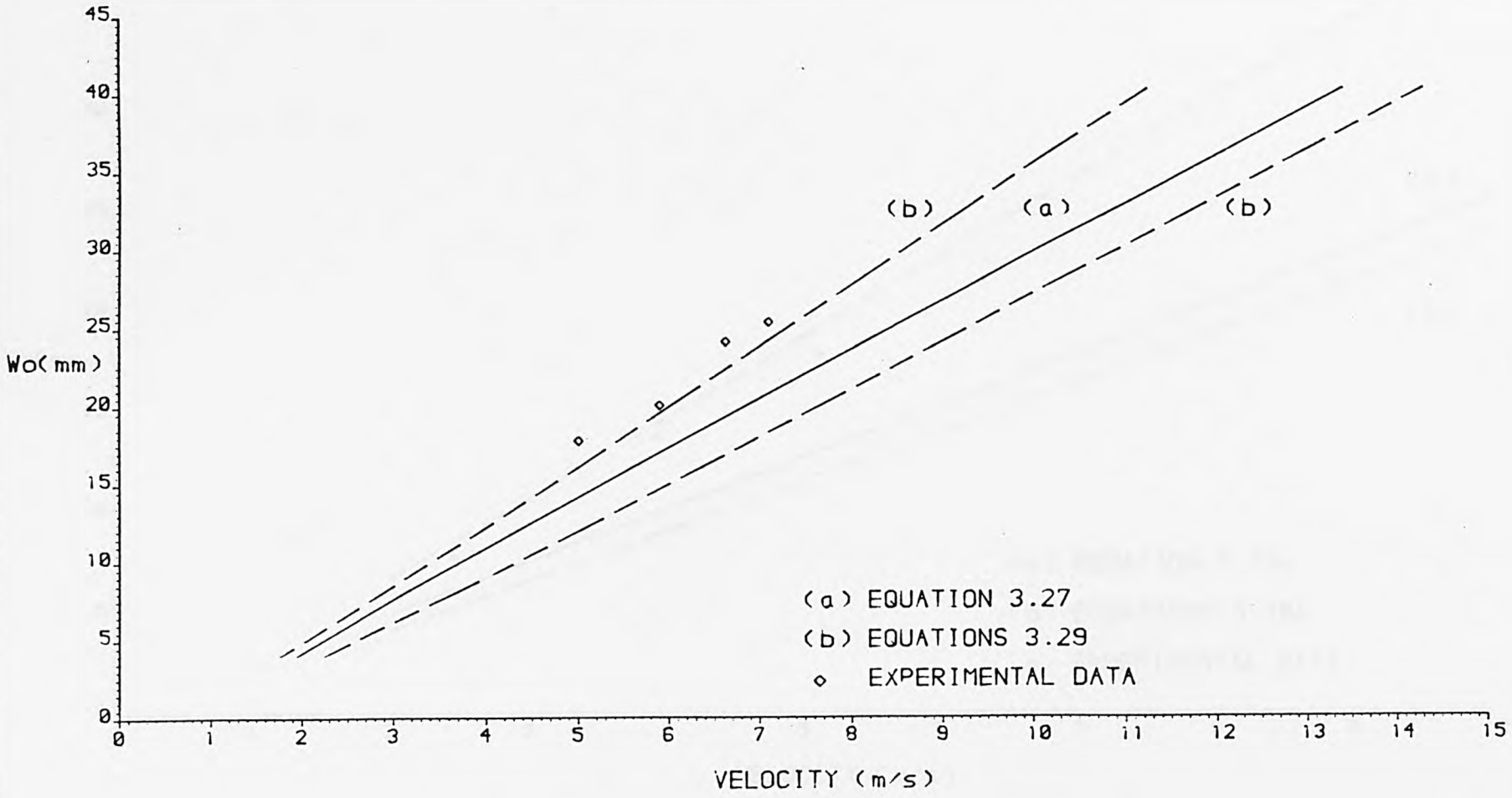

FIGURE 5.14(a) EQUATION 3.42a PLUS BOUND SOLUTIONS - TESTS 'A'

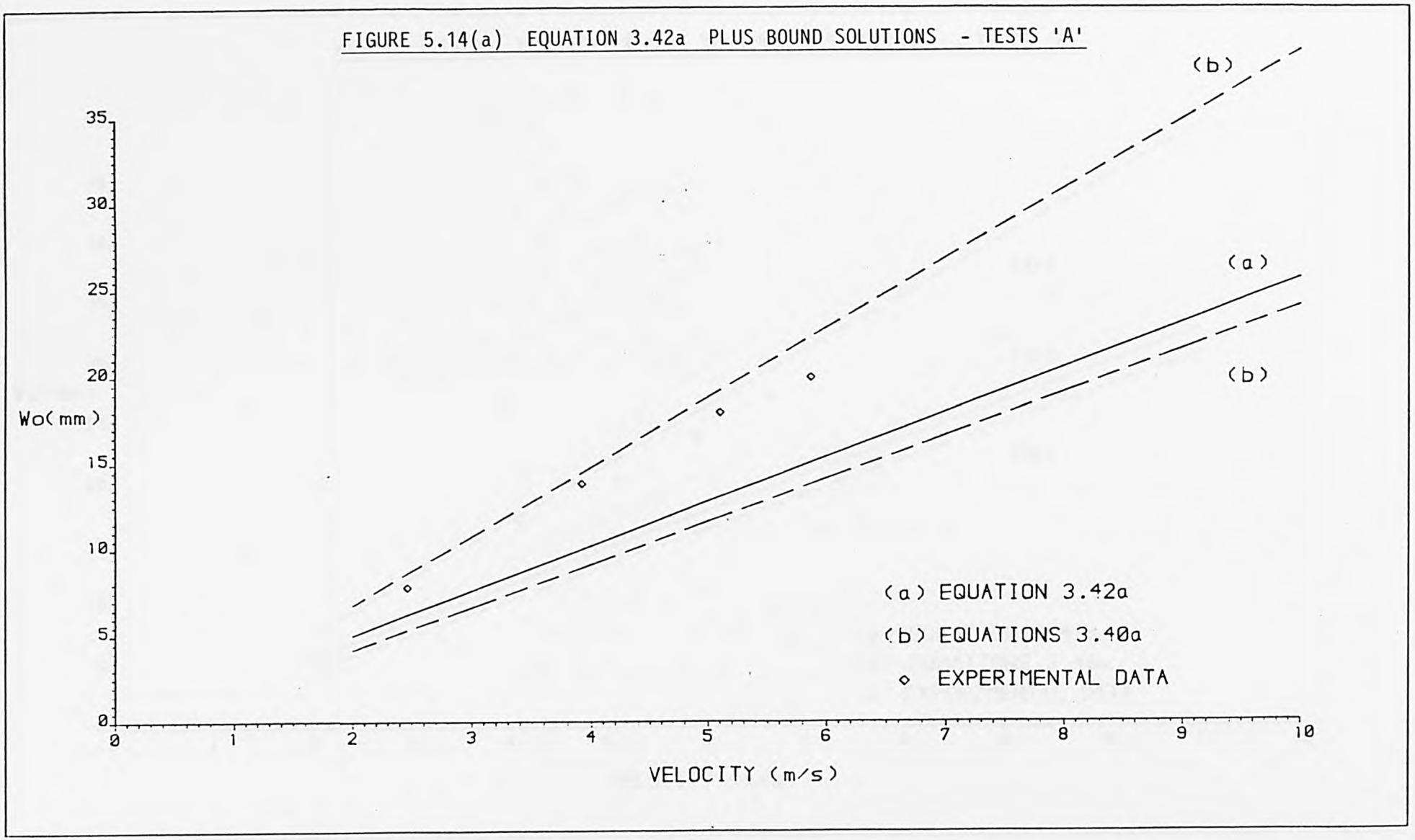

FIGURE 5.14(b) EQUATION 3.42a PLUS BOUND SOLUTIONS - TESTS 'B'

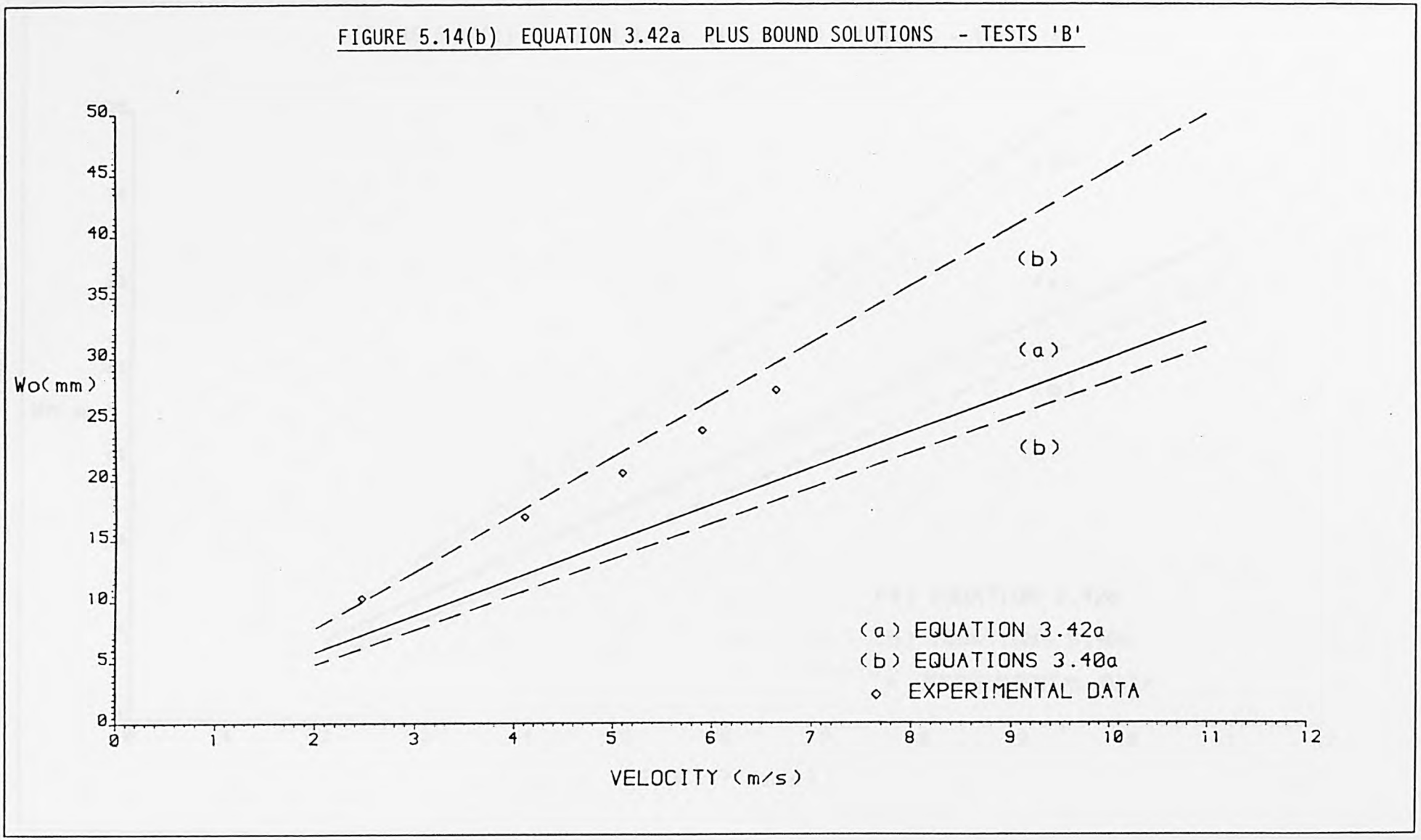

FIGURE 5.14(c) EQUATION 3.42a PLUS BOUND SOLUTIONS - TESTS 'D'

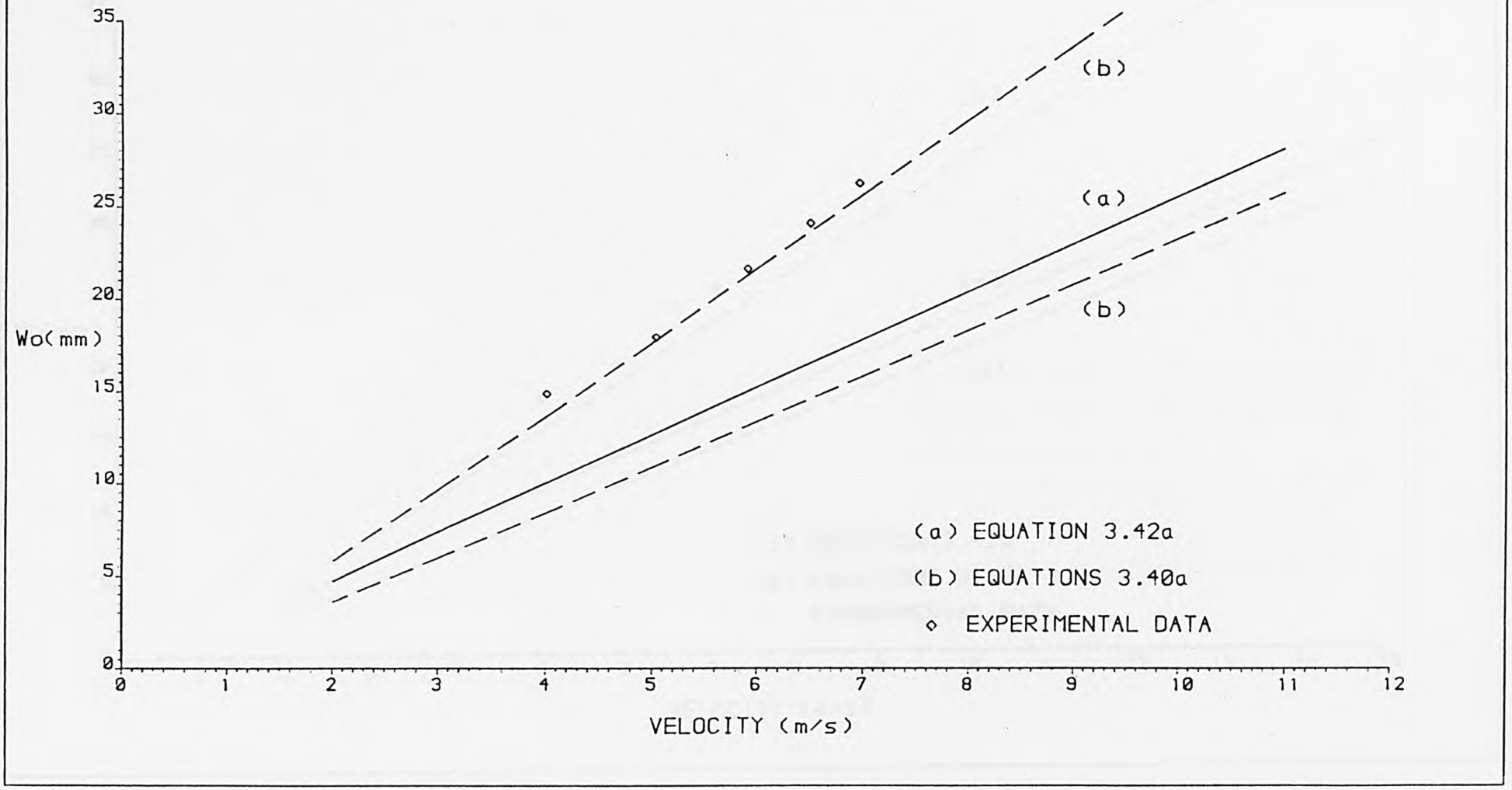

FIGURE 5.14(d) EQUATION 3.42a PLUS BOUND SOLUTIONS - TESTS 'E'

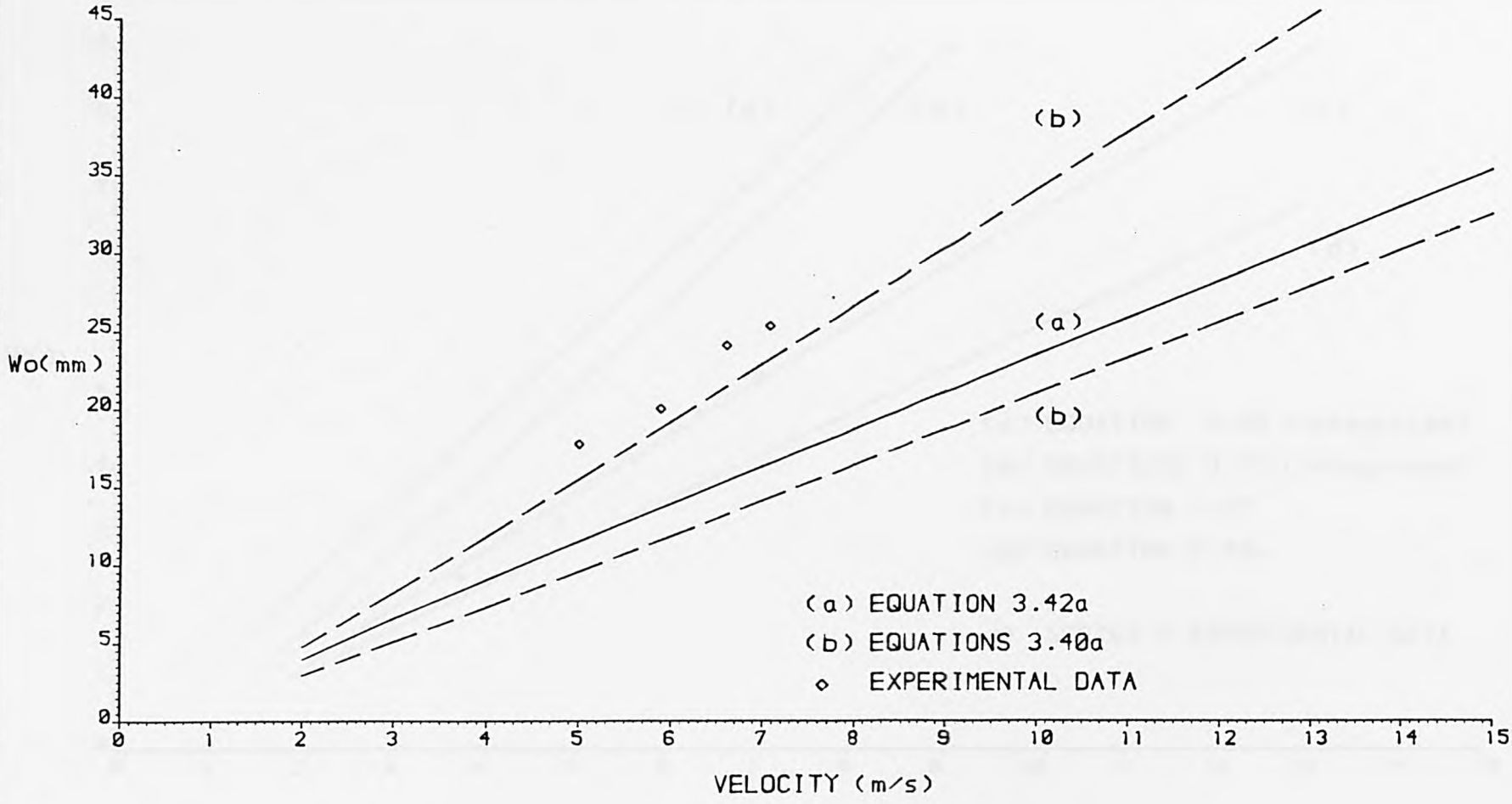

FIGURE 5.15(a) VELOCITY - PERMANENT DEFLECTION - TESTS 'S'

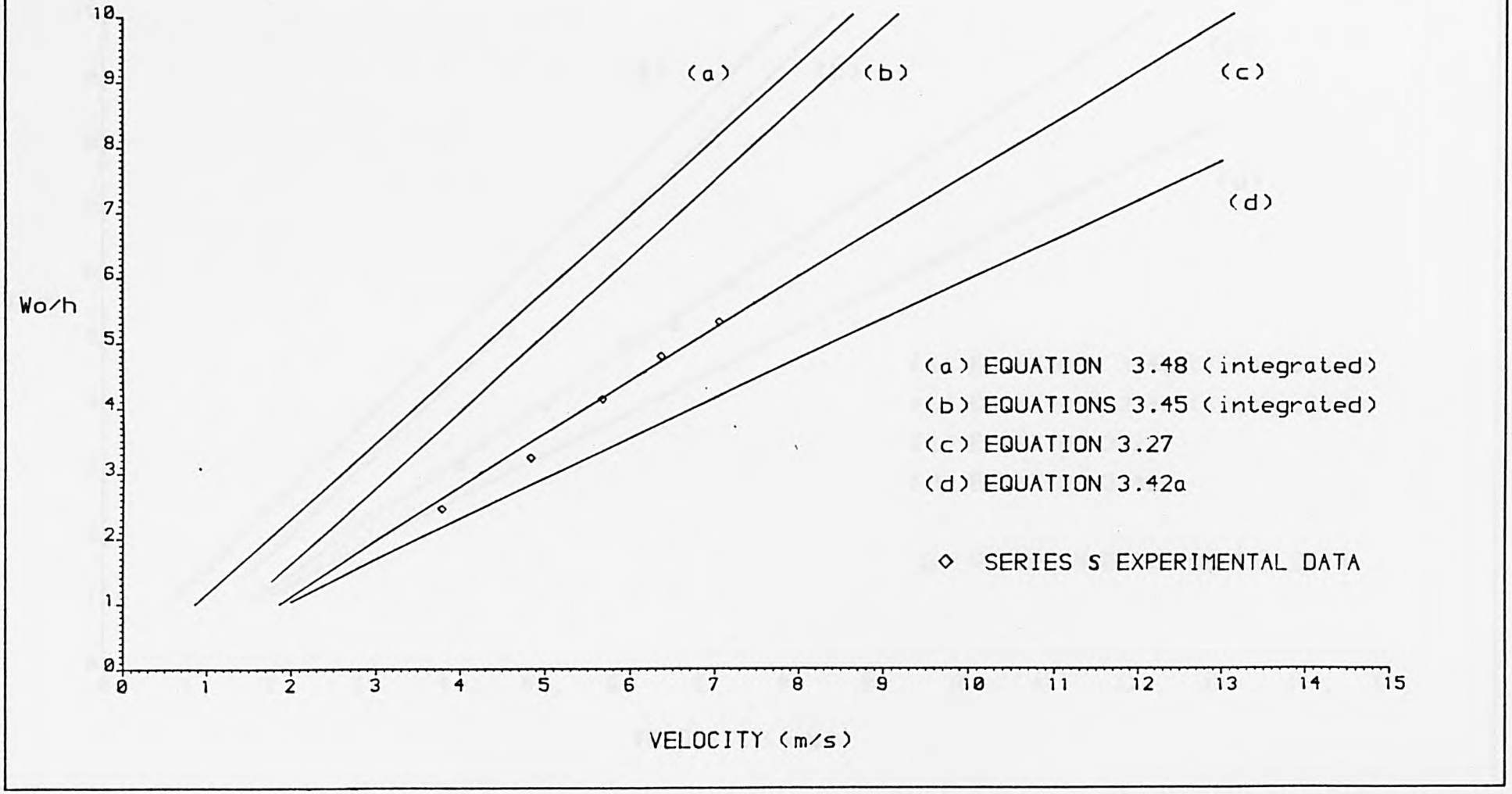

FIGURE 5.15(b) VELOCITY - PERMANENT DEFLECTION - TESTS 'M'

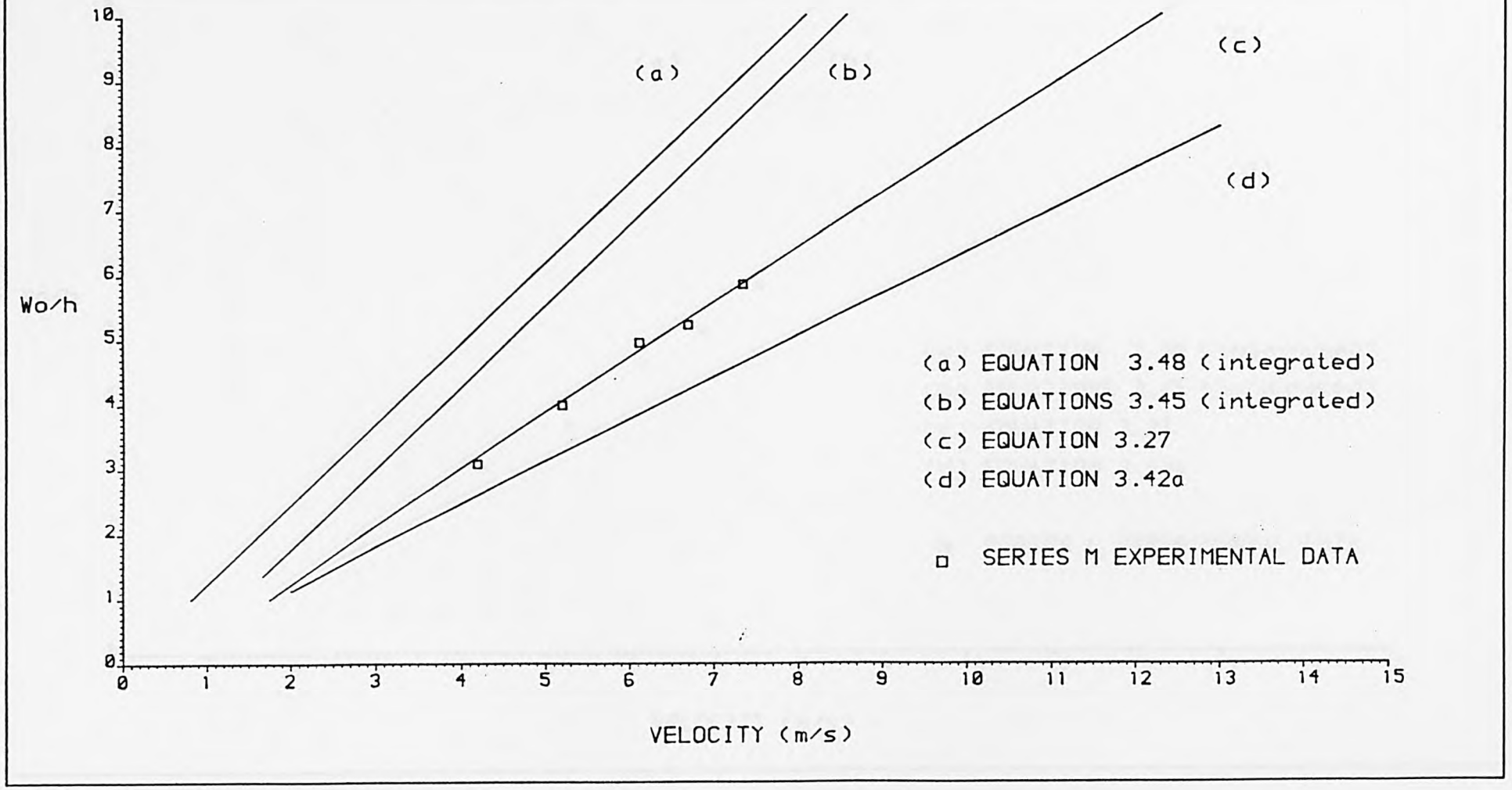

FIGURE 5.15(c) VELOCITY - PERMANENT DEFLECTION - TESTS 'L'

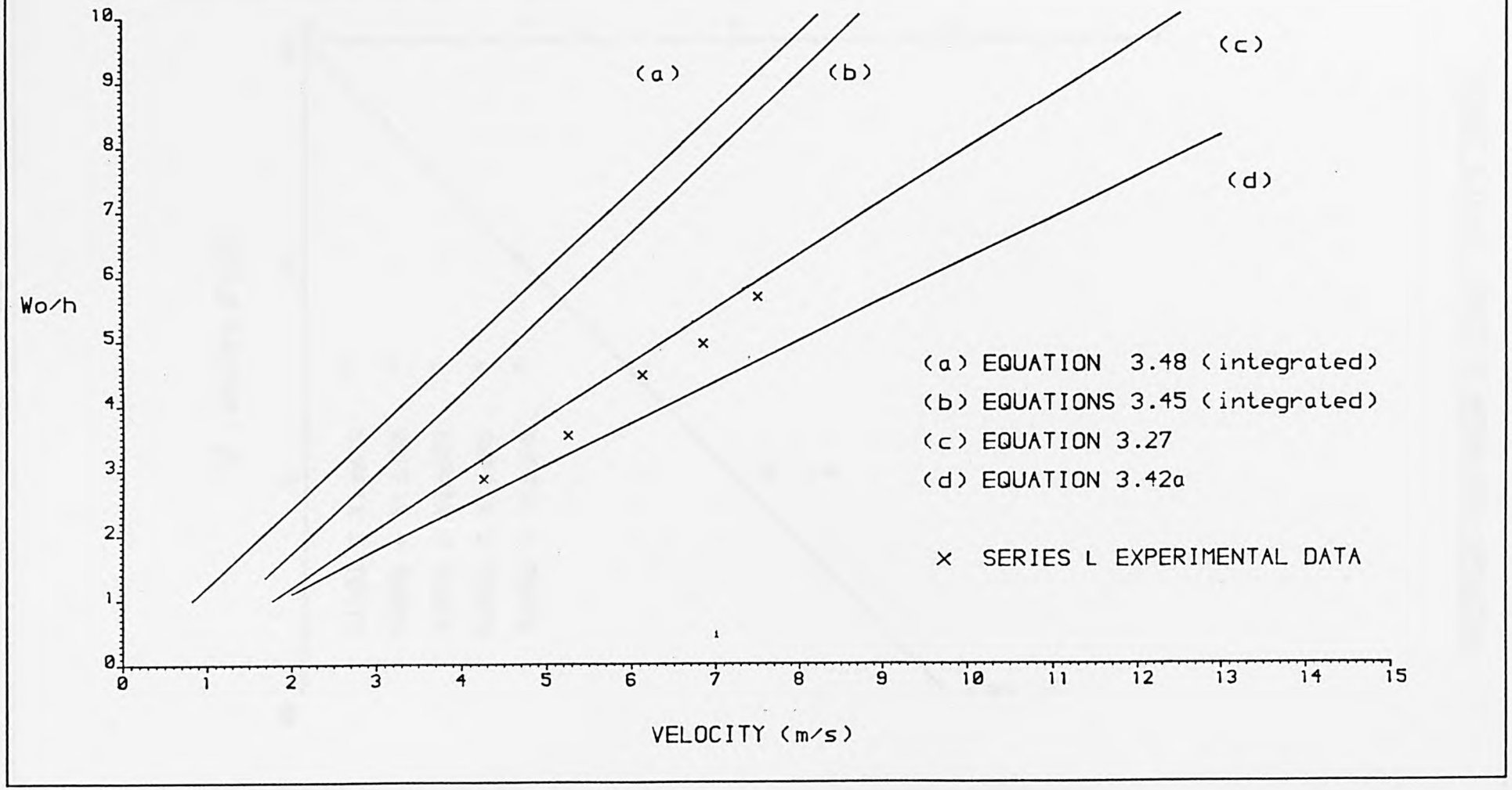

FIGURE 5.16(a) SERIES 2 NORMALISED DEFLECTION

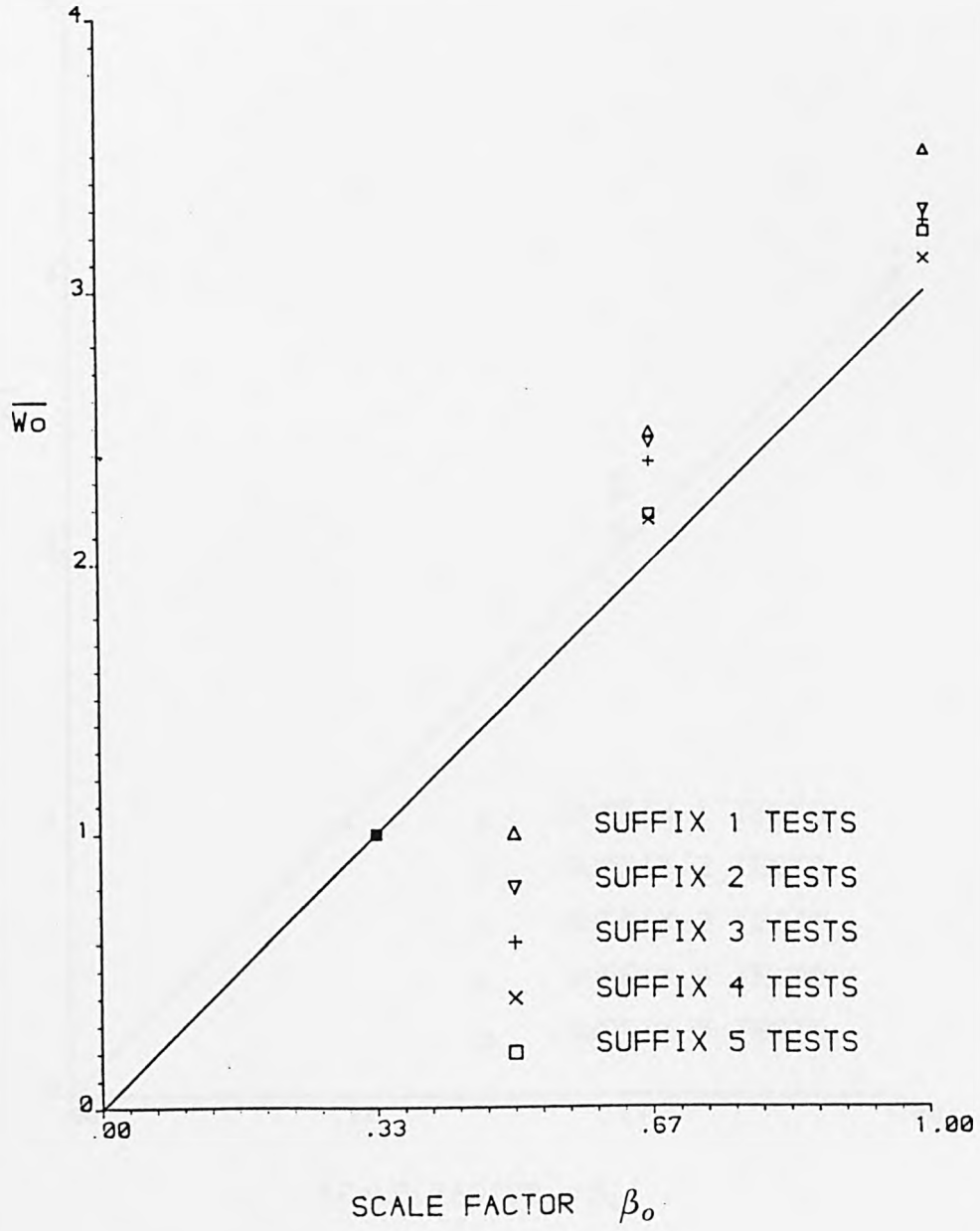

FIGURE 5.16(b) SERIES 2 NORMALISED DEFLECTION - VELOCITY CORRECTED

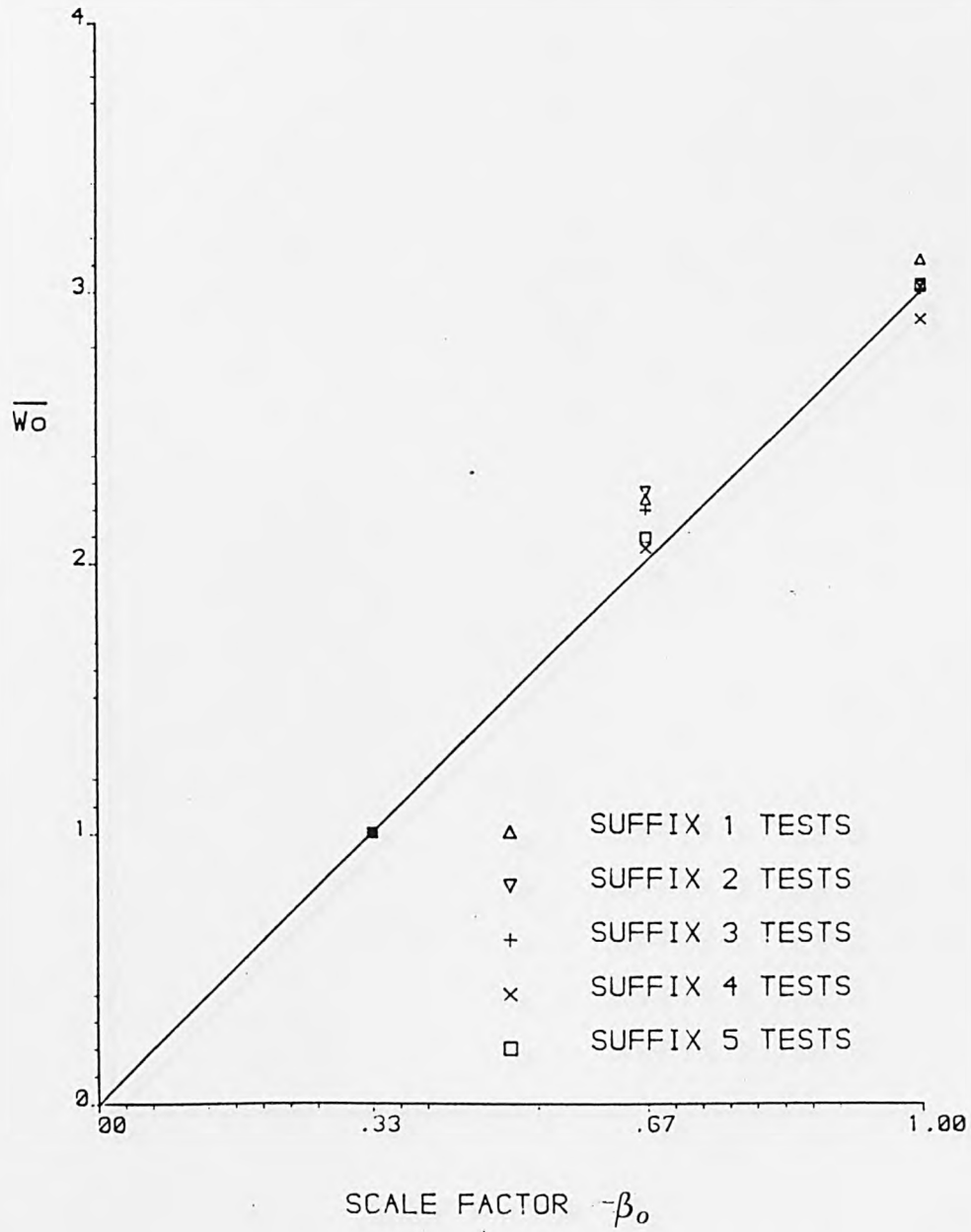

FIGURE 5.16(c) SERIES 2 NORMALISED DEFLECTION - YIELD STRESS CORRECTED

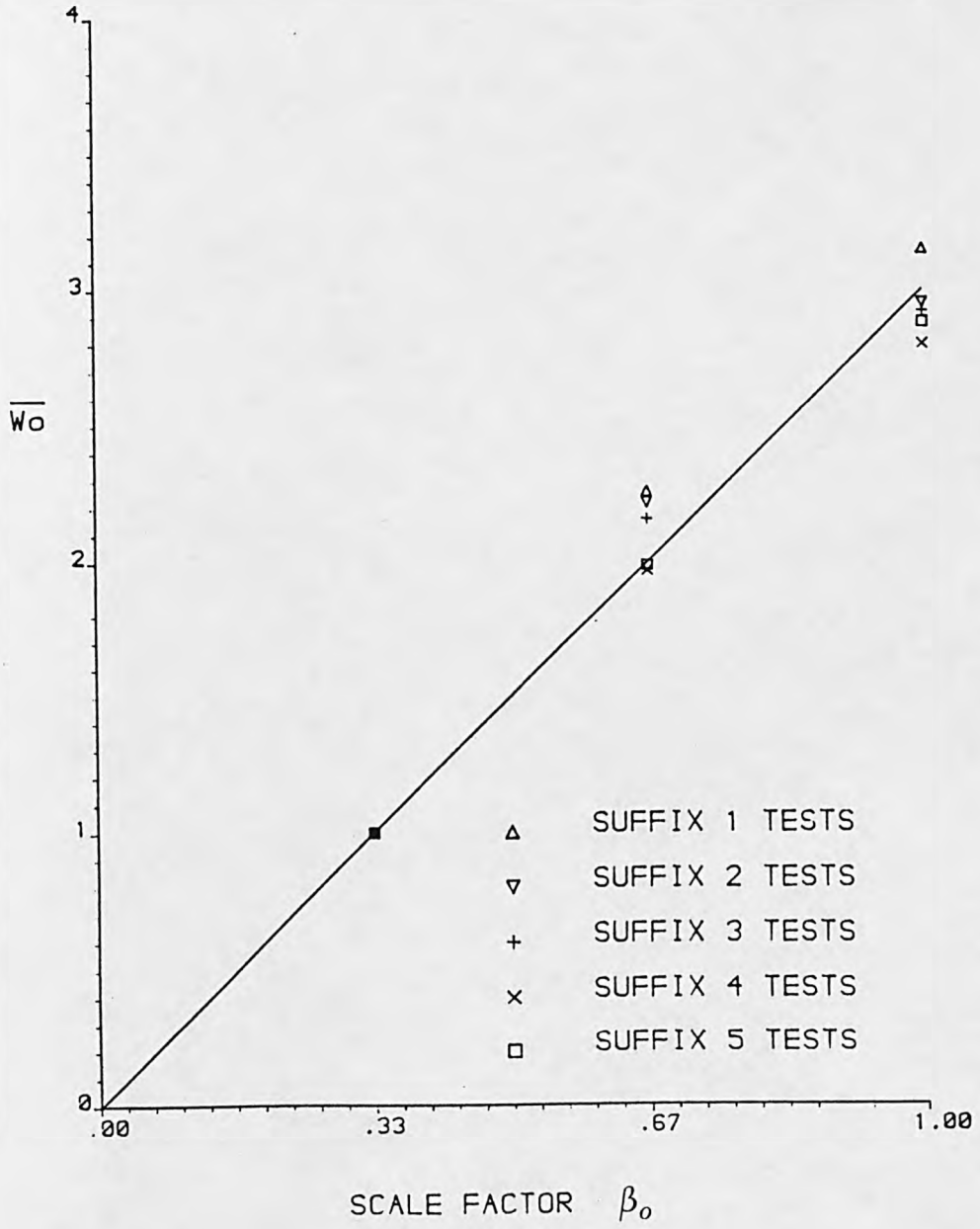

FIGURE 5.17(a) PERMANENT DEFLECTION PROFILES (SUFFIX 5 TESTS)

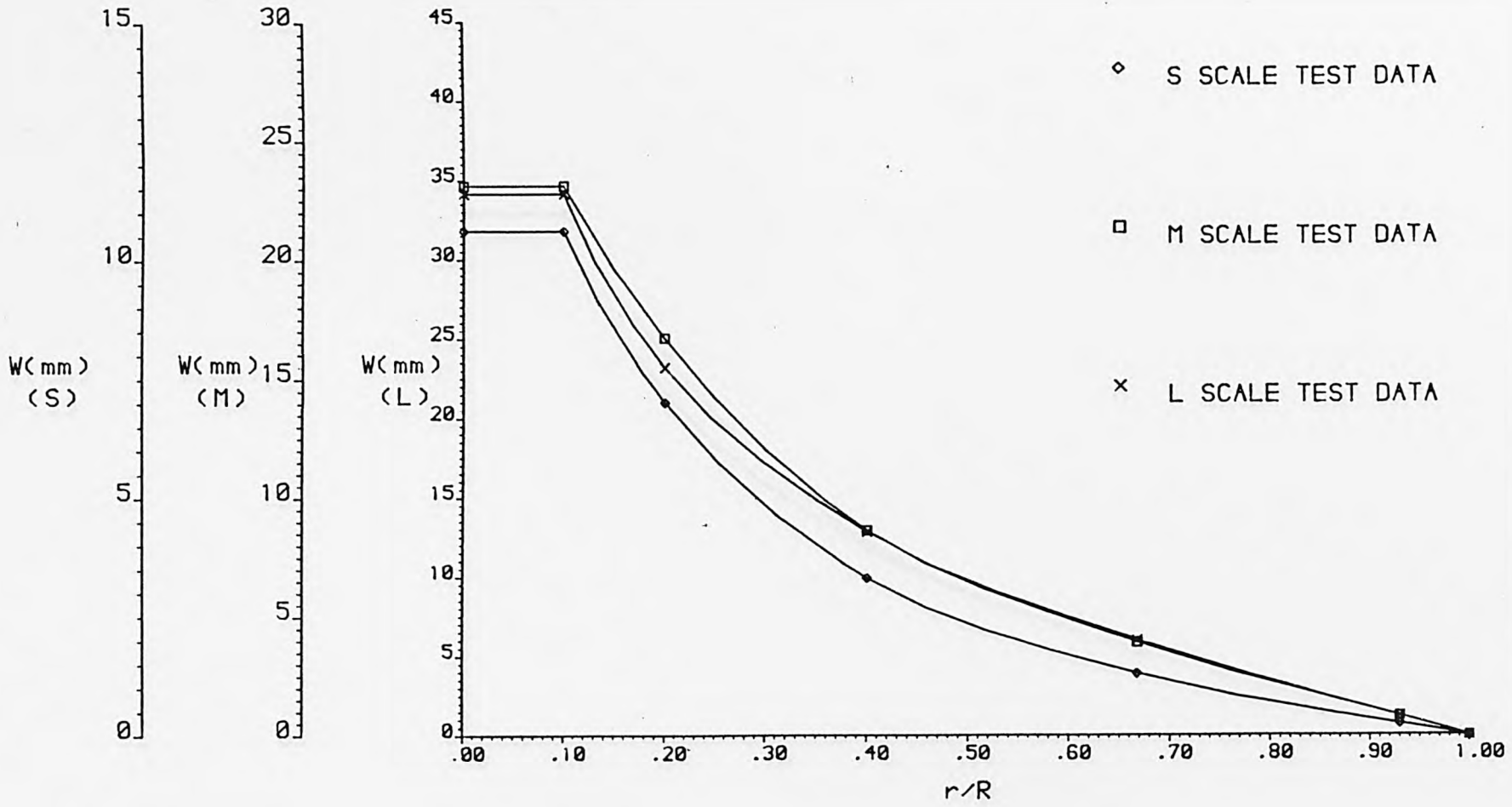

FIGURE 5.17(b) PERMANENT DEFLECTION PROFILES (SUFFIX 5 TESTS) - YIELD STRESS CORRECTED

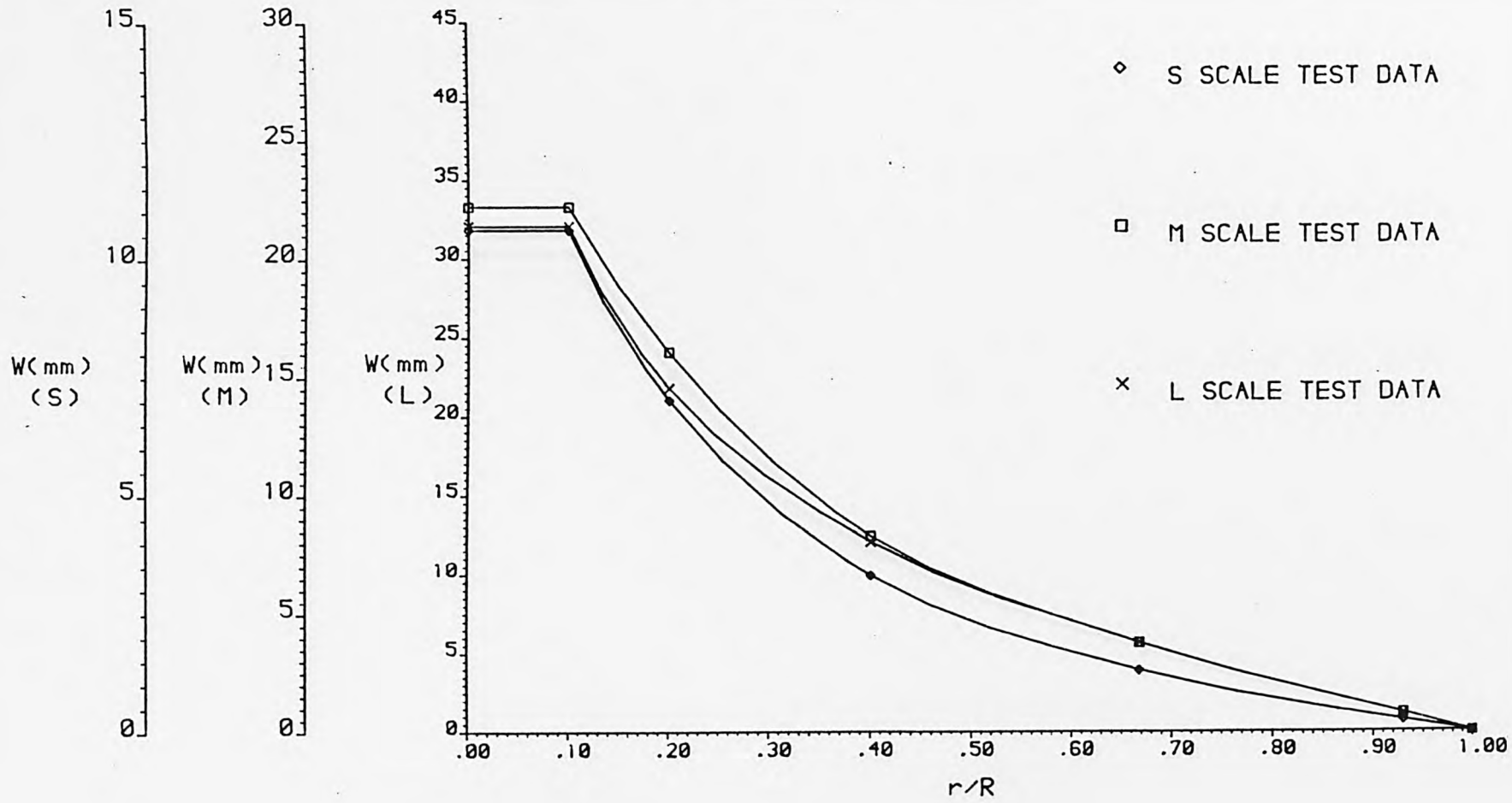

FIGURE 5.17(c) PERMANENT DEFLECTION PROFILES (SUFFIX 5 TESTS) - VELOCITY CORRECTED

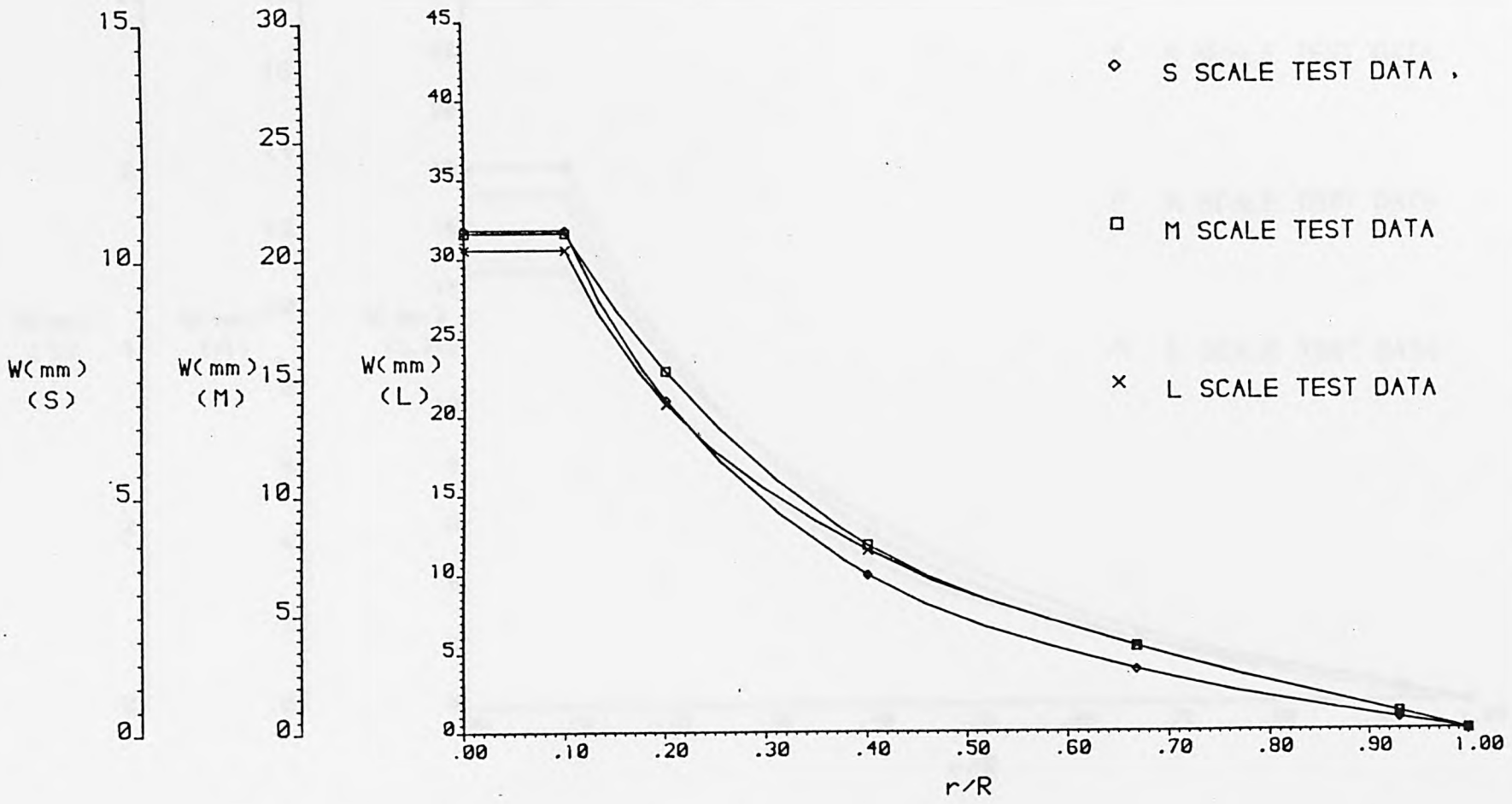

FIGURE 5.17(d) PERMANENT DEFLECTION PROFILES (SUFFIX 1 TESTS)

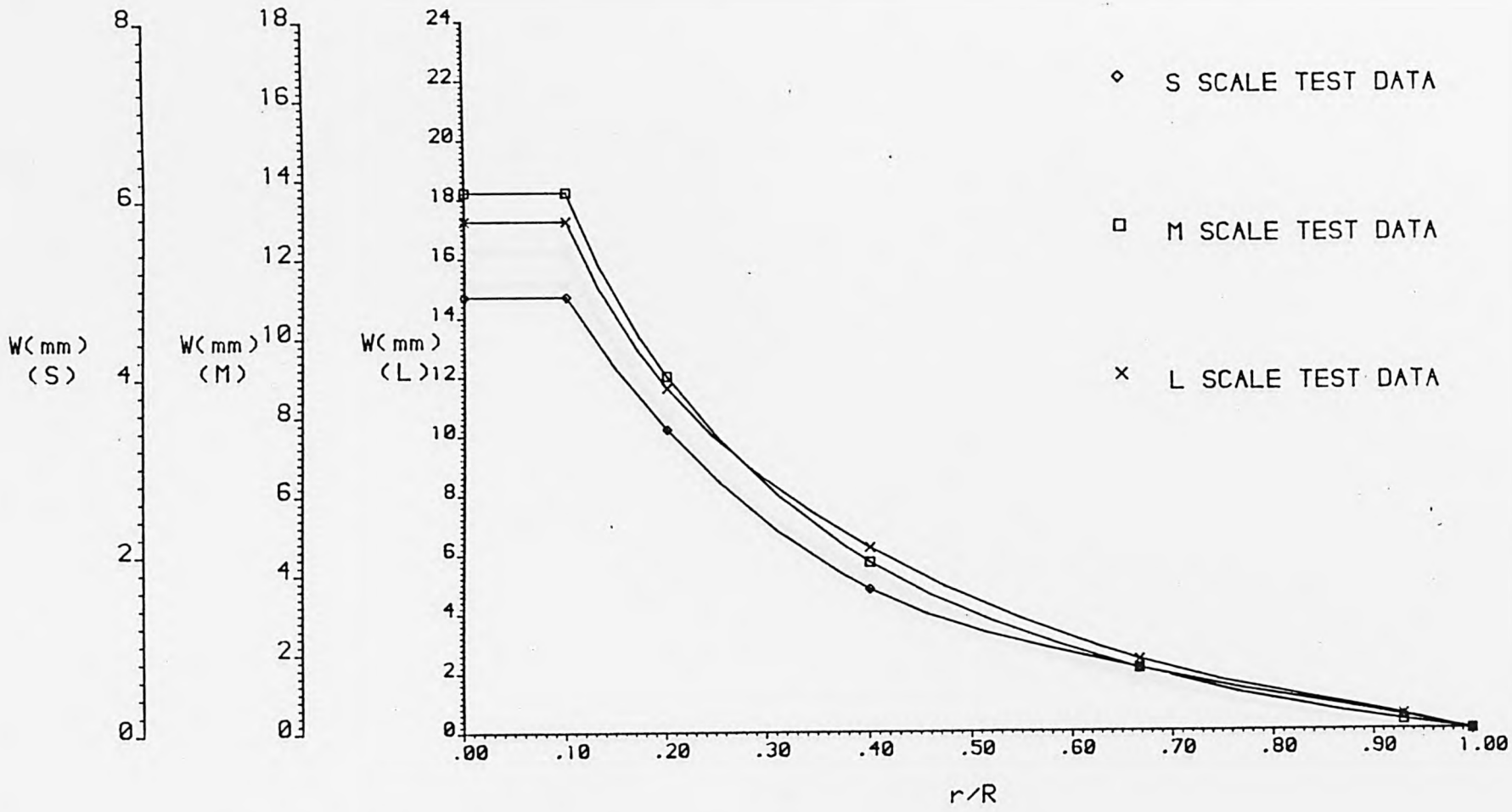

FIGURE 5.17(e) PERMANENT DEFLECTION PROFILES (SUFFIX 1 TESTS) - VELOCITY CORRECTED

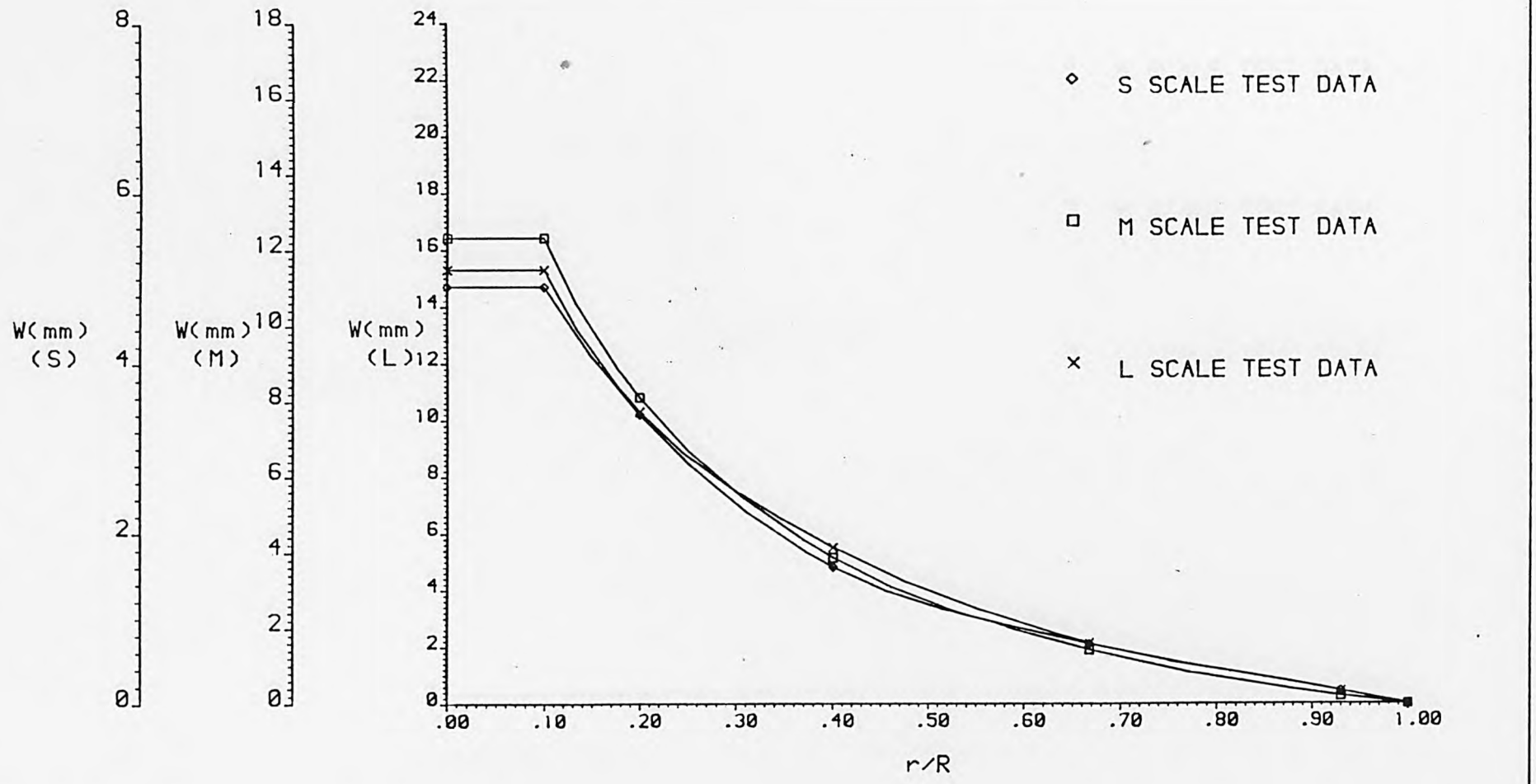

FIGURE 5.17(f) PERMANENT DEFLECTION PROFILES (SUFFIX 1 TESTS) - YIELD STRESS CORRECTED

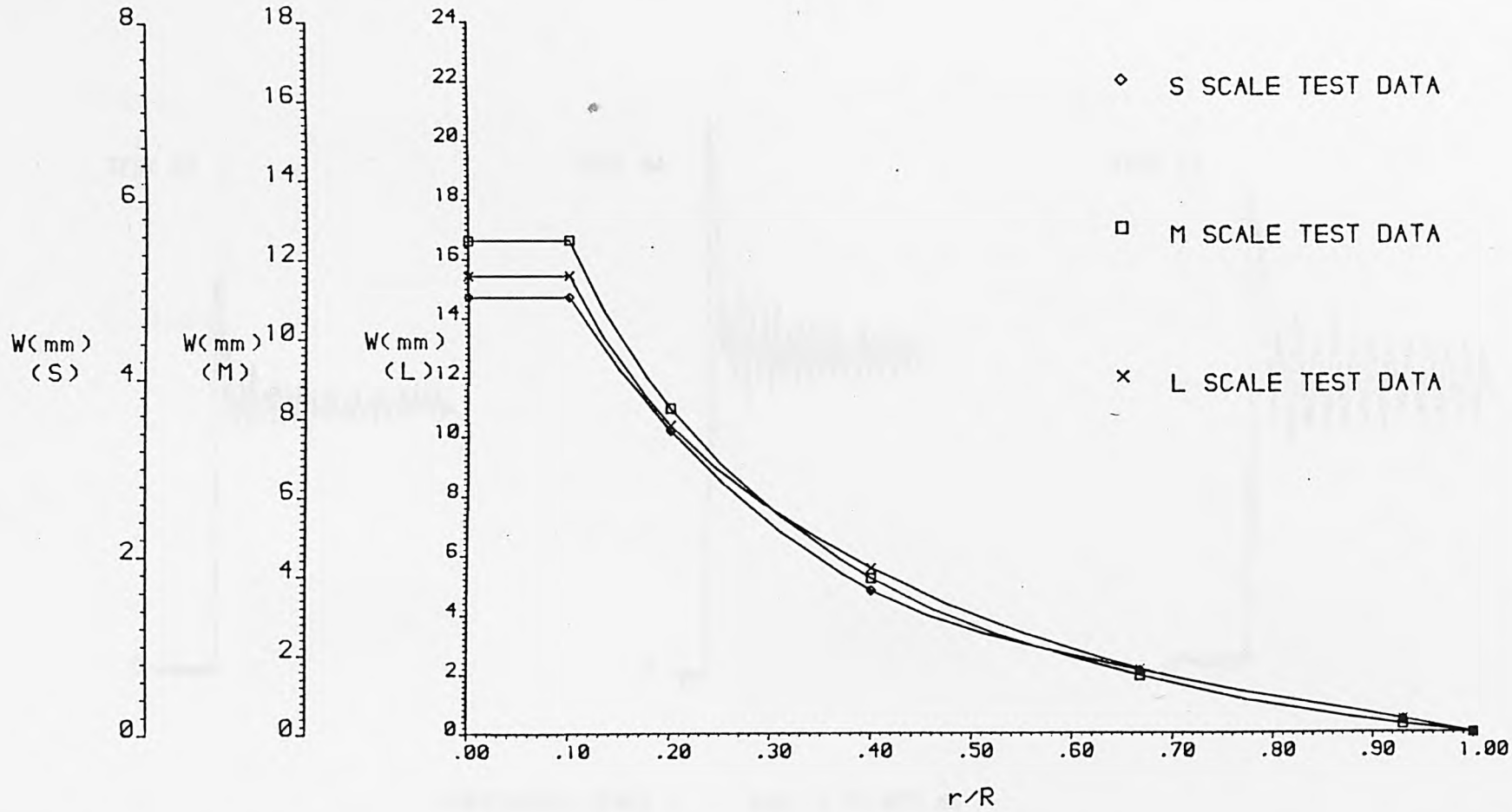

FIGURE 5.18(a) TEST SERIES 2 DYNAMIC STRAIN (GAUGE 2 - See figure 4.27)

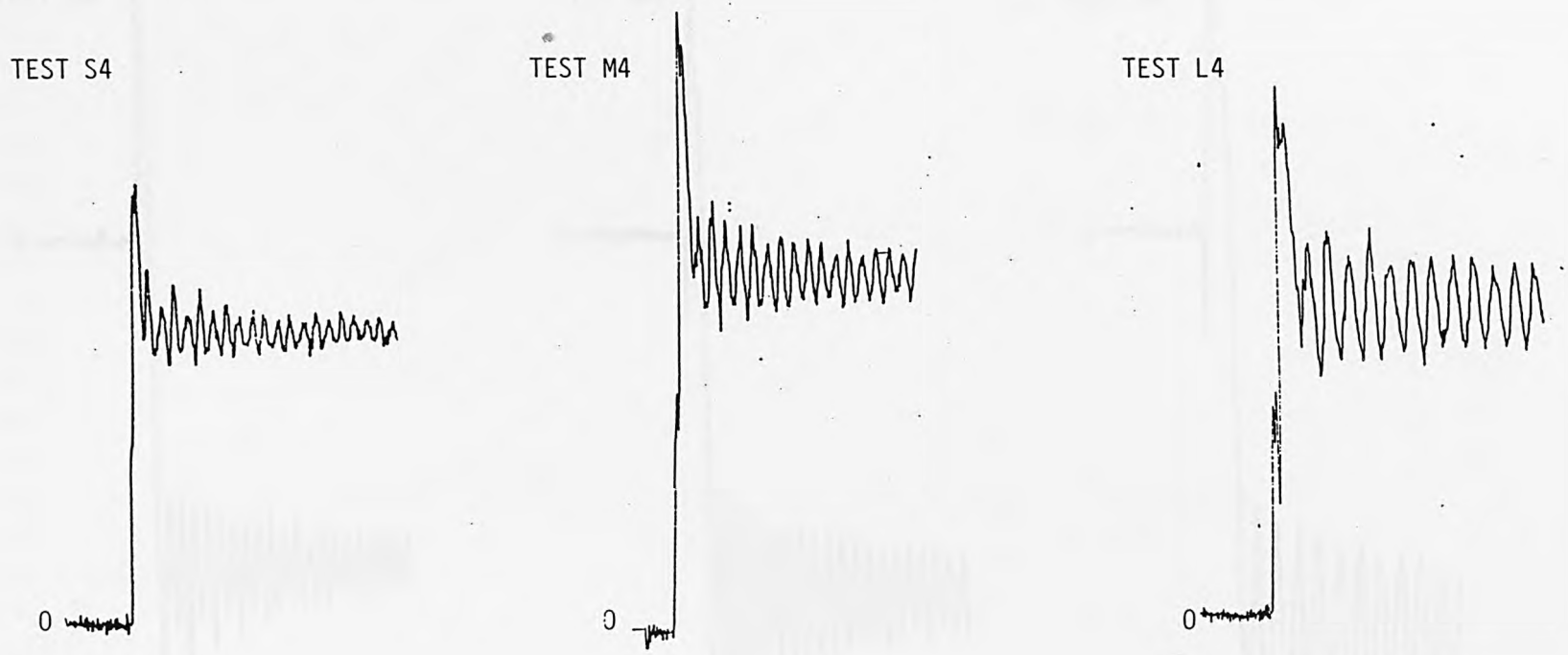

HORIZONTAL SCALE : 5mm = 15.625 ms

VERTICAL SCALE : 5mm = 156$\mu\epsilon$

FIGURE 5.18(b) TEST SERIES 2 DYNAMIC STRAIN (GAUGE 2 - UNLOADED FACE)

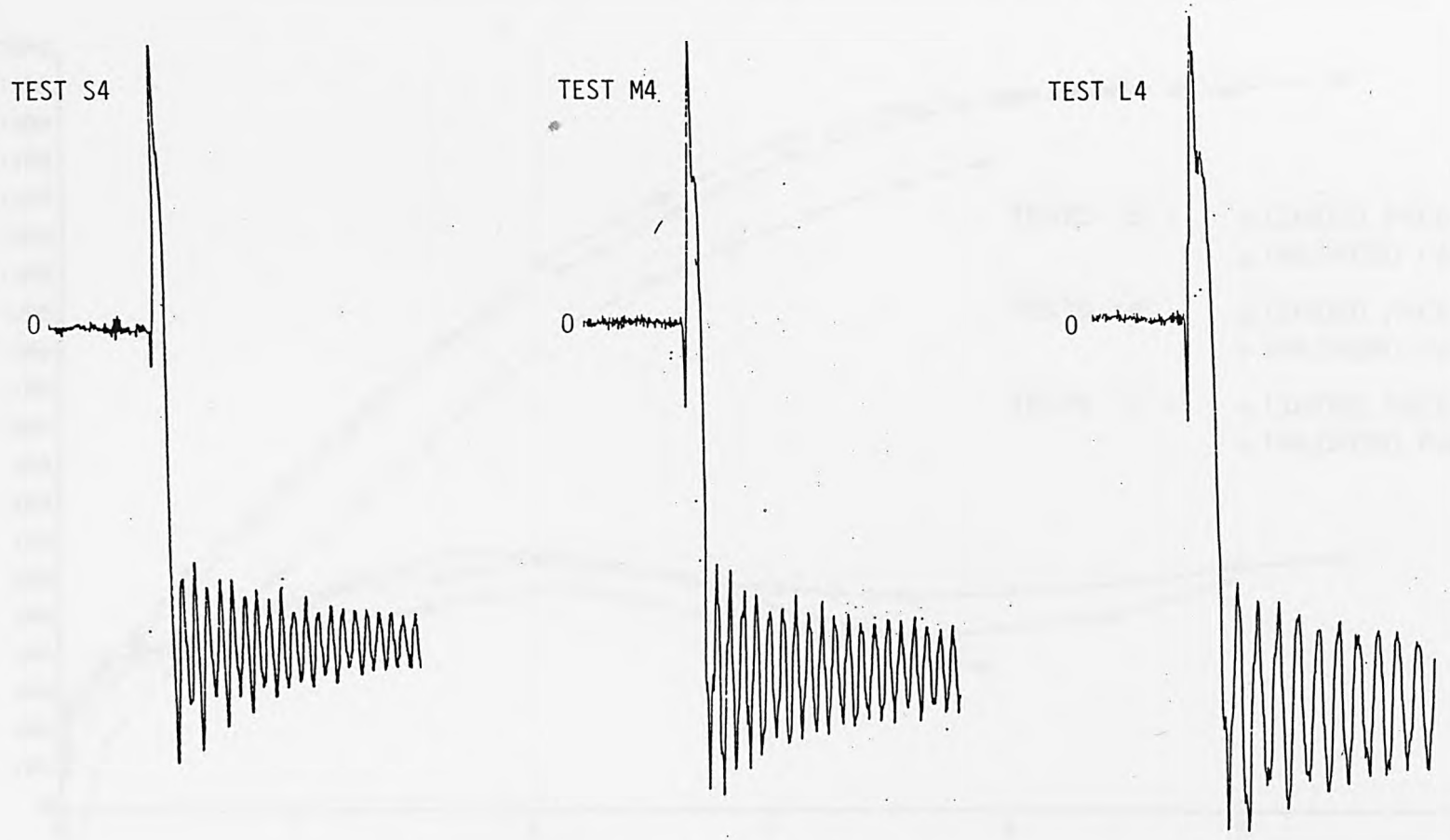

HORIZONTAL SCALE : 5mm = 15.625 ms

VERTICAL SCALE : 5mm = 156$\mu\epsilon$

FIGURE 5.19(a) TEST SERIES 2 STATIC TEST (GAUGE 2)

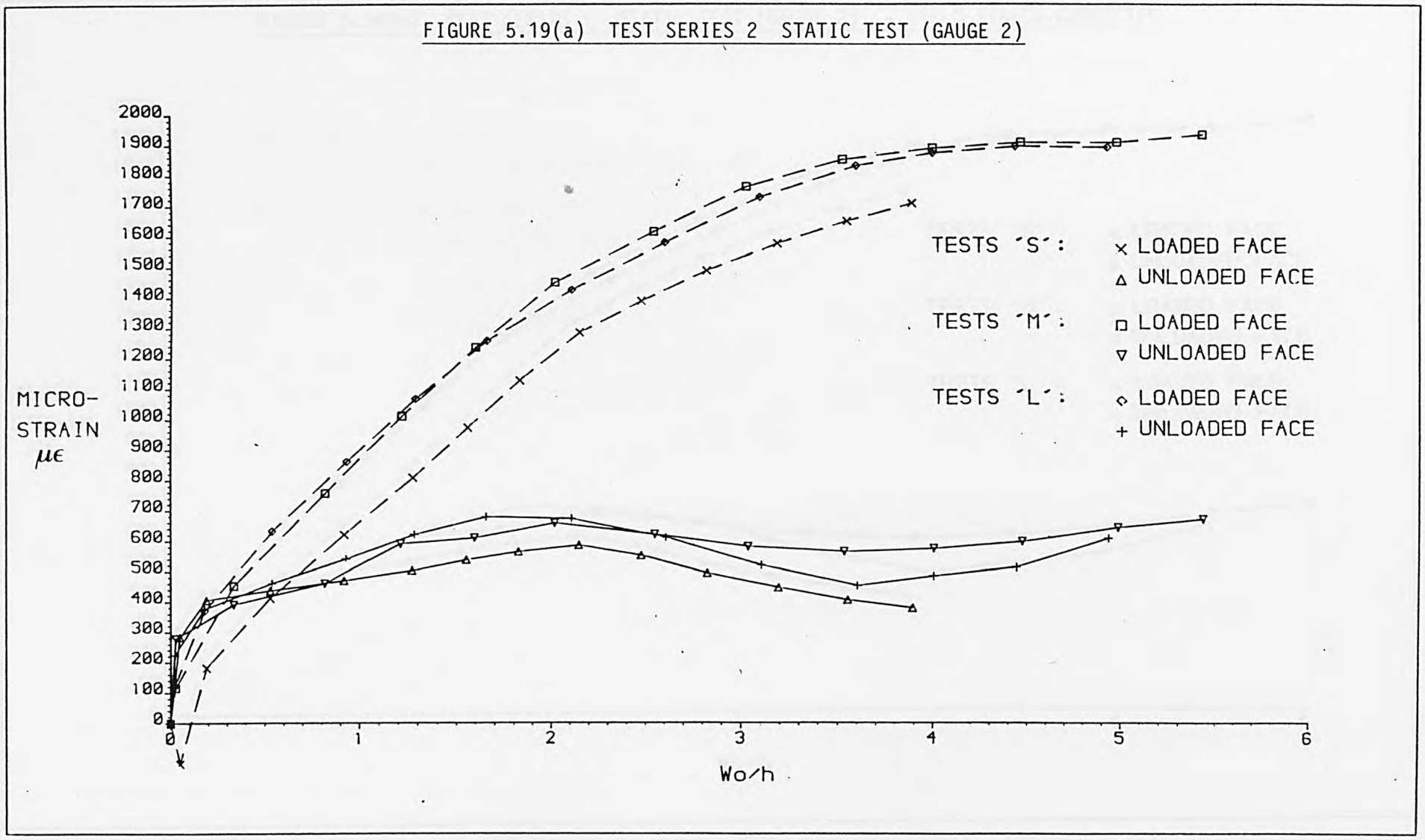

FIGURE 5.19(b) TEST SERIES 2 STATIC TEST (GAUGE 2) - YIELD STRESS CORRECTED

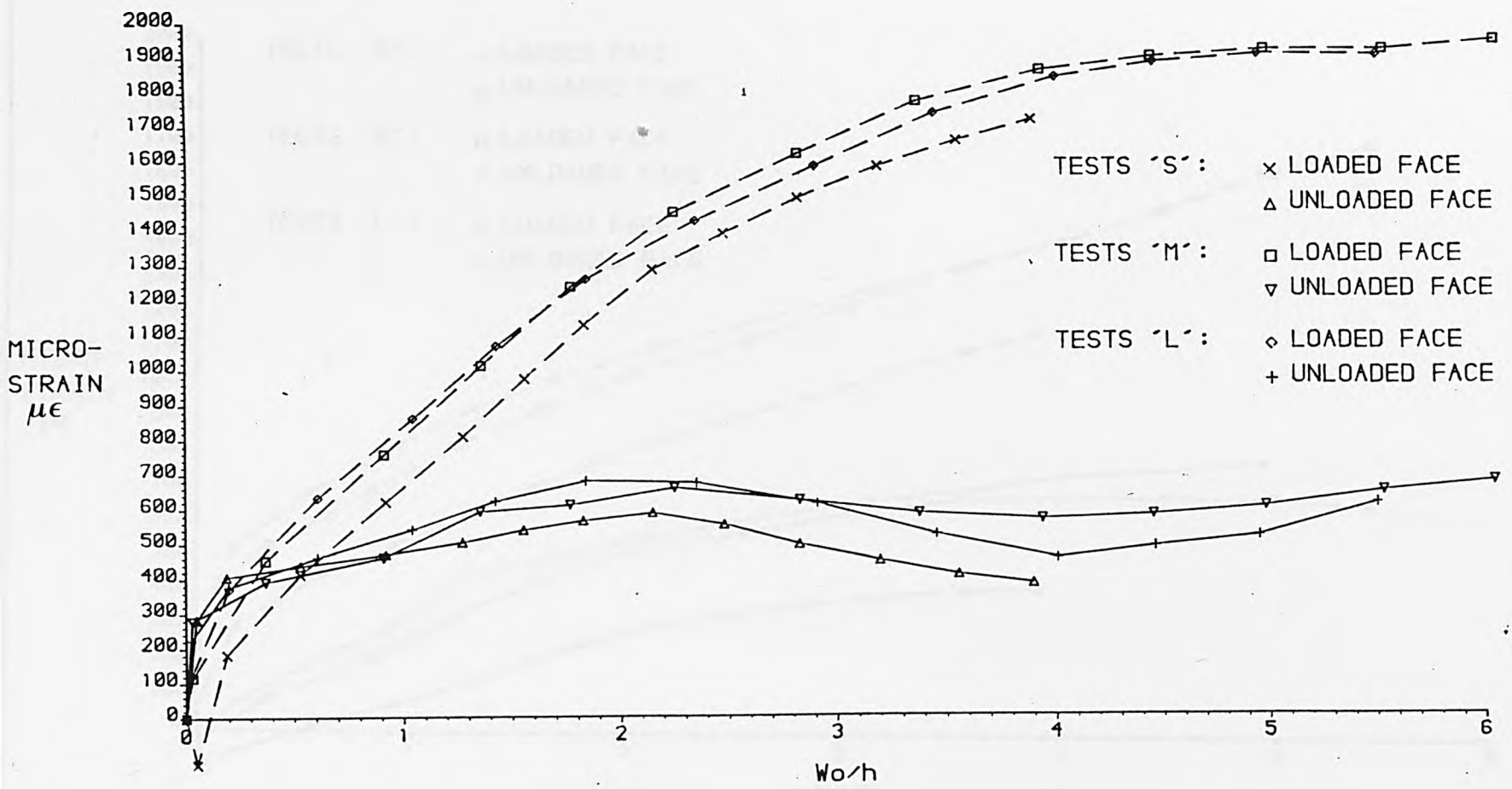

FIGURE 5.19(c) TEST SERIES 2 STATIC TEST (GAUGE 3)

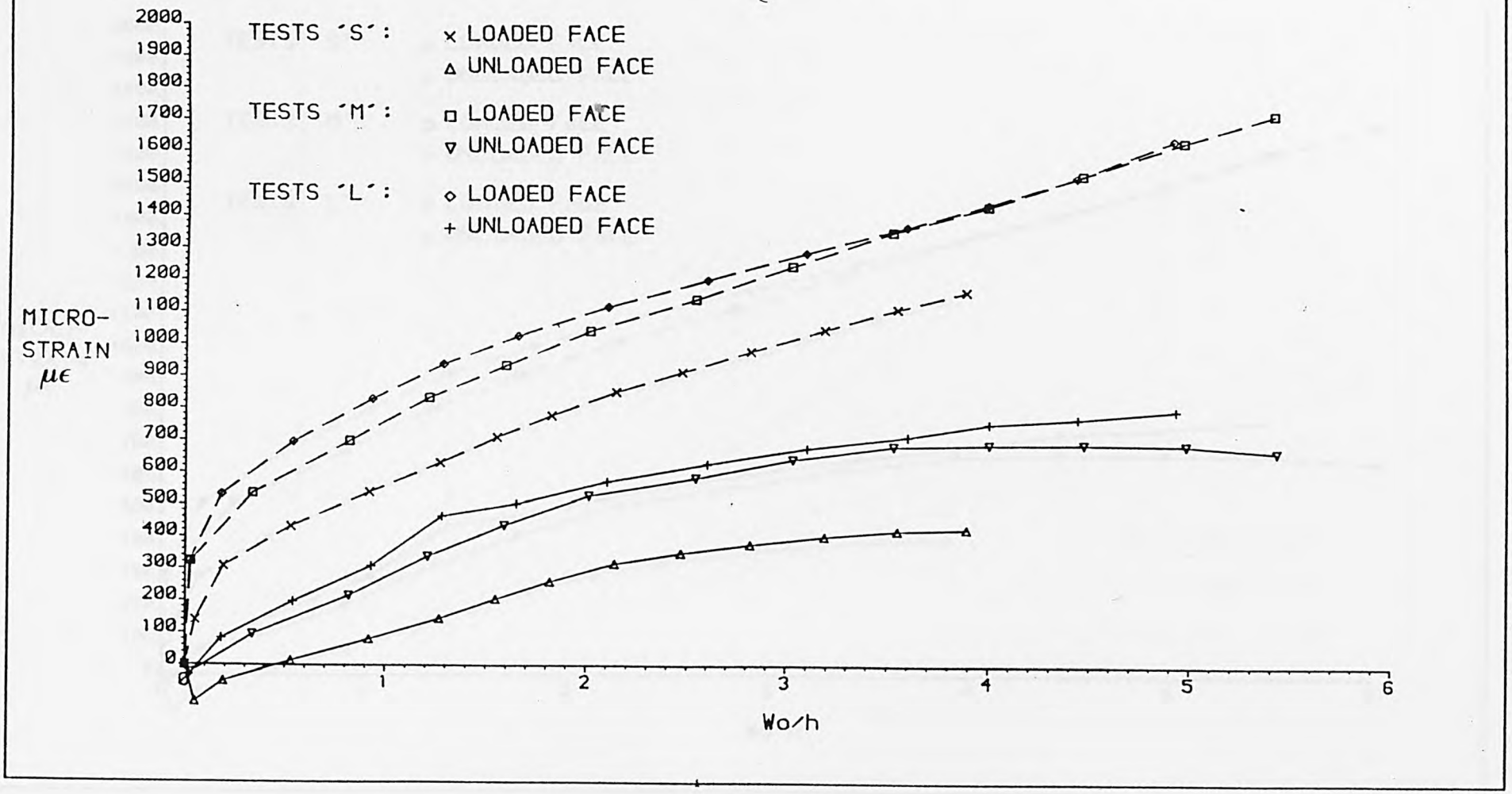

FIGURE 5.19(d) TEST SERIES 2 STATIC TEST (GAUGE 3) - YIELD STRESS CORRECTED

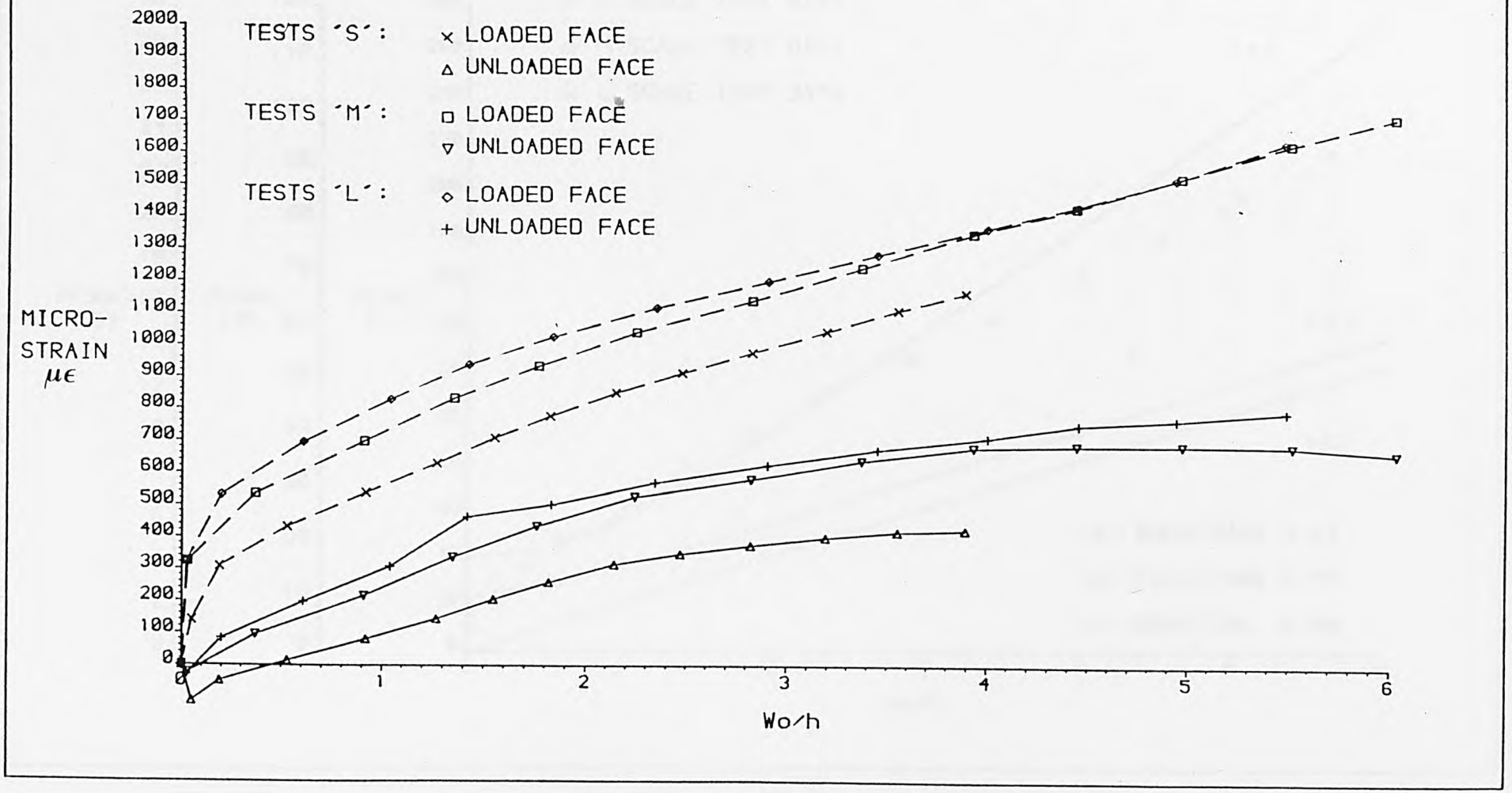

FIGURE 5.20 TEST SERIES 2 STATIC LOAD - DEFLECTION

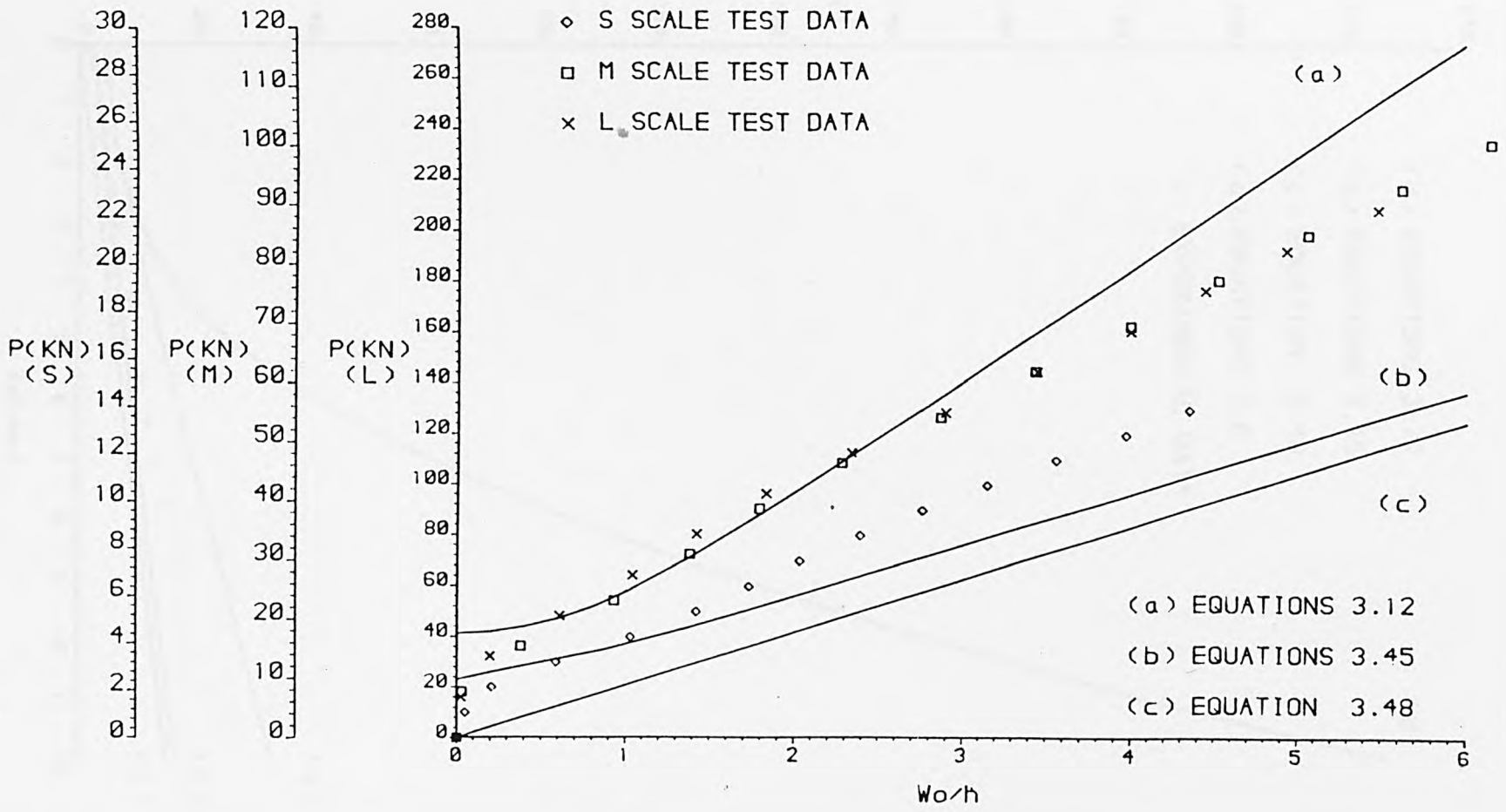

FIGURE 5.21(a) STATIC TEST S6

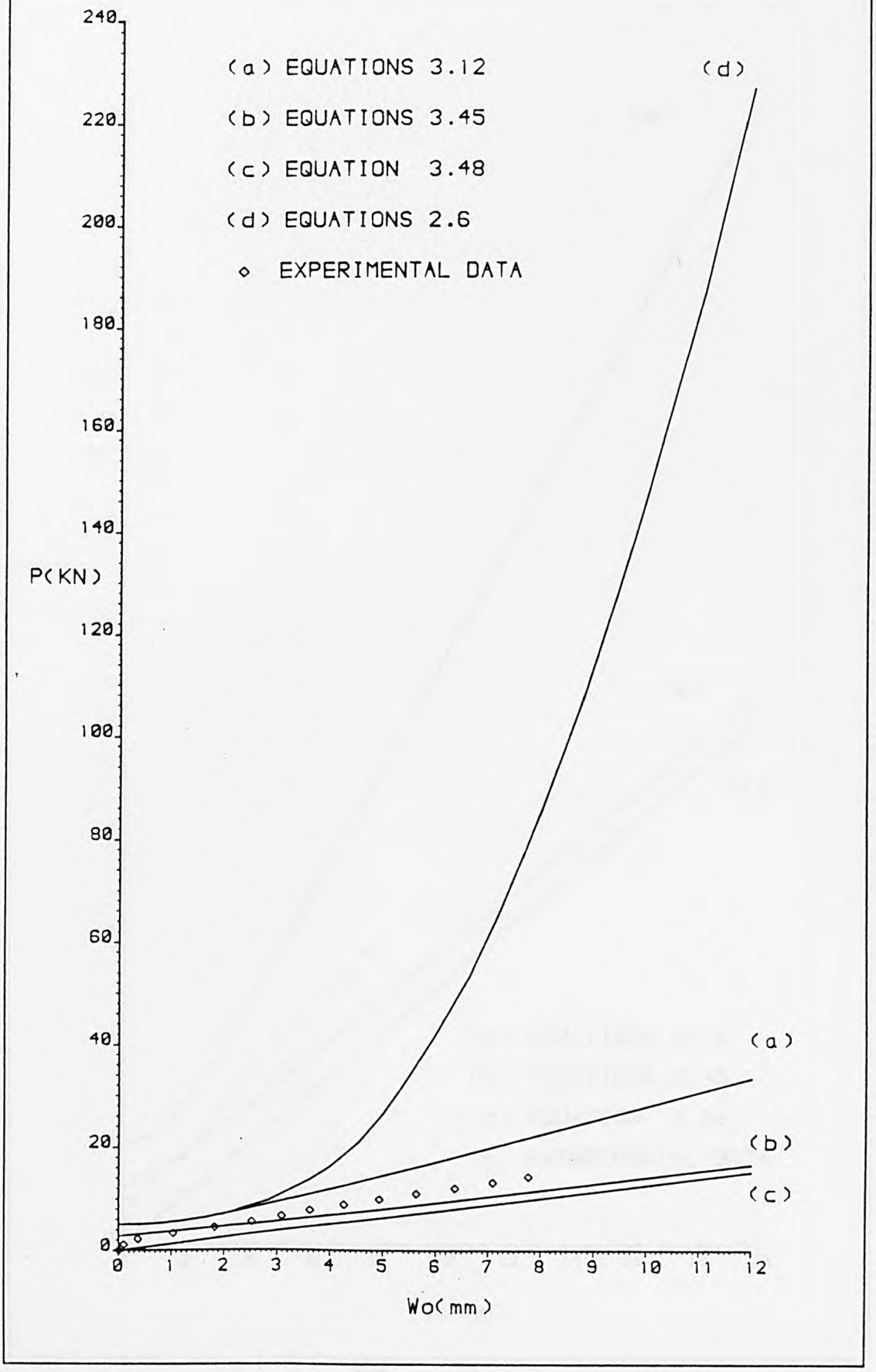

FIGURE 5.21(b) STATIC TEST S6

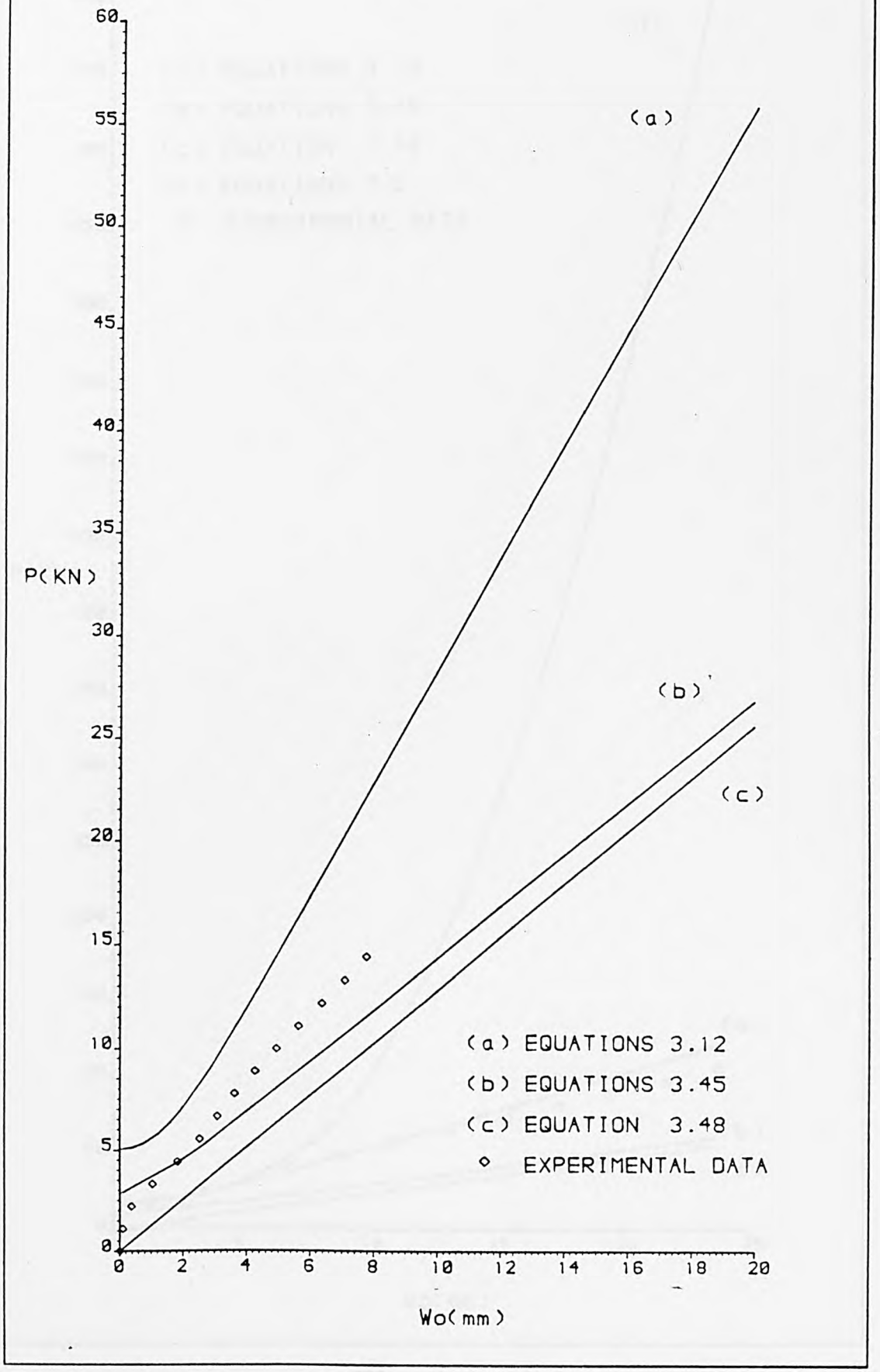

FIGURE 5.21(c) STATIC TEST M6

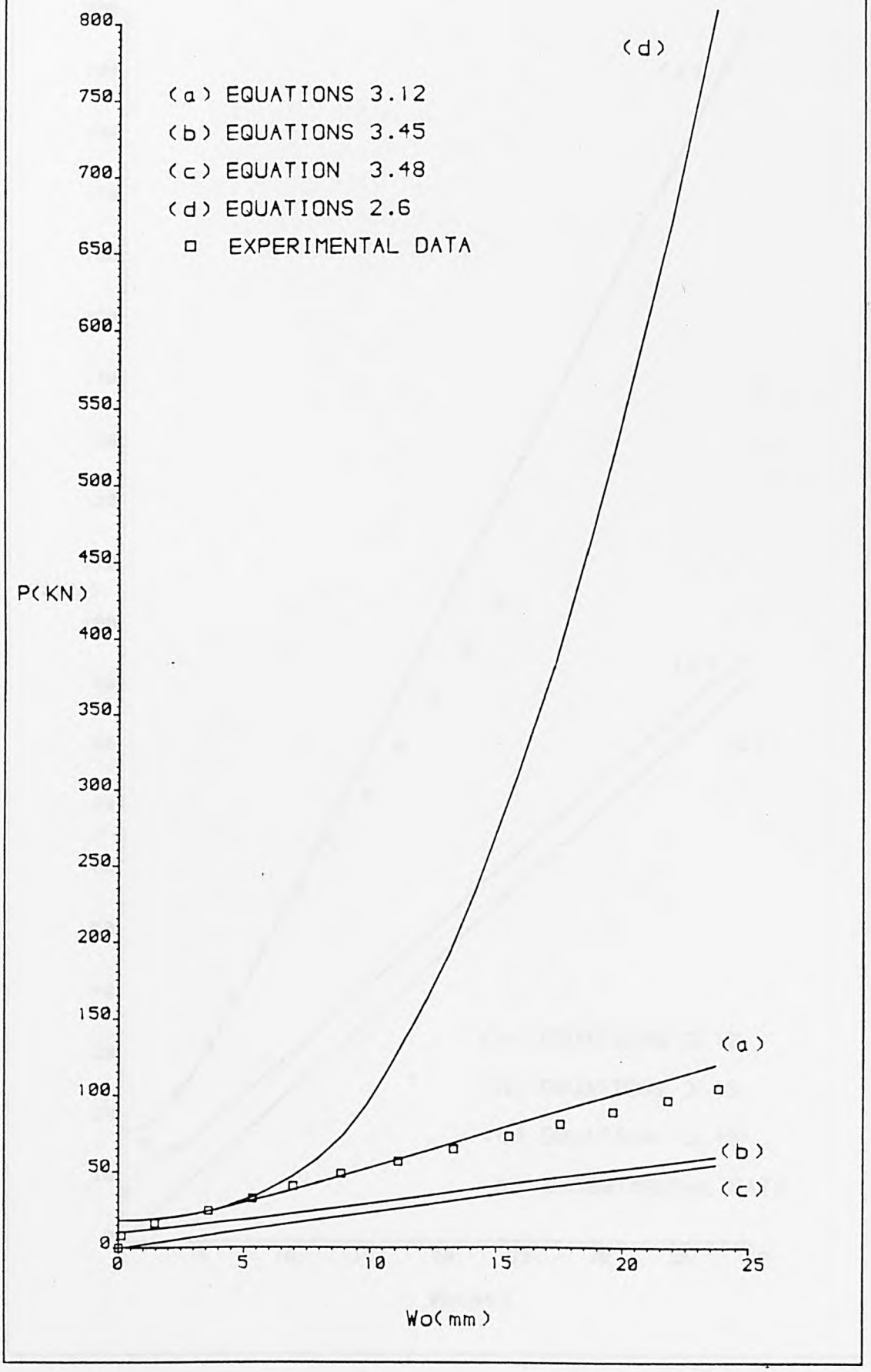

FIGURE 5.21(d) STATIC TEST M6

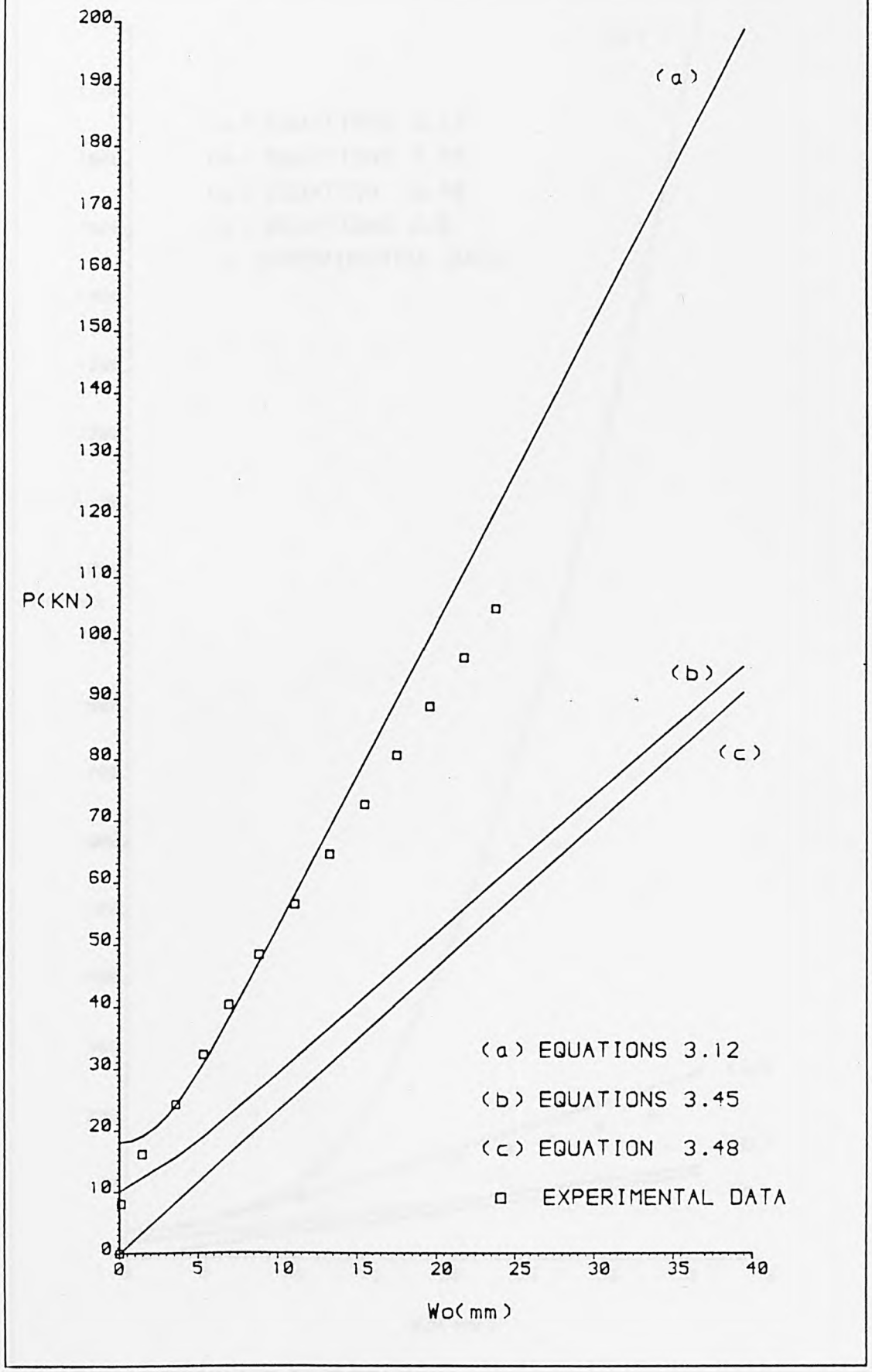

FIGURE 5.21(e) STATIC TEST L6

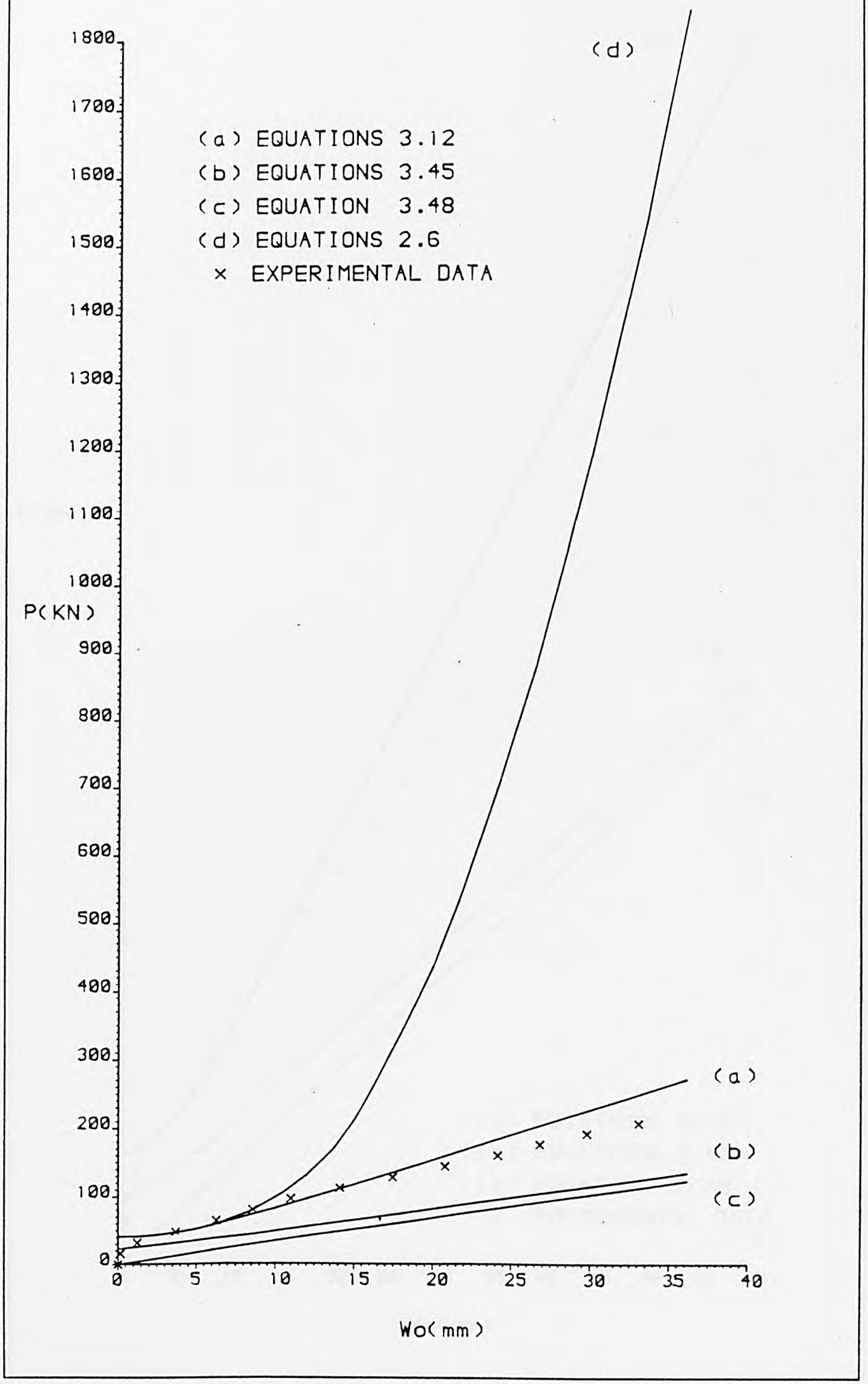

FIGURE 5.21(f) STATIC TEST L6

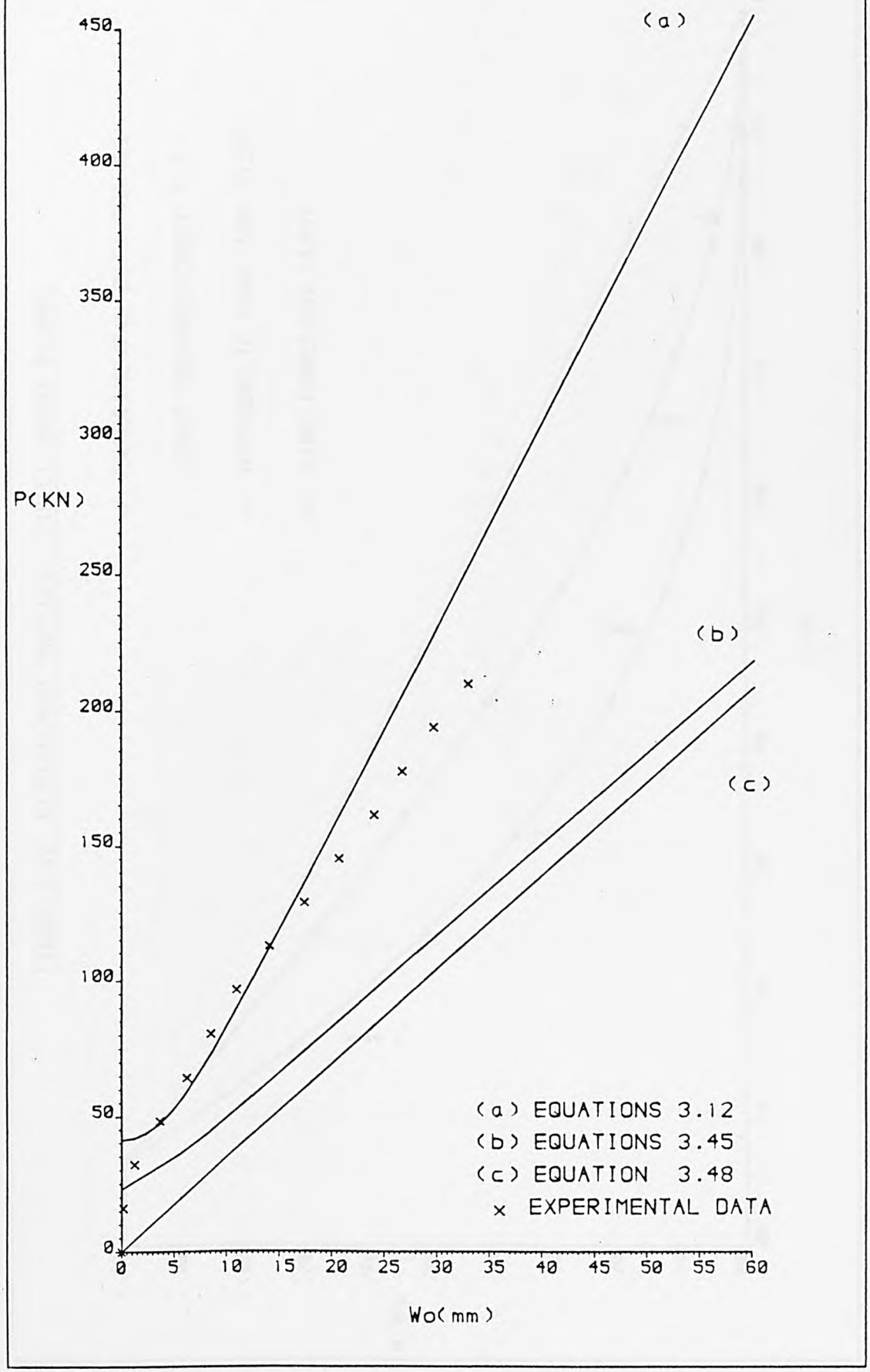

FIGURE 5.22 DISPLACEMENT PROFILES - DIRECT ENERGY BALANCE

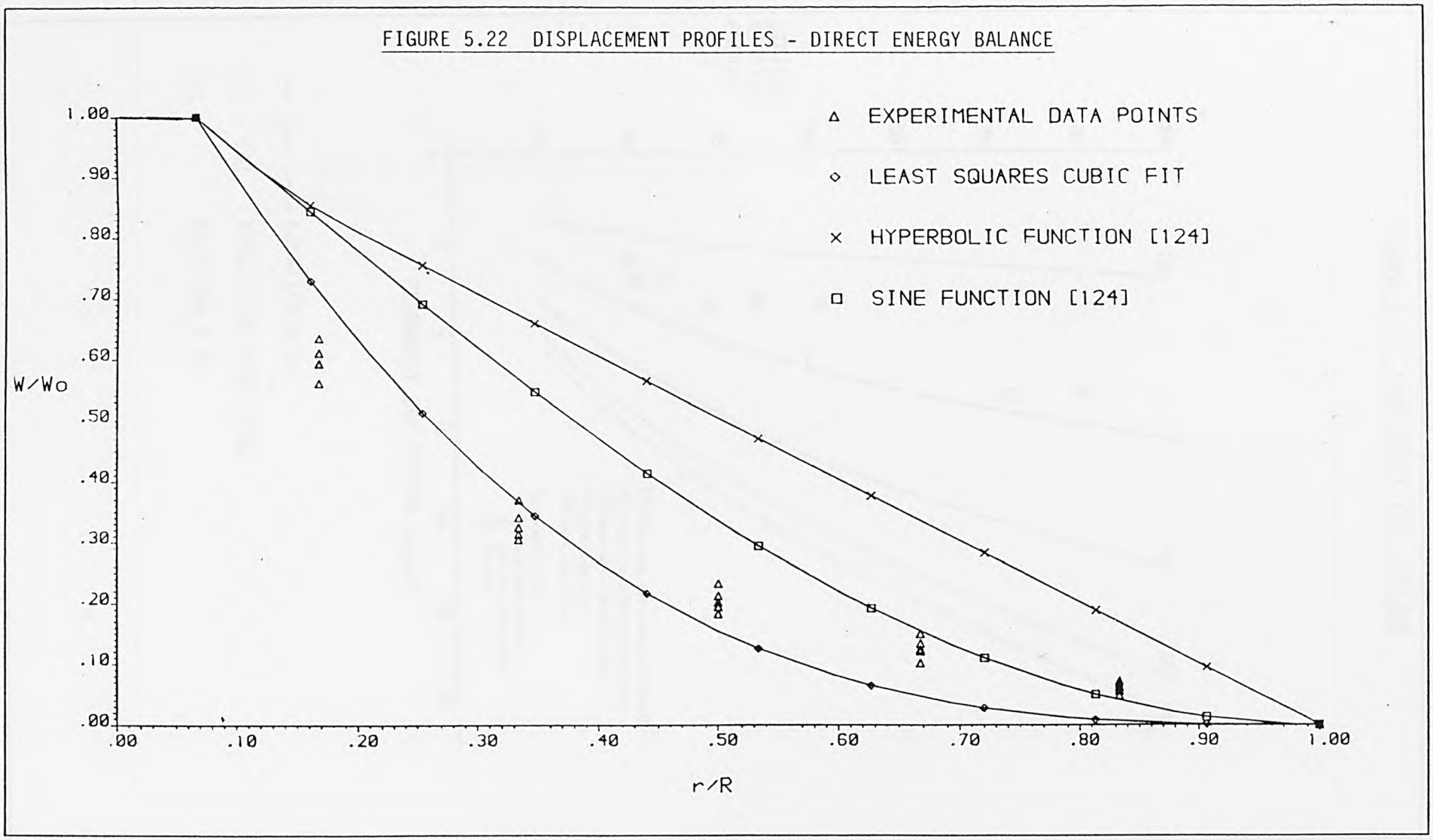

FIGURE 5.23 CASE STUDY (i) [79,80]

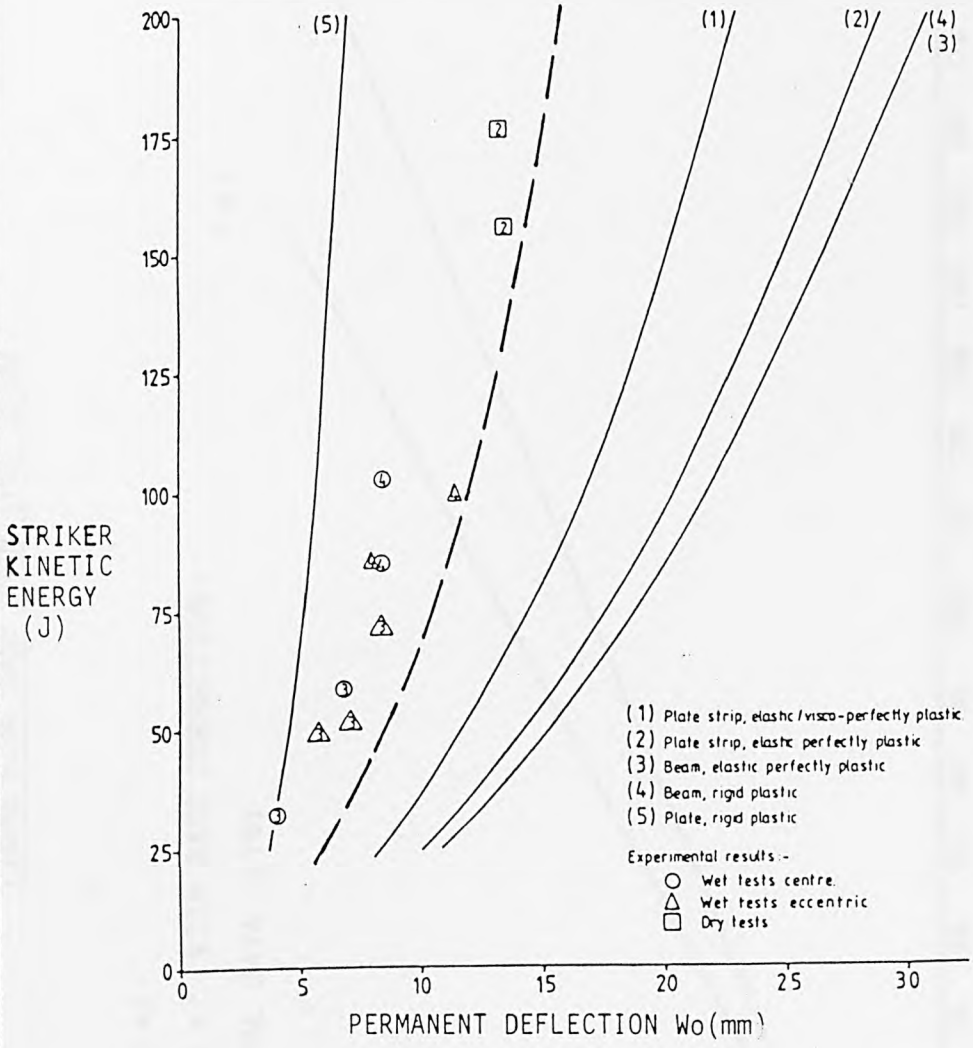

— — — : EQUATION 3.27

(1) - (4) : PREDICTION FROM [79]

(5) : EQUATION 2.8

FIGURE 5.24 CASE STUDY (ii) [118]

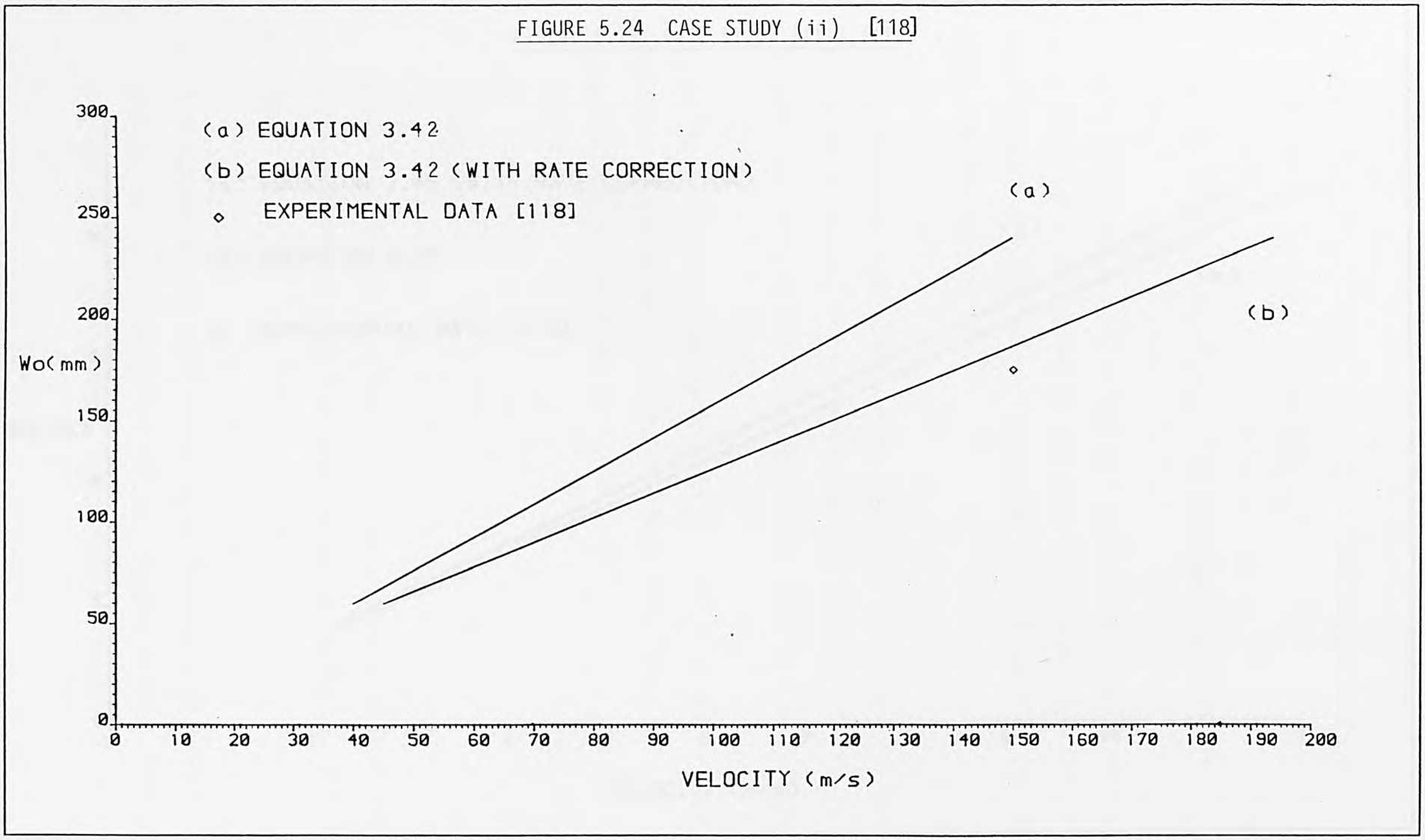

FIGURE 5.25 CASE STUDY (iii) [113]

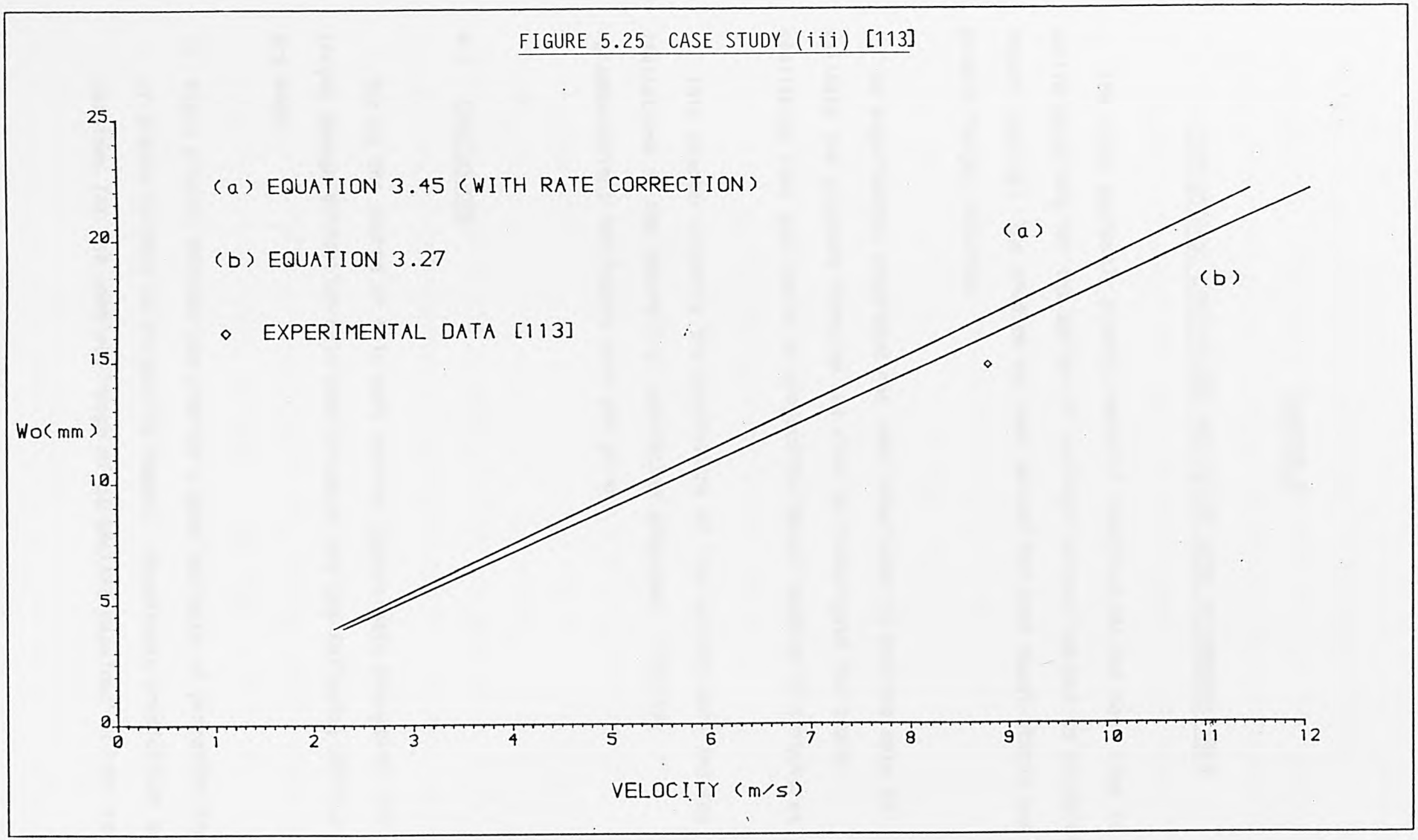

CHAPTER 6

CONCLUSIONS, LIMITATIONS AND FUTURE WORK RECOMMENDATIONS

The rigid perfectly plastic material idealisation has been used to derive equations for the design of isotropic plates subject to projectile impact loading. The problem has been solved for both quasi-static and dynamic target response.

An experimental programme has been undertaken to provide data to validate the proposed formulae and also to investigate the scale similarity laws applicable to projectile impact loading of structures.

This chapter presents the conclusions of the current work and the limitations of the theoretical approaches proposed. Finally, recommendations for future work are given.

6.1 Conclusions

During the course of this work several approximate procedures for target damage estimation have been proposed and the following conclusions are made:

i) Rigid plastic methods can provide a good estimate of permanent damage or plates subject to projectile impact. Reasonable predictions were obtained for the complete range of parameters examined in test series

and 2. In general, energy ratios have ranged from values of approximately three to twelve. In one case, however, the ratio was near unity. The particular analytical approach adopted depends on the initial conditions of the problem. With experience, good predictions should be obtainable for a wide range of problems.

ii) Results from the tests have shown that there are existing published design formulae which seriously underestimate target damage and, therefore, provide potentially unsafe solutions.

iii) The accuracy of equation 3.45 improves with increasing energy ratio magnitude, which may be intuitively expected from rigid plastic analyses. Results are further improved with the inclusion of a correction for material strain rate sensitivity.

iv) The use of an equivalent circular plate to enable axisymmetric analysis of a square plate, is valid for the range of parameters examined here.

v) The strain rate correction employed herein is approximate, both in its original derivation and subsequent execution, equation 2.9. It is evident that any correction for material strain rate sensitivity, in an approximate analytical method, will be essentially 'ad-hoc', because strain rate changes continuously in time and space throughout response. It is usually the order of magnitude which is of importance, however, when strain rate effects are to be considered. Examination of experimental strain output, show the corrections applied, to be of the correct order of magnitude.

vi) The accuracy of equation 3.45 improves with increasing plate thickness. It is likely that this is because the velocity profile assumed in the equation derivation becomes a closer approximation to the actual target profile as plate thickness increases.

vii) The accuracy of equation 3.27 improves with decreasing energy ratio magnitudes and decreasing plate thickness. The reasons for this unexpected behaviour are not clear. It is apparent that the energy dissipation mechanism associated with equation 3.27 has little resemblence to the actual dissipation mechanism. It is perhaps surprising that the equation has produced consistently good results.

viii) The final deflected shapes of the targets change with parametric variation, but were essentially axisymmetric and quasi-static in all cases. Tests incorporating lower energy ratios were associated with higher curvature rates in the final deformed profile. This is due to the proportionately higher elastic recovery associated with the lower energy ratio tests. The influence of bending is greater for low values of energy ratio and this result would be expected.

ix) A dimensionless representation of final maximum target deflection against the initial kinetic energy available from a given missile, provides a useful design aid. It is particularly useful if material properties are common for targets of various thickness.

x) The rigid plastic dynamic analysis did not give good results for the tests reported here. This was not entirely unexpected because impact durations were not short compared to target fundamental

natural periods of vibration. Use of equation 3.42 in case study ii) however provided encouraging results for a higher velocity event where a 'short' duration impact is likely.

xi) The approximate methods developed here are extremely simple and inexpensive to use. For uncomplicated structural configurations it is doubtful whether a more refined theoretical approach is necessary, particularly since the literature survey has shown that these more rigorous solutions are not without their own problems and inaccuracies.

Another aim of the research was to examine the scale similarity laws applicable to impact loading of plates. The following conclusions are made:

i) For the test configurations examined here, the use of scale models will predict the behaviour of prototypes with a good degree of accuracy. The permanent profiles of the plates at three different scales were, at worst, ten percent in error.

ii) This similarity is achieved despite the existence of higher strain rates in the small scale models. These strain rates are evident from the dynamic strain signals recorded. This could mean that, in the tests reported here, strain rates are not of sufficient magnitude to significantly effect material behaviour. Alternatively it may be that the redundant nature of the structures examined, causes a redistribution of strain, which offsets rate effects. Unfortunately, from a scaling point of view, it also means that

strain rates obtained from a model structure will not necessarily be representative of the strain rates in the prototype.

iii) Strain magnitudes agreed well at the different scales tested, but unfortunately equipment problems meant that results were not available to compare similarity of acceleration. In the static tests, strain and force magnitudes scaled well for the medium and large size structures.

iv) A major difficulty associated with tests designed to validate scale similarity laws is obtaining perfect scale models. In the tests reported here, material yield stress varied with plate thickness, and the missile velocity from a given drop height varied with mass. In structures which have bolted or welded connections, it is likely that further difficulties would be encountered.

A total of fifty nine tests were carried out using the equipment described in Chapter 4. The following conclusions are made:

i) The gathering of data from impact tests needs careful planning due to the extremely short time durations involved. Furthermore, it is advisable to attempt to collect as much data as possible, within sensible economic limits even if use of some data is not immediately apparent. Tests involving plastic deformation cannot be repeated.

ii) The measurement of missile velocity is necessary in each impact test. Friction and other losses associated with the test rig guide

mean that missile velocity calibration cannot be achieved simply as a function of drop height.

iii) Impact tests generate high frequency stress waves which may be damaging to equipment. If the missile is assumed rigid the accelerometer should be placed at the far end to make optimum use of mechanical filtering within the system. Alternatively, the transducer should be mounted on a mechanical filter. To prevent overload, a filter is required to condition the acceleration signal before it is converted to voltage by the charge amplifier. Care must be exercised when filtering signals, however, especially if peak values are of interest.

iv) Where many pieces of equipment are in simultaneous use, it is advisable to earth everything through a common ground loop to prevent 'noise' interference.

v) The electromagnetic release mechanism should be powered from an independent d.c. supply to minimise the risk of a voltage surge which may be caused by magnetic field reversal triggering other instrumentation.

6.2 Limitations

The experimental work reported herein has examined a finite range of problems and, therefore, only validated the analytical techniques within this parametric range. The behaviour of the proposed techniques for impact events involving other parameters cannot be guaranteed. In view

of the parametric variation in the tests reported here, however, there is no reason to suppose that extrapolation outside this range should predict inadequate results, providing sensible use is made of the equations.

Only centrally loaded, fully clamped isotropic plates have been considered. Equations have been developed for a simply supported edge condition and the modification of methods to include off-centre impacts would be fairly straightforward. As the impact location approaches a target support, however, the influence of shear will become increasingly important and will eventually determine the mode of failure.

It is unlikely that a fully fixed edge condition was maintained throughout the response of target panels, although this is also likely to be the case in most practical situations. It is worth noting that numerical treatment of this problem would faithfully fix edges and by doing so would perhaps be less representative of the real situation.

All the analysis techniques proposed have ignored the influence of material elasticity and strain hardening effects, and in every test the missile has been significantly heavier than the target. In addition, the techniques developed are only valid for moderate deflections, where $\tan \theta$ can be replaced by θ radians. Further refinement must be made where significant differences exist in these quantities.

Finally, a serious limitation of the methods is the lack of a criterion defining failure. In general, failure criteria are dependent upon material strain and strain determination is dependent on the assumed velocity profile of the target. In view of the variation obtained in

actual and assumed deformation profiles, it is unlikely that a strain based failure criterion can be successfully incorporated into the techniques proposed here.

6.3 Future Work

The following recommendations are made for future work to continue the research:

i) Further tests outside the range of parameters reported here which extend the range of validity of the proposed analytical techniques. The testing of rectangular plates with various aspect ratios would further examine the capabilities of equations 3.27 and 3.42.

ii) The further development of the proposed methods to include off-centre impact. It is likely that the current yield condition is only valid to within a certain distance of a target support. An attempt must be made to determine when shear deformation effects become significant and this is likely to be dependent on the target edge condition.

iii) The development of a failure criterion for use with the proposed analytical techniques. This will depend on many problem parameters including target nose shape, impact location, target support condition and the relative size, mass and stiffness of missile and target.

iv) The current work has examined impact phenomena from a fundamental point of view. Tests and theoretical developments should be carried out for more practical impact situations, for example, targets made of stiffened plate or subject to in-plane loads.

v) The use of scale modelling is shown to be applicable in the current tests, but nevertheless remains a controversial subject. Many more experimental investigations are required before conclusive assertations can be made. Undoubtably, the area of most controversy involves impact events which include tearing, fracture or buckling in structural response. Further tests should be carried out to investigate the scale similarity laws applicable to events involving these phenomena.

REFERENCES

1. WENGER, A., EDUARDSEN, G., OLAFSSON, S., ALVESTADT, T., (1983) "Design for Impact of Dropped Objects", OTC 4471, Houston, Texas.

2. ELLIS, N., PERRET, G.R., RAE, K., (1980) "The Design of an Impact Resistant Roof for Platform Wellhead Modules", OTC 3907, Houston, Texas.

3. DEOLIVEIRA, J.G. (1981) "Design of Steel Offshore Structures against Impact Loads due to Dropped objects", Proc. 3rd Int. Symp. on Offshore Engng.Structures, ed. Carneiro et al, COPPE, Rio de Janeiro, pp 446 - 483.

4. DALLARD, P.R.B., MILES, J.C., (1984) "Design tools for Impact Engineers", in Structural Impact and Crashworthiness, vol.2, ed. J. Morton, Elsevier, London, pp 369-382.

5. GWALTNEY, R.C. (1968) "Missile generation and protection in light water-cooled reactor plants". Report ORNL-NSTL-22, Oak Ridge Nat. Lab., Tenn., U.S.A.

6. WHITE, R.W., BOTSFORD, N.B., (1963) "Containment of fragments from a runaway reactor" (Tech.Report no.6), Report SRIA-113, Stanford Research Labs., Menlo Park, Calif., U.S.A.

7. JONES, N., (1973) "Slamming Damage", Journal of Ship Research, V.17, p.30.

8. JONES, N., (1983) "Structural Aspects of Ship Collisions", in Structural Crashworthiness, eds. N. Jones and T. Wierzbicki, Butterworths, London, pp 308-337.

9. KLING, M., (1980) "Large Deflection of Rectangular Plates subject to Concentrated Loads", M.S. Thesis, Dept. Ocean Engng., M.I.T.

10. BARR, P., (1983) "Studies of the Effects of Missile Impacts on Structures", Atom 318, pp 66-70.

11. SHIOYA, T., STRONGE, W.J. (1984) "Impact on Rotating Fan blades", in Mechanical Properties at High Rates of Strain, 1984, ed. J. Harding, Inst. Phys. Conf. Series no.70, Oxford.

12. BARR, P., (1980) "Studies of Missile Impact with Reinforced Concrete Structures", Nucl. Energy, V19, 3, pp 170-189.

13. BODNER, S.R. (1965) "Strain Rate effects in Dynamic Loading of Structures", in Behaviour of Material under Dynamic Loading, ed. N.J. Huffington, ASME, New York

14. Mechanical Properties at High Rates of Strain 1984, ed. J. Harding, Inst. Phys. Conf. Series no. 70, Oxford.

15. DEROUVRAY, A., ARNAUDEAU, F., DUBOIS, J., CHEDMAIL, J.R., HAUE, E., (1984)
"Numerical techniques and experimental Validations for Industrial Applications", in Structural Impact and Crashworthiness, vol.1, ed. G.A.O. Davies, Elsevier, London, pp 193-242.

16. ZUKAS, J.A., et al (1982)
"Impact Dynamics", John Wiley, London.

17. TRESCA, M.H. (1864)
"Memoire sur L'ecoulement des corps solides soumis a de fortes pressions", Comptes Rendus des Seances de L'Academic des sciences, Vol.59, p 754.

18. VON MISES, R., (1913)
"Mechanik der festen Korper implastisch-deformablen Zustand", Gottinger Nachrichten, Mathematisch-Physikalische Klasse, p. 582.

19. PRANDTL, L., (1924)
"Spannungsverteilung inplastischen Korpern", Proc. Ist Int. Congr. Appl. Mech. Delft, p.45.

20. REUSS, A., (1930)
"Berucksichtigung der elastischen Formanderung inder Plastizitatsthcorie", Zeitschrift fur Angewandte Mathematik und Mechanik, Band 10, Heft 3, Seite 266.

21. HILL, R., (1950)
"The Mathematical Theory of Plasticity", Clarendon Press, Oxford.

22. HILL, R., (1951)
"On the State of Stress in a Plastic-Rigid Body at the Yield Point", Phil.Mag., 42, p 868.

23. DRUCKER, D.C., PRAGER, W., GREENBORE, H.J., (1952)
"Extended Limit Design theorems for Continuous Media", Quart. Appl. Math., 9, p.381.

24. SAVE, M.A., MASSONNET, C.E., (1972)
Plastic Analysis and Design of Plates, Shells and Disks, North-Holland, Amsterdam and London.

25. WOOD, R.H. (1961)
Plastic and Elastic Design of Slabs and Plates, The Ronald Press, New York.

26. JONES, N., (1979)
'Response of Structures to Dynamic Leading', in Mechanical Properties at High Notes of Strain 1979, ed. J.Harding, Inst.Phys.Conf.Series No.47, Oxford.

27. LEE, E.H., SYMONDS, P.S., (1952)
'Large Plastic Deformations of Beams under Transverse Impact', J.Appl.Mech., ASME, V19, p 308.

28. CONROY, M.F., (1952)
'Plastic-rigid analysis of Long Beams under Transverse Impact', J.Appl.Mech., ASME, V19, p 465.

29. BAKER, W.E., (1975)
'Approximate Techniques for Plastic Deformation of Structures under Impulsive Loading', Shock.Vib.Dig., V7, 7, pp 107-117.

30. SYMONDS, P.S., (1953)
'Dynamic Load Characteristics in Plastic Bending of Beams', J.Appl.Mech., ASME, V20, p 475.

31. PARKES, E.W., (1955)
'The Permanent Deformation of a Cantilever Struck Transversely at its Tip', Proc.Royal Soc.London, Series A, V228, p 462.

32. SYMONDS, P.S., FLEMING, W.T., (1984)
'Parkes Revisited: On Rigid Plastic and Elastic-Plastic Dynamic Structural Analysis', Int.J.Impact Engng., V2, No.1, pp 1-36.

33. PARKES, E.W., (1958)
'The Permanent Deformation of an Encastre Beam Struck Transversely at any Point in its Span', Proc.Inst.Civ.Engns., London, V10, p 266.

34. MARTIN, J.B., SYMONDS, P.S., (1966)
'Mode Approximations for Impulsively Loaded Rigid-Plastic Structures', J.Eng.Mech., ASCE, EM5, p 43.

35. MENTEL, T.J., (1958)
'The Plastic Deformation due to Impact at a Cantilever Beam with an attached Tip Mass', J.Appl.Mech., ASME, V25, p 515.

36. BODNER, S.R., SYMONDS, P.S. (1962)
'Experimental and Theoretical Investigation of the Plastic Deformation of Cantilever Beams Subjected to Impulsive Loading', J.Appl.Mech., ASME, V19, p 719.

37. SYMONDS, P.S., MENTEL, T.J.
'Impulsive Loading of Plastic Beams with Axial Constraints', J.Mech.Phys.Solids, V6, pp 186-202.

38. MARTIN, J.B. (1964)
'Impulsive Loading Theorems for Rigid-plastic Continua', Proc.ASCE, V90, pp 27-42.

39. SYMONDS, P.S., (1980)
'Elastic, finite-deflection and Strain-rate effects in a Mode Approximation Technique for Plastic Deformation of Pulse Loaded Structures', J.Mech.Eng.Sci., V22, 4, pp 189-197.

40. NEWMARK, N.M., (1959)
'A Method of Computation for Structural Dynamics',
J.Eng.Mech., ASCE, V85, EM3, p 67.

41. WANG, A.J., (1955)
'The Permanent Deflection of a Plastic Plate under Blast Loading',
J.Appl.Mech., V22m ASME, pp 375-376.

42. FLORENCE, A.L., (1966)
'Clamped Circular Rigid-Plastic Plates under Blast Loading',
J.Appl.Mech., V33, p 256.

43. FLORENCE, A.L., (1966)
'Clamped Circular Rigid-Plastic Plates under Central Blast Loading',
Int.J.Solids Structures, V2, p 319.

44. FLORENCE, A.L., (1966)
'Circular plate under a uniformly distributed impulse', Int.J.Solids
Structures, V2, pp 37-47.

45. WIERZBICKI, T., (1967)
'Impulsive Loading of rigid viscoplastic plates', Int.J.Solids
Structures, V3, 4, pp 635-647.

46. PERRONE. N., (1967)
'Impulsively Loaded Strain-Rate Sensitive Plates', J.Appl.Mech.,
ASME, V89,pp 380-384.

47. JONMES, N., (1968)
'Finite Deflection of a Simply Supported Rigid-Plastic Circular Plate
Loaded Dynamically', Int.J.Solids and Structures, V4, 6, PP 605-615.

48. JONES, N., (1968)
'Impulsive Loading of a Simply Supported Rigid-Plastic Circular
Plate', J.Appl.Mech., ASME, V90, Series E, pp 59-65.

49. JONES, N., (1968)
'Finite Reflections of a Rigid-Viscoplastic Strain-hardening Annular
Plate Loaded Impulsively', J.Appl.Mech., ASME, V35, pp 349-356.

50. JONES, N., (1967)
'Influence of Strain-hardening and Strain-rate Sensitivity on the
Permanent Deformation of Impulsively Loaded Rigid-Plastic Beams',
Int.J.Mech.Sci., V9, 2, pp 777-796.

51. SYMONDS, P.S., JONES, N., (1972)
'Impulsive Loading of Fully Clamped Beams with Finite Plastic
Deflections and Strain-rate Sensitivity', Int.J.Mech.Sci., V14, pp
49-60.

52. WIERZBICKI, T., KELLY, J.M., (1968)
'Finite Deflection of a Circular Viscoplastic Plate Subject to
Projectile Impact', Int.J.Solids and Structures, V4, pp 1081-1092.

53. GOLDSMITH, W., LIU, T.W., CHULAY, S., (1965)
'Plate Impact and Perforation by Projectiles', Exp.Mech., V5, pp 1-20.

54. ONAT, G.T., HAYTHORNTHWAITE, R.M., (1956)
'The Load Carrying Capacity of Circular Plates at Large Deflection', J.Appl.Mech., ASME, V23, pp 49-55.

55. HOPKINS, H.G., PRAGER, W., (1953)
'The Load Carrying Capacities of Circular Plates', J.Mech.Phys. Solids, V2, pp 1-13.

56. CALLADINE, C.R., (1968)
'Simple Ideas in the Large Deflection Plastic theory of Plates and Slabs', in Engineering Plasticity, Eds.J.Heyman and F.A.Leckie, Cambridge University Press.

57. HOOKE, R., RAWLINGS, B., (1969)
'An Experimental Investigation of the Behaviour of Clamped, Rectangular, Mild Steel Plates Subject to Uniform Transverse Pressure', Proc.I.C.E., V42, pp 75-103.

58. HOOKE, R., RAWLINGS, B., (1970)
'Investigation into the Methods of Predicting Post-Elastic Load Carrying Properties of Clamped, Uniformly Loaded, Rectangular Mild Steel Plates', Proc.I.C.E., V49, pp 281-303.

59. HOOKE, R., (1970)
'Post-Elastic Deflection Prediction of Plates', Proc.ASCE, V96, ST4, pp 757-771.

60. JONES, N., WALTERS, R.M., (1971)
'Large Deflections of Rectangular Plates', J.Ship Research, V15,2, pp 164-171.

61. SAWCZUK, A., (1964)
'On Initiation of the Membrane Action in Rigid-Plastic Plates', J.Mec., V3, pp 15-23.

62. SAWCZUK, A., (1964)
'Large Deflection of Rigid-Plastic Plates', Proc.11th Int.Cong. Appl.Mech., pp 224-228.

63. JONES, N., (1971)
'A Theoretical Study of the Dynamic Plastic Behaviour of Beams and Plates with Finite Deflections', Int.J.Solids and Structures, V7, pp 1007-1029.

64. GREENSPON, J.E., (1956)
'An Approximation to the Plastic Deformation of a Rectangular Plate Under Static Load with Design Ap[plication', Int.Shipbuilding Progress, V3, 22, pp 329-340.

65. TAYA, M., MURA, J., (1974)
'Dynamic Plastic Behaviour of Structures Under Impact Loading Investigated by the Extended Hamilton's Principle', Int.J.Solids and Structures, V10, pp 197-209.

66. JONES, N., URAN, T.O., TEKIN, S.A., (1970)
'The Dynamic Plastic Behaviour of Fully Clamped Rectangular Plates', Int.J.Solids and Structures, V6, pp 1499-1512.

67. JONES, N., GRIFFIN, R.N., VANDUZER, R.E., (1971)
'An Experimental Study Into the Dynamic Plastic Behaviour of Wide Beams and Rectangular Plates', Int.J.Mech.Sci., V13, pp 721-735.

68. DRUCKER, D.C., (1956)
'The Effect of Shear on the Plastic Bending of Beams', J.Appl.Mech., V23, pp 509-514.

69. DEOLIVEIRA, J.E., (1982)
'Beams Under Lateral Projectile Impact', J.Eng.Mech., ASCE, EM1, V108, pp 51-71.

70. JONES, N., DEOLIVEIRA, J.G., (1979)
'The Influence of Rotary Inertia and Transverse Shear on the Dynamic Plastic Behaviour of Beams', J.Appl.Mech., V46, 2, pp 303-309.

71. JONES, N., WIERZBICKI, T., (1976)
'A Study of the Higher Modal Dynamic Plastic Response of Beams', Int.J.Mech.Sci., V18, pp 533-542.

72. JONES, N., (1985)
'Bounds on the Dynamic Plastic Behaviour of Structures Including Transverse Shear Effects', Int.J.Impact Engng., V3, 4, pp 273-291.

73. JONES, N., (1973)
'Influence of In-Plane Displacements at the Boundaries of Rigid-Plastic Beams and Plates', Int.J.Mech.Sci., V15, pp 547-561.

74. JONES, N., (1976)
'Dynamic Behaviour of Ideal Fibre-Reinforced Rigid-Plastic Beams', J.Appl.Mech., ASME, V43, 2, pp 319-324.

75. FORRESTAL, M.J., WESENBURG, D.C., (1976)
'Elastic-Plastic Response of 6061-T6 Aluminium Beams to Impulse Loads', J.Appl.Mech., ASME, V43, 2, pp 259-262.

76. FORRESTAL, M.J., WESENBURG, D.C., (1977)
'Elastic-plastic Response of Simply Supported 1018 Steel Beams to Impulse Loads', J.Appl.Mech., ASME, V44, pp 779-780.

77. FORRESTAL, M.J., SAGARTZ, M.J. (1978)
'Elastic-plastic Response of 304 Stainless Steel Beams to Impulse Loads', J.Appl.Mech., ASME, V45, 3, pp 685-687.

78. HAYTHORNTHWAITE, R., (1957()
'Beams with Full End Fixity', Engineering, 183, pp 110-112.

79. SAMUELIDES, E., FRIEZE, P.A., (1983)
'Strip Model Simulation for Low Energy Impacts on Flat-Plated Structures', Int.J.Mech.Sci., V25, 9, pp 669-685.

80. SAMUELIDES, E., FRIEZE, P.A., (1984)
'Experimental and Numerical Simulation of Ship Collisions', Int.J.Mech.Sci., V25, 9, pp 669-685.

81. SYMONDS, P.S., CHON, C.T., (1979)
'Finite Visco-plastic Deflection of an Impulsively Loaded Plate by the Mode Approximation Technique', J.Mech.Phys.Solids, V27, pp 115-133.

82. SYMONDS, P.S., KOLSKY, H., MOSQUERA, J.M., (1984)
'Simple Elastic-plastic Methoid for Pulse Loading - Comparisons with Experiments and Finite Element Solutions', in Mechanical Properties at High Rates of Strain 1984, ed.J.Harding, Inst.Phys.Conf.Series No.70, Oxford.

83. YANKELENSKY, D.Z., (1985)
'Elasto-plastic Blast Response of Rectangular Plates', Int.J.Impact Engng., V3, 2, pp 107-119.

84. GOLDSMITH, W., (1960)
'Impact: The Theory and Physical Behaviour of Colliding Solids', Edward Arnold, London.

85. CRITESCU, N., (1967)
'Dynamic Plasticity', North Holland Publishing Company.

86. JOHNSON, W., (1972)
'Impact Strength of Materials', Edward Arnold, London.

87. JONES, N., WIERZBICKI, T., (1983)
'Structural Crashworthiness', eds. Jones/Wierzbicki, Butterworths, London.

88. DAVIES, G.A.O., MORTON, J., (1984)
'Structural Impact and Crashworthiness', eds. Davies/Morton, Elsevier Applied Science, London.

89. SYMONDS, P.S., (1967)
'Survey of Methods of Analysis for Plastic Deformation of Structures Under Dynamic Loadings', Brown University Report BU/NSDRC/1-67.

90. KEIL, A.H., (1961)
'Problems of Plasticity in Naval Structures: Explosive and Impact Loading', Proc.Second Symp. on Naval Structure Mech., ed. Lee and Symonds, Pergaman Press.

91. JONES, N., (1975)
'A Literature Review of the Dynamic Plastic Response of Structures', Shock Vib.Dig., V7, 8, pp 89-105.

92. JONES, N., (1978)
'Recent Progress in the Dynamic Plastic Behaviour of Structures, Parts I and II', Shock Vib.Dig., V10, 9, pp 21-33 and V10, 10, pp 13-19.

93. JONES, N., (1981)
'Recent Progress in the Dynamic Plastic Behaviour of Structures, Part III', Shock.Vib.Dig., V13, 10, pp 3-16.

94. JONES, N., (1985)
'Recent Progress in the Dynamic Plastic Behaviour of Structures, Part IV', Shock Vib.Dig., V17, 2, pp 35-47.

95. BAKER, W.E., (1979)
'Approximate Techniques for Plastic Deformation of Structures Under Impulse Loading II', Shock Vib.Dig., V11, 7, pp 19-24.

96. BAKER, W.E., (1982)
'Approximate Techniques for Plastic Deformation of Structures Under Impulsive Loading III', Shock Vib.Dig., V14, 11, pp 3-11.

97. GRIFFIN, P.D., MARTIN, J.B., (1983)
'Geometrically Non Linear Mode Approximations for Impulsively Loaded Homogeneous Viscous Beams and Frames', Int.J.Mech.Sci., V25, 1, pp 15-26.

98. BODNER, S.R., (1984)
'Response of Structures to Impact Loading: 'Exact' solutions, Approximate Methods and Experimental Techniques', in Mechanical Properties at High Rates of Strain, ed. J.Harding, Inst.Phys.Conf.Series No.70, Oxford.

99. NEILSON, A.J., (1985)
'Empirical Equations for the Perforation of Mild Steel Plates', Int.J.Impact Engng., V3, 2, pp 137-142.

100. BACKMAN, M.E., GOLDSMITH, W., (1978)
'The Mechanics of Penetration of Projectiles into Targets', Int.J.Engng.Sci., V16, pp 1-99.

101. SHEIH, R.C., (1978)
'Empirical Equations for Puncture Analysis of Lead Shielded Spent Fuel Shipping Casks', Proc. 5th Int.Symp. in Packaging and Transportation of Radioactive Materials, p 341.

102. WILKINS, M.C., (1978)
'Mechanics of Penetration and Perforation', Int.J.Engng.Sci., V16, pp 793-807.

103. BODNER, S.R., (1984)
'Modelling Ballistic Perforation', in Structural Impact and Crashworthiness, eds. G.A.O.Davies and J.Morton, Elsevier, London.

104. CAMBELL, T.I., CHARLTON, T.M., (1973)
'Finite Deformation of a Fully Fixed Beam Comprised of a Non-Linear Material', Int.J.Mech.Sci., V15, 5, pp 415-428.

105. CALDER, C.A., GOLDSMITH, W., (1971)
'Plastic Deformation and Perforation of Thin Plates Resulting from Projectile Impact', Int.J.Solids and Structures, V7, pp 863-881.

106. DUFFEY, T.A., KEY, S.W., (1969)
'Experimental - Theoretical Correlations of Impulsively Loaded Clamped Circular Plates', Eng.Mech., V9, pp 241-249.

107. BEYNET, P., PLUNKET, R., (1971)
'Plate Impact and Plastic Deformation by Projectiles', Exp.Mech., V11, pp 64-70.

108. RAWLINGS, B., (1967)
'Energy Absorption of Dynamically and Statically Tested Mild Steel Beams Under Conditions of Gross Deformation', Int.J.Mech.Sci., V9, pp 633-649.

109. DAVIS, F.C., PIH, H., (1973)
'Plastic Impact Testing of Shipping Cask Fin Specimens', Nucl.Engng. and Design, V24, pp 322-331.

110. ZAID, A.O., TRAVIS, F.W., (1974)
'A Comparison of Single and Multi-Layered Plate Shields Subjected to Impact by a High Speed Projectile; in Mechanical Properties at High Rates of Strain 1974, ed. J.Harding, Inst.Phys.Conf.Series No.21, Oxford.

111. SPILKER, R.L., WITMER, E.A., (1977)
'Theoretical and Experimental Studies of the Non-Linear Transient Response of Plates Subject to Fragment Impact', Trans. 4th Int.Conf., SMiRT, M7/3, San Fransisco.

112. WITMER, E.A., MERUS, F., RODAL, J.J.A., STAGLIANO, T.R., (1977)
'Experimental Transient and Permanent Deformation Studies of Steel-Sphere-Impacted or Impulsively-Loaded Aluminium Panels', MIT Report ASKL TIL 154-12.

113. NEILSON, A.J., (1980)
'Missile Impact on Metal Structures', Nucl.Energy, V19, pp 191-198.

114. NEILSON, A,J., CARTER, P.G., (1979)
'Experimental Validation of the EURDYN and CADROS Finite Element Codes for the Calculation of Metal Target Response to Low Velocity Missiles', Trans. 5th Int.Conf. SMiRT, J8/8, Berlin.

115. CLABBURN, E.J., (1983)
'An Inexpensive Fast Response Displacement Transducer', J.Phys.E: Sci.Instrum., V16, pp 248-250.

116. PERRY, S.H., BROWN, I.C., (1983)
'Model Prestressed Concrete Slabs Subject to Hard Impact Loading', in Design for Dynamic Loading: The Use of Model Analysis, Ed.Armer and Garas, Construction Press, New York/London.

117. PERRY, S.H., BROWN, I.C., (1982)
'An Experimental Method to Investigate Impact on Concrete Slabs', Proc. BAM., Concrete Structures Under Impact and Impulsive Loading, June 82, pp 202-212, Berlin.

118. MIYAMOTO, H., SHIDA, S., CHIBA, N., OHTE, S., YOSHIZAWA, H., (1979)
'Experimental Study on Strength of Steel Plates Subjected to Missile Impact', Trans. 5th Int.Conf. SMiRT, J8/9, Berlin.

119. OHTE,S., YOSHIZAWA, H., CHIBA, N., SHIDA, S., (1981)
'The Strength of Steel Plates Subjected to Missile Impact', Trans. 6th Int.Conf., SMiRT, J7/10,

120. YAMAMOTO, S., OHTE, S., YOSHIZAWA, H., CHIBA, N., SHIDA, S., (1983)
'Nonlinear Dynamic Analysis of Missile Impact on Steel Plates', Trans. 7th Int.Conf., SMiRT, J7/3,

121. CORRAN, R.S., SHADBOLT, P.J., RUIZ, C., (1983)
'Impact Loading of Plates - An Experimental Investigation', Int.J. Impact Engng., V1, 1, pp 3-22.

122. BOOTH, E., COLLIER, D., MILES, J., (1983)
'Impact Scalability of Plated Steel Structures', in Structural Crashworthiness, eds. N.Jones and T Wierzbicki, Butterworths, London.

123. JONES, N., JOURI, W.C., BIRCH, R.S., (1983)
'On the Scaling of Ship Collision Damage', Dept.Mech.Eng. Report ES/09/83, University of Liverpool.

124. DUFFEY, T.A., CHERESH, M.C., SUTHERLAND, S.H., (1984)
'Experimental Verification of Scaling Laws for Punch Impact Loaded Structures', Int.J.Import Engng., V2, 1, pp 103-117.

125. GHOSH, S.K., REID, S.R., JOHNSON, W., (1984)
'The Large Deflection Impulsive Loading of Clamped Circular Membranes', in Structural Impact and Crashworthiness, Vol.2, ed.J.Morton, Elsevier, London.

126. NURICK, G.N., MARTIN, J.B., (1984)
'The Measurement of the Response of Clamped Circular Plates to Impulsive Loading', in Mechanical Properties at High Rates of Strain, Inst.Phys.Conf.Series No.70, Oxford.

127. JONES, N., (1984)
'Scaling of Inelastic Structures Loaded Dynamically', in Structural Impact and Crashworthiness, Vol.1, ed.G.A.O.Davies, Elsevier, London.

128. BUCKINGHAM, E., (1915)
'Model Experiments and the Forms of Empirical Equations', Trans. ASME, V37, p 263.

129. CALLADINE, C.R., (1983)
'An Investigation of Impact Scaling Theory', in Structural Crashworthiness, eds. N.Jones and T.Wierzbicki, Butterworths, London.

130. HAGIWARA, K., TAKAWARE, H., KAWARO, H., (1983)
'A Proposal Method of Predicting Ship Collision Damage', Int.J. Impact Engng., V1, 3, pp 257-279.

131. COWPER, G.R., SYMONDS, P.S., (1957)
'Strain Hardening and Strain Rate Effects in the Impact Loading of Cantilever Beams', Tech.Report 28, ONR, Div.Appl.Mech., Brown University.

132. MANSTONE, R.J., (1975)
'Properties of Material at High Rates of Straining or Loading', Materials and Structures, V8, 44, pp 102-115.

133. MANJOINE, M.J., (1944)
'Influences of rate of Strain and Temperature in Yield Stresses of Mild Steel', J.Appl.Mech., Trans. ASME, V11, p 211.

134. HOBBS, B., (1983)
'Allowing for Strain-Rate Sensitivity in Impulsively Loaded Structures', in Design for Dynamic Loading: The Use of Model Analysis, eds. Armer and Gavos, Construction Press, London/New York.

135. SZILARD, R., (1974)
'Theory and Practice of Plates: Classical and Numerical Methods', Prentice Hall.

136. NEILSON, A.J., (1983)
'A Dyna-3D Calculation for Impact on a Pipe Target', Winfrith UKAEA, Report AEEW-M2058.

137. JONES, N., DUMAS, J.W., GIANNOTTI, J.G., GRASSIT, K.E., (1972)
'The Dynamic Plastic Behaviour of Shells', in Dynamic Response of Structures, eds. G.Herman and N.Perrone, Perguman Press, pp 1-29.

APPENDIX 1 DERIVATION OF YIELD FUNCTION

Stress resultants at a plastic hinge:

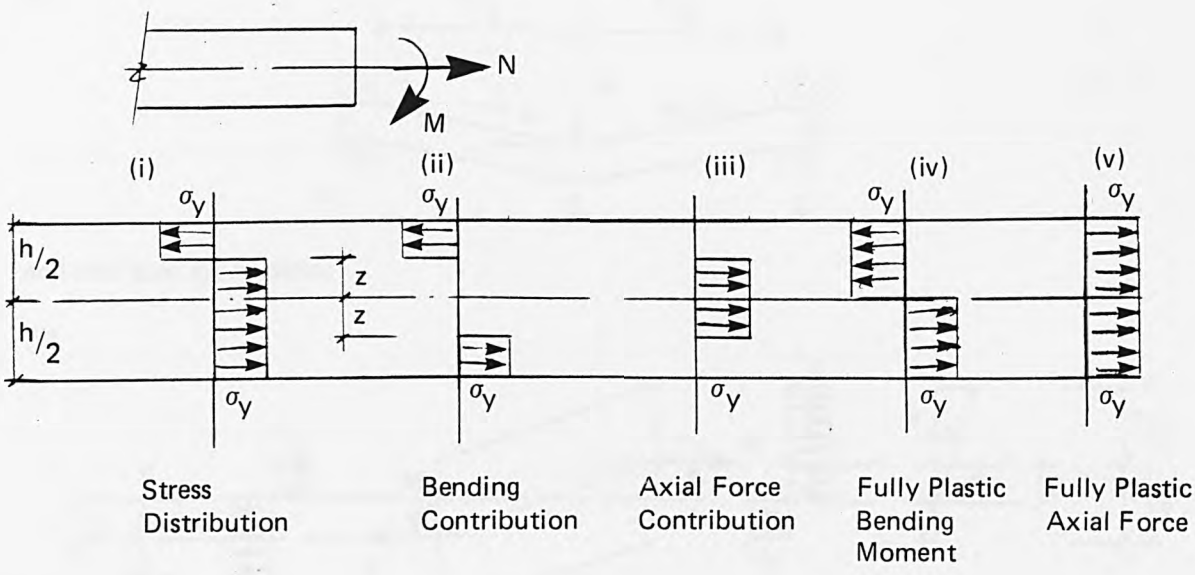

From (ii)

$$M = \sigma_y \left\{ h/2 - z \right\} \left\{ h/2 + z \right\}$$
$$= \sigma_y \left\{ \left(h/2 \right)^2 - z^2 \right\} \quad \ldots\ldots \text{(A1.1)}$$

From (iii)

$$N = 2\sigma_y z \quad \ldots\ldots \text{(A1.2)}$$

From (iv)

$$M_o = \sigma_y \frac{h}{2} \cdot \frac{h}{2} = \frac{\sigma_y h^2}{4} \quad \ldots\ldots \text{(A1.3)}$$

From (v)

$$N_o = \sigma_o h \quad \ldots\ldots \text{(A1.4)}$$

Combining the above equations:

$$\frac{N}{N_o} = \frac{2\sigma_y z}{\sigma_y h} = \frac{2z}{h} \quad \ldots\ldots \text{(A1.5)}$$

$$\frac{M}{M_o} = \frac{\sigma_y \left(h^2/4 - z^2 \right)}{\sigma_y h^2/4} = 1 - \frac{4z^2}{h^2} \quad \ldots\ldots \text{(A1.6)}$$

Combining (A1.5) and (A1.6)

$$\frac{M}{M_o} = 1 - \left(\frac{N}{N_o} \right)^2 \quad \ldots\ldots \text{(A1.7)}$$

APPENDIX 2 DISSIPATION FUNCTIONS

Consider a unit width of a built in plate with plastic hinges at the centre and at the boundaries:

(i)

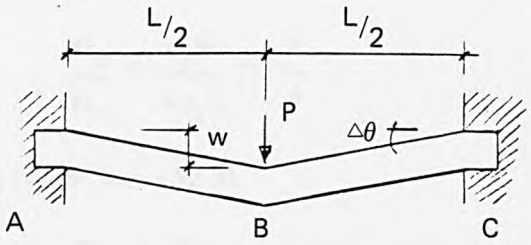

and half span BC in detail:

(ii)

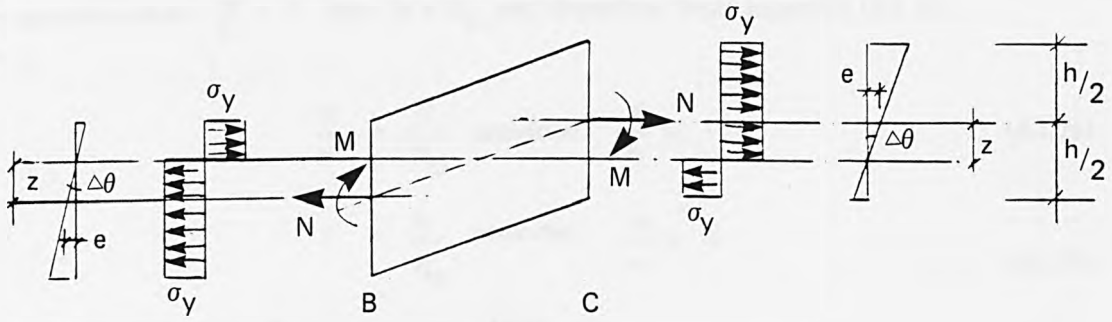

From (ii):

Curvature rate : $\dot{\kappa} \alpha \triangle \theta$

Axial strain rate : $\dot{\epsilon} \alpha e$

$$e = z \triangle \theta$$

$$\therefore \quad \dot{\epsilon} = z \dot{\kappa} \qquad \ldots\ldots \text{(A2.1)}$$

Recall equation (A1.7), yield condition

$$\frac{M}{M_o} = 1 - \frac{N}{N_o}^2$$

$$\therefore \quad \frac{\partial M/M_o}{\partial N/N_o} = -\frac{2N}{N_o}$$

From normality of the yield curve (Figure 3.5):

$$\frac{N_o}{M_o} \cdot \frac{\dot{\epsilon}}{\dot{\kappa}} = \frac{2N}{N_o} \qquad \ldots\ldots \text{(A2.2)}$$

$$\therefore \quad \frac{\dot{\epsilon}}{\dot{\kappa}} = \frac{2NM_o}{N_o^2} \qquad \ldots\ldots \text{(A2.3)}$$

Also from (ii)

$$w = 2Z \qquad \ldots\ldots \text{(A2.4)}$$

and from (A1.3) and (A1.4)

$$\frac{M_o}{N_o} = \frac{\sigma_y h^2}{4\sigma_y h} = \frac{h}{4} \qquad \ldots\ldots \text{(A2.5)}$$

Substituting (A2.5) and (A2.4) into (A2.3)

$$\frac{w}{h} = \frac{N}{N_o} \qquad \ldots\ldots \text{(A2.6)}$$

It is apparent when $\frac{w}{h} = 1$ then $N = N_o$ and therefore, from equation (A1.7), $M = 0$.

$$\therefore \quad \frac{w}{h} = \frac{N}{N_o} \text{ provided } \frac{w}{h} \leqslant 1 \qquad \ldots\ldots \text{(A2.7a)}$$

$$1 = \frac{N}{N_o} \text{ provided } \frac{w}{h} \geqslant 1 \qquad \ldots\ldots \text{(A2.7b)}$$

and using equations (A2.7) with equation (A1.7)

$$\frac{M}{M_o} = 1 - \frac{w^2}{h^2} \quad \text{for } \frac{w}{h} \leqslant 1 \qquad \ldots\ldots \text{(A2.8a)}$$

$$\frac{M}{M_o} = 0 \quad \text{for } \frac{w}{h} \geqslant 1 \qquad \ldots\ldots \text{(A2.8b)}$$

The dissipation function per unit length of straight line hinge is given by equation (3.5a):

$$D_f = (Nw - M)\,\dot{\theta}_m \qquad \ldots\ldots \text{(A2.9)}$$

for $\frac{w}{h} \leqslant 1$:

$$N = N_o \frac{w}{h} = \frac{4M_o}{h} \cdot \frac{w}{h} = \frac{4M_o w}{h^2} \qquad \ldots\ldots \text{(A2.10)}$$

$$M = M_o \left\{ 1 - \left(\frac{N}{N_o} \right)^2 \right\} = M_o \left\{ 1 - \frac{w^2}{h^2} \right\} \qquad \ldots\ldots \text{(A2.11)}$$

Substituting (A2.10) and (A2.11) into (A2.9) gives:

$$D_i = M_o \left(1 + \frac{3w^2}{h^2} \right) \dot{\theta}_m \qquad \ldots\ldots \text{(A2.12)}$$

for $w/h \geqslant 1$:

$$N = N_o \qquad \ldots\ldots \text{(A2.13)}$$

$$M = O \qquad \ldots\ldots \text{(A2.14)}$$

Substituting (A2.13) and (A2.14) into (A2.9) gives:

$$D_i = 4 M_o \frac{w}{h} . \dot{\theta}_m \qquad \ldots\ldots \text{(A2.15)}$$

Equations (A2.12) and (A2.15) give energy dissipation at internal hinges and additional energy is dissipated at the supports:

for $\frac{w}{h} \leqslant 1$:

Use of equation (A2.9) with w = O gives:

$$D_b = M_\theta = M_o \left(1 - \frac{w^2}{h^2} \right) \dot{\theta}_m \qquad \ldots\ldots \text{(A2.16)}$$

for $\frac{w}{h} \geqslant 1$:

$$N = N_o \text{ and } M = O$$

i.e. no further contribution from boundary hinges.

The case of a simply supported plate can be examined in a similar manner, except now the axial extension occurs only at the centrally located plastic hinge. In this circumstance,

$$\frac{N}{N_o} = \frac{2w}{h} \qquad \ldots\ldots \text{(A2.17)}$$

In this case, when $\frac{w}{h} = {}^1/_2$, $N = N_o$ and $M = O$

i.e.

$$\frac{w}{h} = \frac{N}{N_o} \qquad \text{providing} \quad \frac{w}{h} \leqslant {}^1/_2 \qquad \ldots\ldots \text{(A2.18a)}$$

$$1 = \frac{N}{N_o} \qquad \text{providing} \quad \frac{w}{h} \geqslant {}^1/_2 \qquad \ldots\ldots \text{(A2.18b)}$$

Substituting equations (A2.18) and equation (A1.7) into (A2.9)

for $\frac{w}{h} \leqslant {}^1/_2$: $D_i = M_o \left(1 + \frac{4w^2}{h^2} \right) \dot{\theta}_m$ $\qquad \ldots\ldots \text{(A2.19)}$

for $\frac{w}{h} \geqslant {}^1/_2$: $D_i = \frac{4 M_o w}{h} \dot{\theta}_m$ $\qquad \ldots\ldots \text{(A2.20)}$

APPENDIX 3 ELASTIC STRAIN ENERGY CALCULATION

The following provides conservative estimates of elastic strain energy capacity. To estimate the energy absorbed elastically, it is assumed that the plate deforms with a constant stiffness until the load for plastic collapse is reached.

i.e. total elastic energy $= 0.5.P_L \,.\, w$ ..... (A3.1)

and for concentrated loading the limit load is given by: [24]

$$P_L = 4\pi M_o \qquad \text{..... (A3.2)}$$

For square plate under concentrated load with clamped edge condition:

$$w = \frac{0.0056\ PL^2}{D} \qquad \text{..... (A3.3)}$$

where $D = \dfrac{Eh^3}{12(1-\upsilon^2)}$

and stiffness $K = \dfrac{P}{w}$

$$\therefore \quad K = \frac{Eh^3}{12(1-\upsilon^2)\ L^2\ 0.0056} \qquad \text{..... (A3.4)}$$

$$\therefore \quad \text{elastic strain energy capacity} = \frac{0.5P_L{}^2}{K} \qquad \text{..... (A3.5)}$$

Substituting (A3.4) and (A3.2) into (A3.5) gives:

$$S.E = \frac{0.0336\ .\ \pi^2\ .\ h\ (1-\upsilon^2)\ L^2.\ \sigma_y{}^2}{E} \qquad \text{..... (A3.6)}$$

For a circular plate under concentrated load with clamped edge condition:

$$w = \frac{PR^2}{16\pi\ D} \qquad \text{..... (A3.7)}$$

and therefore:

$$K = \frac{16\pi\ Eh^3}{12\ R^2\ (1-\upsilon^2)}$$

which gives:

$$S.E. = \frac{3\pi\ R^2.\ h\ (1-\upsilon^2)\ \sigma_y{}^2}{8E} \qquad \text{..... (A3.8)}$$

An alternative method for strain energy capacity calculation, which in general leads to more conservative results than the above, is given by Jones et al [137].

$$S.E = \frac{\sigma_y^2}{2E} \int_V dV$$

where the integral represents volume integration of the structure under consideration.